Backman, J., Duncan, R. A., et al., 1988
Proceedings of the Ocean Drilling Program, Initial Reports, Vol. 115

5. SITE 707[1]

Shipboard Scientific Party[2]

HOLE 707A

Date occupied: 1930 L, 27 May 1987

Date departed: 1630 L, 28 May 1987

Time on hole: 21 hr

Position: 07°32.72'S, 59°01.01'E

Water depth (sea level; corrected m, echo-sounding): 1552.3

Water depth (rig floor; corrected m, echo-sounding): 1563.8

Bottom felt (m, drill pipe): 1551.9

Penetration (m): 213.3

Number of cores: 24

Total length of cored section (m): 213.3

Total core recovered (m): 160.3

Core recovery (%): 75.1

Oldest sediment cored:
Depth (mbsf): 212.3
Nature: nannofossil ooze
Age: late Eocene
Measured velocity (km/s): 1.548

HOLE 707B

Date occupied: 2005 L, 28 May 1987

Date departed: 0545 L, 29 May 1987

Time on hole: 9 hr, 40 min

Position: 07°32.72'S, 59°01.01'E

Water depth (sea level; corrected m, echo-sounding): 1552.3

Water depth (rig floor; corrected m, echo-sounding): 1563.8

Bottom felt (m, drill pipe): 1551.9

Penetration (m): 124.9

Number of cores: 13

Total length of cored section (m): 124.9

Total core recovered (m): 96.1

Core recovery (%): 76.9

Oldest sediment cored:
Depth (mbsf): 124.1
Nature: foraminifer-bearing nannofossil ooze
Age: middle Miocene
Measured velocity (km/s): 1.537

HOLE 707C

Date occupied: 1750 L, 29 May 1987

Date departed: 0115 L, 1 June 1987

Time on hole: 55 hr, 25 min

Position: 07°32.72'S, 59°01.01'E

Water depth (sea level; corrected m, echo-sounding): 1552.3

Water depth (rig floor; corrected m, echo-sounding): 1563.8

Bottom felt (m, drill pipe): 1551.9

Penetration (m): 443.2

Number of cores: 28

Total length of cored section (m): 259.4

Total core recovered (m): 91.7

Core recovery (%): 35.3

Oldest sediment cored:
Depth (mbsf): 375.6
Nature: calcareous mudstone
Age: early(?) Paleocene
Measured velocity (km/s): 5.172

Basement rocks:
Depth (mbsf): 438.7
Nature: massive basalt
Age: early(?) Paleocene
Measured velocity (km/s): 6.090

Principal results: Site 707 is located in the western tropical Indian Ocean at 7°32.72'S and 59°01.01'E in water depths of 1541.4 m. The northwestern part of the Mascarene Plateau stretches 1300 km, from the Seychelles Bank to the Saya de Malha Bank, and separates the deep Arabian Sea basin to the north from the deep Mascarene basin to the south (Fig. 1). The southward flow of intermediate deep waters across the plateau have scoured a major channel perpendicular to the ridge axis, and Site 707 is located some 6 nmi east of this channel. Small offsets in acoustic basement relief over the region have resulted in variations in the thickness of the sediment from 200 to 400 m on top of the plateau. Seismic reflection data were used to locate this site over a small basement depression, away from the channel, which was estimated to hold some 400 m of sediment.

The main objective at this site was to recover a stratigraphically continuous Neogene sediment sequence for paleoceanographic and paleoclimatologic studies. Since Site 707 is located in comparatively shallow water, this should ensure that the deposition of biogenic carbonate is largely unaffected by dissolution. Thus, the accumulation of carbonate sediment at Site 707 can be used as a reference for the true productivity flux of pelagic carbonate in this part of the western Indian Ocean. The subsequent drilling of sediments at Sites 708 through 711 along the bathymetric profile will allow us to reconstruct carbonate dissolution patterns as a function of (1) increasing water depth and (2) the time-dependent changes in both climate and ocean circulation.

A secondary objective at Site 707 was to recover the lowermost sediments and to sample the basement in order to determine the age and nature of the igneous rocks underlying the plateau. Two alternative models are considered: (1) that Precambrian granitic rocks exposed in the Seychelles Islands extend southeast under Site 707, and

---

[1] Backman, J., Duncan, R. A., et al., 1988. *Proc. ODP, Init. Repts.*, 115: College Station, TX (Ocean Drilling Program).

[2] Shipboard Scientific Party is as given in the list of Participants preceding the contents, with the addition of Isabella Premoli Silva and Silvia Spezzaferria, Dipartimento di Scienze della Terra, Universitá di Milano, Via Mangiagalli 34, I-20129 Milano, Italy.

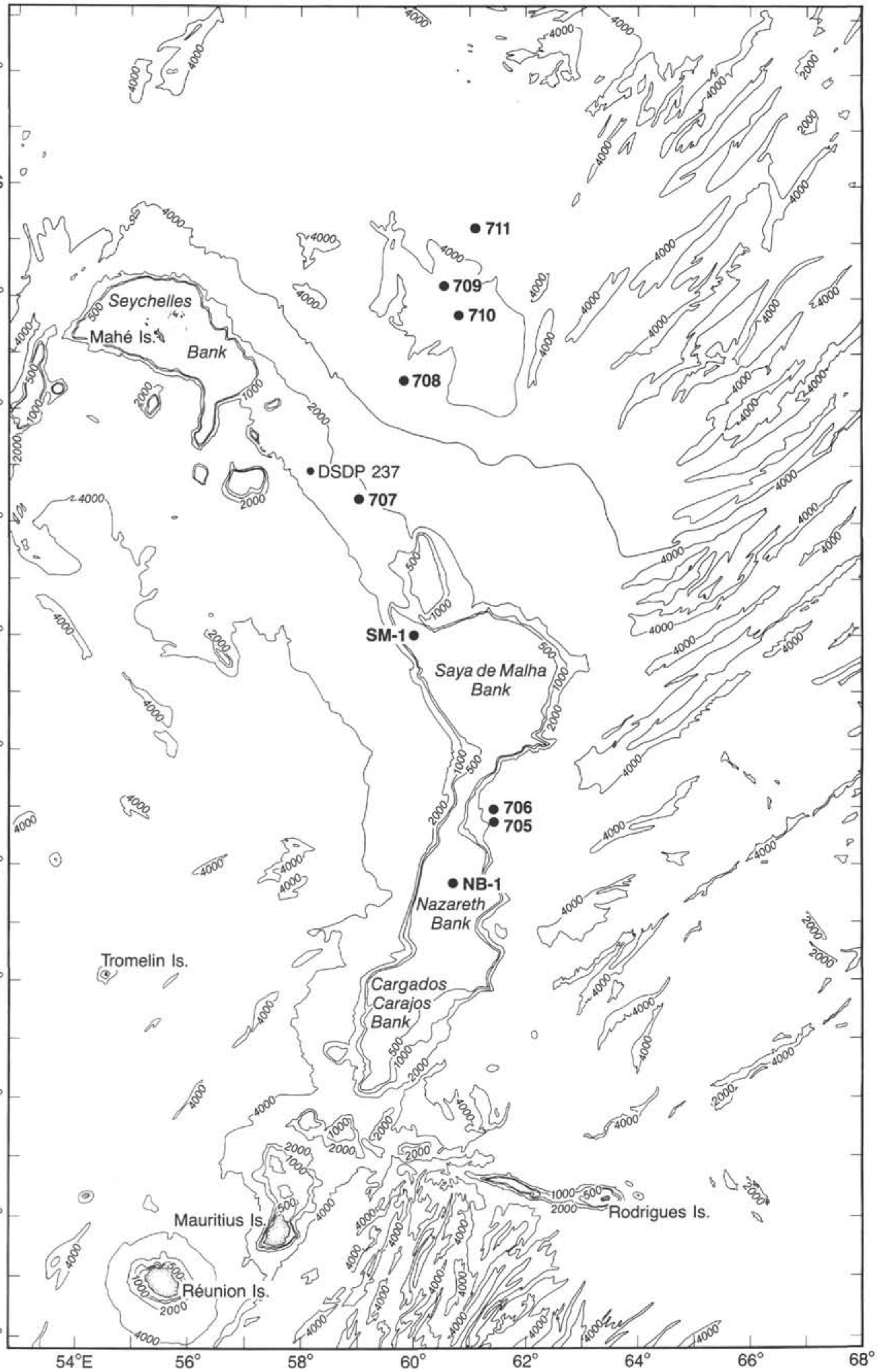

Figure 1. Location and bathymetric map (after Fisher et al., 1971) for sites drilled in the western Indian Ocean during Leg 115. Site 707 is located on an aseismic ridge, midway between the Seychelles Bank and the Saya de Malha Bank in water depths of 1541.4 m.

even on to the Saya de Malha Bank, and that the ridge is thus originally a microcontinent piece in the Gondwanan puzzle; or (2) that basalts equivalent to the Deccan flood basalts of western India, erupted near Cretaceous/Tertiary boundary time when this ridge adjoined India, form the basement for the region.

We drilled three holes at Site 707. In Hole 707A, 19 advanced hydraulic piston (APC) and 5 extended core barrel (XCB) cores were drilled continuously to a terminal depth of 213.3 mbsf, for a recovery rate of 75%. Drilling stopped when the XCB could not penetrate a hard layer, assumed to be a chert stringer. On the basis of the biostratigraphy established from Hole 707A, we decided to core Hole 707B continuously with the APC to a depth of about 120 mbsf. Hole 707B yielded 13 APC cores for a recovery rate of 77%. The total depth was 124.9 mbsf. Thereafter, the drill string was tripped and the RCB system was rigged in order to drill to basement. The upper 183.8 m of the sediment column was washed in Hole 707C, followed by continuous RCB coring. The recovery rate was 26% in the 20 sediment cores retrieved. Basalt was cored from Cores 115-707C-22R to -28R, with an unusually high recovery rate (62%). The average recovery for Hole 707C was 35%. Figure 2 illustrates the geologic column and principal features of the seismic stratigraphy at Site 707, based on data from the three holes drilled.

The lithologic composition and stratigraphic preservation of the sedimentary section at Site 707 show many similarities to DSDP Site 237, located some 60 nmi to the northwest. A fairly expanded sequence of upper Neogene sediments overlies condensed sediments of middle Miocene through Oligocene age, which overlie less condensed lower Paleogene sediments showing increased rates of deposition during Paleocene times (primarily the early part of the late Paleocene). The basaltic basement contains a few intercalated shallow-water limestones. These were virtually unaffected by dolomitization, in stark contrast to the limestones lying on top of the basement. The dominant lithologies and age assignments of the stratigraphic sequence are as follows:

Unit I	0–151.0 mbsf	Nannofossil-bearing foraminiferal ooze to foraminifer-nannofossil ooze of Pleistocene through late Oligocene age.
Unit II	151.0–251.4 mbsf	Nannofossil ooze and chalk of late Oligocene through late Eocene age.
Unit III	251.4–280.3 mbsf	Radiolarian-bearing nannofossil chalk of middle Eocene age.
Unit IV	280.3–358.2 mbsf	Calcareous chalk with interbedded silicified limestone and chert, glauconitic foraminiferal limestone, and shallow-water calcareous mudstones of middle Eocene to late Paleocene age.
Unit V	358.2–375.6 mbsf	Dolomitized shelly, shallow-water grainstones, mudstones, and rudstones of middle to perhaps early Paleocene age.
Basement rock	375.6–443.2 mbsf	Vesicular to compact, massive porphyritic basalt flows with interbedded shallow-water limestones of mid-Paleocene age.

Holes 707A and 707B

Holes 707A and 707B are characterized by decreasing grain sizes going downhole or, in other words, by increasing nannofossil content. The transition is gradual, and this more or less homogeneous lithology essentially lacks sedimentary structures. The carbonate content is on the average over 90%, with opaline silica making up most of the remainder. Volcanic glass, however, occurs in numerous thin horizons throughout the Neogene section. Higher frequency variations in carbonate content as determined from 0.5-m sampling intervals, and ranging between 80% and 95%, are confined to two shorter time intervals, post-2.4 Ma and

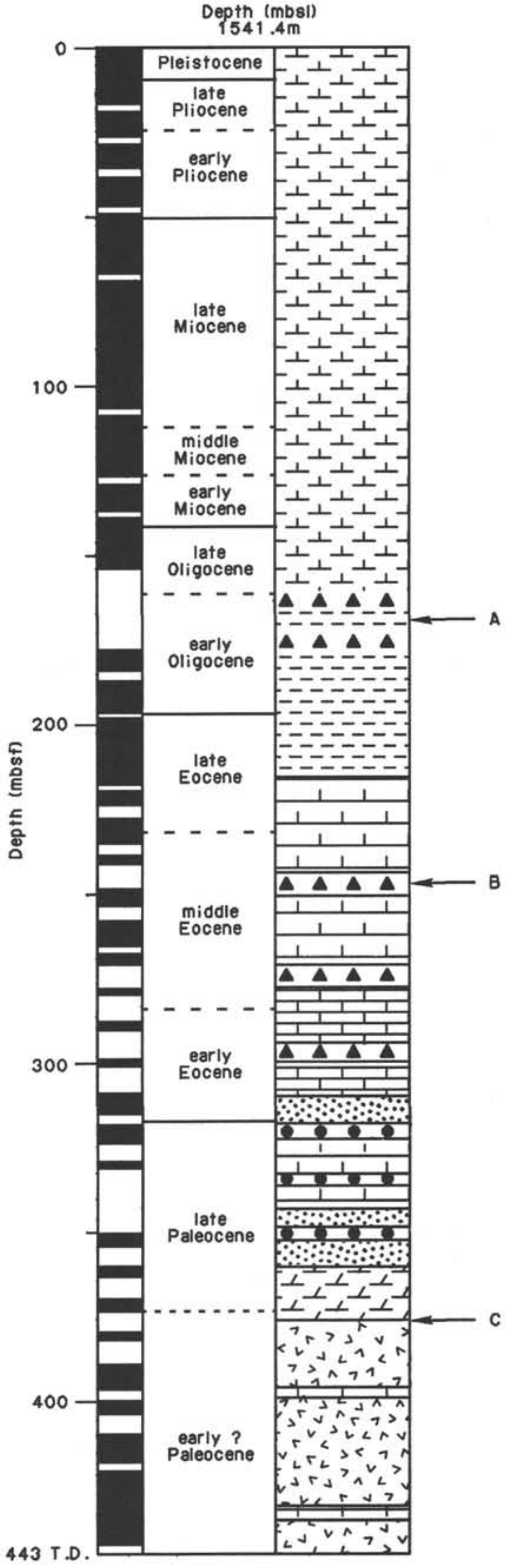

Figure 2. The geologic column for Site 707 as synthesized from lithologic, biostratigraphic, and seismostratigraphic results from cored material. The positions of prominent seismic reflectors are identified by letter (A, B, and C) and are discussed in the "Seismic Stratigraphy" section, this chapter.

between 5 and 6.5 Ma. Thus, the low-resolution shipboard work indicates the existence of possible links between carbonate content in this "shallow" tropical Indian Ocean site and (1) the onset of northern hemisphere glaciation during late Pliocene time and (2) the Messinian event in the latest Miocene.

The rate of bulk sediment accumulation is practically identical to the rate of carbonate accumulation due to the high carbonate percentages (Fig. 3). It is only during the earliest Pliocene and late Miocene that these rates exceed a value of 1 g/cm^2/1000 yr during the past 37 m.y. By assuming that carbonate dissolution has been minimal, the generally low accumulation rates during post-Eocene times presumably reflect the influence of bottom-current erosion and/or winnowing rather than subdued productivity of sediment-forming microplankton.

Condensed sequences characterize the latest Oligocene through middle Miocene interval, which probably implies that this interval contains several hiatuses of shorter duration. This condensed section is preceded by a stepwise reduction in Oligocene mass accumulation rates, presumably indicating progressively greater current strengths. A sharp increase in mass accumulation rates occurs close to the middle/late Miocene boundary at about 10 Ma, which possibly marks the time when modern circulation and productivity patterns became established in the western tropical Indian Ocean. The final late Pliocene/Pleistocene decrease in bulk and carbonate accumulation coincides in time with the onset of large-scale glaciations in the northern hemisphere, which appears to have resulted in intensified winnowing at this intermediate-depth site in the tropical Indian Ocean.

Hole 707C

We intended to wash down to just above the Oligocene-Eocene boundary at this hole and then begin rotary coring. Unfortunately, recovery in the first several cores was very low, so samples for this time horizon were good only in Hole 707A. Better recovery was obtained through the nannofossil oozes and chalks of middle to late Eocene age. The silica content of the sediments increased throughout this interval; and at 270 mbsf we encountered chert, micritic chalk, and silicified limestone of early Eocene age. Recovery then fell off again. Around 310 mbsf we started to observe glauconite-bearing foraminiferal chalks and limestones, which continued down to 355 mbsf. These upper Paleocene to lower Eocene sediments are indicative of a shallow, slow deposition environment. Below this lay calcareous mudstones and silicified limestones of earliest late Paleocene age. The presence of macrofossils (brachiopods, gastropods) is evidence that these sediments were deposited in extremely shallow water.

At 376 mbsf we penetrated basalt. Recovery in this unit was extremely good (62%), and many cores were essentially full. This will be a great boon to petrochemical and paleomagnetic studies. We recognized five distinct flow units within the basalt on the basis of changes in mineralogy and breaks at intercalated macrofossil limestone beds. The basalts are vesicular at the top but become compact downcore. Flow units are thick (one appears to be at least 30 m) and generally fine to medium grained, containing plagioclase, pyroxene, and olivine phenocrysts. No laterite beds were seen, but the absence of chilled margins and the intercalated sediments indicate extremely shallow-water conditions and point to subaerial or littoral eruptions.

The age of the basalts is constrained biostratigraphically to be no younger than the earliest part of the late Paleocene (Zone P3a; see "Biostratigraphy" section, this chapter). The basalts are of uniformly reversed polarity (see "Paleomagnetics" section, this chapter), so it is most likely that they were erupted during Chron C26R, between 62.0 and 63.0 Ma. Plate reconstructions for earliest Paleocene time place this region close to western India (Fig. 4). The origin of the southeastern half of the ridge is thus linked with the Deccan volcanic activity. The main pulse of the Deccan flood basalts occurred rapidly around the time of the Cretaceous/Tertiary boundary, or 67 Ma (Courtillot et al., 1986). The Site 707 basalts are, then, around 4–5 m.y. younger than this and were erupted either after the Deccan event (sensu stricto), as India moved northward away from the hotspot, or during the initial rifting which formed the Arabian basin.

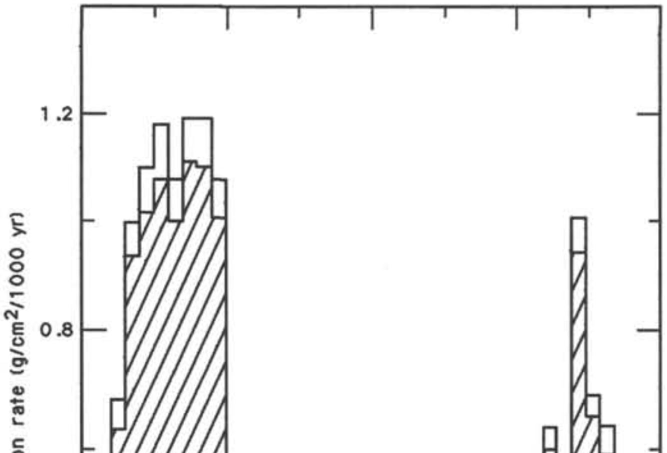

Figure 3. Mass accumulation rates of bulk sediment (unfilled area) and biogenic carbonate (diagonal lines) plotted vs. age at Site 707. The data represent mean values within 1-m.y. time increments.

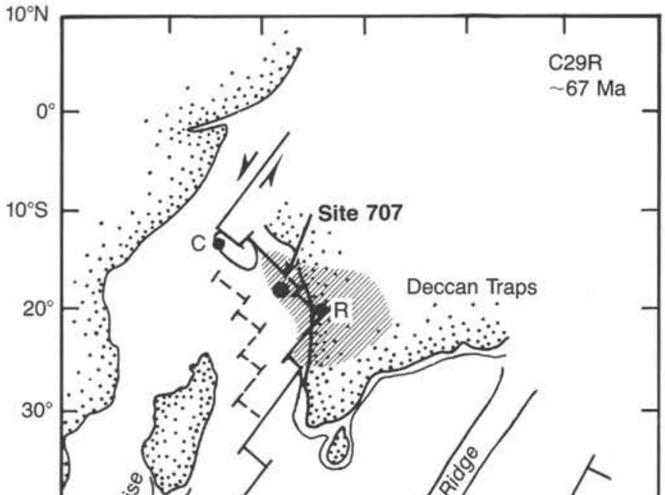

Figure 4. Plate reconstruction for the western Indian Ocean at C29R time (67 Ma), in the hotspot reference frame. Hotspots (Réunion, R; Comores, C; Kerguelen, K; Marion, M) are shown in present coordinates. Deccan volcanic activity occurred as the trailing edge of the Indian plate crossed over the Réunion hotspot. Site 707 basalts show affinities to the Deccan basalts and were probably erupted as part of that volcanic event.

We expect that future radiometric age determinations and geochemical analyses of the basalts will clarify their relationship to the phenomenal Deccan basalt province.

BACKGROUND AND OBJECTIVES

The blanket of calcareous ooze on the deep-sea floor is the chief source material from which we may learn how the global ocean environment has evolved on geologic time scales. The ooze is supplied from the mixed layer in the uppermost part of the water column and is composed mainly of sand- to silt-sized planktonic foraminifers and silt- to clay-sized coccolithophores. These groups provide information primarily about the surface environment at the time they lived. A small percentage of the foraminifers are usually composed of forms which build their shells at or near the sediment/water interface. These benthic foraminifers, although low in relative abundance, are also of paramount importance for the study of ocean history because they provide information about the environment in the deeper waters.

The ocean is everywhere supersaturated with respect to calcium carbonate in its surface layers (Takahashi, 1975), thus making the availability of nutrients the key limiting factor affecting the rate of production of this pelagic rain of calcareous particles to the seafloor. The distribution of nutrients in the world ocean, on the other hand, is a reflection of the balance between the production rate of new deep-water and surface upwelling, and therefore also of the general flow pattern of the deep-ocean circulation (from the North Atlantic through the Indian to the North Pacific; Broecker and Peng, 1982). Moreover, a weak and unstable thermocline enhances the mixing between the nutrient-rich deeper waters and the nutrient-poor euphotic zone, and vice versa. It follows that the time-dependent evolution of the deep- and surface-ocean circulation is linked directly to productivity and, hence, to the input rate of biogenic carbonate to the deep-sea floor.

All deep-water masses are undersaturated with respect to calcium carbonate (Takahashi, 1975), implying that foraminifers and coccolithophores sinking below the depth of the calcite saturation horizon will be subject to dissolution. The depth of the saturation horizon is largely a function of ocean circulation, deeper in the Atlantic and shallower in the Pacific. At present, the deep waters of the Pacific are more acidic than the Atlantic because during the transport from the latter to the former basin these deep waters steadily receive organic material from the surface which oxidizes at intermediate depths. The end result is that this process increases the concentration of dissolved carbon dioxide along the deep-water flow path, and hence the corrosiveness of these deep-water masses with respect to calcite (Broecker and Peng, 1982).

Two factors more than anything else influence ocean circulation. On shorter time scales, it is climate which regulates both deep and surface circulation. If longer time scales are considered, the geometric evolution of the ocean basins also has to be taken into account, particularly the closing and opening of critical passageways. Examples of these include the final closure of the Tethyan Seaway which connected the low-latitude Indo-Pacific and Atlantic regions during pre-middle Miocene times, or the increasing isolation of Antarctica, with respect to Australia, during late Eocene times.

The main purpose of the paleoenvironmental program of Leg 115 was to study the interplay between the flux in carbonate production and the dissolution of this material as a function of water depth, in the perspective of the evolving climate and ocean circulation during Neogene times. The key to achieving this objective was to obtain a tightly spaced transect of continuous Neogene sediments from sites spanning a wide range of water depths. The requirements for such a transect also included the following: (1) the sites should be located in a small geographic area to ensure that the pelagic rain to all sites is similar; (2) the shallowest site should be located well above the depth of the calcite saturation horizon to ensure that little or no calcite dissolution has occurred; (3) the sites should cover a wide depth range so that a wide range of calcite saturation levels become represented; and (4) the sites should be located in an area with reasonably high sediment accumulation rates to ensure that high-resolution studies are possible (e.g., detection of precessional cycles).

The northeastern flank of the Seychelles–Saya de Malha platform fulfilled these requirements within the tropical Indian Ocean, and Site 707 (Fig. 5) is the shallow end-member of five sites in a bathymetric transect in water depths ranging from 1550 to 4430 m. Site 707 is located in the saddle separating the Seychelles Bank from the Saya de Malha Bank on the Mascarene Plateau, and the seismic records upon which the site selection was made indicated a total sediment thickness of about 440 m at this target. Judging from the drilling results of the nearby DSDP Site 237, we anticipated encountering a virtually complete Neogene section and a less continuous Paleogene strata.

Site 707 was aimed at fulfilling the role as a reference site for the remaining, deeper sites in the carbonate profile. Since the biogenic carbonate accumulation at Site 707 presumably is unaffected by dissolution, these sediments should reflect the true productivity flux in this region of the tropical Indian Ocean. By assuming that productivity has been similar over the area encompassing the transect sites, the deeper sites along the carbonate profile can be used to monitor temporal variations in dissolution as a function of increasing water depth.

An additional objective at Site 707 was to determine the nature and origin of the basement rocks that underlie the ridge between the Seychelles Bank and the Saya de Malha Bank. Granitic rocks of age 600 to 650 Ma, or latest Precambrian, outcrop on the Seychelles Islands and are presumed to form the base of the entire Seychelles Bank, on which carbonate reefs have grown. From industry drilling it is known that the Saya de Malha Bank consists of 2400 m of Paleocene to Recent shallow-water carbonate built on at least 850 m of basalt. The two banks are connected by a 600-km linear ridge with shallows of 1500 m or less. The basement rocks at Site 707 could, therefore, be a submerged extension of the Seychelles granites. Indeed, granitic rocks could even underlie the basalts at the Saya de Malha Bank. In this case, the Seychelles microcontinent, left behind in the rifting between India, Madagascar, and Africa, is a significant piece to be fit in western Indian Ocean plate reconstructions.

In plate reconstructions of the western Indian Ocean for latest Cretaceous time, this region is joined with the western margin of India (Fig. 6). Hence, the clear alternative origin is that the basement rocks at Site 707 and beneath the Saya de Malha Bank are entirely basaltic and were erupted as part of the Deccan volcanism about 67 Ma. This, of course, requires that this ridge had to be attached to western India at that time. Rifting began during Chron C27 time (63–64 Ma), and seafloor spreading moved India rapidly away to the northeast. From studies of benthic foraminifer assemblages, we expect to determine the subsidence history of the ridge since rifting.

OPERATIONS

Site CARB-1B is located 3 nmi east-northeast of the original site, CARB-1. At 0100 hr, 26 May 1987, the ship was under way. We streamed the seismic gear for a pre-site evaluation and dropped a retrievable beacon at 1300 hr, 27 May 1987, to establish Site 707. The ship was in dynamic positioning (DP) mode at 1410 hr.

Hole 707A

We lowered the bottom hole assembly (BHA) to the seafloor and established the mud line at 1541.4 m. The hole was cored

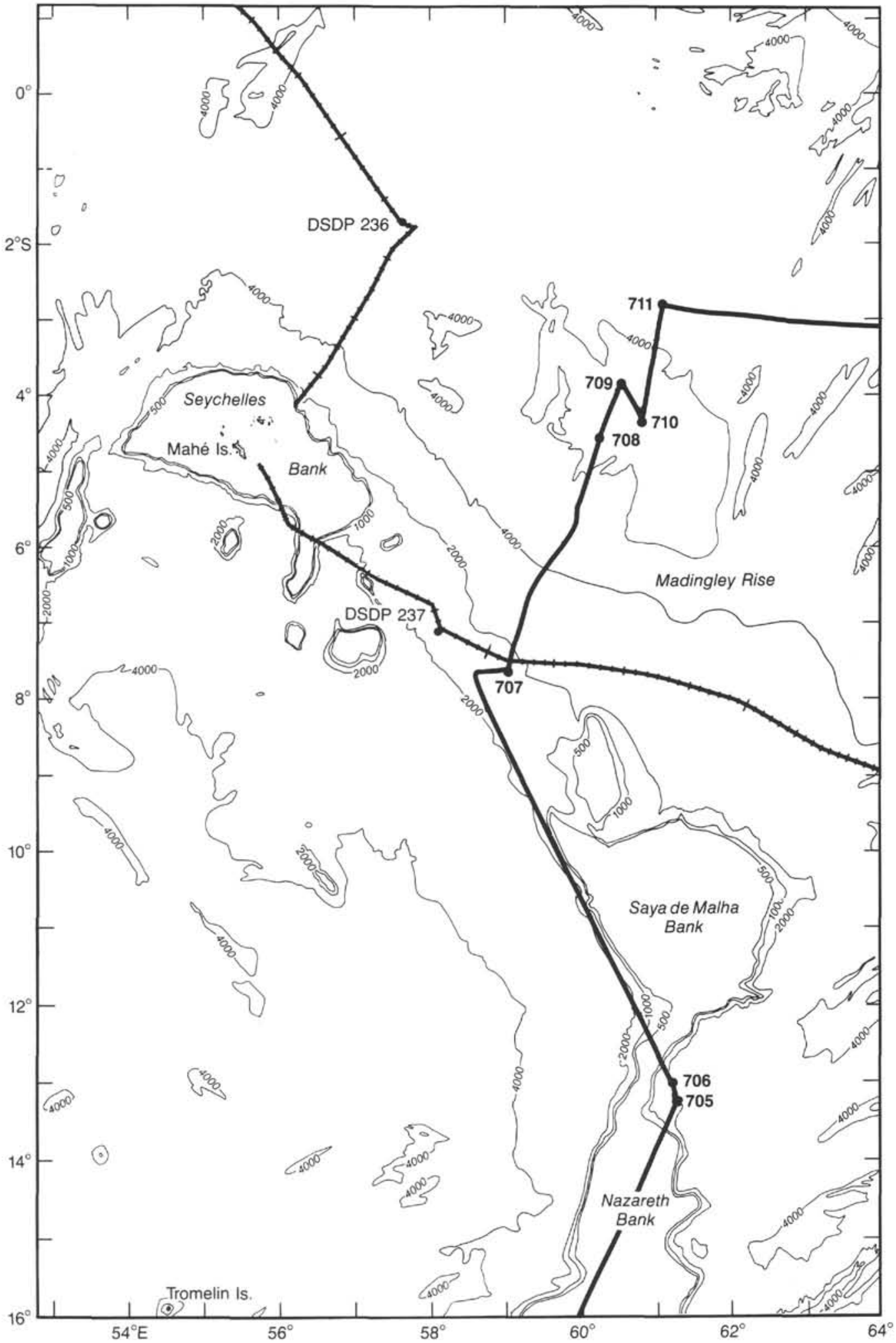

Figure 5. Expanded view of bathymetric features around the northern Mascarene Plateau and the location of Site 707 (after Fisher, Bunce, et al., 1974). Shown for reference is the track line of the *Glomar Challenger* on DSDP Leg 24 as well as the track line for ODP Leg 115 made by *JOIDES Resolution.*

with the APC to 1715.1 m (173.7 mbsf) when penetration and recovery fell off. Orientation instruments were deployed from Core 115-707A-4H at 1567.2 m through Core 115-707A-19H. Coring with the APC recovered 127.7 m of core for a recovery rate of 73.5%.

Coring with the XCB was employed from Core 115-707A-20X at 1715.1 m through Core 115-707A-24X at 1754.7 m (213.3 mbsf), when a hard formation, presumably chert, was encountered. At this point we retrieved the XCB and installed an amalgamated synthetic diamond cutting shoe. The synthetic dia-

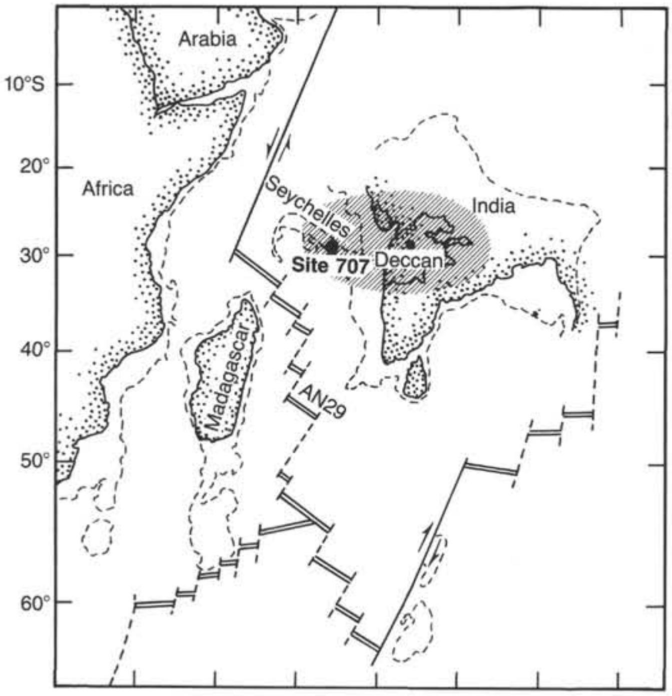

Figure 6. Paleoreconstruction of the Indian plate and surrounding oceanic plateaus and ridges at the time of Chron C29R, the Cretaceous-Tertiary boundary, when the Deccan flood basalts are thought to have erupted. Identification of Deccan-type basalts at Site 707 greatly extends the original bounds of this flood basalt event. The Seychelles Bank–Saya de Malha Bank ridge adjoins western India (from Courtillot et al., 1986).

mond cutting shoe was unable to penetrate the hard formation, so we decided to pull clear of the mud line, offset the ship 10 m south, and initiate Hole 707B. Coring with the XCB recovered 32.6 m of core, for a recovery rate of 82.3%.

Total penetration was 213 mbsf to 1754.7 m, with 160.3 m of core recovered for a total recovery rate of 75.1% (Table 1).

Hole 707B

At 2005 hr, 28 May 1987, we lowered the BHA to the seafloor again and established the mud line at 1541.4 m. Hole 707B was cored 13 times with the APC to 1666.3 m. Total penetration was 124.9 mbsf, with 96.1 m of core recovered for a total recovery rate of 76.9% (Table 1). The scientists wanted to double APC core the top 120 m only. With that objective met, the APC/XCB was tripped out and replaced with a standard RCB. The ship was offset 10 m south to initiate Hole 707C.

Hole 707C

The RCB was lowered to the seafloor (1541.4 m), and the hole was washed down 183.8 mbsf to 1725.2 m. Coring commenced at this depth, with the ultimate objective of penetrating the hard formation encountered in Hole 707B at 1754.4 m (213 mbsf).

At approximately 1753 m (212 mbsf) while drilling in a soupy chalk ooze, the drill string became stuck, presumably because of sand falling back into the hole. The drill string was worked for half an hour before it was jarred free. The hard formation, previously encountered at 213 mbsf in Hole 707A, was never encountered, even though the ship had been offset only 20 m.

Basalt was recovered with Core 115-707C-22R at 1917.4 m (376 mbsf). After Core 115-707C-28R at 1984.6 m (443.2 mbsf), it was decided by the Co-Chiefs to stop drilling and prepare to

Table 1. Coring summary, Site 707.

Core no.	Date (1987)	Time (local)	Depth (mbsf)	Cored (m)	Recovered (m)	Recovery (%)
115-707A-						
1H	May 27	2000	0–6.6	6.6	6.60	100.0
2H	27	2045	6.6–16.2	9.6	9.15	95.3
3H	27	2115	16.2–25.8	9.6	6.31	65.7
4H	27	2215	25.8–35.5	9.7	6.93	71.4
5H	27	2315	35.5–45.1	9.6	8.15	84.9
6H	28	0030	45.1–54.7	9.6	9.51	99.0
7H	28	0115	54.7–64.3	9.6	8.92	92.9
8H	28	0200	64.3–74.0	9.7	9.76	100.0
9H	28	0250	74.0–83.6	9.6	9.54	99.4
10H	28	0345	83.6–93.2	9.6	8.74	91.0
11H	28	0430	93.2–102.8	9.6	0.99	10.3
12H	28	0515	102.8–112.4	9.6	8.77	91.3
13H	28	0615	112.4–122.0	9.6	7.44	77.5
14H	28	0730	122.0–131.6	9.6	6.90	71.9
15H	28	0815	131.6–141.3	9.7	8.37	86.3
16H	28	0900	141.3–151.0	9.7	10.03	103.4
17H	28	0930	151.0–160.7	9.7	1.51	15.5
18H	28	1015	160.7–170.3	9.6	0	0
19H	28	1100	170.3–173.7	3.4	0	0
20X	28	1200	173.7–183.4	9.7	4.81	49.6
21X	28	1300	183.4–193.1	9.7	9.12	94.0
22X	28	1345	193.1–202.7	9.6	9.37	97.6
23X	28	1445	202.7–212.3	9.6	9.35	97.4
24X	28	1530	212.3–213.3	1.0	0	0
115-707B-						
1H	28	2030	0–9.5	9.5	5.91	62.2
2H	28	2115	9.5–19.1	9.6	7.50	78.1
3H	28	2200	19.1–28.7	9.6	6.82	71.0
4H	28	2245	28.7–38.4	9.7	7.72	79.6
5H	28	2330	38.4–48.0	9.6	8.59	89.5
6H	29	0015	48.0–57.6	9.6	6.93	72.2
7H	29	0115	57.6–67.2	9.6	9.75	101.0
8H	29	0200	67.2–76.9	9.7	8.55	88.1
9H	29	0245	76.9–86.5	9.6	5.45	56.8
10H	29	0330	86.5–96.1	9.6	8.80	91.6
11H	29	0415	96.1–105.7	9.6	8.96	93.3
12H	29	0500	105.7–115.3	9.6	2.31	24.0
13H	29	0545	115.3–124.9	9.6	8.79	91.5
115-707C-						
1W	29	1800	0–183.8	183.8	0.10	0.1
2R	29	1915	183.8–193.5	9.7	0	0
3R	29	2015	193.5–203.1	9.6	9.74	101.0
4R	29	2200	203.1–212.8	9.7	0	0
5R	29	1145	212.8–222.5	9.7	0.65	6.7
6R	30	0100	222.5–232.1	9.6	4.37	45.5
7R	30	0215	232.1–241.8	9.7	6.41	66.1
8R	30	0315	241.8–251.4	9.6	1.22	12.7
9R	30	0400	251.4–261.0	9.6	3.78	39.4
10R	30	0500	261.0–270.6	9.6	6.18	64.4
11R	30	0600	270.6–280.3	9.7	1.16	11.9
12R	30	0715	280.3–289.8	9.5	0.69	7.3
13R	30	0845	289.8–299.3	9.5	1.28	13.5
14R	30	0945	299.3–308.9	9.6	0.55	5.7
15R	30	1100	308.9–318.2	9.3	3.97	42.7
16R	30	1215	318.2–327.9	9.7	3.16	32.6
17R	30	1330	327.9–337.5	9.6	0.09	0.9
18R	30	1445	337.5–347.1	9.6	0	0
19R	30	1600	347.1–356.7	9.6	1.68	17.5
20R	30	1730	356.7–366.0	9.3	1.82	19.5
21R	30	1950	366.0–375.6	9.6	2.55	26.5
22R	31	0115	375.6–385.3	9.7	2.03	20.9
23R	31	0445	385.3–394.9	9.6	5.11	53.2
24R	31	0715	394.9–404.5	9.6	3.33	34.7
25R	31	1105	404.5–414.3	9.8	8.57	87.4
26R	31	1600	414.3–423.9	9.6	9.41	98.0
27R	31	2230	423.9–433.6	9.7	8.73	90.0
28R	Jun 1	0115	433.6–443.2	9.6	5.08	52.9

log the hole. Cores 115-707C-25R through -28R recovered 31.7 m of basalt for an 82% recovery rate, much to the pleasure of the petrologists. Total penetration was 443.2 mbsf to 1984.6 m. The total cored interval was 259.4 m, with 91.3 m of core recovered for a total recovery rate of 35.3% (Table 1).

The first suite of logging tools (DIL-GR-SLT-MCD) was run with no problems. The second suite of logging tools (GST-ACT-CNT-NGT) encountered a bridge at 1934.5 m. The GST was redeployed and again did not function properly. The GST was retrieved and the third suite of logging tools (LDT-CNL-NGT-GPIT) was deployed. Another bridge was encountered at 1721.5 m, and the logging tools were retrieved and rigged down.

On 30 May 1987 at approximately 0200 hr, the ship, in DP mode, was heading into a half-knot current with light winds when it was hit broadside by a rip current moving at approximately 6 kt. The DP system reacted immediately by sounding alarms and bringing on-line another skid to supply sufficient power to hold position. The ship immediately headed into the oncoming rip current; however, the DP system kept the ship within 91.4 m (6% of water depth) of the hole with no adverse affect on the drill string. We observed the rip current on radar and at first believed it to be a rain shower. It was approximately 6 nmi wide and 4 nmi long with a velocity of 3 kt. Another rip current of lesser strength hit the ship at 0300 hr, 31 May 1987, causing the ship to move off position only 46.6 m, or 3% of water depth.

Site 707 to Site 708 (CARB-4)

With all the coring objectives met and logging time depleted, the drill string was tripped out and the beacon recalled and retrieved.

LITHOSTRATIGRAPHY

Introduction

Three holes were drilled at Site 707 which provide a relatively complete cross-section of the sedimentary sequence overlying the basaltic basement of the Mascarene Plateau. This sequence can be divided into five major units (Fig. 7). Unit I is composed of nannofossil-bearing foraminiferal ooze and foraminifer-nannofossil ooze ranging in age from Pleistocene to late Oligocene. Unit II is composed of nannofossil ooze and nannofossil chalk ranging in age from late Oligocene to middle Eocene. Unit III consists of a relatively thin middle Eocene sequence of radiolarian-bearing nannofossil chalk that contains minor amounts of chert. Unit IV is composed of a sequence of interbedded lithologies that include micritic chalk, chert and silicified limestone, glauconitic foraminiferal limestone, and calcareous grainstones of middle Eocene to late Paleocene age. Finally, Unit V consists of dolomitized and partially dolomitized shallow-water grainstones, rudstones, and mudstones of middle to early Paleocene age which directly overlie basement and which were also found in two thin horizons intercalated within the massive porphyritic basalt flows.

The five sedimentary units are described in detail below.

Unit I: Cores 115-707A-1H to -16H (0–151.0 mbsf) and Cores 115-707B-1H to -13H (0–124.9 mbsf); Age: Pleistocene to late Oligocene.

Unit I in Holes 707A and 707B consists of a nannofossil-bearing foraminiferal ooze at the top which grades gradually downhole into a foraminifer-nannofossil ooze, the dominant lithology of the unit. Calcareous nannofossils typically form 15%–20% of the sediment at the top of the unit and progressively increase in abundance to its base, where they comprise 60%–80% of the unit. Planktonic foraminifers show the opposite trend, forming from 70%–90% of the sediment near the mud line to 25%–35% near the base of Unit I. Minor (<10%) and trace components include sponge spicules, radiolarians, diatoms, volcanic glass, dolomite rhombs, and feldspar.

The sediments of Unit I are very homogeneous and typically show few or no sedimentary structures. The carbonate content of the sediments averages >90% (see "Geochemistry" section, this chapter). Sediment color is predominantly white (10YR 8/1–8/2, 2.5Y 8/2, N9) to very pale brown (10YR 8/3), although a number of thin light gray (10YR 7/1 to N8), very light yellowish gray (2.5Y 7/2), and very light green (5G 8/2) horizons are faintly visible throughout the unit. Many of these slightly darker intervals have a well-defined base and a gradational upper contact, suggesting rapid deposition and subsequent bioturbation from above. There is no evidence from the cores themselves or from smear slides that these layers represent turbidites. Our preferred interpretation is that these faint gray to green horizons represent thin, highly altered and disseminated volcanic-ash layers, as volcanic glass is found in greater than trace amounts only within these darker intervals. A similar explanation has been put forth by Gardner et al. (1986) to explain the occurrence of pale green laminae observed in pelagic sediments from the Lord Howe Rise that were drilled on DSDP Leg 90.

With the exception of one short interval in Hole 707A (131.6–138.9 mbsf), there was no evidence of significant consolidation in the oozes of Unit I. The sole exception occurs in Core 115-707A-15H where foraminifer-nannofossil ooze was found to be interbedded with semi-indurated chalk "nodules" throughout the first 7.3 m of the core. Much of the fine carbonate in both the ooze and chalk in this interval could not be identified, although heavy overgrowths on recognizable coccoliths and discoasters argue strongly for a nannofossil origin. Curiously, nannofossils below Section 115-707A-15H-5, 130 cm, and in deeper cores, are very well preserved.

The stratigraphic distribution of Unit I sediments at Site 707 is shown in Figure 7. Because the increase in nannofossil content downhole in this unit is systematic and not sudden, we have not tried to further divide Unit I into formal subunits. Shown, however, for reference purposes is the approximate level of transition from a foraminifer-dominated sediment (nannofossil-bearing foraminiferal ooze) to a nannofossil-dominated sediment (foraminifer-nannofossil ooze) in both Holes 707A and 707B. The similar sub-bottom depths of this transition in both holes suggest that, despite the uniform lithology of this unit, excellent between-hole correlations will be possible using more refined stratigraphic tools.

Unit II: Cores 115-707A-17H to -24X (151.0–212.3 mbsf) and Cores 115-707C-3R to -8R (193.5–251.4 mbsf); Age: late Oligocene to middle Eocene.

Unit II in Holes 707A and 707C is composed of nannofossil ooze which grades downhole into a sequence of nannofossil ooze and chalk couplets. The carbonate fraction in this unit is formed almost exclusively of nannofossils (90%–100%), with foraminifers consistently making up less than 10% of the sediment. Noncarbonate components which are found in variable but minor and trace amounts include radiolarians, sponge spicules, silicoflagellates, clay, volcanic glass, mica, and opaque minerals (pyrite?). Sediment texture reflects the dominance of nannofossils, being typically 5%–15% sand, 10%–30% silt, and 60%–95% clay. In appearance, the sediments are remarkably uniform with few sedimentary structures.

Changes in sediment color in Unit II are limited to subtle shades of white, predominantly 10YR 8/1, 10YR 8/2, 2.5Y 8/2, and N9. As in the overlying Unit 1, a number of faint light gray horizons (10YR 7/2, N7–N8) occur throughout Unit II. In one such light gray interval (Section 115-707A-17H, CC), the sediment contains enough volcanic glass (15%) to be properly pre-

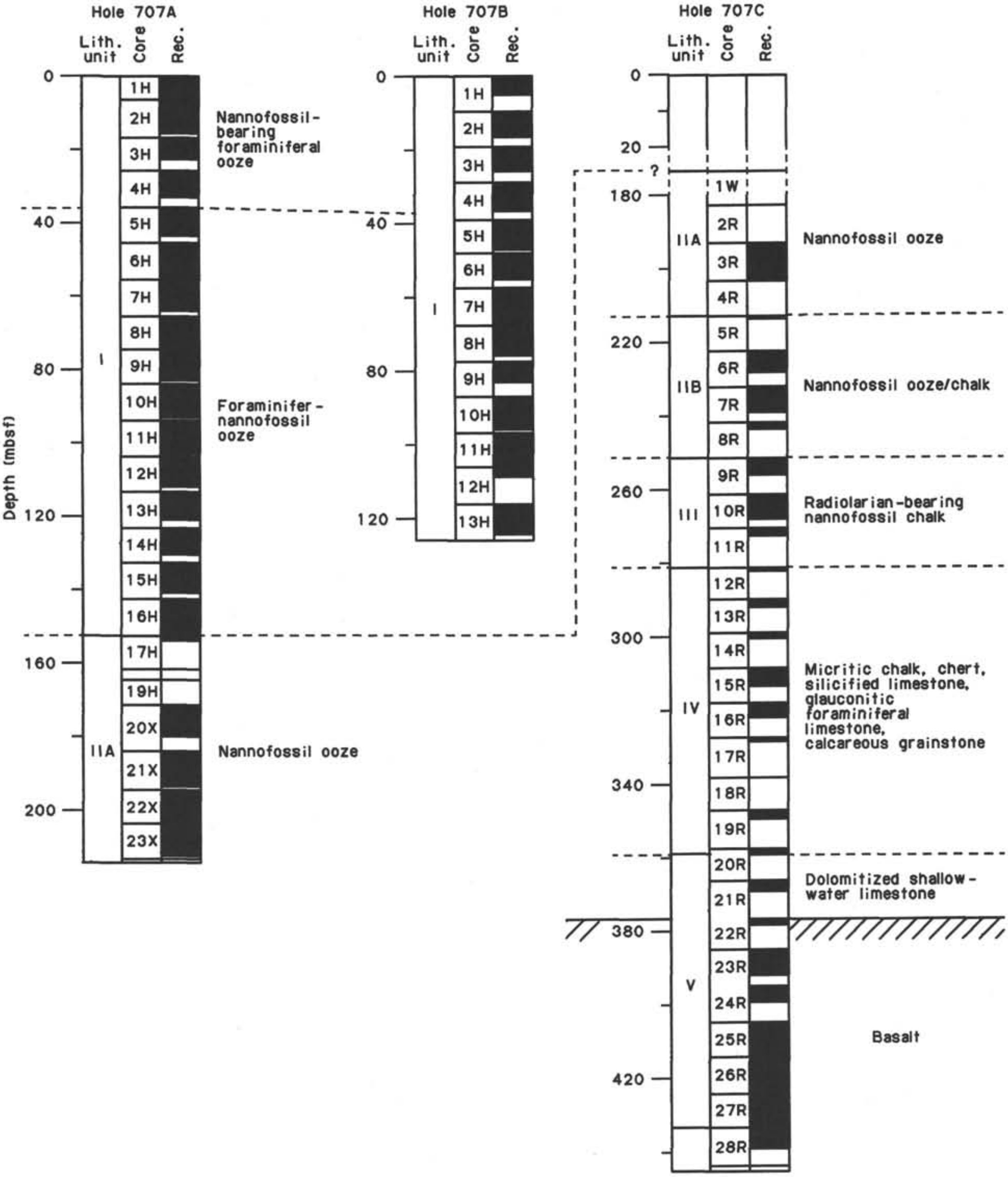

Figure 7. Summary of lithologic units recognized at Site 707. Black bars represent recovery in Holes 707A, 707B, and 707C.

fixed with "volcanic-ash-bearing." This association between color and composition again supports the hypothesis that these faint bands represent highly altered and disseminated ash layers.

Unit II sediments can be divided into two subunits to accommodate slight variations in the degree of lithification: Subunit IIA in Hole 707A is 151.0–212.3 mbsf and in Hole 707C, 193.5–212.8 mbsf; and Subunit IIB in Hole 707C is 212.8–251.4 mbsf. Subunit IIB does not appear in Hole 707A.

Subunit IIA consists of nannofossil ooze with the general characteristics discussed above. Subunit IIB differs only in that it contains alternating couplets of nannofossil ooze and nannofossil chalk, usually on a scale from 5 to 20 cm. Chalk layers in Subunit IIB are typically fractured and subrounded, and are surrounded by a soft to semifirm ooze matrix. The general degree of induration tends to increase with depth, with chalk "nodules" becoming thicker and ooze layers proportionately thinner and more irregularly spaced.

Of considerable interest is the question of whether the ooze-chalk couplets of Subunit IIB are real diagenetic features or artifacts of the rotary drilling process used in Hole 707C. If the sediments are truly undeformed, then the chalk nodules probably represent chalk layers from an original ooze-chalk depositional sequence which have been broken through and slightly eroded by friction with the rotating RCB core liner. Alternatively, the degree of drilling disturbance may be considerable, with what was originally a well-indurated chalk sequence partially ground up into a drilling paste which forms the observed ooze matrix. Observational data from this site cannot definitively answer this question, and in reality both mechanisms may be operative under different sets of lithologic and drilling conditions. In Site 709A, however, a similar sequence of ooze-chalk couplets was recovered using the APC-coring system (see "Principal Results" section, "Site 709" chapter, this volume), which suggests that such couplets may be truly diagenetic in their origin.

Unit III: Cores 115-707C-9R to -11R (251.4–280.3 mbsf); Age: middle Eocene.

Unit III consists of a relatively thin sequence of radiolarian-bearing nannofossil chalks that contain minor amounts of chert fragments. Calcareous nannofossils are moderately well preserved and still form the bulk of the unit (60%–80%), but radiolarians make up as much as 25% of the sediment and siliceous sponge spicules are also common (5%–10%). Minor and trace components include foraminifers (3%–5%), quartz, volcanic glass, mica, feldspar, and glauconite. Sediment texture is typically 10%–20% sand, 10%–15% silt, and 70%–80% clay.

The radiolarian-bearing nannofossil chalk of Unit III is predominantly white (N9), but it grades slightly to very pale green (5GY 8/1) near its base in Core 115-707C-11R. Glauconite observed in trace amounts in the latter interval is probably responsible for the subtle color change. A number of pale gray (N7–N8) horizons are again visible against the mostly white chalk, as are preserved burrow structures of the same pale gray color. Thus, the sediments of Unit III are the first of Site 707 to show significant visible evidence of faint mottling due to bioturbation.

Chert occurs only as a few granule- to pebble-sized fragments of white (10YR 8/1) to very pale brown (10YR 7/3) color near the top of Section 115-707C-9R-1 and interspersed within the chalk of Core 115-707C-11R. In general, the chalk itself is well indurated and compositionally homogeneous.

Unit IV: Core 115-707C-12R to Section 115-707C-20R-2, 52 cm (280.3–358.2 mbsf); Age: middle Eocene to late Paleocene.

Unit IV is composed of a mixed sequence of interbedded lithologies that include calcareous chalk, chert, and silicified limestone; glauconitic foraminiferal limestones; and calcareous grainstones (Fig. 8). Because the recovery within this unit was so poor (15%) and much of the material was highly fractured, further division into stratigraphically significant subunits seemed unrealistic. We will discuss each end-member lithology separately, therefore.

Foraminifer-bearing calcareous chalk was found in Cores 115-707C-12R and -13R. Calcareous nannofossils are thought to make up the bulk of these very fine-grained chalks, but the degree of alteration and recrystallization makes this identification tentative. Foraminifers, although similarly recrystallized, are nevertheless identifiable as planktonic species, and they make up 10%–15% of the sediment. Radiolarians, sponge spicules, and volcanic glass are present in minor and trace amounts. The calcareous chalk of Unit IV ranges from white to pale yellow (N9, 2.5Y 8/2–8/4) and gray (N6) to pinkish white (5YR 8/2) in color. It is also weakly bioturbated.

Chert and well-indurated, partially silicified limestones were identified in Cores 115-707C-12R through -16R. Chert nodules and fragments are generally darker in color, being typically dark brown (7.5YR 3/2–3/4), dark yellowish brown (10YR 4/6), to very dark grayish brown (10YR 3/2). The intervals of silicified limestone are lighter in color, ranging from olive brown (2.5Y 4/4), light brownish gray and light gray (2.5Y 6/2 to N6), to white (10YR 8/1).

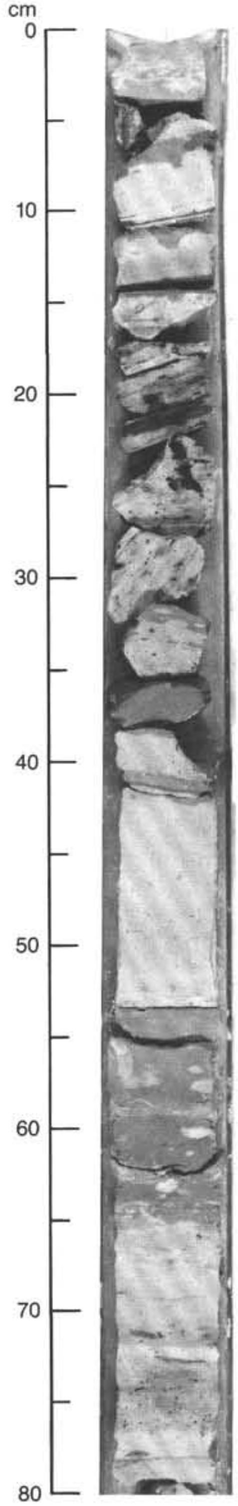

Figure 8. An example of the mixed, interbedded lithologies characteristic of Unit IV found in Section 115-707C-13R-1. From top to bottom, these include chert (0–14 cm), foraminifer-bearing silicified limestone (14–23 cm), micritic chalk (23–38 cm), claystone (38–53 cm), micritic chalk (53–65 cm), and partially silicified limestone (65–80 cm).

Glauconite-rich foraminiferal limestones and foraminifer-bearing nannofossil limestones were recovered in Cores 115-707C-14R through -16R. Glauconite grains make up as much as 5% of their total composition and give the materials their overall pale green to grayish green to moderate yellowish green hue (5G 6/2, 5G 4/2, 10GY 6/4). These rocks are well lithified and range in texture from grain-supported, glauconitic foraminiferal limestones to much finer grained, foraminifer-bearing nannofossil limestones. In the latter, much of the fine carbonate is again heavily recrystallized but apparently of nannofossil origin. Minor and trace components include quartz, feldspar, volcanic glass, and fish debris, with siliceous microfossils notably absent. This particular lithology exhibits slight to moderate amounts of bioturbation, enhanced by the presence of glauconite infilling (Fig. 9).

The last major lithology of Unit IV is calcareous grainstone, which is restricted to the base of the unit in Section 115-707C-17R, CC, and in Cores 115-707C-19R and -20R. The grainstone is well lithified. The grains range in size from fine sand to medium sand, most of which are not identifiable. Foraminifers, poorly preserved, make up as much as 15% of the total composition, but they are usually much less abundant. Glauconite is present in minor amounts (0%–3%), and trace components include feldspar and quartz. The calcareous grainstones of Unit IV are gray to greenish gray (5GY 5/1–6/1) in color, and are weakly to moderately bioturbated throughout.

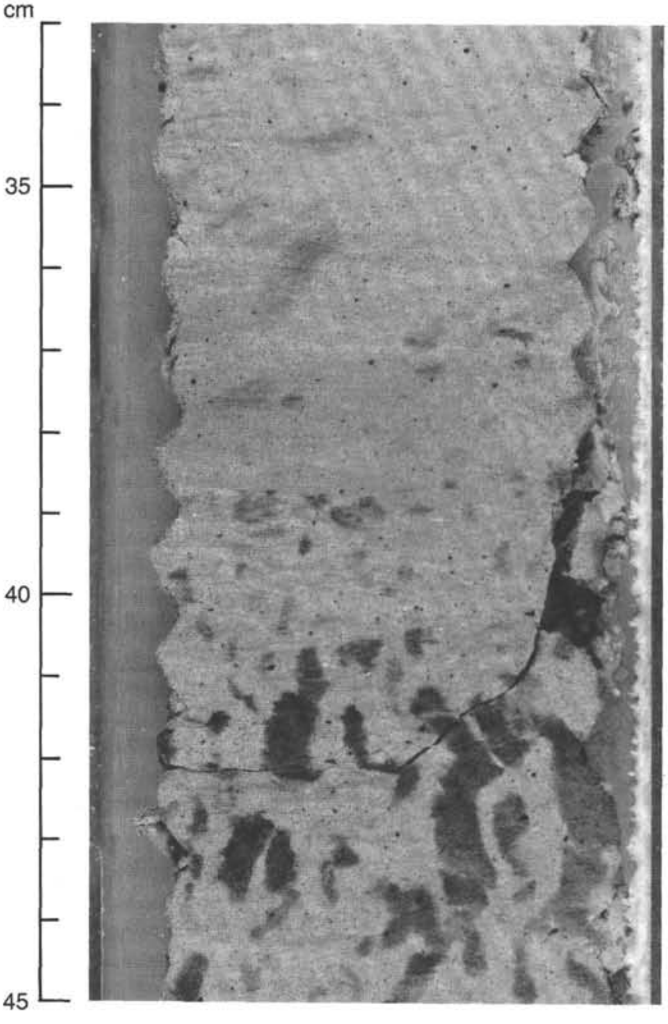

Figure 9. Evidence of bioturbation in a glauconitic foraminifer-bearing nannofossil limestone (Unit IV) from Section 115-707C-15R-3. Preserved burrow traces are enhanced by the presence of glauconite.

A thin (15 cm) layer of reddish brown (5YR 8/2) claystone, a very minor lithology, was observed in Core 115-707C-13R interbedded between micritic chalk and partially silicified limestone. The carbonate content of this layer is negligible, with the exception of *Zoophycos* burrows infilled with chalk from the overlying lithology. The sharp bottom contact, gradational upper contact, and dominance of clay minerals suggest that this claystone represents a relatively thick, but highly altered, volcanic ash. Lastly, a manganese nodule 7–8 cm in diameter was recovered in Core 115-707C-14R.

Unit V: Section 115-707C-20R, CC, to Core 115-707C-21R (358.2–375.6 mbsf); Section 115-707C-24R-1, 0–91 cm (394.9–395.8 mbsf); Section 115-707C-28R-1, 0–35 cm (433.6–434.0 mbsf); Age: late to early Paleocene.

Unit V consists of dolomitized to partially dolomitized shelly grainstones, mudstones, and rudstones of shallow-water origin. The first dolomite appears in the core catcher of Core 115-707C-20R and continues into Core 115-707C-21R. The dolostone in this very basal part of the Site 707 sequence is light olive gray (5Y 6/2) and dark olive gray (5Y 3/2) to dark gray (5Y 4/1) in color; it is commonly shelly and often shows fine flaser structure. An example of the fossiliferous nature of dolostone found in the core catcher of Core 115-707C-21R is shown in Figure 10. Directly underlying this specimen was a single piece of basalt.

Sediments were also recovered from two thin horizons intercalated within the massive basalt flows near the top of basement. Unlike the shallow-water facies directly overlying the basalt, these grainstones, mudstones, and rudstones have been only partially dolomitized. Macrofossils with a shallow-water (reefal) affinity are common and include small bivalves, brachiopods, gastropods, worm tubes, and calcareous algae. Glauconite grains (<2 mm) are a minor, but visible, constituent. The color of

Figure 10. Dolostone with preserved bivalve molds recovered from Section 115-707C-21R, CC.

these partially dolomitized limestones ranges from grayish and dark grayish brown (2.5Y 5/2–4/2) to greenish gray (5GY 7/1–6/1).

Depositional Setting

The five lithologic units recognized at Site 707 indicate that this locality has been a site of pelagic carbonate sedimentation since at least the Paleocene. The discovery of a shallow-water reef fauna in the partially dolomitized early Paleocene limestones within the basement rocks indicates that the site was very close to sea level at the conclusion of basaltic volcanism.

The pelagic part of the sedimentary sequence at Site 707 is characterized by a gradual increase in the calcareous nannofossil content and a corresponding decrease in the foraminifer content downhole. Sediment texture is largely a function of these two components, and average grain size thus gradually decreases downhole as well. The origins of this long-term trend are not clear. One possibility is that this transition from a nannofossil-dominated sediment below to a foraminifer-dominated sediment above reflects a gradual change in their relative rates of biogenic production in the overlying equatorial waters. Alternatively, the coarsening of sediments in the late Neogene may reflect winnowing related to gradual flow changes in the intermediate waters which bathe this shallow site.

In general, lithification of the carbonate-rich sediments increases with burial depth, with nannofossil oozes grading into nannofossil chalks in Unit II. The explanation for the ooze-chalk couplets observed in Subunit IIA is not apparent at this time. Strong recrystallization of carbonate begins in the early Eocene sediments of Unit IV and continues with increasing depth.

Radiolarians and siliceous sponge spicules are especially abundant in the middle Eocene chalks of Unit III but are rare in older sediments, suggesting that opaline skeletons are a material source for the silicification observed in Unit IV. Chert first appears in minor amounts in the middle Eocene and is common in the lower Eocene and Paleocene.

Finally, the presence of thin pale gray to greenish gray horizons throughout much of the predominantly white, high-carbonate pelagic sequence, and their tentative interpretation as altered and disseminated ash layers, suggests that Site 707 has recorded the existence of volcanic activity in the area throughout much of the Tertiary.

BIOSTRATIGRAPHY

Introduction

The 375.6-m-thick sedimentary sequence penetrated in the three holes of Site 707 consists from top to bottom of:

1. 114 m of continuous Pleistocene to upper Miocene calcareous ooze (recovered in Holes 707A and 707B);
2. 28 m of condensed middle and lower Miocene calcareous ooze with at least one significant hiatus in the lower Miocene;
3. 233 m of Paleogene calcareous ooze and chalk apparently continuous from Oligocene to upper Paleocene (recovered in the lower part of Hole 707A and in Hole 707C). The lowermost sediments overlying basement, as well as sediment inclusions 30 m below the top of basement, indicate a Paleocene age.

Calcareous nannofossils are abundant throughout the Pleistocene to upper Paleocene sequence. Preservation is good in the Neogene with significant overgrowth of the discoasters, especially in the lower Pliocene and upper Miocene. Preservation is good to moderately good in the Oligocene through the upper Paleocene, although nannofossil assemblages are rare and preservation is poor below Core 115-707C-17R.

Planktonic foraminifers are abundant in Pleistocene through Eocene sediments. They are very rare in the Paleocene interval where recrystallization is significant. Preservation is good in the Pleistocene through the upper Miocene. It is moderately good in the middle and lower Miocene and in the Oligocene to upper Eocene, poor in the lower Eocene and upper Paleocene, and very poor in the lower Paleocene.

Benthic foraminifers are rare throughout most of the sedimentary sequence, except in the lower Oligocene and the upper Eocene where a higher concentration results from increased dissolution. The assemblages reflect intermediate water depths from the Pleistocene through the Eocene, shoaling to middle bathyal depths in the lowermost Eocene. A substantial shoaling to shelf depth is recorded by the benthic foraminiferal assemblages in the Paleocene. Limestone microfacies included in the basement show a shallow reefal environment rich in calcareous algae.

Siliceous microfossils are present only in some intervals. Radiolarians occur in two intervals: (1) in the lower Pliocene–upper Miocene and (2) in the Oligocene–middle Eocene (with common to poor occurrence and good to poor preservation in both intervals). Diatoms have a restricted occurrence. They are present in significant amounts only in the lower Pliocene to the upper part of the upper Miocene; their occurrence in the Paleogene section is very scattered. They are poorly preserved in both intervals.

A biostratigraphic summary for Site 707 is presented in Figure 11.

Calcareous Nannofossils

Hole 707A

Abundant Pleistocene to upper Eocene calcareous nannofossil assemblages were identified from the 23 cores retrieved from this hole. Preservation is good in the Pleistocene sequence, whereas deeper cores show moderate preservation. Specifically, lower Pliocene and upper Miocene discoasters are so overgrown that their recognition at the species level is severely restricted. As a result, the determination of some zonal boundaries based on discoasters could be done only tentatively.

Pleistocene

Pleistocene sediments recovered in this hole consist mostly of loose foraminiferal sands, with nannofossils generally being scarce. Nevertheless, the stratigraphic succession of the Pleistocene flora can be recognized within this sequence, although frequent occurrences of reworked specimens make precise identification difficult for some marker events. We examined a set of closely spaced samples (10–20 cm intervals) for the Pliocene/Pleistocene sequence. We subsequently located the Pliocene/Pleistocene boundary within the lower part of Section 115-707A-2H-3, making the total thickness of the Pleistocene sequence approximately 11 m.

The interval between Samples 115-707A-1H-1, 1 cm, and 115-707A-1H-2, 40–41 cm, is assigned to Zone CN15 or Subzone CN14b. *Emiliania huxleyi* is relatively scarce even in the upper portion of this sequence, making the identification of its first occurrence (FO) at the base of Zone CN15 difficult. Gephyrocapsids of medium and large size are the dominant forms in the assemblage. Other typical elements include *Syracosphaera* spp., *Calcidiscus leptoporus, Helicosphaera hyalina*, and *Umbilicosphaera sibogae*. A few reworked *Pseudoemiliania lacunosa* were noticed in some samples taken from this interval.

Pseudoemiliania lacunosa is not an abundant member of the flora above Sample 115-707A-1H-3, 40–42 cm, but it does occur consistently below Sample 115-707A-1H-2, 50–52 cm, indicating the top of Subzone CN14a at this sample.

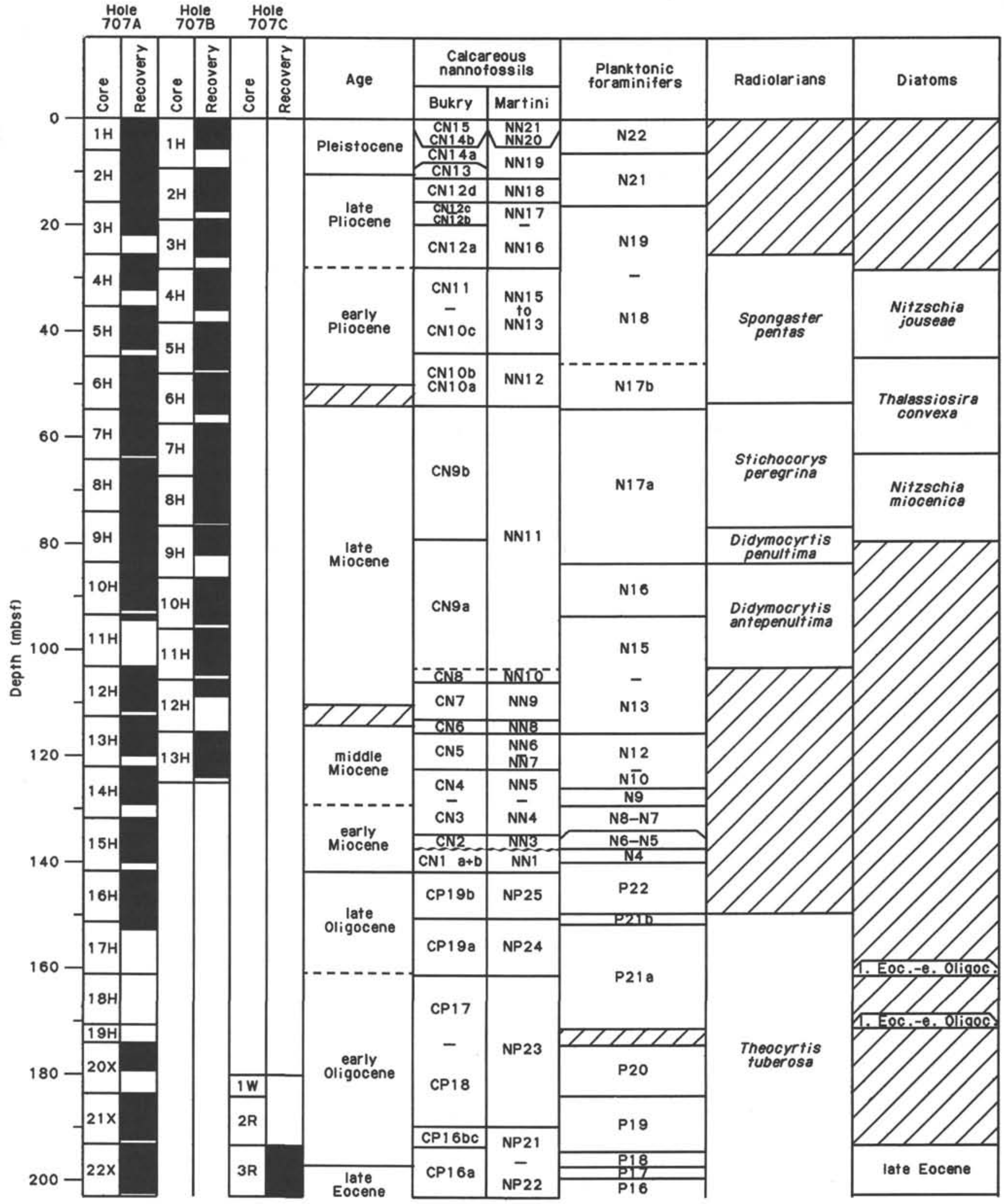

Figure 11. Biostratigraphic summary, Site 707, as based on Holes 707A (0–212.3 mbsf) and 707C (from 212.3 mbsf to basement).

A short interval between Samples 115-707A-1H-4, 10–12 cm, and 115-707A-1H-4, 120–121 cm, is assigned to the small *Gephyrocapsa* Zone of Gartner (1977). We identified the last occurrences (LO) of *Helicosphaera sellii* (1.37 Ma) and *Calcidiscus macintyrei* (1.45 Ma) in Samples 115-707A-2H-1, 45–46 cm, and 115-707A-2H-3, 5–6 cm, respectively.

The FO of *Gephyrocapsa oceanica* was detected in Sample 115-707A-2H-3, 95–96 cm, and the base of Subzone CN14a was placed between this sample and Sample 115-707A-2H-3, 105–106 cm. Rare specimens of *Gephyrocapsa caribbeanica* were noticed in two samples (105–106 cm and 125–126 cm levels) of Section 115-707A-2H-3; thus, these samples are referred to Sub-

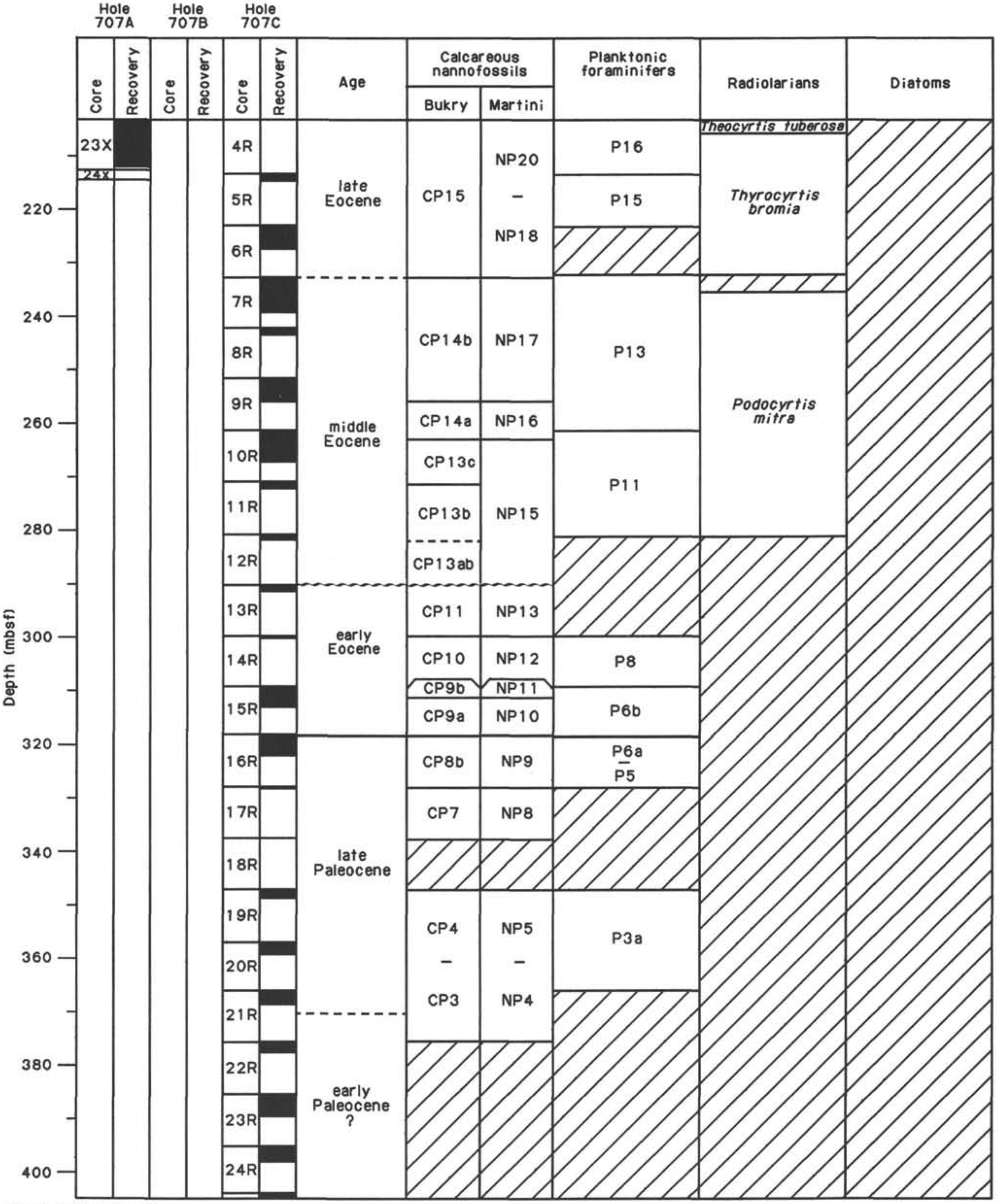

Figure 11 (continued).

zone CN13b. The Pliocene/Pleistocene boundary should be located, therefore, between Samples 115-707A-2H-3, 95–96 cm, and 115-707A-2H-3, 125–126 cm.

Pliocene

Whereas the Pliocene/Pleistocene boundary is well constrained in Hole 707A, the Miocene/Pliocene boundary is difficult to locate. The calcareous nannofossil events which we used to determine the Miocene/Pliocene boundary (4.9 Ma) are the LO of *Discoaster quinqueramus* (5.0 Ma) and the FO of *Ceratolithus acutus*. Because the discoasters are heavily overgrown and ceratoliths are rare in the samples we studied, the events mentioned above are difficult to pinpoint in Hole 707A. A few specimens of *C. acutus* were observed in Sample 115-707A-6H-4, 40 cm, and the last specimens of *D. quinqueramus* have been detected in Sample 115-707A-6H-7, 40 cm. We tentatively located the boundary between the Miocene and the Pliocene, therefore, between these two samples (i.e., between 50.0 and 54.5 mbsf). The Pliocene is thus represented by about 40 m of sediments.

All nannofossil events of the late Pliocene have been recognized. The LOs of *Discoaster brouweri, D. pentaradiatus, D. surculus*, and *D. tamalis* were observed in Sample 115-707A-2H-4, 115 cm, Section 115-707A-2H, CC, and Samples 115-707A-3H-1, 1 cm, and 115-707A-3H-2, 90 cm, respectively. All of the zones of Martini (1971) and the subzones of Zone CN12 of Okada and Bukry (1980) can be determined.

The LO of *Reticulofenestra pseudoumbilica*, which defines the boundary between Zones CN11 and CN12 (or between NN15 and NN16), and which is generally used to approximate the boundary between the lower and upper Pliocene, occurs in Sample 115-707A-4H-2, 30 cm.

The detailed biostratigraphic classification of the lower Pliocene has proven to be more difficult because the LO of *Amaurolithus delicatus* (definition of the NN14/NN15 boundary and of the CN10/CN11 boundary) and the FO of *Discoaster asymmetricus* (NN13/NN14 or CN11a/CN11b boundary) have not been identified. The ceratoliths are poorly represented in the material investigated. *Discoaster asymmetricus*, which occurs in the upper Miocene, is generally rare and its acme is hard to detect. In Sample 115-707A-5H-5, 130 cm, we recorded the first *Ceratolithus rugosus* together with *C. acutus*. These two forms are known to overlap for a short interval (Backman and Shackleton, 1983), so the observed FO of *C. rugosus* (calibrated at about 4.6 Ma) is probably reliable in the investigated section in spite of its rare and scattered distribution. The appearance of *C. rugosus* allows us to recognize the NN12/NN13 (CN10b/CN10c) boundary between Sample 115-707A-5H-5, 130–131 cm, and Section 115-707C-5H, CC.

Miocene

As discussed above, we tentatively located the upper boundary of the Miocene between 54 and 50 mbsf in Hole 707A. The lower boundary of the Miocene is one of the most debated boundaries in the Neogene chronostratigraphic scale. Nannofossil paleontologists generally recognize this boundary in deep-sea sediments by means of the LO of *Dictyococcites bisectus* or of the LO of *Sphenolithus ciperoensis*. These two events are often spaced apart, with the LO of *S. ciperoensis* preceding the LO of *D. bisectus* (Berggren et al., 1985). In Hole 707A, these two events occur simultaneously in the same sample (115-707A-16H-1, 40 cm). Therefore, the Oligocene/Miocene boundary can be placed at about 141 mbsf in the investigated sequence. The total thickness of the Miocene sequence in Hole 707A is represented by about 90 m of sediments. The sedimentation rate is uneven, however, being high during the late Miocene and low in the middle and in the early Miocene.

Within the upper Miocene interval, the FO of *Amaurolithus primus*, defining the boundary between Subzones CN9a and CN9b, has been recognized in Sample 115-707A-9H-3, 130 cm. The base of Zone CN9a (equivalent to the base of NN11) is placed in Section 115-707A-11H, CC. The placement of this boundary is tentative because of the overgrowth problems on *Discoaster quinqueramus* and *D. berggrenii*. The upper Miocene nannofossil assemblages are dominated by discoasters, sphenoliths, and reticulofenestrids. Among the discoasters, *D. neohamatus, D. surculus*, and *D. pentaradiatus* have been confidently identified.

Triquetrorhabdulus rugosus is present in the upper Miocene sequence but is heavily overgrown, and the identification of its LO, which defines the top of Subzone CN10a, again proved difficult. The LO of *Discoaster hamatus*, which defines the CN7/CN8 (NN9/NN10) boundary, has been detected in Sample 115-707A-12H-2, 130 cm. The FO of *D. hamatus*, which defines the CN6/CN7 (NN8/NN9) boundary and is generally used to approximate the middle-late Miocene boundary, occurs in Sample 115-707A-13H-1, 40 cm. Zone CN7, with a calculated duration of 1.1 m.y., is represented in an 8-m-thick interval of sediments. The FO of *Catinaster coalitus*, defining the base of Zone CN6 (NN8), was observed in Sample 115-707A-13H-2, 130 cm.

The LO of *Cyclicargolithus floridanus*, a secondary marker for the lower boundary of Subzone CN5a, was identified in Section 115-707A-13H, CC. The LO of *Sphenolithus heteromorphus*, which defines the base of Zone CN5, was detected in Sample 115-707A-14H-1, 65 cm. Therefore, Zone CN5 (NN6–NN7) is represented by approximately 9 m of sediments.

In the five sections recovered in Core 115-707A-14H, delicate (slender) discoasters are more abundant than robust *Discoaster deflandrei*, thus making possible the assignment of this core to Zone CN4. The large form of *Reticulofenestra pseudoumbilica* (larger than 7 μm), known to occur from the latest part of Zone CN4, was first detected in Sample 115-707A-14H-2, 65–66 cm. The FO of *S. heteromorphus*, defining the CN2/CN3 boundary, was detected in Sample 115-707A-15H-2, 65–66 cm.

We detected the presence of *Sphenolithus belemnos* only in Sample 115-707A-15H-3, 65–66 cm, which was assigned to the lower Miocene Zone CN2. The lower portion of Core 115-707A-15H, between Sample 115-707A-15H-4, 40–41 cm, and Section 115-707A-15H, CC, can be assigned to the lowermost Miocene Zone NN1 (CN1a and CN1b). This observation seems to indicate the presence of a hiatus corresponding to the NN2 (CN1c) interval.

Oligocene

The interval from approximately 141 mbsf to the bottom of the hole (213.3 mbsf) yielded abundant upper Eocene and Oligocene nannofossil assemblages. Although the state of preservation varies from good to moderate, it is generally better than the preservation observed in the Miocene sequence.

We observed the LOs of *Dictyococcites bisectus* and *Sphenolithus distentus* in Samples 115-707A-16H-1, 65–66 cm, and 115-707A-16H-7, 65–66 cm, respectively. Since these two evolutionary events are used to define the upper and lower boundaries of Subzone CP19b, we assigned the upper six sections of Core 115-707A-16H to this uppermost Oligocene subzone. *Sphenolithus ciperoensis*, whose disappearance is another boundary marker for the top of Subzone 19b, occurs throughout the entire interval assigned to this subzone, becoming more abundant in the lower sections. In this upper Oligocene interval, sphenoliths and *Cyclicargolithus floridanus* are abundant, and *Coccolithus pelagicus, Cyclicargolithus abisectus, Discoaster deflandrei, Triquetrorhabdulus carinatus*, and *Zygrhablithus bijugatus* are well represented.

We recognized the FO of *Sphenolithus ciperoensis* in Section 115-707A-17H, CC. The lower three sections of Core 115-707A-16H and all of Core 115-707A-17H were thus assigned to the upper Oligocene Subzone CP19a.

The assignment of Zones CP18–CP16 is difficult because the sequence of events employed for the "standard" zonation of Martini (1971), as well as for that of Okada and Bukry (1980), is somewhat different from the actual sequence observed here. The identification of the FO of *S. distentus* is difficult due to strong recrystallization. The lowest sample in which clearly recognizable specimens occur is Sample 115-707A-20X-2, 65–66 cm.

Sporadic occurrences of rare to few specimens which resemble *S. distentus* were observed in the underlying sediment down to Sample 115-707A-21X-4, 65–66 cm. The LO of *Reticulofenestra umbilica* is also difficult to locate because this species is generally rare in the lower Oligocene sequence and some reworked(?) specimens showed up occasionally in Core 115-707A-21X. The LO of *Ericsonia formosa* was detected in Sample 115-707A-21X-5, 65–66 cm, and the end of the acme interval of *Ericsonia subdisticha* was observed in Sample 115-707A-22X-1, 65–66 cm.

Considering the stratigraphic occurrences mentioned above, the lower Oligocene zones and subzones were tentatively assigned as follows:

CP18–CP17:	Sections 115-707A-18H, CC, to 115-707A-21X-4
CP16c–CP16b:	Sections 115-707A-21X-5 to 115-707A-21X, CC
CP16a:	Sections 115-707A-22X-1 to 115-707A-22X-6

Eocene

The LO of *Discoaster saipanensis*, which defines the boundary between Zones CP15 and CP16, occurs in Sample 115-707A-22X-7, 5 cm. This event is generally used to approximate the Eocene-Oligocene boundary, although it has recently been determined that its LO precedes the true Eocene/Oligocene boundary by approximately 0.5 m.y., and also precedes the extinction of *Hantkenina* by approximately 0.7 m.y. (Nocchi et al., 1986). *Chiasmolithus grandis*, whose disappearance defines the CP14/CP15 boundary, was not detected in the material recovered from this hole.

Hole 707B

We drilled this hole in order to recover a duplicate sequence of the upper Neogene strata retrieved at Hole 707A. Only core-catcher samples were studied, and the results indicate that the sequence recovered from this hole is identical to Hole 707A. The Pliocene/Pleistocene boundary is located within Core 115-707B-2H, and the Miocene/Pliocene boundary within Core 115-707B-6H. The FO of *Amaurolithus* spp., indicative of the latest Miocene, is observed within Section 115-707B-9H, CC. The deepest sample recovered from this hole (Section 115-707B-13H, CC) yields a nannoflora indicative of the lower middle Miocene Zone CN4.

Hole 707C

Oligocene

The sedimentary sequence recovered from this hole yields lower Oligocene to basal upper Paleocene assemblages. Nannofossils are abundant in the sequence above Core 115-707C-16R, but they do become rare in the lower upper Paleocene sediments. The preservation is moderate to good throughout the entire sequence, with nannofossils showing slight evidence of etching coupled with slight to moderate recrystallization.

The first core, 115-707C-1W, recovered no sediment. Approximately 10 cm of sediment was recovered in Core 115-707C-2R. Due to possible contamination, however, we excluded this sample.

Ericsonia formosa and *E. subdisticha* are common in the six sections of Core 115-707C-3R, and Section 115-707C-3R, CC, yielded rare specimens of *Discoaster saipanensis*. Because the LO of *D. saipanensis* marks the top of Zone CP15, all sections of Core 115-707C-3R were assigned to the lowermost Oligocene Subzone CP16a. *Coccolithus pelagicus, Cyclicargolithus floridanus*, and *Dictyococcites bisectus* are abundant species observed in this flora.

Since the CP15/CP16 boundary precedes the Eocene/Oligocene boundary by approximately 0.5 m.y. (see Table 3 in the "Explanatory Notes" chapter, this volume), the latter boundary is assumed to be located within Core 115-707C-3R.

Eocene

The interval between Sections 115-707C-3R, CC, and 115-707C-6R, CC, yields an upper Eocene assemblage assignable to Zone CP15. In addition to the abundant taxa mentioned above, the major species encountered in this sequence are *Bramletteius serraculoides, Calcidiscus kingii, Discoaster barbadiensis, D. saipanensis, D. tanii, Sphenolithus moriformis, S. pseudoradians*, and *Zygrhablithus bijugatus*. *Cribrocentrum reticulatum* does not occur in Section 115-707C-3R, CC, but it is an abundant member of the flora below Sample 115-707C-5R-1, 50–51 cm.

The LO of *Chiasmolithus grandis* was detected in Sample 115-707C-7R-1, 50–51 cm, whereas the LO of *Chiasmolithus solitus* was observed in Section 115-707C-9R, CC. The interval between Sections 115-707C-7R-1 and 115-707C-9R-3 can be assigned, therefore, to the upper Eocene Subzone CP14b. The FO of *Reticulofenestra umbilica* (defined as a form larger than 14 μm) was observed in Sample 115-707C-10R-1, 57–58 cm, and Sections 115-707C-9R, CC, and 115-707C-10R-1 were assigned to Subzone CP14a. In addition to the major species mentioned for the CP15 flora, common occurrences of *Campylosphaera dela* and *Sphenolithus furcatolithoides* characterize the CP14 flora. *Cribrocentrum reticulatum*, although still common in the upper part of CP14, is greatly reduced in abundance in the lower part of the sequence.

We assigned the interval between Sections 115-707C-10R-2 and 115-707C-12R, CC, to the middle Eocene Zone CP13. The LO of *Chiasmolithus gigas* was recognized in Sample 115-707C-11R-1, 50–51 cm. The interval between this sample and Sample 115-709C-12R-1, 30–31 cm, which yielded rare but consistent occurrences of *C. gigas*, was assigned to Subzone CP13b. The interval between Sample 115-707C-10R-2, 62–63 cm, and Section 115-707C-10R, CC, yielded an assemblage which is assigned to Subzone CP13c. Only a few and poorly preserved nannofossils occur in Section 115-707C-12R, CC; a single specimen which resembles *Nannotetrina pappii* was used to place this sample tentatively within Zone CP13. *Cruciplacolithus staurion, Discoaster bifax, Helicosphaera lophota, Pedinocyclus larvalis, Reticulofenestra samodurovii*, and *Sphenolithus radians* are common members characterizing the CP13 flora observed in this hole.

Discoaster sublodoensis was not observed, whereas few to common specimens of *Toweius*? *crassus* were recognized in Sample 115-707C-13R-1, 20–21 cm, and Section 115-707C-13R, CC. Core 115-707C-13R, therefore, was assigned to Zone CP11. Thus, Zone CP12 and possibly a part or all of Subzone CP13a are missing at this site. *Ericsonia formosa* is abundant, and common occurrences of *Discoaster lodoensis, Helicosphaera seminulum, Sphenolithus editus*, and *Toweius*? *gammation* characterize the CP11 flora.

The entire Core 115-707C-14R can be assigned to Zone CP10. *Campylosphaera dela, Coccolithus pelagicus, E. formosa, Toweius pertusus*, and *T. gammation* are abundant; and *Coronocyclus prionion, Cruciplacolithus cribellum, Ellipsolithus macellus, Lophodolithus mochloporus, Neococcolithes dubius, Sphenolithus conspicuus*, and *S. editus* are common in the assemblage of this core.

Sample 115-707C-15R-1, 50–51 cm, yields common *Tribrachiatus orthostylus*, but we did not observe *Discoaster lodoensis*. *Tribrachiatus bramlettei* and *T. contortus* are also absent; therefore, this sample was assigned to the lower Eocene Subzone CP9b. *Discoaster binodosus* and *D. diastypus* are common members of the flora.

The interval between Sample 115-707C-15R-2, 50–51 cm, and Section 115-707C-15R, CC, is referred to the lowermost Eocene

Subzone CP9a. Small forms of the genus *Toweius* dominate the flora, and the absence of previously consistent members of Eocene forms like *D. barbadiensis* is obvious. *Rhomboaster cuspis* is fairly common in some samples, and rare to few *T. bramlettei* occur in the upper portion of this sequence. *Tribrachiatus contortus*, whose FO defines the base of Subzone CP13a, was also observed in this sequence.

Paleocene

The entire portion of Core 115-707C-16R yielded abundant and well-preserved nannofossils assignable to the uppermost Paleocene Subzone CP8b. The nannoflora show a high diversity, and all typical components of this subzone, such as *Campylosphaera eodela, Fasciculithus alanii, Discoaster multiradiatus, Sphenolithus anarrhopus*, and *Rhomboaster calcitrapa* are present in this flora.

Core 115-707C-17R recovered only 9 cm of sediment, containing few moderately preserved nannofossils. The species diversity, however, is fairly high and the assemblage is assigned to the upper Paleocene Zone CP7. In addition to the dominant *Coccolithus pelagicus*, and rare but significant *Discoaster nobilis*, species observed here include *Chiasmolithus consuetus, Chiasmolithus californicus*, large *Cruciplacolithus primus, Cruciplacolithus tenuis, Ellipsolithus macellus, Ericsonia subpertusa, Fasciculithus clinatus, Markalius inversus, Prinsius bisulcus, Prinsius martinii, Sphenolithus anarrhopus*, and *Sphenolithus primus*.

Samples taken from Sections 115-707C-19R, CC, 115-707C-20R, CC, and 115-707C-21R, CC, yielded few and moderately preserved nannofossils. Besides the dominant *Prinsius martinii*, other species include *Cruciplacolithus subrotundus, C. pelagicus, C. primus, Ellipsolithus macellus, Ericsonia subpertusa, Prinsius bisulcus*, and *Toweius*? sp. Primarily because of the presence of *C. subrotundus*, this assemblage was tentatively assigned to the early late Paleocene Zones CP3 or CP4.

After drilling two core lengths of basalt, Section 115-707C-24R-1 recovered yellowish brown sandy silt underlain by a skeletal grainstone. The nannofossils observed in this sandy silt (Sample 115-707C-24R-1, 6 cm) are rare and forms are small. The only species identified are *Prinsius martinii* and small forms resembling *Prinsius bisulcus*. Because of the sketchy evidence, we tentatively identified the age of this sediment (and the age of the volcanism itself) as the late part of Danian (early Paleocene) or the early part of the late Paleocene (Zones CP3–CP4).

Planktonic Foraminifers

Neogene

The Neogene planktonic foraminifer biostratigraphy of Hole 707A is based on data from core catchers for the upper 10 cores and from core catchers and additional samples in the interval between Cores 115-707A-11H and -15H.

In the upper Neogene (Cores 115-707A-1H through -11H), planktonic foraminifers are abundant and well preserved. In the middle to lower Miocene (Cores 115-707A-12H through -15H), they are abundant and moderately well preserved. In the latter interval, small-sized fauna dominate the assemblages, possibly as a result of the dissolution of larger forms. Throughout the section the fauna yield warm-water assemblages typical of tropical areas.

Section 115-707A-1H, CC, is assigned to Pleistocene Zone N22. The assemblage is dominated by *Globorotalia tumida, Neogloboquadrina dutertrei*, and *Globigerinoides sacculifer*. The presence of *Globorotalia tosaensis* indicates an age older than 0.6 Ma. Section 115-707A-2H, CC, is assigned to the upper Pliocene Zone N21 based on the presence of rare *G. tosaensis*. The assemblage is dominated by *Dentoglobigerina altispira, Globorotalia limbata* (right coiling), and *Globigerinoides sacculifer*. Rare *Sphaeroidinellopsis* indicate an age greater than 3.0 Ma. Sections 115-707A-4H, CC, through 115-707A-5H, CC, assigned to the lower Pliocene zonal interval N18–N19, yield assemblages dominated by *G. tumida* (including flexuous forms), *G. limbata* (right coiling), *D. altispira*, and *Sphaeroidinellopsis*.

Sections 115-707A-6H, CC, to 115-707A-9H, CC, are assigned to upper Miocene Zone N17. They contain common *G. limbata, G. plesiotumida*, and *G. sacculifer. Sphaeroidinellopsis* spp. and *D. altispira* fluctuate in abundance, being more common in Sections 115-707A-4H, CC, and 115-707A-5H, CC, and less common in the interval from Sections 115-707A-6H, CC, to 115-707A-8H, CC. The first occurrence of *Pulleniatina primalis* in Section 115-707A-6H, CC, marks the subzonal boundary between N17b and N17a. All the menardiforms from the complex *G. limbata–G. plesiotumida* change coiling direction in Section 115-707A-8H, CC, from right-coiling above to left-coiling below.

Sections 115-707A-10H, CC, and 115-707A-11H, CC, contain a fauna similar to that of Sections 115-707A-6H, CC, through 115-707A-9H, CC, but we assigned these sections to Zone N16 based on the presence of *Neogloboquadrina acostaensis* and the absence of *G. plesiotumida*. The first occurrence of *G. plesiotumida*, however, is not unequivocal here and must be identified more precisely after further investigation. There is a taxonomic ambiguity between the two species *G. plesiotumida* and *G. limbata*, which both occur commonly and change coiling direction simultaneously at the same levels.

A change in fauna occurs in Core 115-707A-12H. Samples in the interval between Cores 115-707A-12H and 115-707A-15H yield an abundant small-sized fauna with few larger forms. This middle to lower Miocene interval is condensed and mixed assemblages were found in a number of samples, especially in Cores 115-707A-14H and -15H. The base of Zone N13 is placed in upper Core 115-707A-13H at the first occurrence of *Sphaeroidinellopsis subdehiscens*, the base of Zone N10 in Section 115-707A-14H-3 at the first occurrence of *Globorotalia peripheroacuta*, the base of Zone N9 in Section 115-707A-14H-4 at the first occurrence of *Orbulina*, and the base of N7 in Section 115-707A-15H-2 at the last occurrence of *Catapsydrax dissimilis*. The occurrence of small-sized *Globorotalia kugleri* in Section 115-707A-15H-5 identifies Zone N4. No true *G. kugleri* (whose first appearance approximates the Oligocene/Miocene boundary) were found below this level.

Paleogene

Paleogene planktonic foraminifers were recovered from Cores 115-707A-16H through -23X and Cores 115-707C-2R through -20R. Samples examined below Section 115-707C-20R, CC, were barren, the foraminifers having been replaced by dolomite. Foraminiferal preservation throughout the section varied from moderately good at a few levels in the Oligocene, to moderately poor in the upper Eocene radiolarian-rich residues, to poor in the lower Eocene and mid to upper Paleocene.

Oligocene

A discontinuous Oligocene section, containing levels in all planktonic foraminiferal biozones except Zone P21b, was recovered in Core 115-707A-16H through Sample 115-707A-22X-3, 121 cm. The moderately well-preserved samples were located in Zones P22 and P21a. Moderately well-preserved faunas from the upper portion of Zone P22 contained high concentrations of the intermediate (250 μm to 149 μm) and fine (149 μm to 63 μm) fractions. Coarse fraction species, such as the large globoquadrinids, were few and fragmented. Most other residues were composed of such solution-resistant species as the globoquadrinids and catapsydracids. This resulted in low foraminiferal diversity, but high dominance.

Criteria for zonal recognition included:

1. Zone P22 (Sample 115-707A-16H-1, 120 cm, through Section 115-707A-16H, CC): very rare *Streptochilus* with *Globoquadrina binaiensis*, but no *Paragloborotalia opima* or *Globorotalia kugleri*.
2. Zone P21a (Section 115-707A-17H, CC): presence of abundant *Streptochilus* together with *P. opima*.
3. Zone P20 (Section 115-707A-18H, CC): abundant *Streptochilus* together with common *Globigerina praebulloides* and infrequent *Globigerina angulisuturalis*, in the absence of *P. opima* as well as the zonal marker, *Globigerina ampliapertura*; the presence of *G. angulisuturalis* locates this section in the upper portion of Zone P20.
4. Zone P19 (Section 115-707A-20X, CC): the co-occurrence of *Globoquadrina sellii* and very rare *Pseudohastigerina naguewichiensis* locates this section in the uppermost levels of Zone P19.
5. Zone P18 (Section 115-707A-21X, CC): presence of *Turborotalia pseudoampliapertura* and *G. ampliapertura* together with *Globigerina tapuriensis*, but no *G. sellii*.

Eocene

The Eocene/Oligocene boundary was located between Samples 115-707A-22X-3, 121 cm, and 115-707A-22X-4, 38 cm, on the basis of the extinction of all hantkeninids. It is possible at this site to confirm the evolutionary event sequence proposed in the Umbrian area of Italy. Following the disappearance of *Cribrohantkenina inflata*, which defines the P16/P17 zonal boundary, all members of the *Turborotalia cerroazulensis* group go extinct well below the extinction of the other hantkeninids, equated to the Eocene/Oligocene boundary. The FO of *Globigerina tapuriensis* immediately below the boundary in Umbria, could not be used here because this species occurred much earlier at this site, in Zone P16. The FO of *G. tapuriensis* in the temperate Umbrian region is apparently delayed, while its FO is located in late Eocene Zone P16 in tropical areas.

Eocene faunas occurred in Hole 707A sediments in Sections 115-707A-22X, CC, and 115-707A-23X, CC, and in Sections 115-707C-3R, CC, through 115-707C-15R, CC, in Hole 707C sediments. Middle and late Eocene coarse fractions were dominated by radiolarians which comprised nearly 90% of several latest Eocene samples. In such sediment the foraminifers were few and badly preserved, and benthic foraminifers were concentrated at the expense of planktonic specimens. Early Eocene faunas were badly recrystallized so that the solution-resistant morozovellids and acarininids were concentrated at the expense of most other forms. Because many Eocene marker species are dissolution resistant, a firm stratigraphy could be determined in this interval.

We recognized the following zones:

1. Zone P17 (Samples 115-707A-22X-4, 38 cm, through 115-707A-22X-4, 121 cm): determined by the presence of *Cribrohantkenina lazzarii*. The uppermost sample, 115-707A-22X-4, 38 cm, represents the topmost portion of Zone P17 after the extinction of *Turborotalia cunialensis*. The top of the zone could not be recognized on the basis of the first appearance of *G. tapuriensis*.
2. Zone P16 (Sample 115-707A-22X-5, 38 cm, through Section 115-707A-23X, CC, and Section 115-707C-3R, CC): determined by the presence of *T. cerroazulensis* and the globigerinathekids, but the absence of *Globigerinatheka semiinvoluta*. The presence of *T. cunialensis* and the rarity of the globigerinathekids places all these samples in the upper portion of Zone P16.
3. Zone P15 (Section 115-707C-5R, CC): identified by the presence of the nominate taxon, *G. semiinvoluta*. Section 115-707C-6R, CC, may also belong in this zone, but the planktonic assemblage was too dissolved for biostratigraphic assignment. The lack of acarininids in the small fauna suggests a late Eocene age.
4. Zone P13 (Sections 115-707C-7R, CC, through 115-707A-9R, CC): identified by the presence of the nominate taxon, *Orbulinoides beckmanni*.
5. Zone P11 (Sections 115-707C-10R, CC, and 115-707C-11R, CC): identified by the overlap of *Morozovella aragonensis, M. lehneri, Acarinina pentacamerata*, and the *Globigerinatheka subconglobata* group.
6. Zone P8 (Section 115-707C-14R, CC): identified by the abundance of the nominate taxon, *Morozovella aragonensis*, together with *M. formosa* and *M. subbotinae*, prior to the first appearance of the globigerinathekids or turborotaliids.
7. Zone P6b (Section 115-707C-15R, CC): identified by the presence of the nominate taxon, *Morozovella subbotinae*, but the absence of *M. edgari* and *M. formosa*.

Paleocene

This incomplete Paleocene sequence is very poorly preserved. Below the late Paleocene, faunas consisted of only three or four barely recognizable juveniles in a matrix of micritized carbonate, echinoid and bryozoan remains, and recrystallized shelf benthic foraminifers. Zonal recognition was based on:

1. Zone P5 (Section 115-707C-16R, CC): abundance of the nominate taxon, *Morozovella velascoensis* and absence of *Planorotalites pseudomenardii*.
2. Zone P3a (Sections 115-707C-19R, CC, and 115-707C-20R, CC): tentatively identified on the basis of some morozovellids with angular chambers, belonging to *Morozovella angulata*.

Benthic Foraminifers

Benthic foraminifers were recovered in all core catchers from Hole 707A and in core catchers from the first 21 cores in Hole 707C. Benthic foraminifers were infrequent in most Neogene samples, rare in earliest Miocene levels (Section 115-707A-14H, CC), and frequent as dissolution concentrations in early Oligocene Zone P18 (Section 115-707A-21X, CC) and late Eocene Zone P15 (Sections 115-707C-5R, CC, and 115-707C-6R, CC). Below the late Eocene (Sections 115-707C-7R, CC, through 115-707C-21R, CC), benthic foraminifers were rare and poorly preserved.

Pleistocene

Only a few specimens were found in the rich carbonate oozes in Section 115-707A-1H, CC. The species such as *Planulina wuellerstorfi, Uvigerina auberiana*, and *Globocassidulina subglobosa* are cosmopolitan. The intermediate size of *G. subglobosa* and the presence of *Planulina ariminensis* suggest intermediate-water depths.

Pliocene

Pliocene benthic faunas (Sections 115-707A-2H, CC, through 115-707A-5H, CC) are composed of a large cosmopolitan element and numerous species (*Textularia lythostrota, Uvigerina proboscidea, U. hispida, Osangularia bengalensis, Stilostomella insecta, Cibicidoides cicatricosus*) originally named from Car Nicobar. This Car Nicobar fauna occurs in numerous low-latitude, mid-depth localities and can be used as an index for intermediate-water depths and subtropical waters.

The species *Uvigerina hispida* occurs only in Section 115-707A-5H, CC. This taxon is usually associated with enhanced production and sediment accumulation rates at mid-depth locations. The first occurrence of *Uvigerina hispidocostata* (Section 115-707A-2H, CC) is the result of the benthic shoaling event which occurred in the late Gauss of the Indo-Pacific.

Miocene

Miocene benthic faunas (Sections 115-707A-6H, CC, through 115-707A-15H, CC) are divisible into three main types. The middle middle through late Miocene cosmopolitan fauna characterized by high diversity and large-sized individuals first occurs in Section 115-707A-11H, CC, probably associated with the development of the middle Miocene glacial event. This fauna contains a number of planulinids (*Planulina lucida, P. wuellerstorfi*, and *P. marialana*), some buliminids (*Bulimina tuxpamensis* and *B. consanguinea*), and *Globocassidulina subglobosa*.

The FO of true *P. wuellerstorfi* and the extinction of *B. tuxpamensis* in Section 115-707A-11H, CC, represent the true FO's and LO's of these species. A small number of hispid uvigerinids are present, but all other uvigerinids are rare to absent. The hispid group is usually associated with oxidizing conditions at the bottom in an area of low sediment accumulation rates. Incursions of uvigerinids in this fauna are periodic and, in other areas of the Indo-Pacific, can be correlated with glacials and with the enhanced sediment accumulation found during the Pacific late Miocene low-oxygen episode.

The late early to middle middle Miocene, low-diversity faunas (Sections 115-707A-12H, CC, and 115-707A-13H, CC) are dominated by the *Planulina marialana* group, but they are low in numbers of benthic specimens. The *P. marialana* group predominates also at intermediate depths on the Ninetyeast Ridge. Present in these faunas are the apparent predecessors of several middle Miocene forms, such as *Osangularia* trans. *bengalensis, Planulina* trans. *wuellerstorfi*, and *Textularia* trans. *lythostrota*. These ancestral types occur in the early Miocene of other Indo-Pacific low-latitude sites such as Site 588 in the Coral Sea.

A depauperate early Miocene fauna (Sections 115-707A-14H, CC, and 115-707A-15H, CC) is associated with extensive sediment dissolution and the removal of coarse-fraction planktonic foraminifers. The very small and rare specimens in this sediment include *Pullenia bulloides, Globocassidulina subglobosa, Orthomorphina rohri*, and *Uvigerina subproboscidea*. The fact that coeval, depauperate faunas of this age have also been found on the Walvis Ridge, the Lord Howe Rise, and the Rio Grande Rise at intermediate depth sites suggests that this is an oceanwide, mid-depth event in the early Miocene.

Oligocene

Oligocene faunas recovered in Sections 115-707A-16H, CC, through 115-707A-21X, CC, are moderately well preserved but relatively low in diversity and numbers of specimens per species. These faunas differ from those of the Miocene by the presence of *Discorbis subvillardeboanus, Cibicidoides subspiratus, Bolivinopsis cubensis, Rotaliatina mexicana, Cassidulina crassa, Hanzawaia cushmani*, an unnamed strio-costate buliminid typical of Atlantic upper deep-water sites of the latest Eocene and Oligocene, and *Uvigerina ongleyi*.

Unlike the Oligocene faunas of Site 706, morphotypes of Atlantic rather than Mediterranean origin predominate at Site 707. This suggests a greater affinity with Atlantic and Caribbean intermediate waters. A somewhat deeper intermediate-water depth is also suggested by the presence of *U. ongleyi* and *D. subvillardeboanus*, which rarely occur in deep-water sites, and by the lack of lenticulinids, which occur at and above intermediate depths.

Site 707 is assigned to slightly greater paleodepths than Site 706 (600–1000 m) because of the co-occurrence of middle bathyal species with a large cosmopolitan deep-water element typical of the Barbados fauna. This includes *Pleurostomella subcylindrica, Stilostomella abyssorum, Bulimina tuxpamensis*, common costate buliminids, dentalinids, and pleurostomellids inter alia. An Oligocene paleodepth from 1,500 to 2,000 m is estimated.

As at Site 706, the typical Eocene form *Plectofrondicularia lirata* occurs well up into the Oligocene (Section 115-707A-20X, CC, of uppermost Zone P19 age). This represents a new LO for this species, the disappearance of which is apparently diachronous between the Atlantic and Indian Oceans. Because *P. lirata* is constrained to intermediate and shallower sites, its presence further corroborates an assignment of intermediate paleodepths to Site 707 in the Oligocene.

Eocene

Benthic foraminifers are rarely common in Eocene samples, either in the radiolarian oozes of the late Eocene (Sections 115-707A-22X, CC, and 115-707A-23X, CC; Sections 115-707C-3R, CC through 115-707C-7R, CC) or the recrystallized carbonates of the middle and early Eocene (Sections 115-707C-8R, CC, through 115-707C-15R, CC). Most faunas are dominated by *Nuttalides truempyi, Oridorsalis umbonatus*, and *Bulimina semicostata*, with accessory stilostomellids and a few cibicidids.

The admittedly poor faunas contain species typical of intermediate depths; *N. truempyi* is large, also a feature of intermediate depth sites. Upon going downhole, a number of upper bathyal elements appear in Section 115-707C-15R, CC, suggesting that the site is shoaling. Because of the paucity of benthic foraminifers, a good paleodepth estimate is difficult; middle bathyal depths (600–1000 m) are tentatively estimated.

A major benthic boundary is encountered in middle Eocene Zone P11 (Sections 115-707C-10R, CC, and 115-707C-11R, CC) when benthic specimens become large for the first time in the Eocene and remain relatively large throughout its remainder. Uvigerinids also occur for the first time in this zone. Improved preservation of Zone P11 sediments can account for higher diversity but not for the individual size increase. In the world ocean, middle Eocene Zone P11 represents a time of cooling at the bottom (eutrophication) and invigorated circulation and upwelling associated with an expanded oxygen minimum zone. This Zone P11 benthic fauna may be the middle Eocene analog of the larger, more diverse benthic faunas found at the middle Miocene glacial.

Paleocene

Despite the very poor preservation of all Paleocene foraminiferal faunas, substantial shoaling of the site from middle bathyal to shelf depths can be documented. This shoaling occurred between late Paleocene Zone P5 (Section 115-707C-16R, CC) and earliest late Paleocene Zone P3a (Section 115-707C-19R, CC) when only small rotalid benthic foraminifers characteristic of inner shelf depths are found.

Radiolarians

Samples were prepared and examined for radiolarians in four samples per core from Holes 707A and 707C. No samples were examined from Hole 707B, since this hole exactly duplicates the stratigraphic interval recovered at Hole 707A.

Hole 707A

Sections 115-707A-1H, CC, through 115-707A-3H, CC, are barren of identifiable radiolarian taxa. Sponge spicules are abundant; the only radiolarians observed are poorly preserved fragments of collosphaerids.

Samples 115-707A-4H-2, 101 cm, through 115-707A-6H-6, 101 cm, belong to the *Spongaster pentas* Zone of early Pliocene age. Diagnostic taxa include *Phormostichoartus doliolum, P. fistula, Anthocyrtidium michelinae, A. jenghisi, A. prolatum*, and *Lychnodictyum audax*.

We assigned Section 115-707A-6H, CC, through Sample 115-707A-9H-2, 101 cm, to the *Stichocorys peregrina* Zone of late Miocene age. Diagnostic taxa include *Solenosphaera omnitubus, Didymocyrtis penultima, Anthocyrtidium michelinae*, and *A. pliocenica*.

Sample 115-707A-9H-4, 101 cm, through Section 115-707A-9H, CC, belong to the *Didymocyrtis penultima* Zone of late Miocene age. Diagnostic taxa include *Stichocorys delmontensis, Didymocyrtis penultima, D. prismatica*, and *Dendrospyris bursa*.

Sample 115-707A-10H-2, 101 cm, through Section 115-707A-11H, CC, belong to the *Didymocyrtis antepenultima* Zone of late Miocene age. Diagnostic taxa include *Diartus hughesi, Didymocyrtis antepenultima*, and *D. prismatica*.

Section 115-707A-12H, CC, through Sample 115-707A-16H-6, 101-103 cm, are barren of radiolarians. Sponge spicules and zeolite crystals are common in some of the samples within this interval.

Section 115-707A-16H, CC, through Sample 115-707A-23X-2, 101 cm, belong to the *Theocyrtis tuberosa* Zone of early Oligocene age. Preservation of specimens is poor at the top of this interval and improves downward. Diagnostic taxa include *Theocyrtis tuberosa, Artophormis gracilis, Lithocyclia angusta, Didymocyrtis prismatica*, and *Dorcadospyris triceros*. Scattered specimens of apparently upper Eocene forms (e.g., *Carpocanistrum azyx* and *Thyrsocyrtis bromia*) may be reworked or may indicate nonsynchroneity between the Indian Ocean datum levels and corresponding radiolarian events in the equatorial Pacific (Sanfilippo et al., 1985).

Sample 115-707A-23X-4, 101 cm, through Section 115-707A-23X, CC, belong to the *Thyrsocyrtis bromia* Zone of late Eocene age. Taxa present which are diagnostic of this zone include *Thyrsocyrtis bromia, T. tetracantha, Dictyoprora mongolfieri, Calocyclas turris, Eusyringium fistuligerum*, and *Cryptoprora ornata*. The Eocene/Oligocene boundary corresponds approximately with, or may lie slightly below, the top of the *T. bromia* Zone.

Hole 707C

Section 115-707C-3R, CC, lies approximately at the boundary between the *T. tuberosa* and the *T. bromia* Zones. The presence of *Lithocyclia angusta* and *Artophormis gracilis* suggests the *T. tuberosa* Zone. However, common specimens of *Sethochytris babylonis, Dictyoprora armadillo*, and *Cryptoprora ornata* suggest the uppermost *T. bromia* Zone. More detailed study of closely spaced samples will be required to resolve this uncertainty. However, the relatively poor core recovery in Cores 115-707C-2R through -5R precludes a detailed analysis of the Eocene/Oligocene boundary transition in Hole 707C.

Sections 115-707C-5R, CC, through 115-707C-6R, CC, lie within the *Thyrsocyrtis bromia* zone of late Eocene age. Diagnostic taxa include *T. bromia, Calocyclas turris, Thyrsocyrtis tetracantha, Dictyoprora mongolfieri, Carpocanistrum azyx*, and *Lithocyclia aristotelis*.

Sample 115-707C-7R-2, 78 cm, through Section 115-707C-11R, CC, belong to the *Podocyrtis mitra* Zone of middle Eocene age. Diagnostic taxa include *P. mitra, P. trachodes, P. helenae, Lithocyclia ocellus, Thyrsocyrtis triacantha, T. rhizodon, Lithochytris vespertilio, Calocyclas hispida*, and *Dictyoprora mongolfieri*.

All samples between Section 115-707C-13R, CC, and the bottom of the hole (Core 115-707C-28R, 443.2 mbsf) are barren of identifiable radiolarians.

Diatoms

Diatoms have a restricted stratigraphic occurrence in the core-catcher samples from the three holes of Site 707. Their occurrence is consistent in the lower Pliocene–upper Miocene sections of Holes 707A and 707B, and they are scattered throughout the Paleogene intervals of Holes 707A and 707C.

Neogene

The abundance of diatoms in the lower Pliocene–upper Miocene sections of Holes 707A and 707B is generally fairly low, and they are fragmented and moderately preserved. The Neogene assemblages yield a fair amount of radiolarians and sponge spicules in addition to diatoms.

Of the diatom-bearing core-catcher samples from Hole 707A, Sections 115-707A-4H, CC, and 115-707A-5H, CC, are referred to the *Nitzschia jouseae* Zone based on the presence of *N. jouseae*. The poorly preserved assemblages in Section 115-707A-6H, CC, are placed in the *Thalassiosira convexa* Zone based on the occurrence of *Thalassiosira miocenica* and *Nitzschia cylindrica*. We placed Sections 115-707A-7H, CC, and 115-707A-8H, CC, in the *Nitzschia miocenica* Zone, based on the occurrence of *Thalassiosira praeconvexa*.

Of the diatom-bearing samples from Hole 707B, Sections 115-707B-4H, CC, and 115-707B-5H, CC, represent the *N. jouseae* Zone in which *T. convexa* var. *aspinosa* is present, but *Rhizosolenia praebergonii* is lacking. The poorly preserved assemblages in Sections 115-707B-6H, CC, and 115-707B-7H, CC, are placed in the *T. convexa* Zone. Age-diagnostic species include *T. convexa* var. *aspinosa* and *T. miocenica*. Section 115-707B-8H, CC, is referred to the *N. miocenica* Zone based on the occurrence of *Nitzschia reinholdii, N. porterei*, and *N. miocenica*.

Paleogene

Sections 115-707A-17H, CC, and 115-707A-18H, CC, provide very poorly preserved diatom assemblages that include a fair amount of fresh-water specimens from the genera *Grammatophora* sp. and *Biddulphia* sp. of late Eocene or early Oligocene age. The sporadic and poorly preserved diatoms in Sections 115-707A-22X, CC, and 115-707C-3R, CC, are presumably of late Eocene age, and those in Section 115-707C-9R, CC, of middle Eocene age.

PALEOMAGNETICS

Introduction

The quality of the paleomagnetic data produced from Site 707 ranges from poor (from the sediments) to excellent (from the basalts), with little between these two extremes. Since the paleomagnetic results from the sediments proved to be unreliable, our discussion of these data will be brief. In contrast, the basement rocks appear well behaved and their paleomagnetic results are described in more detail.

Results

Cores 115-707A-1H through -15H were measured using the pass-through magnetometer. These measurements almost invariably showed that the intensity of magnetization is quite high at the top of each core and decreases with increasing depth in the core. A typical example of this behavior is shown in Figure 12. The decrease in intensity between the top and bottom sections was typically 2–3 orders of magnitude, with the larger magnetization values tending to correspond with what appears to be rust contamination in the section. Discrete samples obtained from Hole 707A displayed low magnetic moments (the NRM intensity of 7-cm^3 samples was typically 0.02×10^{-4} emu or less).

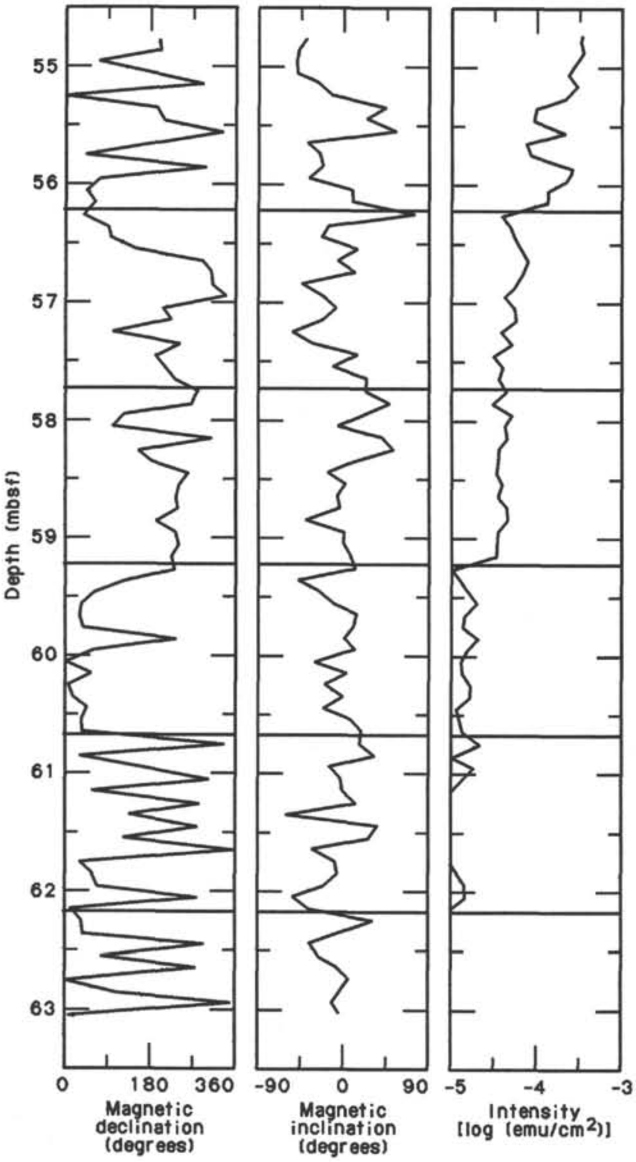

Figure 12. Pass-through magnetometer record from Core 115-707A-7H after demagnetization at 5 mT. Declination is given in core coordinates. Horizontal lines indicate section breaks.

We could not measure these samples reliably with the shipboard magnetometers, and as of yet we have not undertaken any further analysis of them.

Among the sediments analyzed, only the glauconitic sediments recovered in Cores 115-707C-15R and -16R produced reliable paleomagnetic directions. Unfortunately, the recovery rate in these two cores was poor, so relatively little material was sampled. Pass-through measurement of these cores gave erratic results; however, progressive alternating field (AF) demagnetization of four discrete samples appeared to give stable directions (Fig. 13). The magnetic moment of these glauconitic samples is relatively low, so the data are of limited quality. Nevertheless, three of the samples gave results which appear to show a stable component of remanence. This component has a positive inclination in Samples 115-707C-15R-1, 69–71 cm, and 115-707C-16R-1, 112–114 cm, while the intermediate sample (115-707C-15R-2, 56–58 cm) shows a negative inclination.

The basalt cores (115-707C-22R to -28R) recovered material from five petrologic units. The basalt pieces were often sufficiently well oriented so that pass-through measurements were possible. Nearly all the basalt sections were measured with the pass-through magnetometer (Fig. 14) before and after 9-mT AF demagnetization. This method often showed a consistent direction of magnetization over segments of 1 m in length (e.g., Section 115-707C-26R-3 as shown in Fig. 14). These particularly stable intervals indicate a paleomagnetic inclination between 25° and 50°. In addition, 30 discrete basalt samples were subjected to progressive AF demagnetization, and 26 to thermal demagnetization; these results are given in Tables 2 and 3. In general, AF demagnetization revealed one stable component of magnetization, while the thermal treatment often showed two components. Nevertheless, the high blocking temperature component was readily isolated. The average inclination of the high temperature/coercivity component from the five units is 43.2° (SD = 3.7°).

Discussion

The intensity pattern which emerged from our measurements on the sedimentary sections confirmed what is apparent visually and from susceptibility measurements: each core was contaminated with rust particles, the amount of contamination being greatest near the top of each core. Though the lowermost (i.e., most rust-free) sections generally show negative inclinations, we hesitated to interpret these directions in terms of magnetic polarity.

Because most of the sediments recovered at Site 707 were very light-colored, one could easily see the ubiquitous contamination. However, it was difficult to determine whether the contamination is disseminated throughout or restricted only to the surface of the cores.

Three glauconitic sediment samples which gave stable directions suggest that multiple polarity intervals may have been sampled in Cores 115-707C-15R and -16R. Given so few data points, however, a correlation with the magnetic polarity time scale can only be speculative.

With the basalt results, a comparison of the discrete measurements with the whole-core measurements showed a discrepancy between the directions measured with these two different methods. The difference in measured inclination may be on the order of 10°–20°; thus, it appears that the pass-through method gave only a general indication of direction. It did, however, show the consistently reversed polarity of the flows.

Measurements from the discrete basalt samples provided inclinations from each of the identified flows; however, the small scatter in these results (as we can see from Tables 2 and 3) suggests that the time between the emplacement of the various units may not have been adequate to allow the proper averaging of secular variation of the geomagnetic field.

The average inclination obtained from the basalt samples computed with the maximum likelihood technique is 43.3° (N = 5, kappa = 205.2, alpha 95 = 4.9°) and corresponds to a paleolatitude of 25.2° ± 3.8°. The average value may be revised if further geochemical work reveals new divisions in the five lithologic units. Thus, we regard the paleolatitude estimate as tentative, since the unit definitions may be revised and the averaging of secular variation may be inadequate.

Magnetic Susceptibility

Whole-core measurements of low-frequency (0.47 kHz) magnetic susceptibility were made on all sections of cores recovered from Hole 707A. Measurements were made with a Bartington Susceptibility Meter (Model MS1) and whole-core, pass-through sensor coil of 80-mm inner diameter (Model MSC2). Susceptibility was measured at varying intervals in Hole 707A (3 cm, 5 cm, or 6 cm), depending on the degree of disturbance and lith-

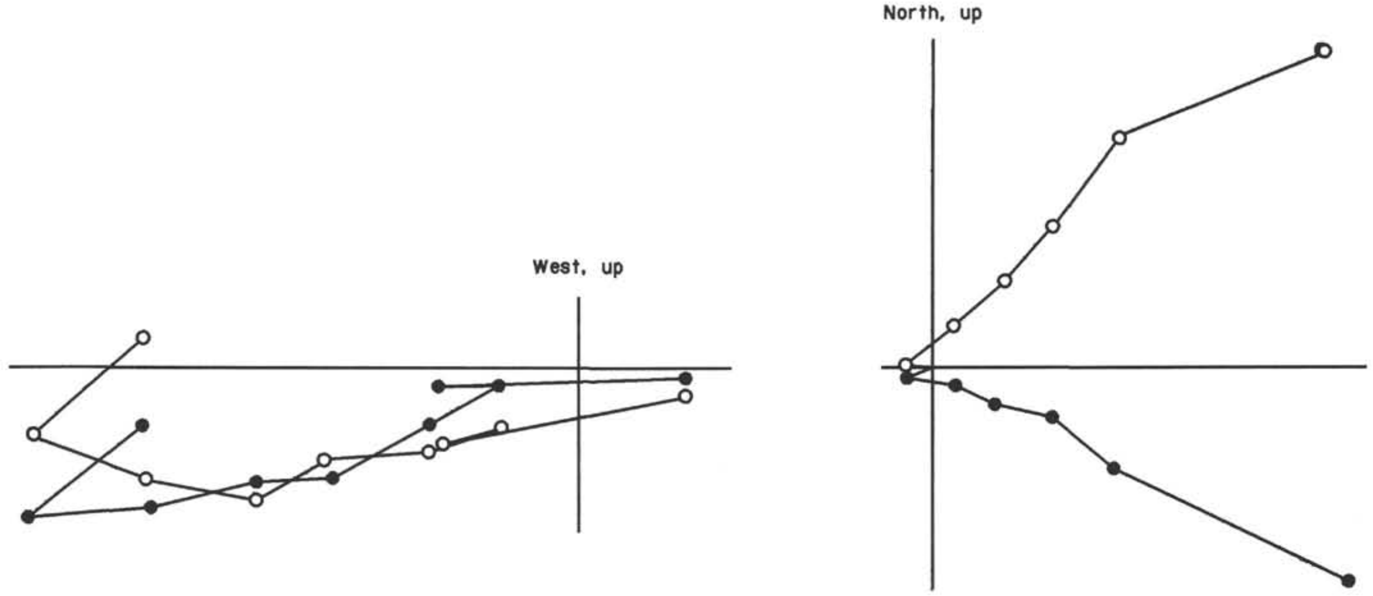

Sample 115-707C-15R-1, 69-71 cm

Sample 115-707C-15R-2, 56-58 cm

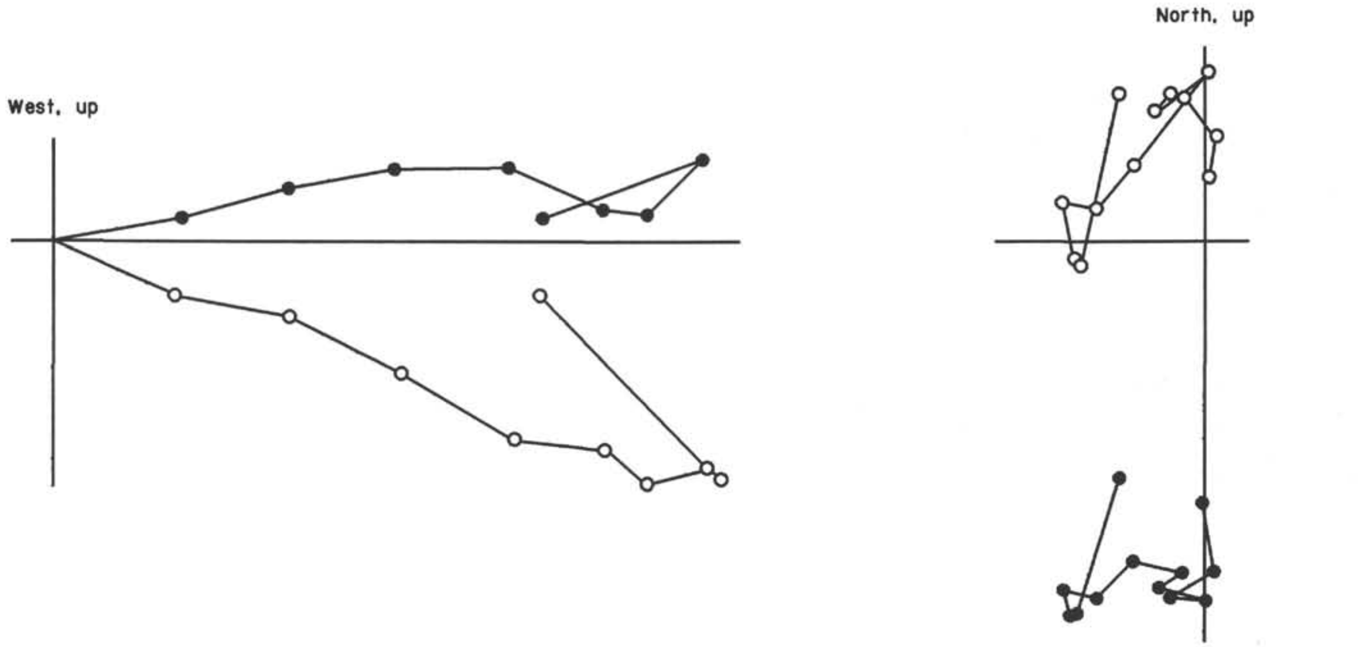

Sample 115-707C-16R-1, 112-114 cm

Sample 115-707C-16R-2, 112-114 cm

Figure 13. Zijderveld orthogonal projection diagrams of glauconitic sediment samples subjected to alternating-field (AF) demagnetization. Open points represent projection in the vertical plane; closed points, in the horizontal plane.

ologic homogeneity of the cores, but no measurements were made on core material from Holes 707B and 707C.

Magnetic susceptibility measurements provide an indication of the concentration of magnetizable material in the sediment, which not only includes magnetic (NRM-carrying) minerals but also a large proportion of the lithogenous fraction of the sediment (see "Explanatory Notes" and "Paleomagnetics" section, "Sites 705 and 706" chapter, this volume). Magnetic susceptibility is very much more sensitive, however, to the presence of ferrous metal contaminants in the sediment, such as particles of pipe rust or related artifacts of drilling disturbance.

Figures 15–17 show the results of whole-core susceptibility measurements made at Site 707. The susceptibility profile of Hole 707A (Fig. 15) displays a series of regularly spaced, asymmetric peaks of similar amplitude (around 20 × 10^{-6} cgs), plus some of greater amplitude (up to around 85 × 10^{-6} cgs), each consisting of a number of subsidiary or "parasitic" peaks of decreasing amplitude downhole. These asymmetric clusters of peaks are all superimposed on "background" fluctuations in susceptibility values which are of extremely low amplitude, that is, between 1 × 10^{-7} and 2 × 10^{-6} cgs, from 0 to 140 mbsf, but rising slightly to around 2.5 to 5 × 10^{-6} cgs below 140 mbsf.

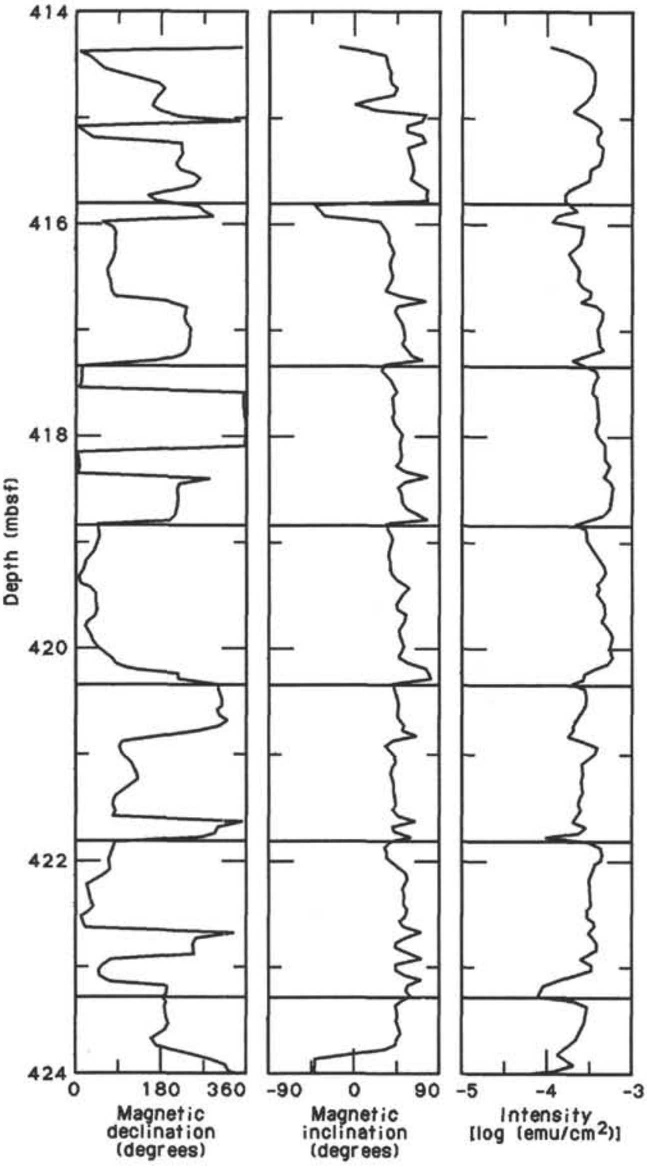

Figure 14. Pass-through magnetometer record from basalt Core 115-707C-26R after a demagnetization treatment of 9 mT. Conventions as in Figure 12.

Table 2. Directions of primary component of magnetization in basalt samples from Site 707 as determined with principal component analysis after alternating-field (AF) demagnetization.

Sample interval (cm)	Number of samples	MAD	Inclination (degrees)	Intensity (A/m)	Hard rock unit
115-707C-					
22R-1, 62–64 (Piece 10A)	5	2.1	53.6	0.094	1
22R-2, 40–42 (Piece 2)	4	0.9	46.9	0.567	1
23R-1, 44–46 (Piece 1G)	9	2.2	42.0	0.104	2
23R-1, 133–135 (Piece 1Q)	3	0.6	43.5	0.101	3
23R-2, 58–60 (Piece 1E)	6	5.6	44.9	0.130	3
23R-3, 69–71 (Piece 1E)	9	2.2	43.5	0.095	3
23R-4, 4–6 (Piece 1A)	4	2.8	45.8	0.130	3
24R-2, 86–88 (Piece 15)	4	2.8	48.6	0.313	3
24R-3, 108–110 (Piece 7)	6	1.8	38.4	3.668	4
25R-1, 124–126 (Piece 1J)	6	1.2	38.8	3.958	4
25R-2, 67–69 (Piece 1F)	4	0.5	39.6	2.694	4
25R-3, 63–65 (Piece 1H)	6	1.0	39.1	2.212	4
25R-4, 50–52 (Piece 1G)	5	2.6	39.3	3.280	4
25R-5, 118–120 (Piece 1N)	6	1.7	41.1	3.023	4
26R-1, 94–96 (Piece 1P)	5	1.4	48.7	2.048	4
26R-2, 50–52 (Piece 1D)	3	2.6	43.9	4.107	4
26R-3, 50–52 (Piece 1F)	7	2.0	47.2	1.527	4
26R-4, 113–115 (Piece 1H)	3	1.3	44.7	2.171	4
26R-5, 90–92 (Piece 1M)	5	2.9	42.6	2.154	4
26R-6, 84–86 (Piece 1I)	6	2.4	47.3	3.278	4
26R-7, 69–71 (Piece 1G)	5	3.4	47.0	6.993	4
27R-1, 88–90 (Piece 4G)	6	1.9	42.7	3.588	4
27R-2, 86–88 (Piece 5D)	5	2.4	40.7	1.879	4
27R-3, 80–82 (Piece 4A)	6	1.3	43.0	2.780	4
27R-6, 11–13 (Piece 1B)	6	2.6	38.8	4.304	4
27R-7, 49–51 (Piece 9)	6	1.3	43.3	3.637	4
28R-1, 137–139 (Piece 16)	7	0.9	49.7	4.050	5
28R-3, 104–107 (Piece 10)	4	0.9	40.1	5.427	5
28R-4, 37–39 (Piece 4)	4	2.1	43.3	3.293	5
28R-4, 80–83 (Piece 9C)	7	0.8	41.5	7.336	5

Note: MAD = mean angular deviation of fit.

Table 3. Directions of primary component of magnetization in basalt samples from Site 707 as determined with principal component analysis after thermal demagnetization.

Sample interval (cm)	Number of samples	MAD	Inclination (degrees)	Intensity (A/m)	Hard rock unit
115-707C-					
23R-3, 111–113 (Piece 1G)	2	0	37.9	0.655	3
23R-4, 39–42 (Piece 1C)	5	0.9	26.0	0.913	3
24R-2, 36–38 (Piece 8)	3	5.5	36.9	2.319	4
24R-2, 126–128 (Piece 17D)	3	1.5	39.2	4.971	4
24R-3, 76–78 (Piece 5)	4	1.3	39.0	3.170	4
25R-1, 68–70 (Piece 1F)	9	2.9	43.9	2.948	4
25R-2, 18–20 (Piece 1C)	4	3.5	43.2	3.355	4
25R-3, 113–115 (Piece 1M)	5	3.0	38.4	4.035	4
25R-4, 112–114 (Piece 1Q)	4	2.0	34.7	3.740	4
25R-5, 89–91 (Piece 1K)	3	4.1	43.2	1.329	4
26R-1, 106–108 (Piece 15)	3	3.1	40.0	2.048	4
26R-2, 126–128 (Piece 1O)	3	2.5	33.6	3.922	4
26R-3, 129–131 (Piece 1L)	6	3.8	35.5	4.835	4
26R-4, 84–86 (Piece 1F)	5	3.3	58.8	2.775	4
26R-5, 143–145 (Piece 1U)	5	8.0	44.6	3.363	4
26R-6, 105–107 (Piece 1J)	7	13.6	31.8	3.094	4
26R-7, 10–12 (Piece 1A)	6	14.6	36.4	2.329	4
27R-1, 132–134 (Piece 4O)	6	8.3	52.4	1.697	4
27R-2, 130–132 (Piece 7D)	4	8.7	33.4	1.804	4
27R-3, 40–42 (Piece 2B)	3	4.0	45.8	2.992	4
27R-4, 40–42 (Piece 2)	5	7.6	21.7	5.273	4
27R-5, 85–87 (Piece 9A)	6	5.4	26.7	6.678	4
27R-6, 37–39 (Piece 3A)	3	6.9	39.2	2.937	4
27R-7, 73–75 (Piece 14)	4	2.8	29.3	1.989	4
28R-2, 72–74 (Piece 7)	3	0.8	40.4	7.547	5
28R-3, 126–128 (Piece 11)	5	1.2	41.4	7.229	5

Note: MAD = mean angular deviation of fit.

The abrupt increase in background values of susceptibility at approximately 140 mbsf corresponds to (1) a small change in sediment color, from white to light gray; (2) greater clarity with which bioturbation features can be discerned; and (3) an overall trend toward lower carbonate content in the sediment below this point in the sequence (see core photographs and barrel sheet lithologic descriptions of Cores 115-707A-15H and -16H and "Geochemistry" section, this chapter). These attributes suggest that an increase in the proportion of lithogenous material in the sediment occurs below a depth of 140 mbsf. Most or all of the remaining features of the susceptibility profile of Hole 707A, however, are unrelated to natural changes in sediment composition and result from contamination of the cores by drilling artifacts.

Individual particles of pipe rust, as long as 5 mm, were clearly visible through the plastic core liner in Sections 1 and 2, and sometimes also Section 3, of each core. More significantly, an examination of split-core sections revealed that several fragments of pipe rust and, in some cores, a much larger number of

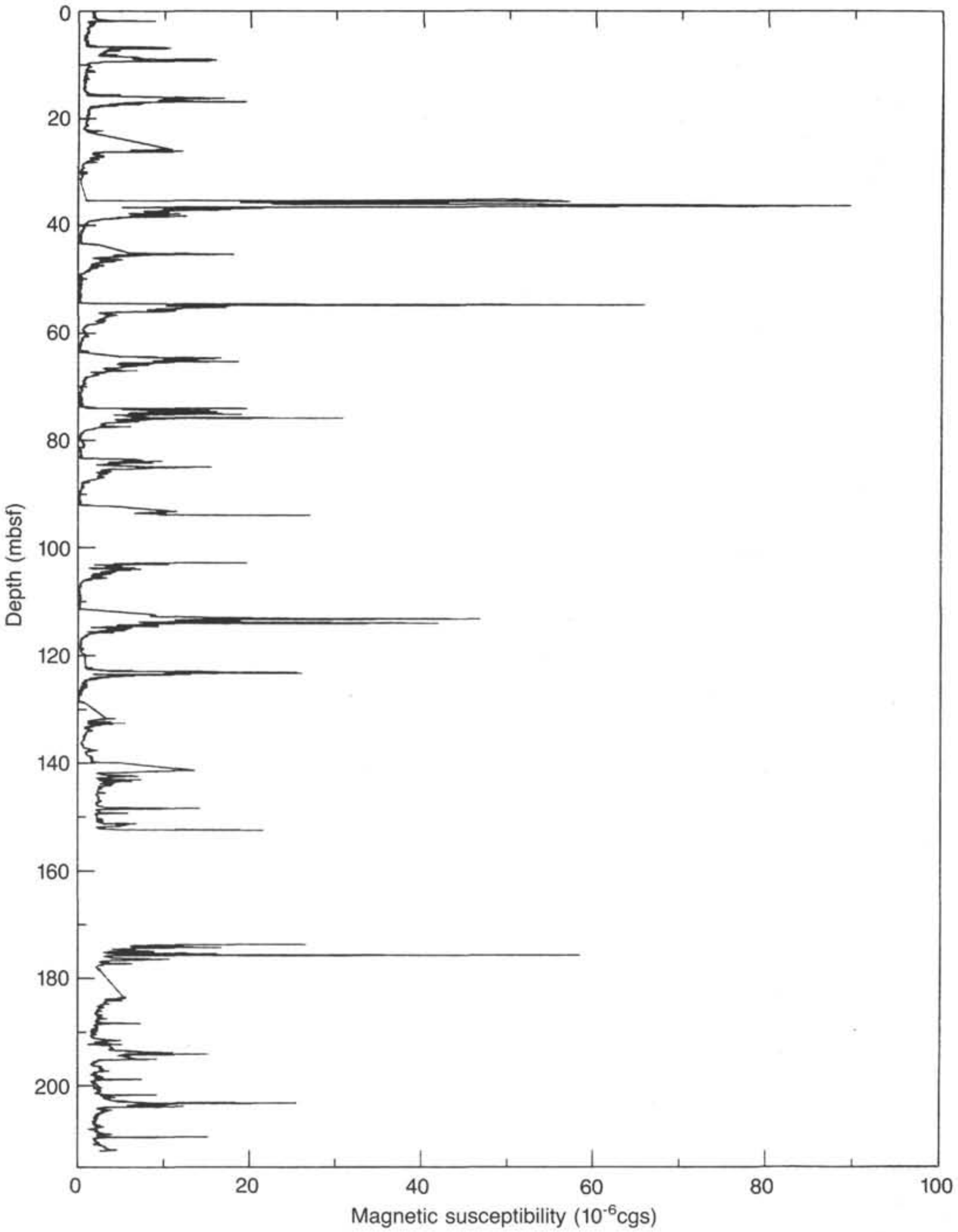

Figure 15. Whole-core magnetic susceptibility profile of Hole 707A.

finely divided, unoxidized ferrous metal particles were disseminated throughout Section 1 and occasionally at the top of Section 2 of each core. Freshly abraded particles of drill pipe or bit, resembling iron filings, were particularly noticeable in Section 115-707A-5H-1 and are responsible for the very large peak in the susceptibility profile of Hole 707A at 35–40 mbsf (Fig. 15). Below Section 1, and the uppermost horizons of Section 2 in some cores, particles of pipe rust were apparent only at the interface between the exterior of the core and the core liner. This suggests that pervasive contamination by drilling artifacts is generally restricted to the uppermost section(s) of each core, and below this the presence of contaminants is related to sediment smearing inside the core liner, which occurs during penetration of the core barrel.

The regular spacing of the asymmetric peaks in the susceptibility profile of Hole 707A corresponds exactly to that of individual cored intervals of the sequence (Fig. 16). The apex of each of the asymmetric peaks occurs, almost invariably, in Section 1 of each core and usually near the top of the section. Subsequent peaks in the susceptibility profile of individual cored intervals are then superimposed on a gradual decline in susceptibility values with depth in core—the diminution often spanning a depth in core between one-third and one-half of its total length—before reaching "background" levels again. Clearly, within each interval cored, the overall trend in susceptibility values is related to a single event or process. Similarly, all of the asymmetric peaks, or clusters of related peaks, in the susceptibility profile of the entire hole must surely be the result of the

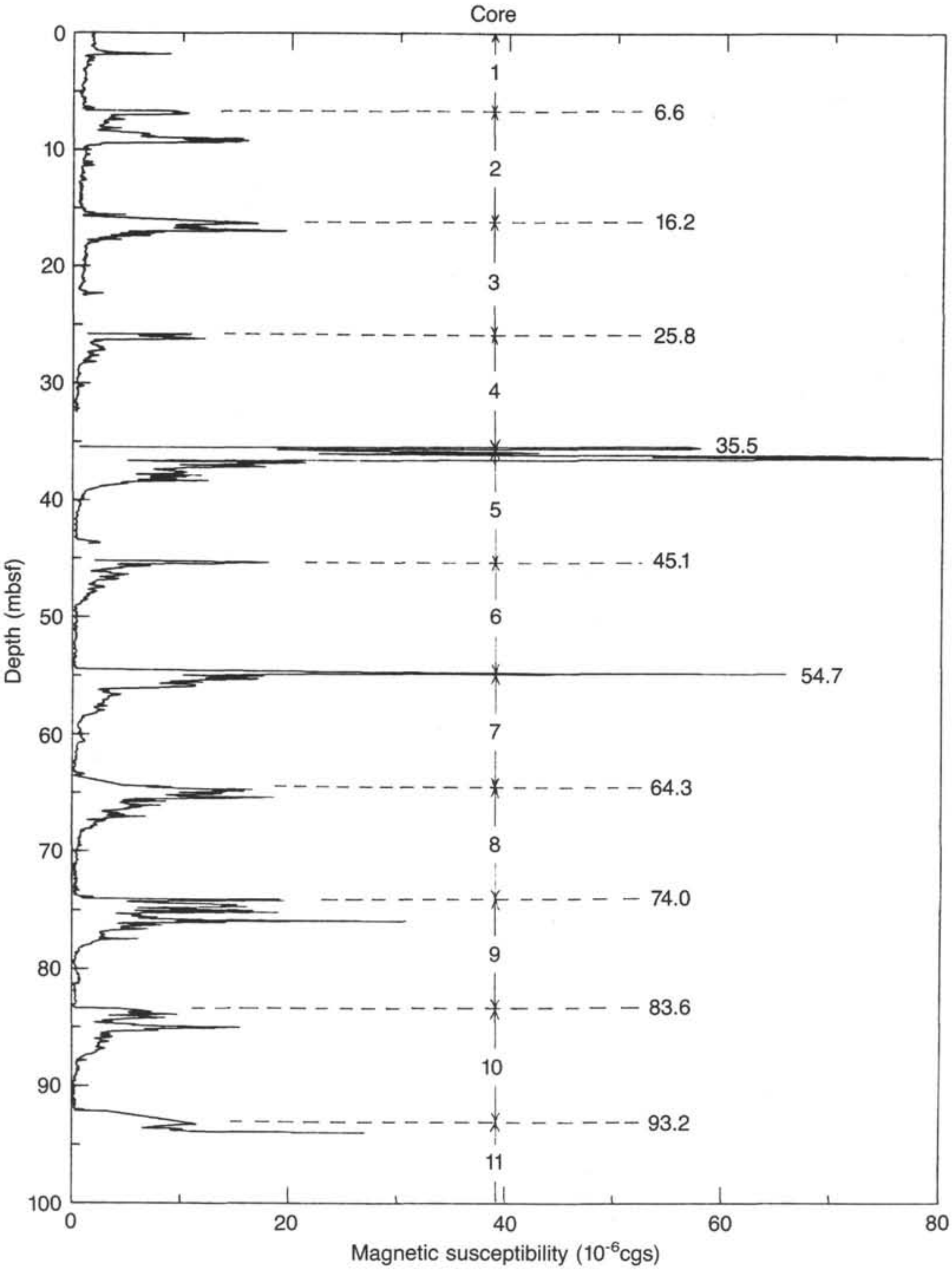

Figure 16. Whole-core magnetic susceptibility profile of the first 100 mbsf of Hole 707A, showing the correspondence between peaks in susceptibility and individual cored intervals of the sequence.

same effect. The consistent frequency, intensity, position, and configuration of peaks in the susceptibility profile of Hole 707A all suggest that the unusual "sawtooth" geometry of this profile is an artifact of drilling contamination.

The occurrence of pervasive, as distinct from superficial, contamination by drilling artifacts may be explained by one or both of the following two processes, or possibly by some other effect not considered here.

1. Sager (1986) suggested that pervasive contamination of ODP Leg 101 cores signified the presence of material "washed-in" from uphole each time the core barrel was withdrawn from the hole. Subsequently, this slumped material, which contains particles of rust and/or drilling abrasion debris deposited from the outer surface of the drill string, becomes incorporated into the upper section of the next interval cored in the sequence.

2. Pervasive contamination can also occur when superficially smeared particles of rust, etc., become incorporated into the bulk of the sediment column as a result of spontaneous liquefaction of the sediment during penetration of the core barrel. The first section of almost every HPC core recovered from Hole 707A (and at several other sites) was "soupy," presumably as a result of coring disturbance of this kind.

The first explanation has adverse implications for the stratigraphic continuity and the apparent accumulation rates of the sequence. The second explanation, in contrast, does not require that pervasively contaminated material in the first section of each core be washed-in from uphole. Thus, in explanation 2, the contaminated sediment in the first section of each core may still be in the correct stratigraphic position, albeit thoroughly disturbed. This explanation, however, does require that the first explanation be partly correct, in that material containing metal contaminants smeared around the exterior of the core (inside its liner) during penetration of the core barrel must have been deposited from uphole, presumably by the mechanism described by Sager (1986).

The extent of contamination in each cored interval of Hole 707A, inferred by the whole-core susceptibility profile, appears to be much greater than the norm for APC coring. However, the actual extent of pervasive contamination of each core may be less than that which is suggested by its susceptibility profile as a result of sediment smearing inside the core liner. In Figure 17A we attempted to distinguish between intervals within each core which are (1) not contaminated, (2) only contaminated superficially as a result of smearing, or (3) pervasively contaminated either as a result of spontaneous liquefaction of the sediment during penetration of the corer or as a result of coring material washed-in from uphole.

Below a depth of 183 mbsf in Hole 707A, the configuration of susceptibility anomalies associated with drilling contamination changes considerably. This lower interval corresponds to sediments which were recovered using the XCB method, rather than the APC system used to core the upper horizons of the sequence. Figures 17A and 17B contrast the different motifs in the susceptibility profile of Hole 707A, associated with drilling contamination by the two different methods of coring. Figure 17A illustrates the characteristic "sawtooth" geometry associated with contamination of APC cores. Figure 17B shows that, in the case of drilling contamination in XCB cores, the sharp peak in susceptibility values occurs below the top of the core and tapers off uphole—directly opposing the trend in susceptibility anomalies associated with contamination in APC cores. This effect is probably the result of coring "density-stratified slurries" which form at the bottom of rotary-drilled holes on removal of each interval of core (Sager, 1986).

Within these graded slumped horizons, particles of rust and/or other drilling artifacts settle out of suspension toward the bottom of the hole. Thus, on retrieval of the next interval of core, the contaminants tend to be concentrated in discrete horizons at the base of spurious graded beds. Because smearing of sediment along the exterior of the core, inside the core liner, is more pronounced with rotary piston (e.g., XCB) coring than with HPC coring, more of the contaminants in slumped horizons become redistributed (superficially) throughout the cored interval above and below the contaminated horizon. This results in misleading susceptibility profiles which imply that more pervasive contamination (indicating slumped horizons) of the core

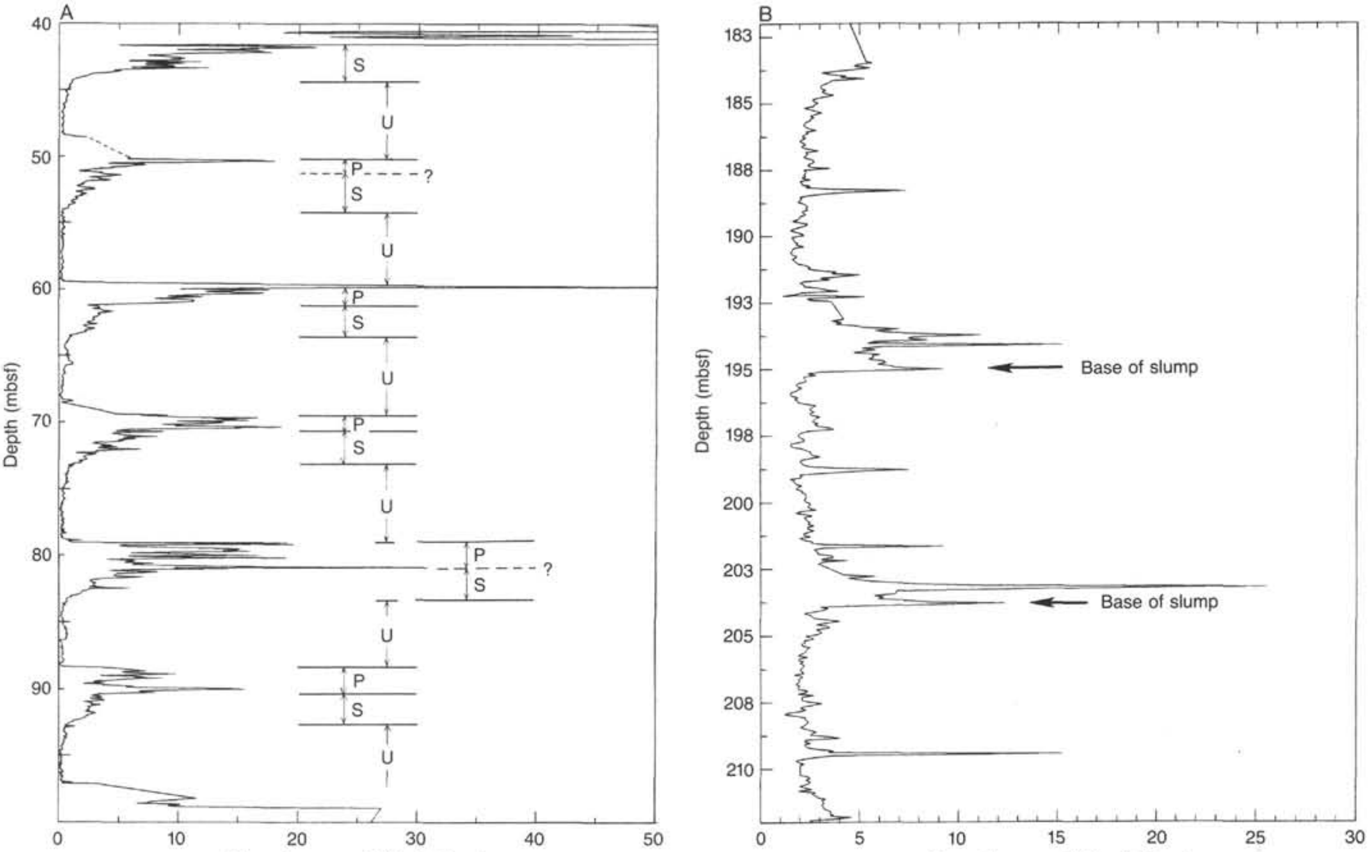

Figure 17. **A.** Whole-core susceptibility profile of a subsection from Hole 707A, showing the characteristic "sawtooth" motif associated with contamination by drilling artifacts in APC cores. The probable extent and nature of contamination (i.e., pervasive or superficial) in each core is also indicated by the following letter codes: P = pervasive contamination, S = superficial contamination, and U = uncontaminated. **B.** Whole-core susceptibility profile of a subsection from Hole 707A showing the characteristic "graded" (density-stratified) motif associated with drilling contamination of XCB cores. The bases of spurious, graded beds (horizons consisting of sediment washed-in from uphole) are indicated by arrows.

has occurred than is actually the case. Also, the rotary-smearing effect makes the identification of drilling contamination using susceptibility profiles much more difficult for XCB cores than for APC cores (cf. Figs. 17A and 17B).

Conclusions

The high degree of contamination (implying disturbance) of core material from Hole 707A suggested by the whole-core susceptibility profile—although exaggerated by the effects of smearing—may have adverse implications with regard to whole-core NRM measurements as well as to all single sample NRM or biostratigraphic analyses of samples taken from the first section of each core. The extent of disturbance and/or contamination at this site, however, is probably abnormal as a result of the following adverse drilling conditions.

1. Hole 707A contained a high proportion of sandy, foraminifer-rich oozes which were poorly cohesive and only weakly consolidated. Such sediments are obviously prone to liquefaction during penetration of the core barrel, or to slumping on removal of the corer if drilling mud is not used to support the hole. Coring disturbance and/or rust contamination tends to be much less of a problem in nannofossil-rich oozes, or in sediments with a higher lithogenous clay content than those encountered at Site 707A.
2. Loose, sandy foraminifer oozes are also extremely effective at scouring rust particles from the surface of the drill pipe.
3. An even more effective abrasive agent, however, was the cherty horizons encountered at various points in the sequence. Chert fragments not only stripped the drill pipe of paint and rust in places but also abraded the underlying surface of the metal. Abrasion of the drill pipe or bit by chert fragments was probably responsible for the pervasive contamination by particles resembling iron filings in Section 115-707A-5H-1, as noted above.
4. The drill pipe in use onboard *JOIDES Resolution* during Leg 115 was last rustproofed approximately 2 yr previously (first used on ODP Leg 103), and many sections of the pipe used during the leg were visibly rusted.

Based on our experience during Leg 115, we recommend that regular inspections to determine the condition of the drill pipe be carried out at intervals of less than 2 yr. It is also essential that both the internal and external surfaces of the drill pipe are rustproofed (effectively zinc-plated) in order to prevent further contamination of the kind experienced at Site 707.

SEDIMENTATION RATES

Sedimentation rates are represented in Figures 18–20 based on the biostratigraphic datums for the various fossil groups given in Table 4. No corrections were made for the effect of compaction. Curves have been constructed for the best fit with the biostratigraphic datums; they show average rates for the various intervals considered, without taking into account short-term fluctuations which may occur. More detailed fluctuations may be determined by further biostratigraphic studies with shorter sampling intervals. Figures 18 and 19 show sedimentation rate curves constructed from Hole 707A for the late Neogene, and from Hole 707C for the Eocene-Paleocene, respectively. In Figure 20 data from both Holes 707A and 707C were combined to give sedimentation rates for the entire stratigraphic sequence at the site.

Between 62.2 and 60 Ma, during the earliest late Paleocene, sediments accumulated in a neritic environment at a rate exceeding 12 m/m.y. After deepening of the site in the latest Paleocene, pelagic sedimentation proceeded at an average rate of 6 m/m.y. during the Eocene (from 60 to 40 Ma), with a high (10 m/m.y.) around the Eocene/Oligocene boundary. Sedimentation during the remainder of the Oligocene and through the early and middle Miocene occurred at a reduced rate, averaging 2.9 m/m.y.

A marked change in sedimentation occurred approximately 9 m.y. ago near the middle/late Miocene boundary: sediments accumulated during the entire late Miocene, Pliocene, and Pleistocene at an average rate of 9 m/m.y. Sedimentation rates, however, were higher during the late Miocene and early Pliocene (from 9 to 3.5 Ma) with an average rate of 15 m/m.y. Rates subsequently decreased to 8 m/m.y. between 3.5 and 0.9 Ma in late Pliocene and earliest Pleistocene times, and then to 5 m/m.y. during the remainder of the Pleistocene.

The Neogene trend in sedimentation rates observed at Site 707 is similar to that observed at nearby DSDP Site 237 (in 1640-m water depth) and other DSDP sites of the western Indian Ocean. Vincent (1974, 1977) reported that, following the Oligocene epoch of reduced sedimentation (after Antarctic Bottom Water moved northward into the Indian Ocean in the late Eocene to earliest Oligocene), sedimentation remained low in the early and middle Miocene (about 2 m/m.y. for that time interval at Site 237). Near the end of the middle Miocene, rates of sedimentation again increased significantly (average value of approximately 11 m/m.y. for the remainder of the Neogene at Site 237).

The pronounced increase in sedimentation rate in the late Miocene was suggested by Vincent (1974, 1977) to be related to higher productivity resulting from the development of the modern surface equatorial circulation pattern at the time when the tip of India moved north of the equator. It is probable, however, that the marked change in sedimentation regime in the tropical Indian Ocean at approximately 9 Ma, near the middle/late Miocene boundary, is related to a global oceanic circulation change associated with a cooling event. Equatorial Pacific records show near the middle/late Miocene boundary a cooling event recorded by a δ^8O increase, the widespread presence of a hiatus (NH4–NH5 of Barron and Keller, 1982), and pronounced calcium carbonate dissolution (Barron et al., 1985a, 1985b).

GEOCHEMISTRY

Interstitial Water Geochemistry

Of the three closely spaced holes drilled at Site 707, interstitial water samples were taken from Holes 707A and 707C only. For purposes of comparison, interstitial water data have been plotted on the same diagram (Fig. 21) and are reported in Table 5.

Calcium and Magnesium

Concentrations of calcium and magnesium are inversely correlated at Site 707, showing a Ca^{2+}/Mg^{2+} gradient of -1.19 (Fig. 22). Calcium values increase from 10.94 to a maximum of 18.52 mmol/L at 254.35 mbsf, while magnesium decreases from 52.66 to 44.52 mmol/L over the same interval. The inverse relationship between Ca^{2+} and Mg^{2+} was apparent as shallow as 100 mbsf, which led to the prediction of a basaltic basement at depth. This was later confirmed when basement was penetrated (see "Basement Rocks" section, this chapter). We did not expect a negative correlation between Ca^{2+} and Mg^{2+} because at DSDP Site 237, only 10 km to the northwest of Site 707, a Ca^{2+}/Mg^{2+} gradient greater than -0.5 was measured (Sandstrom and Gieskes, 1974).

Although basement rocks were not penetrated at the older Site 237, positive gradients have been attributed to the presence of more felsic rocks. If such differences are representative of the underlying basement, then Site 707 and DSDP Site 237 may

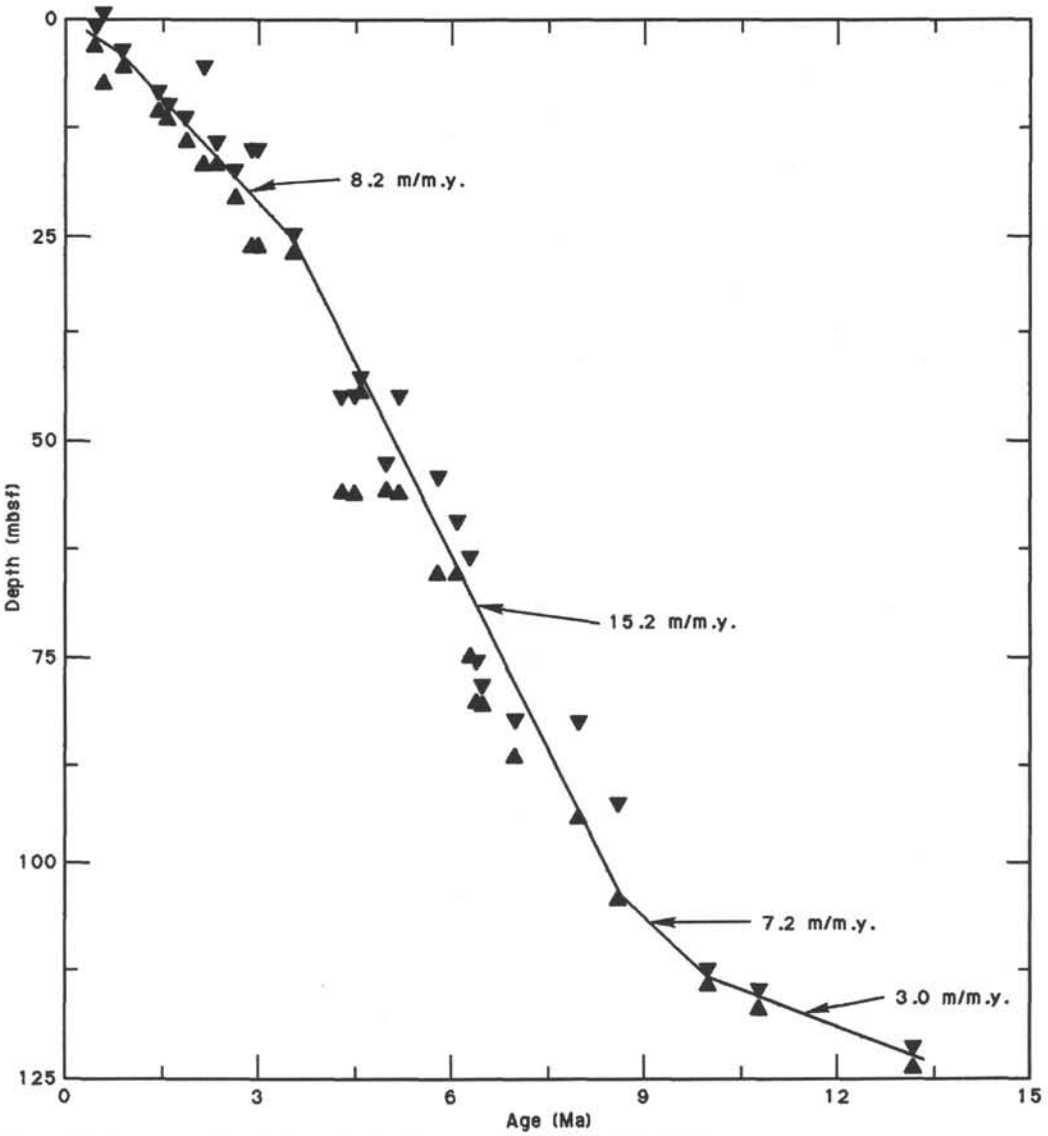

Figure 18. Average sedimentation rates for the upper Neogene in Hole 707A.

have been drilled extremely close to the boundary between continental and oceanic crust, postulated to occur between the Seychelles Islands and the Nazareth Bank on the Mascarene Plateau.

Sulfate and Alkalinity

Sulfate concentrations increase in the top two core samples from a surface seawater value of 28.06 to 29.75 mmol/L. It is believed that this change simply reflects an increase in salinity of the sediment pore waters. In fact, the magnitude of the increase in chlorinity is larger than sulfate, suggesting a small amount of oxidation. This can be seen as a small rise in alkalinity from 2.90 mmol/L in Core 115-707A-1H to 3.29 mmol/L in Core 115-707A-12H.

Silica

The concentration of dissolved silica at Site 707 increases from surface values of <1 to 1000 μmol/L at depth. The increase is caused by the dissolution of biogenic silica (opal-A). Toward the lower interval of the section, the pore fluids become supersaturated with respect to opal-CT, and extensive silicification of the sediments occur (see "Lithostratigraphy" section, this chapter). The rise of silica is limited, therefore, by the solubility product of opal-CT.

X-ray Mineralogy, Carbonate, and Organic Carbon Analyses

X-ray Mineralogy

X-ray analyses of the sediments from which the interstitial water samples were taken show them to be predominantly low-magnesium calcite. Minor amounts of clay minerals and opal-A were not detected by X-ray methods. In Hole 707C, however, the limestones were dolomitized near the basaltic basement (for a description of the basaltic units, see "Basement Rocks" section, this chapter).

Carbonate Content

In Hole 707A, the carbonate content was determined on three samples per section, in addition to the physical properties specimens. These data, and the analyses from Hole 707B and 707C, are shown in Figure 23 and recorded in Table 6. Although the percent carbonate appears to be relatively constant, with a mean value of 92.93 wt% (± 3.17), there are intervals in which the carbonate content shows a much larger variation. Using a running average plot, we identified seven reversals in carbonate concentration (Fig. 24). The first decrease, from 93 to 90.5 wt%, occurs from the upper Pliocene to the lower Pleistocene (10–20

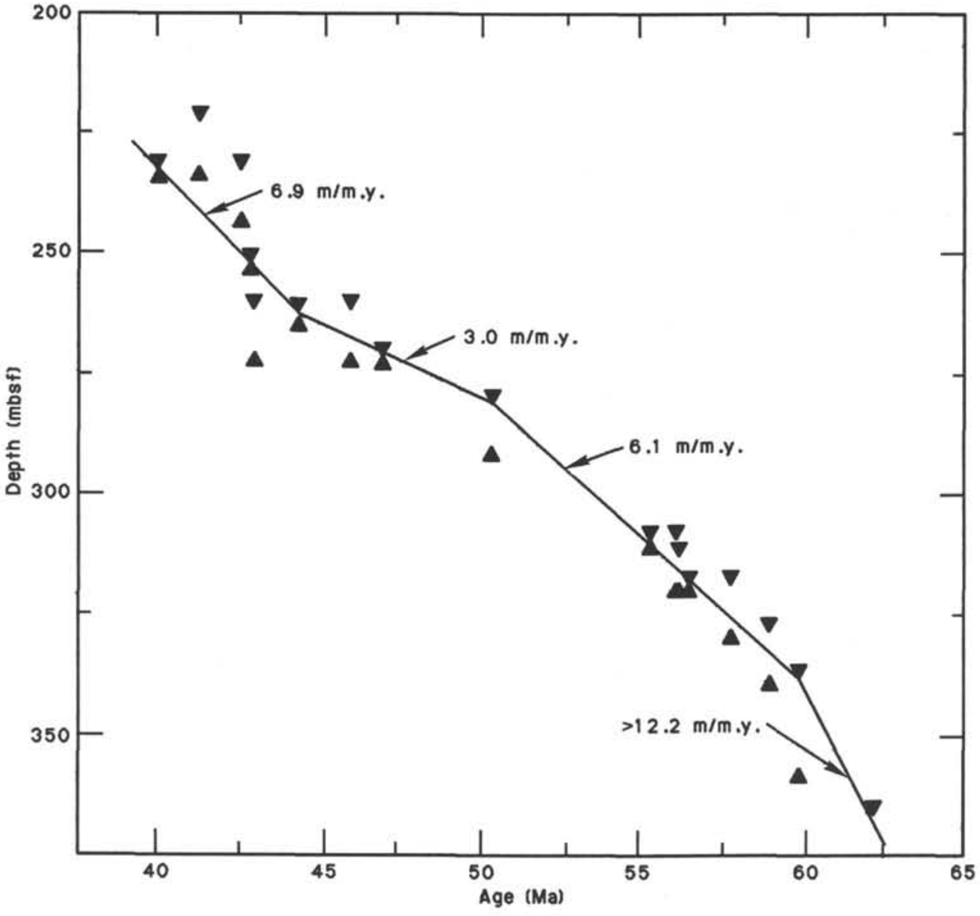

Figure 19. Average sedimentation rates in Hole 707C.

mbsf). The carbonate concentration increases sharply in the upper to middle Pliocene and then gradually decreases to 91 wt%, coincident with the Miocene/Pliocene boundary (50–60 mbsf).

In the middle to upper Miocene, there are three further changes in the carbonate content, ranging from 94 to 92 wt%. The highest carbonate content was reached near the boundary between the Oligocene and Miocene. In the upper Oligocene, the carbonate content once again falls. Recovery was extremely poor between 152 and 173 mbsf; therefore, we did not perform any analyses. By the lower Oligocene, the carbonate content was again as high as 94 wt%, and thereafter it decreased to below 90 wt% in the upper Eocene.

Organic Carbon and Gaseous Hydrocarbons

The amount of organic carbon was at or below detection limits throughout Hole 707A. It is estimated that the error in weighing a sample is at least ±50 μg using shipboard equipment. For organic carbon determinations, two samples are weighed, which means that the error is at least ±100 μg for a sample weighing 2.0 mg. Excluding any errors in the technique itself, the minimum detection limit for this technique is 0.05% or 500 ppm.

Headspace analyses of low-weight alkanes showed these species to be below detection limits.

BASEMENT ROCKS

Introduction

We attempted to penetrate basement rock only in Hole 707C. Rotary coring in this hole encountered basaltic lavas at depths of 375.6 mbsf. We stopped drilling at 443.2 m, after penetrating a total of 67.6 m for an average recovery rate of 62.4%.

Five basalt units were identified, with thin intercalated, mollusc-rich, shallow-water, limestone beds occurring above and below Unit 4. A thin basaltic breccia occurred at the base of the sediments, directly overlying Unit 4. All units are clinopyroxene-plagioclase basalt, and some of them are olivine bearing.

Boundaries between units were recognized on the basis of grain size and texture changes, with the broad chilled lower surfaces of the units usually juxtaposed against highly vesicular, altered upper portions of underlying flows. The units ranged from 0.62 to 37.61 m in apparent thickness, and each appears to represent a single flow. Narrow, chilled, glassy or celadonite-rich contacts were absent.

A detailed description of the macroscopic and microscopic characteristics of each unit and the basalt breccia are given below; features of each are summarized in Figure 25. Shipboard X-ray fluorescence (XRF) data on major and trace element chemistry of Site 707 basalts are summarized in Table 7.

Macroscopic Characteristics

Unit 1

This unit was encountered between 375.6 and 385.35 mbsf, of which only 2.54 m was recovered. It contains microphenocrysts but appears aphyric in hand specimens. The vesicle content decreases rapidly from about 20% in the upper 0.5 m to about 5% 1 m below the flow top. The unit is moderately altered, with green clay and calcite filling vesicles, and high-angle and subhorizontal fractures and veins.

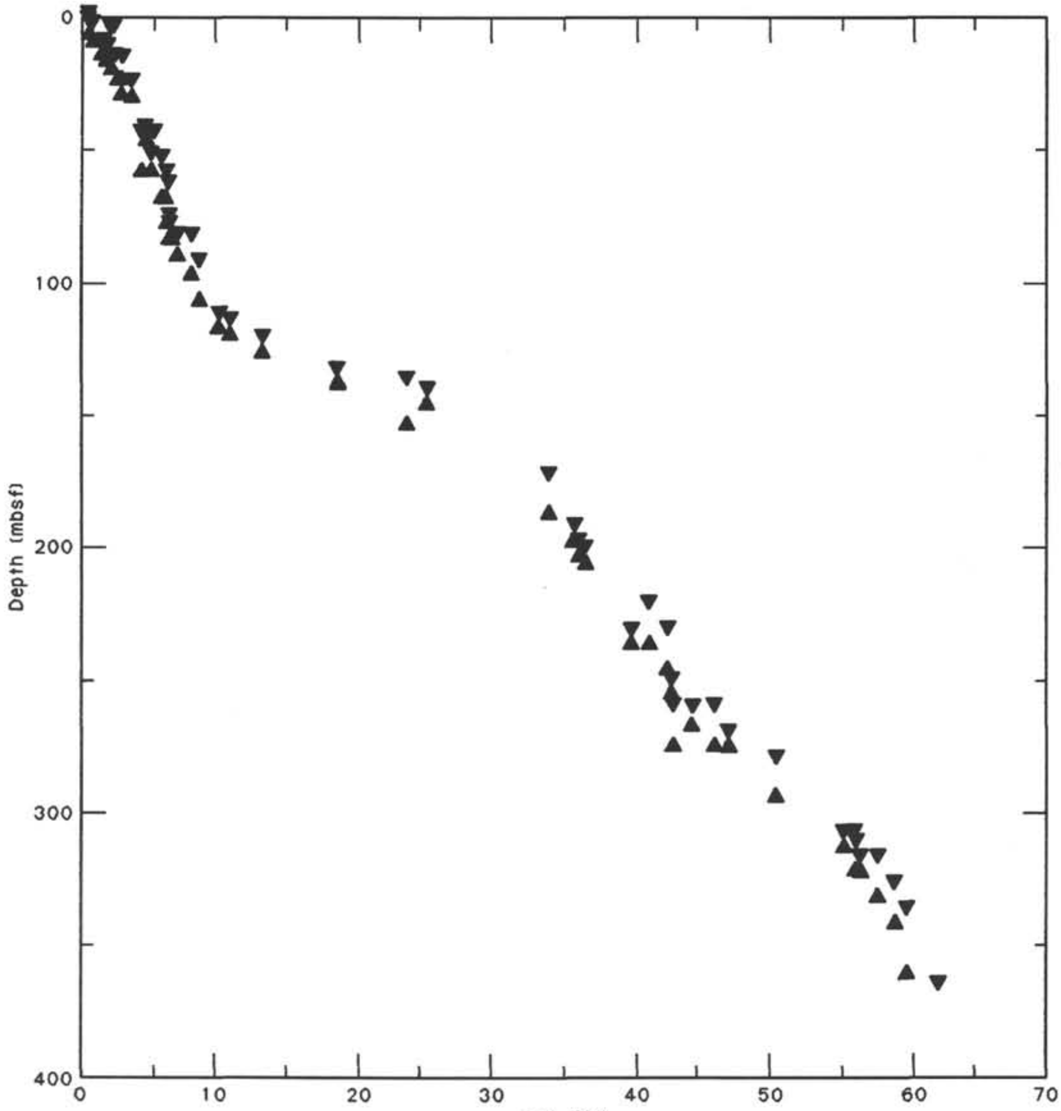

Figure 20. Synthesis of estimated sedimentation rates at Site 707.

Unit 2

We encountered basalt between 0.05 and 0.67 m of the 5.2 m recovered in Core 115-707C-23R (385.35–385.97 mbsf), which we recognized as the second unit in this hole. Macroscopically, it is a fine-grained, clinopyroxene-plagioclase basalt which is moderately to highly altered, with dark green clay filling pervasive veins.

Unit 3

This unit forms the lower 4.5 m of the 5.2 m of core recovered in Core 115-707C-23R (385.97–394.90 mbsf). It is a moderately altered, sparsely vesicular, highly porphyritic clinopyroxene plagioclase basalt. The major alteration products are dark green and brown clays that occur both in the matrix and as a fracture filling with calcite. The lower 1.0 m of the unit shows a progressively developed chill facies (cf. Sample 115-707C-23R-4, 1–12 cm, with Sample 115-707C-23R-4, 86–90 cm).

Shelly Limestone

We recovered 1.09 m of sediment at the top of Core 115-707C-24R, which consisted of silicified, glauconitic, shelly, calcareous mudstones that became grainstone with depth. Flaser bedded, the microfossil assemblage of brachiopods, oysters, and gastropods suggests shallow marine (< 100 m) sedimentation. The lower 0.18 m of this 1.09-m segment comprises a basaltic breccia with subangular vesicular basalt clasts as much as 5 cm in diameter. Many of the fragments display small-scale crenulate boundaries with the silicified fine-grained matrix.

Unit 4

This unit is approximately 37.61 m thick, of which 29.50 m was recovered, extending from 396.0 mbsf (Core 115-707C-24R) to 433.6 mbsf (base of Core 115-707C-27R). It is a porphyritic olivine-clinopyroxene-plagioclase basalt, moderately vesicular (10%), with vesicle diameters as much as 1 cm and typically irregular to ellipsoidal. The unit is moderately altered, with vesicles and high-angle fractures partially filled by green clays and calcite. Local vesicle-rich zones occur. The lowermost 0.1 m of this massive unit is highly altered; the main alteration phases are calcite and green clays (chlorite?).

Carbonate Sands

We recovered 36 cm of silicified carbonate sands and muds from the top of Core 115-707C-28R at 433.60 mbsf, overlying Unit 5.

Table 4. Biostratigraphic datum levels, Holes 707A and 707C.

	Species event	Depth (mbsf)	Age (Ma)
LO	*P. lacunosa* (N)	1.8–2.1	0.46
LO	*G. tosaensis* (F)	0–6.6	0.60
Top	Small *G. oceanica* Zone (N)	4.5–4.6	0.90
LO	*C. macintyrei* (N)	9.4–9.9	1.45
FO	*G. oceanica* (N)	10.75–10.90	1.60
LO	*D. brouweri* (N)	12.4–13.5	1.89
LO	*G. limbata* (F)	6.6–16.2	2.15
LO	*D. pentaradiatus* (N)	15.4–16.2	2.35
LO	*D. tamalis* (N)	18.6–20.1	2.65
LO	*D. altispira* (F)	16.2–25.8	2.90
LO	*Sphaerodinellopsis* sp. (F)	16.2–25.8	3.00
LO	*R. pseudoumbilica* (N)	26.1–26.6	3.56
LO	*S. omnitubus* (R)	45.1–54.7	4.30
FO	*N. jouseae* (D)	45.1–54.7	4.50
	C. acutus/C. rugosus (N)	42.8–42.8	4.60
LO	*D. quinqueramus* (N)	53.0–54.5	5.00
FO	*G. tumida* (F)	45.1–54.7	5.20
FO	*P. primalis* (F)	54.7–64.3	5.80
FO	*T. convexa* var. *aspinosa* (D)	60.0–64.3	6.10
FO	*T. praeconvexa* (D)	64.3–74.0	6.30
	S. delmontensis/S. peregrina (R)	76.5–79.5	6.40
FO	*A. primus* (N)	79.3–79.8	6.50
LO	*D. hughesi* (R)	83.3–86.1	7.00
FO	*G. plesiotumida* (F)	83.6–93.2	8.00
FO	*N. acostaensis* (F)	93.2–102.8	8.60
FO	*D. hamatus* (N)	112.8–113.0	10.00
FO	*C. coalitus* (N)	115.2–115.8	10.80
LO	*S. heteromorphus* (N)	122.0–122.7	13.20
FO	*S. heteromorphus* (N)	133.8–134.4	18.60
LO	*S. belemnos* (N)	133.8–133.4	18.60
FO	*G. kugleri* (F)	138.0–149.5	23.70
LO	*S. ciperoensis* (N)	141.3–141.7	25.20
LO	*Pseudohastigerina* sp. (F)	173.7–183.4	34.00
Acme	*E. subdisticha* (N)	193.0–193.7	35.90
LO	*Hantkenina* (F)	198.8–199.5	36.20
LO	*D. saipanensis* (N)	201.3–202.3	36.70
LO	*C. grandis* (N)	232.1–232.6	40.00
FO	*G. semiinvoluta* (F)	222.5–232.1	41.30
LO	*O. beckmanni* (F)	232.1–241.8	42.60
FO	*D. bisectus* (N)	251.4–251.6	42.90
FO	*O. beckmanni* (F)	261.0–270.6	43.00
FO	*R. umbilica* (N)	261.6–263.2	44.40
LO	*M. aragonensis* (F)	261.0–270.6	46.00
LO	*C. gigas* (N)	270.6–271.1	47.00
LO	*D. lodoensis* (N)	280.6–290.0	50.40
FO	*D. lodoensis* (N)	308.9–309.4	55.30
FO	*M. formosa* (N)	308.9–318.2	56.10
Trans.	*T. orthostylus/contortus* (N)	312.4–318.2	56.20
FO	*D. diastypus* (N)	318.2–318.2	56.50
LO	*M. velascoensis* (F)	318.2–327.9	57.80
FO	*D. multiradiatus* (N)	327.9–337.5	59.00
FO	*D. nobilis* (N)	337.5–356.7	59.90
	Zone P3a/P2 boundary (F)	366.0	62.20

Note: LO = last occurrence, FO = first occurrence, N = nannofossil, F = foraminifer, R = radiolarian, and D = diatom. Ages are those given in "Explanatory Notes" chapter, this volume.

Unit 5

This unit, which is represented by 5.33 m of core between 433.96 mbsf and the drilling end-point at 443.20 mbsf, is a porphyritic olivine-clinopyroxene-plagioclase basalt with a fine-grained groundmass. The upper 2.5 m contains 10%–20% vesicles, but their abundance rapidly declines to 1%–2% below this zone. Vesicles range from 1 to 5 mm, typically have irregular shapes, and are filled by calcite and a fine green acicular phase growing radially from vesicle interiors. Large vugs filled with botryoidal chalcedony are locally developed (Sample 115-707C-28R-2, 65–70 cm).

Petrography

Unit 1

This is a fine-grained, sparsely microporphyritic augite-plagioclase basalt with 5%–7% total phenocrysts and a clinopyroxene to plagioclase ratio of 3:5. Glomerocrysts of augite and plagioclase are common. Plagioclase phenocryst compositions are An_{60}–An_{65}. The matrix consists of plagioclase, clinopyroxene, titaniferous magnetite, and abundant interstitial brown clays, probably replacing quenched groundmass. The thin section from Sample 115-707C-22R-1, 15–17 cm, near the top of the unit contains segregation pockets with a strong zonation of augite to aegerine-augite rims, plagioclase from An_{60} to An_{65}, and abundant titaniferous magnetite. Alteration phases include calcite and microcrystalline brown clays (smectite?).

Unit 2

This is a strongly porphyritic clinopyroxene-plagioclase basalt. Plagioclase averages 25 modal percent, and clinopyroxene is roughly half that amount. Glomerocrysts of clinopyroxene and plagioclase as much as 1 cm in diameter are common. Alteration of the groundmass is extensive, averaging 50%, the main secondary minerals being smectite clays and calcite.

Unit 3

This is a fine-grained, strongly porphyritic olivine-clinopyroxene-plagioclase basalt. Total phenocryst content is 15%–30% with less than 2% olivine typically and a clinopyroxene to plagioclase ratio of 0.3:1.0. Olivine is always totally replaced by calcite and iddingsite in contrast to the fresh augite and plagioclase (An_{55}–An_{65}). Alteration averages 20%–25% with brown clays and calcite replacing interstitial glass and filling vesicles. Unit 3 shows a complete transition from microporphyritic, fine-grained facies through glomeroporphyritic textures, to medium-grained intersertal varieties, possibly controlled by the cooling rate.

Basalt Breccia

The groundmass of the porphyritic basalt fragments in the breccia, and their contacts with the overlying shelly limestone sediment matrix, show conspicuous evidence of pyritization. Replacement of feathery, quench clinopyroxene by pyrite has occurred, but the iron-titanium oxide phase was apparently unaffected.

Unit 4

This is a strongly porphyritic olivine-clinopyroxene-plagioclase basalt. Total phenocryst content varies from 11% to 27% with a clinopyroxene to plagioclase ratio of 0.2:1.0. Olivine phenocrysts form less than 3% of the rock and are always replaced totally by calcite (plus serpentine-group minerals). Augite and plagioclase microphenocrysts are fresh, with plagioclase compositions ranging from An_{50} to An_{65}. Groundmass is typically interstitial, with brown smectite clays forming as much as 30% of the rock as a replacement of quenched groundmass. Vesicles are partially filled by calcite (plus brown clay) and are abundant only in the uppermost part of the unit, where they form about 20% of the rock. Elsewhere they form less than 1%.

Unit 5

This is a moderately to highly porphyritic olivine-clinopyroxene-plagioclase basalt. Olivine typically forms less than 1% of the mode and is always replaced by calcite and iddingsite. Augite and plagioclase (An_{50}–An_{70}) microphenocrysts are fresh.

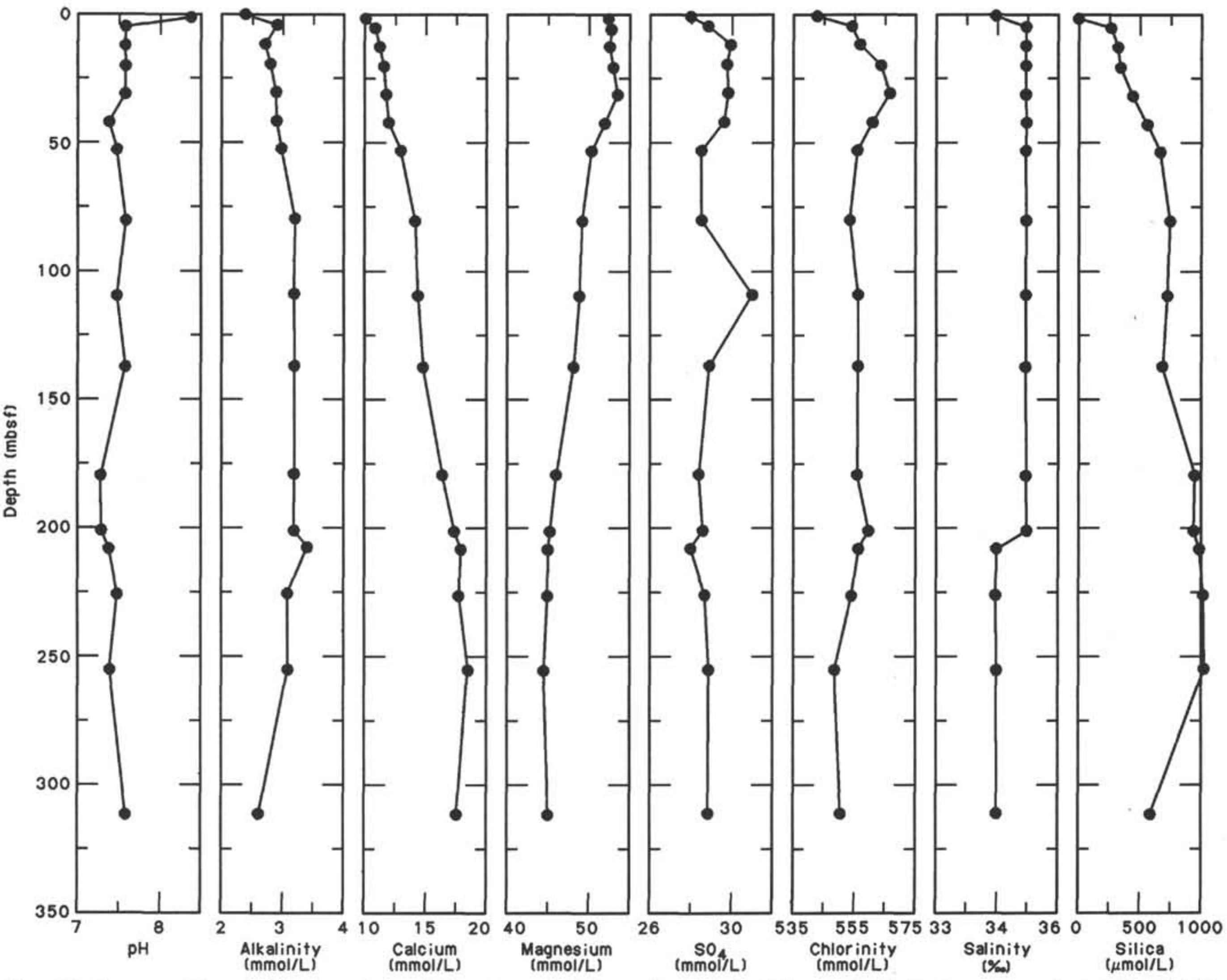

Figure 21. Summary of interstitial water analyses, Holes 707A and 707C, as a function of sub-bottom depth. Surface seawater is plotted at 0 mbsf.

Glomeroporphyritic textures are sporadically developed. The uppermost parts of the flow are fine grained, with a quenched groundmass carrying feathery clinopyroxene and skeletal titaniferous magnetite. Pyrite sporadically occurs in voids and shows a distinct framboidal habit. Alteration products form 15%–55% of the rock, largely replacing interstitial glass and infilling vesicles. Alteration phases are brown clays and calcite. Upper parts of the flow carry 15%–25% vesicles, reducing downward to 2%–5%.

Opaque Minerals and Magnetic Susceptibility

The predominant to exclusive opaque mineral is titaniferous magnetite. Within individual units or subunits, it is present in relatively uniform amounts, grain sizes, and textures; it varies significantly, however, in one or more of the parameters between units (Table 8, Units 4A, 4B, and 4C). A significant variation in the texture of the magnetite was noted in different core segments in the thick Unit 4 (also in magnetic susceptibility; see Table 8).

The most spectacular oxyexsolution of ilmenite from magnetite was noted in what possibly represents the upper chilled border (4A). The magnetite in this, and the basal zone of the unit (4C), tends to occur as subequant but anhedral interstitial aggregates, whereas that from the central zone (4B) is characterized by fine skeletal titaniferous magnetite. This textural variation may be a reflection of the cooling and crystallization profile in this unit. In general, the grains appear homogeneous throughout and rarely show evidence of high-temperature oxyexsolution of ilmenite. We could not determine whether the grains have undergone any low-temperature alteration to titanomaghemite. Ilmenite was observed only as very rare lamellae in magnetites of Unit 4 and in one polished section from Unit 3.

Average magnetic susceptibility (measured on 85 minicores taken for paleomagnetic study) varies systematically between units and appears to correlate with the relative abundance of modal magnetite (see Table 8 and Fig. 26). While the susceptibility of Units 4 and 5 is within the range of that typical of oceanic tholeiites away from ridges ($2.41 \pm 0.22 \times 10^{-3}$ emu/cm$^3\cdot$Oe, on DSDP Leg 37), Units 1, 2, and 3 are significantly below. Of these three units, Unit 2 has particularly low potassium and appears to have the lowest magnetite content; in general, it is more altered than the others. Some magnetite grains in one thin section of Unit 3 contain trellis intergrowths of ilmenite indicative of high-temperature oxidation; these factors may contribute to the lowered potassium in Unit 2. The top of Unit 5 has the highest potassium, even though it is fine-grained and contains as much as 20% vesicles. It also contains the coarsest magnetite grains noted (as large as 4 mm).

Table 5. Interstitial water analyses, Site 707.

Sample interval (cm)	Depth (mbsf)	Ca (mmol/L)	Mg (mmol/L)	Cl (mmol/L)	Alk (mmol/L)	pH	Salinity (‰)	Si (μmol/L)	SO_4 (mmol/L)
Seawater	0	10.18	52.38	542.56	2.43	8.4	34.2	0.4	28.06
115-707A-									
1H-3, 145–150	4.45	10.94	52.66	554.16	2.90	7.6	35.5	266.3	28.92
2H-3, 145–150	11.05	11.37	52.55	557.07	2.79	7.6	35.5	329.0	29.91
3H-2, 145–150	19.15	11.62	52.94	563.84	2.86	7.6	35.6	346.0	29.75
4H-3, 145–150	30.25	11.85	53.34	566.74	2.92	7.6	35.5	441.0	29.75
5H-4, 145–150	41.45	12.03	51.97	560.93	2.90	7.4	35.0	557.0	29.58
6H-5, 145–150	52.55	13.09	50.35	556.10	3.08	7.5	35.2	665.0	28.56
9H-4, 145–150	79.95	14.21	49.15	553.20	3.21	7.6	35.2	735.0	28.56
12H-4, 145–150	108.75	14.40	48.88	556.13	3.29	7.5	35.2	720.0	30.93
15H-3, 145–150	136.05	14.96	48.16	556.10	3.27	7.6	35.2	677.0	28.90
20X-3, 145–150	178.15	16.40	46.00	556.10	3.21	7.3	35.2	946.0	28.49
23X-3, 145–150	207.15	17.96	45.08	556.10	3.41	7.4	34.8	979.0	28.07
115-707C-									
3R-5, 145–150	200.95	17.49	45.31	559.97	3.23	7.3	35.0	945.0	28.66
6R-2, 145–150	225.45	17.88	45.00	554.16	3.18	7.5	34.8	1011.0	28.75
9R-2, 145–150	254.35	18.52	44.52	548.36	3.19	7.4	34.2	1027.0	28.90
15R-1, 145–150	310.35	17.65	45.14	550.30	2.62	7.6	34.0	585.0	28.92

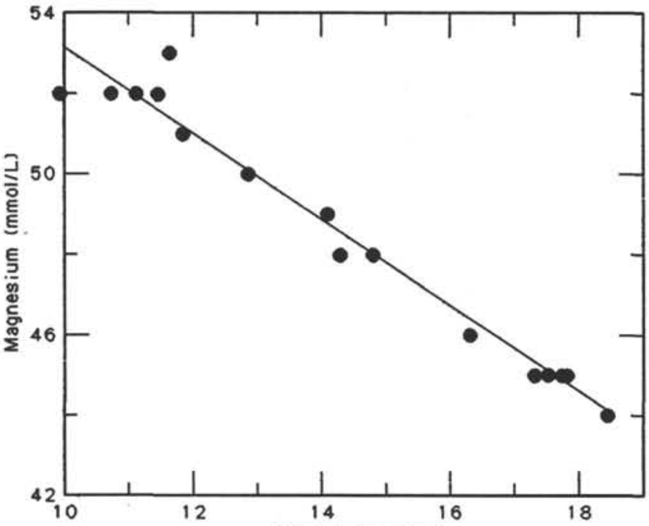

Figure 22. Correlation between calcium and magnesium in Hole 707A.

Discussion

Petrographic contrasts between Site 707 and 706 basalts largely result from the much thicker nature and inferred slower cooling rates of the former. The Site 707 basalts are characterized by a much more crystalline groundmass, with quenched groundmass that is always altered restricted to interstitial areas. While the phenocryst and groundmass phases are similar, clinopyroxenes from Site 707 show no signs of the titanium enrichment common in clinopyroxenes from Site 706. This probably indicates that Site 707 basalts are less alkaline. Glomerocrysts of clinopyroxene plus plagioclase are common in Site 707 basalts but not in Site 706 units, possibly reflecting the slower cooling rates of the thicker flows.

Site 707 lavas frequently display vesicle concentration in the upper parts of the units, and broad, progressively developed chill facies at their lower contacts. Flow boundaries are always subhorizontal; in contrast, Site 706 lavas frequently display variably oriented flow or pillow contacts, with narrow, glassy, or celadonitic margins. Other than these features, detailed thin-section analysis indicates that Site 707 basalts display no systematic intraflow petrographic variation.

Available evidence suggests that while Site 706 basalts formed as submarine, thin-pillow lava units, those from Site 707 formed either subaerially or in very shallow water, with the paucity of high-temperature oxidation of magnetite suggesting the latter. The absence of any matching upper and lower chills in any of the thick units from Site 707 suggests they are not likely to represent sills.

Whole-core physical property measurements show a broad correlation with the relatively subjective and less representative thin-section assessments of degree of alteration and average vesicle abundance. The *P*-wave velocity generally increases downward, as does density, while net porosity declines with depth. The latter change may contribute to the overall increase in magnetic susceptibility with depth. The general sense of change in physical properties is consistent with the observed upward increase in vesicle content and alteration in flows.

An approximate age of earliest late Paleocene (62–63 Ma) is indicated for Site 707 basalts, based on microfossil assemblages in the sediments immediately overlying Unit 1 and intercalated between Units 3 and 4. This contrasts with a similarly derived minimum age of early Oligocene (36 Ma) for Site 706 lavas.

Estimates of a paleolatitude for Site 707 basalts derived from magnetic measurements on all five units give a value of 25° ± 4°S. This is 4° south of the present Réunion hotspot latitude and, within the measured uncertainty, is consistent with the requirements of a hotspot model for the origin of the Deccan-Chagos-Laccadive Ridge-Mascarene Plateau lineament.

PHYSICAL PROPERTIES

Introduction

We drilled Site 707 at a water depth of 1541.4 m on an elevation between the Seychelles Bank and the Saya de Malha Bank on the Mascarene Plateau, approximately 200 km southeast of DSDP Site 237. At Hole 707A, 127 m of sediments were recovered by APC coring, and an additional 32 m by XCB coring. The recovered sediments were composed of uncohesive, homogeneous nannofossil-bearing foraminiferal ooze (as encountered

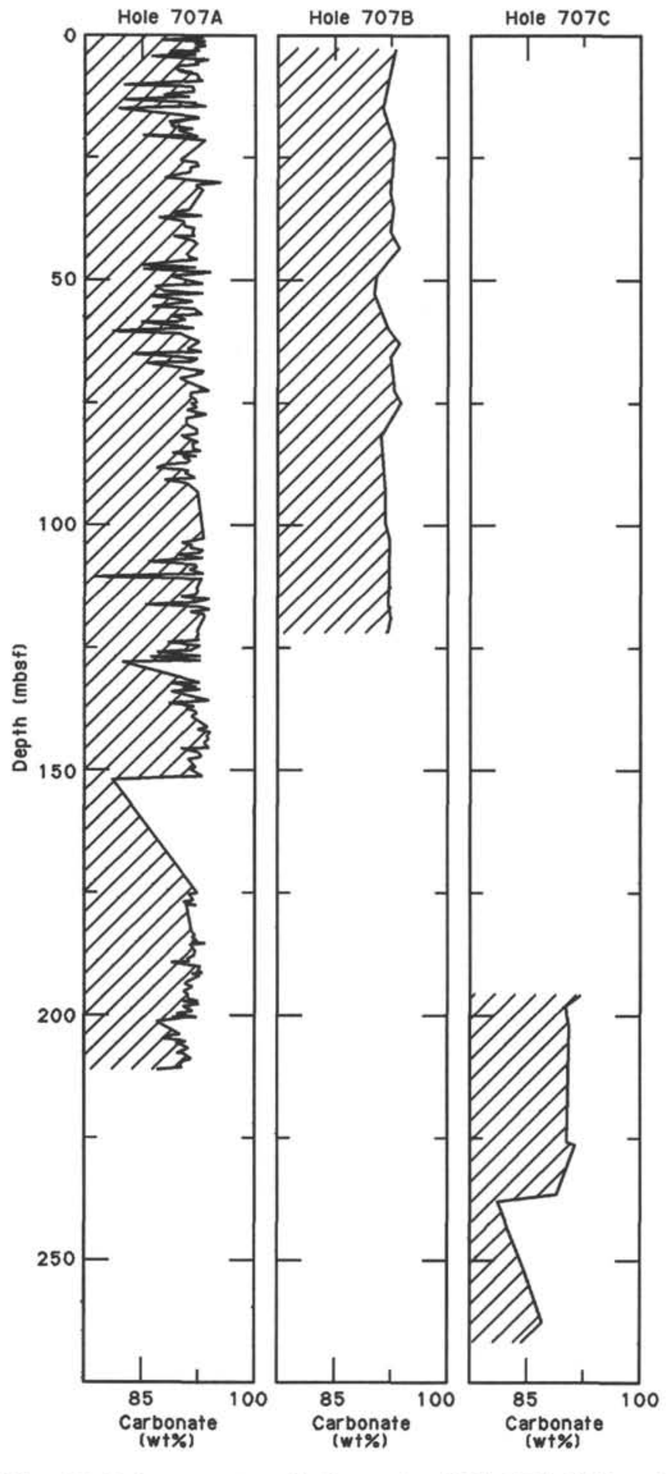

Figure 23. Carbonate content of sediments from Holes 707A, 707B, and 707C.

at Sites 705 and 706), which graded into nannofossil ooze and nannofossil chalk. At Hole 707B, 96 m of sediments were recovered by APC techniques: 64 m of "soupy" homogenous foraminiferal nannofossil ooze, and a further 32 m of soft nannofossil ooze with incipient hard chalk layers. Hole 707C was washed down to a depth of 183 mbsf, and we recovered 92 m of sediments and basement basalts using the RCB. These sediments consisted of a soft nannofossil ooze, chalk, and limestone sequence, underlain by interbedded silicious limestones and basalts.

Table 6. Carbonate content of samples from Holes 707A, 707B, and 707C.

Sample interval (cm)	Depth (mbsf)	Carbonate (wt%)
115-707A-		
1H-1, 80–81	0.80	95.61
1H-1, 133–134	1.33	88.17
1H-2, 20–21	1.70	96.13
1H-2, 60–67	2.10	93.94
1H-2, 80–81	2.30	96.21
1H-2, 133–134	2.83	94.17
1H-3, 20–21	3.20	94.91
1H-3, 80–81	3.80	89.77
1H-3, 133–134	4.33	94.35
1H-4, 20–21	4.70	86.58
1H-4, 65–67	5.15	91.87
1H-4, 80–81	5.30	96.65
1H-4, 133–134	5.83	94.15
1H-5, 20–21	6.20	95.03
2H-1, 20–21	6.80	91.18
2H-1, 80–81	7.40	91.03
2H-1, 133–134	7.93	93.85
2H-1, 138–140	7.98	91.46
2H-2, 20–21	8.30	94.53
2H-2, 80–81	8.90	94.80
2H-2, 133–134	9.43	94.79
2H-3, 20–21	9.80	95.55
2H-3, 35–37	9.95	91.84
2H-3, 80–81	10.40	81.76
2H-3, 133–134	10.93	93.87
2H-4, 20–21	11.30	94.00
2H-4, 80–81	11.90	94.01
2H-4, 133–134	12.43	88.66
2H-5, 20–21	12.80	93.30
2H-5, 80–81	13.40	81.78
2H-5, 133–134	13.93	94.59
2H-6, 20–21	14.30	93.63
2H-6, 80–81	14.90	96.00
2H-6, 84–86	14.94	89.70
2H-6, 133–134	15.43	80.86
3H-1, 80–81	17.00	94.78
3H-1, 133–134	17.53	94.92
3H-2, 20–21	17.90	92.41
3H-2, 55–57	18.25	89.56
3H-2, 80–81	18.50	90.01
3H-2, 133–134	19.03	90.09
3H-3, 20–21	19.40	93.94
3H-3, 80–81	20.00	91.23
3H-4, 20–21	20.90	94.77
3H-4, 30–32	21.00	85.00
3H-4, 80–81	21.50	93.41
3H-4, 133–134	22.03	96.19
4H-1, 20–21	26.00	91.50
4H-1, 80–81	26.60	94.61
4H-1, 90–92	26.70	94.54
4H-1, 133–134	27.13	94.71
4H-2, 20–21	27.50	93.45
4H-2, 80–81	28.10	93.44
4H-2, 133–134	28.63	92.69
4H-3, 20–21	29.00	91.98
4H-3, 80–81	29.60	88.92
4H-3, 133–134	30.13	94.89
4H-4, 20–21	30.50	98.74
4H-4, 80–81	31.10	94.40
4H-4, 133–134	31.63	95.28
4H-5, 20–21	32.00	95.87
5H-1, 20–21	35.70	93.70
5H-1, 80–81	36.30	92.82
5H-1, 133–134	36.83	90.23
5H-2, 20–21	37.20	95.32
5H-2, 80–81	37.80	87.93
5H-2, 133–134	38.33	90.62
5H-3, 20–21	38.70	92.37
5H-3, 80–81	39.30	92.46
5H-3, 133–134	39.83	94.17
5H-4, 20–21	40.20	94.09
5H-4, 80–81	40.80	93.88
5H-4, 133–134	41.33	94.23
5H-5, 20–21	41.70	90.59
5H-5, 80–81	42.30	94.07

Table 6 (continued).

Sample interval (cm)	Depth (mbsf)	Carbonate (wt%)
5H-5, 133–134	42.83	94.67
5H-6, 20–21	43.20	94.65
6H-1, 20–21	45.30	92.78
6H-1, 80–81	45.90	93.42
6H-1, 133–134	46.43	94.83
6H-2, 20–21	46.80	93.00
6H-2, 80–81	47.40	85.16
6H-2, 133–134	47.93	94.38
6H-3, 20–21	48.30	85.17
6H-3, 80–81	48.90	96.97
6H-3, 133–134	49.43	90.88
6H-4, 20–21	49.80	89.93
6H-4, 80–81	50.40	93.29
6H-4, 133–134	50.93	95.65
6H-5, 20–21	51.30	95.30
6H-5, 80–81	51.90	87.14
6H-6, 20–21	52.80	89.08
6H-6, 80–81	53.40	95.70
6H-6, 133–134	53.93	90.42
6H-7, 20–21	54.00	86.44
7H-1, 20–21	54.90	93.88
7H-1, 80–81	55.50	89.03
7H-1, 133–134	56.03	86.80
7H-2, 20–21	56.40	94.31
7H-2, 80–81	57.00	94.60
7H-2, 133–134	57.53	95.50
7H-3, 20–21	57.90	90.06
7H-3, 80–81	58.50	92.64
7H-3, 133–134	59.03	91.06
7H-4, 20–21	59.40	84.83
7H-4, 80–81	60.00	94.12
7H-4, 133–134	60.53	93.90
7H-5, 20–21	60.90	79.84
7H-5, 80–81	61.50	91.94
7H-6, 20–21	62.40	94.69
7H-6, 80–81	63.00	94.98
8H-1, 20–21	64.50	92.79
8H-1, 80–81	65.10	95.36
8H-1, 133–134	65.63	83.29
8H-2, 20–21	66.00	93.20
8H-2, 54–56	66.34	94.70
8H-2, 80–81	66.60	94.13
8H-2, 133–134	67.13	93.69
8H-3, 20–21	67.50	85.92
8H-3, 80–81	68.10	92.39
8H-3, 133–134	68.63	94.25
8H-4, 20–21	69.00	95.82
8H-4, 80–81	69.60	95.27
8H-4, 133–134	70.13	92.76
8H-5, 20–21	70.50	91.56
8H-5, 80–81	71.10	92.78
8H-5, 133–134	71.63	93.53
8H-6, 20–21	72.00	94.44
8H-6, 56–58	72.36	94.08
8H-6, 80–81	72.60	95.64
8H-6, 133–134	73.13	96.80
8H-7, 20–21	73.50	93.82
9H-1, 20–21	74.20	93.61
9H-1, 80–81	74.80	94.50
9H-1, 133–134	75.33	94.86
9H-2, 20–21	75.70	93.65
9H-2, 80–81	76.30	94.98
9H-2, 133–134	76.83	92.98
9H-3, 20–21	77.20	94.47
9H-3, 80–81	77.80	96.42
9H-3, 133–134	78.33	94.61
9H-4, 20–21	78.70	92.80
9H-4, 80–81	79.30	92.81
9H-4, 133–134	79.83	92.80
9H-5, 20–21	80.20	93.84
9H-5, 80–81	80.80	94.55
9H-5, 133–134	81.33	94.72
9H-6, 20–21	81.70	94.83
9H-6, 80–81	82.30	91.97
9H-6, 133–134	82.83	93.82
9H-7, 20–21	83.20	95.03
10H-1, 20–21	83.80	93.90
10H-1, 80–81	84.40	94.01

Table 6 (continued).

Sample interval (cm)	Depth (mbsf)	Carbonate (wt%)
10H-1, 133–134	84.93	94.17
10H-2, 20–21	85.30	95.32
10H-2, 80–81	85.90	90.43
10H-2, 133–134	86.43	94.77
10H-3, 20–21	86.80	92.10
10H-3, 80–81	87.40	93.68
10H-3, 133–134	87.93	92.98
10H-4, 20–21	88.30	88.81
10H-4, 80–81	88.90	87.68
10H-4, 133–134	89.43	93.29
10H-5, 20–21	89.80	92.34
10H-5, 80–81	90.40	94.15
10H-5, 133–134	90.93	94.34
10H-6, 20–21	91.30	89.16
10H-6, 80–81	91.90	93.17
11H-1, 46–57	93.66	94.86
12H-1, 20–21	103.00	95.94
12H-1, 80–81	103.60	93.65
12H-1, 133–134	104.13	92.08
12H-2, 20–21	104.50	94.08
12H-2, 80–81	105.10	93.40
12H-2, 133–134	105.63	95.82
12H-3, 20–21	106.00	95.32
12H-3, 80–81	106.60	91.25
12H-3, 133–134	107.13	95.75
12H-4, 20–21	107.50	95.10
12H-4, 80–81	108.10	86.24
12H-4, 110–111	108.40	94.48
12H-5, 20–21	109.00	94.69
12H-5, 80–81	109.60	93.16
12H-5, 133–134	110.13	95.87
12H-6, 20–21	110.50	95.47
12H-6, 80–81	111.10	76.75
12H-6, 110–111	111.40	95.57
13H-1, 20–21	112.60	94.99
13H-1, 133–134	113.73	94.65
13H-2, 20–21	114.10	94.99
13H-2, 80–81	114.70	94.68
13H-2, 133–134	115.23	91.83
13H-3, 20–21	115.60	96.68
13H-3, 80–81	116.20	94.35
13H-3, 133–134	116.73	85.73
13H-4, 20–21	117.10	95.00
13H-4, 80–81	117.70	97.06
13H-4, 133–134	118.23	93.50
13H-5, 20–21	118.60	96.03
13H-5, 80–81	119.20	96.15
14H-1, 20–21	122.20	94.77
14H-1, 80–81	122.80	95.15
14H-1, 133–134	123.33	94.39
14H-2, 20–21	123.70	95.23
14H-2, 54–57	124.04	93.46
14H-2, 80–81	124.30	89.64
14H-2, 133–134	124.83	95.32
14H-3, 20–21	125.20	95.11
14H-3, 80–81	125.80	93.41
14H-3, 133–134	126.33	87.55
14H-4, 20–21	126.70	94.75
14H-4, 47–50	126.97	95.55
14H-4, 80–81	127.30	86.52
14H-4, 133–134	127.83	95.50
14H-5, 20–21	128.20	81.62
15H-1, 20–21	131.80	93.5
15H-1, 80–81	132.40	95.34
15H-1, 133–134	132.93	90.26
15H-2, 20–21	133.30	94.61
15H-2, 58–60	133.68	92.19
15H-2, 80–81	133.90	95.34
15H-2, 133–134	134.43	90.26
15H-3, 20–21	134.80	92.74
15H-3, 80–81	135.40	93.76
15H-4, 20–21	136.30	96.92
15H-4, 54–57	136.64	92.40
15H-4, 80–81	136.90	89.87
15H-4, 133–134	137.43	94.55
15H-5, 20–21	137.80	92.72
15H-5, 80–81	138.40	94.89
15H-5, 133–134	138.93	94.16

Table 6 (continued).

Sample interval (cm)	Depth (mbsf)	Carbonate (wt%)
15H-6, 20-21	139.30	93.71
16H-1, 20-21	141.50	96.86
16H-1, 80-81	142.10	94.72
16H-1, 133-134	142.63	97.12
16H-2, 20-21	143.00	96.71
16H-2, 54-56	143.34	96.10
16H-2, 80-81	143.60	96.90
16H-2, 133-134	144.13	96.56
16H-3, 20-21	144.50	96.04
16H-3, 80-81	145.10	96.04
16H-3, 133-134	145.63	96.85
16H-4, 20-21	146.00	91.91
16H-4, 80-81	146.60	95.08
16H-4, 133-134	147.13	95.68
16H-5, 20-21	147.50	95.29
16H-5, 80-81	148.10	93.20
16H-5, 133-134	148.63	93.56
16H-6, 20-21	149.00	94.17
16H-6, 80-81	149.60	94.52
16H-6, 133-134	150.13	93.51
16H-7, 20-21	150.50	94.32
16H-7, 80-81	151.10	95.06
17H-1, 20-21	151.20	95.70
17H-1, 80-81	151.80	94.51
17H-1, 125-127	152.25	84.15
17H-1, 130-131	152.30	80.04
20X-1, 20-21	173.90	93.58
20X-1, 80-81	174.50	94.06
20X-1, 133-134	175.03	94.33
20X-2, 20-21	175.40	94.90
20X-2, 80-81	176.00	93.39
20X-3, 20-21	176.90	94.36
20X-3, 80-81	177.50	92.31
20X-3, 133-134	178.03	94.50
20X-3, 143-145	178.13	92.80
21X-1, 20-21	183.60	94.03
21X-1, 80-81	184.20	94.59
21X-1, 133-134	184.73	93.77
21X-2, 20-21	185.10	94.82
21X-2, 80-81	185.70	93.78
21X-2, 81-83	185.71	96.24
21X-2, 133-134	186.23	93.62
21X-3, 20-21	186.60	93.63
21X-3, 80-81	187.20	94.57
21X-3, 133-134	187.73	94.25
21X-4, 20-21	188.10	94.31
21X-4, 80-81	188.70	92.97
21X-4, 133-134	189.23	92.88
21X-4, 141-143	189.31	93.68
21X-5, 20-21	189.60	90.16
21X-5, 80-81	190.20	95.22
21X-5, 133-134	190.73	95.00
21X-6, 20-21	191.10	94.97
21X-6, 80-81	191.70	95.66
21X-6, 84-86	191.74	93.96
21X-6, 128-129	192.18	95.31
22X-1, 20-21	193.30	92.98
22X-1, 80-81	193.90	92.66
22X-1, 133-134	194.43	94.05
22X-2, 20-21	194.80	93.04
22X-2, 80-81	195.40	92.46
22X-2, 133-134	195.93	93.20
22X-3, 20-21	196.30	92.98
22X-3, 80-81	196.90	93.36
22X-3, 133-134	197.43	94.77
22X-3, 140-142	197.50	92.22
22X-4, 20-21	197.80	95.05
22X-4, 80-81	198.40	92.37
22X-4, 133-134	198.93	93.38
22X-5, 20-21	199.30	94.15
22X-5, 80-81	199.90	91.19
22X-5, 133-134	200.43	94.81
22X-5, 140-142	200.50	90.44
22X-6, 20-21	200.80	92.17
22X-6, 80-81	201.40	87.74
22X-6, 133-134	201.93	87.72
23X-1, 20-21	202.90	89.45
23X-1, 80-81	203.50	90.76
23X-1, 133-134	204.03	91.82
23X-2, 20-21	204.40	89.20
23X-2, 50-52	204.70	90.30
23X-2, 80-81	205.00	88.89
23X-2, 133-134	205.53	92.90
23X-3, 20-21	205.90	90.97
23X-3, 80-81	206.50	93.01
23X-3, 133-134	207.03	93.35
23X-4, 20-21	207.40	91.93
23X-4, 80-81	208.00	92.43
23X-4, 85-87	208.05	91.38
23X-5, 20-21	208.90	93.82
23X-5, 80-81	209.50	92.43
23X-6, 20-21	210.40	91.85
23X-6, 80-81	211.00	92.09
23X-6, 133-134	211.53	87.84
23X-6, 136-138	211.56	88.19
115-707B-		
1H-3, 48-50	3.48	95.83
2H-4, 117-119	15.17	93.52
3H-3, 36-38	22.46	95.78
3H-5, 45-47	25.55	95.34
4H-3, 118-120	32.88	95.04
4H-5, 120-122	35.90	95.56
5H-2, 63-66	40.53	95.01
5H-4, 85-88	43.75	96.81
6H-2, 25-28	49.75	92.45
6H-4, 64-67	53.14	92.19
7H-2, 134-137	60.44	94.80
7H-4, 113-116	63.23	96.79
7H-6, 113-116	66.23	95.01
8H-2, 93-96	69.63	95.49
8H-4, 113-116	72.83	95.94
8H-6, 56-58	75.26	97.03
9H-4, 65-69	82.05	93.45
10H-5, 111-114	93.61	94.27
11H-3, 106-109	100.16	94.02
11H-5, 132-135	103.42	94.91
13H-1, 100-102	116.30	94.75
13H-3, 100-102	119.30	95.24
13H-5, 100-102	122.30	94.62
115-707C-		
3R-2, 89-91	195.89	94.69
3R-4, 23-25	198.23	92.03
3R-6, 133-137	202.33	92.72
6R-3, 65-67	226.20	92.26
6R-3, 96-98	226.51	93.84
7R-3, 142-144	236.52	90.54
7R-5, 6-8	238.16	79.79
9R-1, 128-130	252.68	84.90
10R-2, 33-36	262.83	87.83
10R-4, 114-116	266.64	84.21

This section presents the physical properties measurements for index properties, compressional- and shear-wave velocities, shear strength, and thermal conductivities of sediments and basement rocks from Site 707. The section is divided into two subsections, "Sediments" and "Basement," although the base of the sedimentary sequence is included in the latter subsection.

Sediments

Index Properties

The results of the index property measurements at Site 707 are presented in Figures 27–30 and Table 9.

The wet-bulk density of the nannofossil-foraminifer-rich ooze recovered in Holes 707A and 707B increases from 1.45 to 1.74 g/cm^3 from the seafloor to 211.56 mbsf (Fig. 27 and Table 9). The variability of the data is predominantly due to disturbance

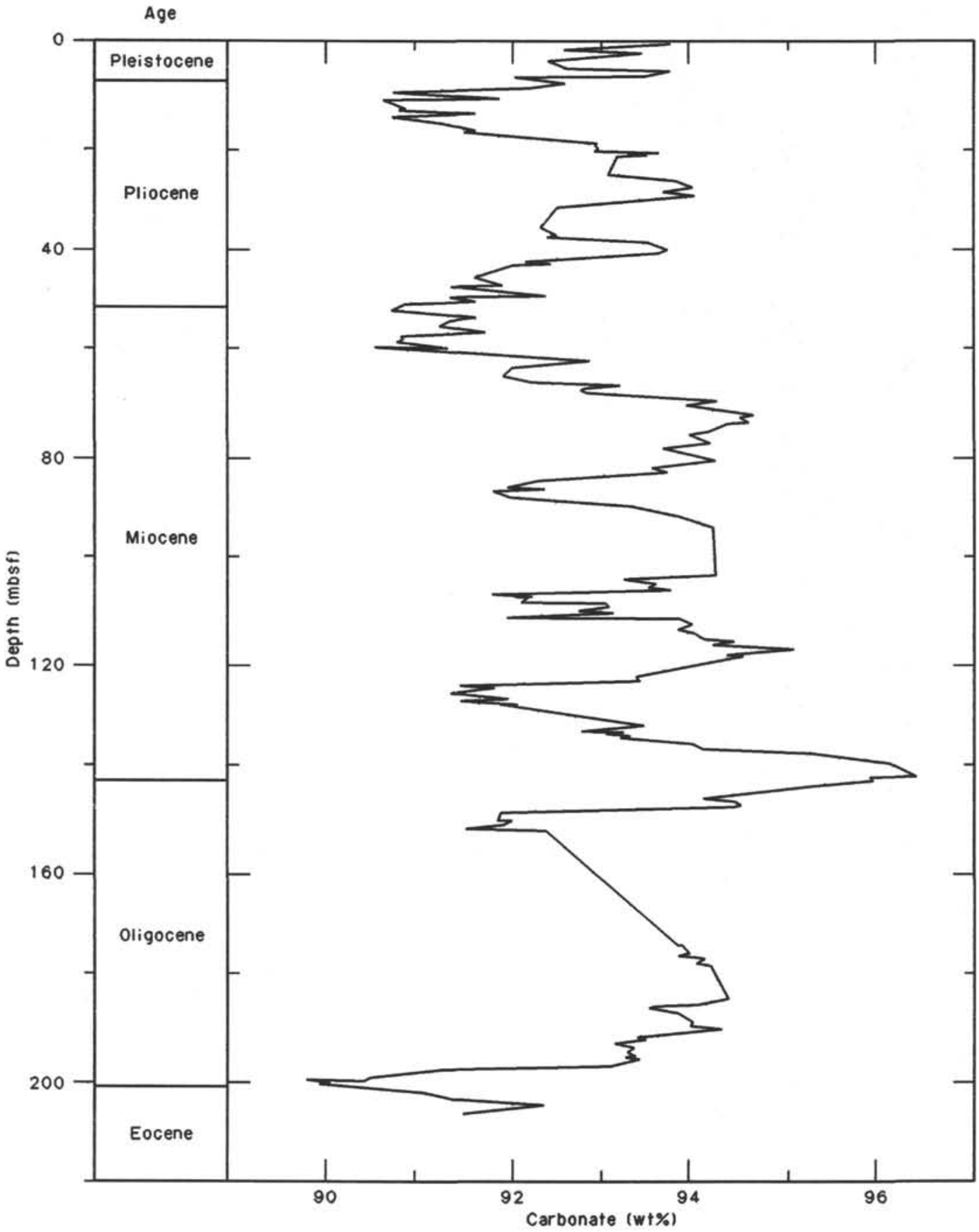

Figure 24. Smoothed record of carbonate content (based on a 10-point running mean) for Hole 707A.

of the sediment and is not related to lithologic layering. This is clearly demonstrated by comparing wet-bulk density values from Holes 707A and 707B. The wet-bulk density values in Hole 707C vary from 1.70 to 1.82 g/cm^3 within the nannofossil-foraminifer ooze sequence between depths of 195.89 and 238.16 mbsf (Fig. 27 and Table 9). These are slightly greater than those wet-bulk densities measured in 707A and 707B and are the result of greater compaction of the deeper 707C samples.

Porosity decreases gradually with depth in Hole 707A from 77.83% at 7.98 mbsf to 59.64% at 211.56 mbsf (Fig. 28 and Table 9). A reduction from 55.51% to 35.68% can be seen for the water content over the same depth interval. In Hole 707B porosity decreases from 74.17% at 3.48 mbsf to 67.12% at 122.30 mbsf, and the water content decreases from 51.12% to 42.43% in the same interval. Porosity and water content in Hole 707C are fairly constant between 55% and 60% and between 32% and 35%, respectively, except for the drastic decrease at 236.52 mbsf to 20.45% porosity and 12.13% water content. Similar observations were made by Fisher et al. (1974) at DSDP Site 237. They concluded that the rapid decrease in porosity marked

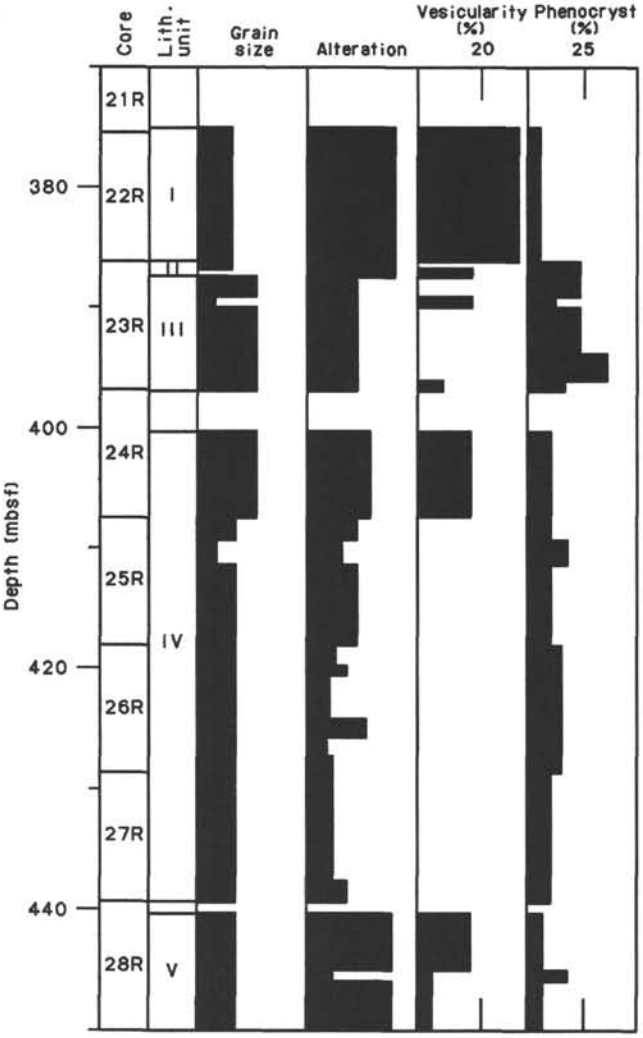

Figure 25. Graphic summary (assuming core recovered is directly proportional to core drilled) of basalt stratigraphy and major characteristics at Site 707. The first column shows the core number and letter, and the second column gives the unit number. The space between Units 3 and 4 is shelly limestone and basalt breccia, and the space between Units 4 and 5 represents silicified carbonate sand. Grain size is indicated by bars of increasing length for microcrystalline, fine grain size, and medium grain size. Alteration is on a scale of 0%–100%; vesicularity is on a scale of 0%–30%, and total phenocryst abundance is from 0%–50%.

the onset of compaction from ooze to chalk. Interestingly, there is a corresponding drop in grain density over this interval and little net resultant change in wet-bulk density.

In the homogeneous nannofossil-foraminifer ooze and foraminifer-nannofossil ooze, no major variation in the grain density was observed. The measured values shown in Figure 29 and Table 9 lie within the range of 2.50 and 2.83 g/cm^3 that is typical for a carbonate-rich sediment. The low values of 2.13 and 2.09 g/cm^3 at 21.00 and 26.70 mbsf, respectively, are probably erroneous since there was no indication of large amounts of biogenic silica from smear slides. High amounts of biogenic silica, with a grain density of 1.7–2.2 g/cm^3 (Baas Becking and Moore, 1959; Hurd, 1983), would reduce the net grain density, consequently reducing the wet-bulk density significantly (Hempel and Mayer, in press). Grain-density values above 3.10 g/cm^3 in Hole 707B are also most likely erroneous. Through most parts of Holes 707A, 707B, and 707C, the grain density values follow the carbonate content curve (Fig. 30).

A comparison of the porosity, grain density, and wet-bulk density curves shown in Figures 27–29, shows that wet-bulk density is relatively insensitive to variations in grain density. Therefore, porosity is the key parameter controlling the wet-bulk density of the sediments at this site.

Compressional-Wave Velocities

The compressional-wave velocity (V_p) was determined on discrete samples and from continuous *P*-wave logs. The quality of the measurements was often poor with evidence of disturbance. Only limited data were collected with the *P*-wave logger due to hardware and software problems. In addition, many core sections were only partially filled with sediment, which created whole-round-core logging problems.

Results of V_p vs. depth are summarized in Table 10 and displayed in Figure 31. We observed that Hamilton frame velocity measurements made on discrete samples agree well with the velocities obtained from the *P*-wave logger. These results do not show any velocity gradient, and an average value of 1550 m/s is characteristic for V_p measurements made in a laboratory.

Shear-Wave Velocities and Shear Strength

Shear-wave velocity (V_s) and shear strength are the physical properties most severely affected by core disturbance. Both properties strongly depend upon the rigidity of the cemented sediment framework, which can be reduced drastically through drilling disturbance. Results for V_s vs. depth at Site 707 are presented in Table 11 and Figure 32. A gradual increase of V_s with depth can be seen from this data, representing an increase in rigidity due to cementation.

For Holes 707A and 707B, V_s values below 40 mbsf are similar to those for the foraminifer ooze at Sites 705 and 706, but they increase slightly to nearly 120 m/s in the underlying nannofossil ooze. At 152 mbsf in Hole 707A, we changed drilling modes from the APC- to the XCB-coring system. The sudden decrease in V_s is attributed to increased disturbance within the XCB cores.

Shear strength was evaluated at selected intervals within the sedimentary sequence. Although a few measurements were made upon consolidated sediment "chunks," the majority of measurements were obtained in soft-sediment intervals. The results for peak shear strength at Site 707 are illustrated in Figure 33 and given in Table 12. From these values we observed a general increase in shear strength with depth. The scatter among the data is significant, but we have greater confidence in the larger values since these measurements were obtained on less disturbed intervals.

Acoustic Impedance

The acoustic impedance (the product of compressional velocity and wet-bulk density) shows no major variations within the ooze sections of Holes 707A, 707B, and 707C (Fig. 34). It varies only by about 20% between 2.21 and 2.78 g/cm$^2 \cdot$s$\cdot 10^5$, which leads to weak reflectors in the seismic profile. Impedance contrasts are more sensitive to wet-bulk density variations (>20%) than to variations in velocity (7%).

In the lower part of Hole 707C, wet-bulk density and velocity changes run parallel, so the impedances match well with both curves. The peaks at 370 mbsf (Fig. 35) represent the silicified hard limestone layer which occurs toward the base of the sedimentary section. The large impedance contrast at 375 mbsf corresponds to the strongest reflector in the seismogram (see Fig. 39).

Thermal Conductivity

Thermal conductivity measurements were made at intervals of about one per section (1.5 m) in Hole 707A and Hole 707C,

Table 7. XRF major and trace element chemistry of Site 707 basalts.

Core, Section Interval (cm)	22R-1 94–98	22R-2 40–42	23R-1 24–27	23R-1 123–127	23R-3 137–140	23R-4 32–34	25R-1 39–43	25R-3 44–47	26R-2 126–128	26R-5 82–84	26R-6 115–118	27R-6 143–147	27R-7 46–50	28R-4 37–39	28R-4 133–134
wt%:															
SiO_2	51.51	50.32	49.92	50.20	50.23	50.19	49.60	49.70	50.08	48.99	49.88	49.89	49.36	49.79	49.61
TiO_2	0.82	0.71	0.65	0.58	0.69	0.69	1.38	1.45	1.47	1.44	1.39	1.45	1.40	1.47	1.46
Al_2O_3	15.11	13.44	16.22	15.86	16.20	15.70	14.90	15.10	15.38	15.11	14.41	15.04	14.73	14.33	14.48
Fe_2O_3	12.03	14.56	10.18	10.44	10.98	11.69	13.49	13.32	13.03	13.91	14.27	13.77	14.05	14.06	14.13
MnO	0.08	0.07	0.10	0.13	0.12	0.14	0.16	0.17	0.15	0.18	0.19	0.19	0.20	0.16	0.17
MgO	9.21	10.88	8.72	9.01	8.39	8.13	7.10	7.15	6.96	7.17	6.92	6.44	6.64	7.11	7.08
CaO	9.65	8.30	12.24	12.61	12.53	12.22	11.50	11.24	11.05	11.37	11.32	11.66	11.99	11.01	11.17
Na_2O	2.37	2.29	1.88	1.87	1.89	1.91	2.15	2.23	2.27	2.20	2.10	2.16	2.13	2.52	2.26
K_2O	0.16	0.19	0.05	0.05	0.06	0.08	0.13	0.09	0.07	0.07	0.08	0.07	0.06	0.11	0.09
P_2O_5	0.03	0.03	0.03	0.02	0.03	0.03	0.10	0.11	0.11	0.11	0.10	0.11	0.10	0.11	0.10
Total	100.97	100.79	99.99	100.77	101.06	100.78	100.93	99.56	100.57	100.55	100.66	100.78	100.66	100.67	100.55
Ignition loss	1.48	2.23	0.87	0.14	0.59	0.52	0.48	0.23	0.73	0.75	−0.27	0.35	0.26	0.31	0.13
ppm:															
Nb	2.1	2.3	1.8	2.3	1.7	2.5	5.3	6.4	5.9	6.2	5.7	6.0	6.7	5.8	6.1
Zr	34.8	28.6	27.9	22.2	28.5	28.6	78.6	82.9	80.7	82.6	80.1	83.5	80.3	82.8	81.3
Y	17.8	24.8	18.3	18.1	19.1	24.5	34.1	37.1	34.5	34.4	34.3	33.6	34.8	32.7	31.8
Sr	59.7	57.1	104.4	73.5	53.7	53.3	98.3	98.6	101.8	101.3	95.2	105.0	101.0	110.9	110.7
Rb	1.5	0.9	0.8	1.2	0.8	0.6	1.5	0.8	0.6	0.9	0.1	0.3	1.1	1.8	1.4
Zn	88.6	76.2	69.2	67.7	74.2	78.0	103.3	111.6	100.3	100.8	102.6	101.1	109.4	89.1	88.5
Cu	167.6	142.6	137.5	103.6	143.4	133.9	248.9	168.5	232.9	230.9	232.3	247.0	218.9	232.0	195.0
Ni	101.2	91.1	101.5	101.2	103.5	91.1	68.9	67.2	69.5	66.4	66.5	68.8	72.3	63.3	60.6
Cr	130.0	113.4	173.1	169.7	213.0	139.2	85.6	87.7	126.2	86.4	85.6	102.5	87.9	63.5	62.5
V	371.0	311.9	297.7	275.2	314.0	311.9	414.4	436.4	427.2	430.2	422.1	434.7	420.9	365.6	375.8
Ce	0.1	0.1	0.1	0.1	0.1	0.1	6.9	7.4	9.6	8.8	5.6	5.4	8.2	7.1	8.6
Ba	18.9	15.4	8.5	16.5	12.4	14.3	29.5	28.4	30.2	27.7	37.6	39.7	29.1	43.3	36.8

Table 8. Magnetic susceptibility and oxide mineralogy for Site 707.

Unit	Mt. conc. (%)	Grain size (mm)	Texture	PTS	Average magnetic susceptibility	N
1	~1	<0.15	skeletal	4	1.6	4
2	~1.5	~0.3	subequant to subskeletal	1	1.4	1
3	~1	~0.15	subequant irregular anhedral	6	1.2	10
4A	~2	~0.25	subequant irregular subskeletal	2	2.25	6
4B	~2	~0.1–0.15	fine skeletal	16	2.0	16
4C	~2	~0.15–0.25	subequant anhedral interstitial	13	2.75	41
5	2–3	0.15–0.40	subequant	2	4.0–2.8	8

Note: Mt. conc. = magnetite concentration; PTS = polished thin sections studied; K = cgs × 10^{-4} emu/cm^3·Oe; N = number of cores used in determining average susceptibility (K).

where recovery permitted. The results are shown in Figure 36 and Table 13. The thermal conductivity shows a gradual increase with depth with a large degree of small-scale variability. This is not uncharacteristic of carbonate sediments with a high water content (and is the reason we measured the thermal conductivity so frequently).

There are three extraordinarily high values in Hole 707A (above 2.0 $W \cdot m^{-1} \cdot K^{-1}$). These measurements may not be valid. Only two measurements were made in Hole 707B, and they are similar to the values at the top of Hole 707A. Measurements were resumed in Hole 707C, but problems were encountered due to low recovery and a long interval where most of the cores recovered were too hard to measure with the needle-probe technique, yet too soft to risk removing from the core liner and immersing in the water bath for the "slab-probe" technique.

Basement

Physical properties results for the assemblage of lithified sediments and interbedded volcanics cored at Hole 707C are reported below. The lithified sediments encountered at 280.3 mbsf were comprised predominantly of silicified limestone and glauconitic grainstones overlain by chert and chalk. The actual basement volcanics were encountered at 375.6 mbsf and consisted of basalts which had been hydrothermally altered to various degrees.

Discrete compressional-wave velocity and density measurements were made on minicore samples using similar methods to those used at Site 706. Acoustic impedances were then calculated. Thermal conductivities were evaluated on large split-core fragments at frequent intervals.

The variability in compressional-wave velocity, bulk density, and acoustic impedance for the various basement lithologies are given in Table 14 and illustrated in the lower portion of Figure 35. Compressional velocities measured perpendicular to the core axis varied between 2402 and 6090 m/s, whereas the velocity of 2402 m/s in the uppermost recovered basalt is caused by fractures. The average value for the velocity in the basalts is approximately 4000 m/s.

There is a general increase in the average velocity within the different basaltic flow units: 2860 m/s for Unit 1, 4270 m/s for Unit 2, 4710 m/s for Unit 3, 4960 m/s for Unit 5, and 4630 m/s for Unit 6. The only prominent boundary is located between Unit 3 and Unit 5 at 396.25 mbsf, where a dramatic increase in velocity and density occur. The gradual increase in velocity and density within Units 5 and 6 is disturbed by a few anomalously low measurements. These low values were most likely due to fractures within the samples.

Thermal Conductivity

The thermal conductivity within the uppermost units of the basement was significantly lower (1.3 $W \cdot m^{-1} \cdot K^{-1}$) than the conductivity of the overlying silicified sediments (1.8 $W \cdot m^{-1} \cdot K^{-1}$). Unit 3 of the basalt exhibited much higher conductivity (1.66–2.18 $W \cdot m^{-1} \cdot K^{-1}$), perhaps due to its decreased porosity. The low values for the top of Core 115-707C-24R are from a highly vesicular piece. The conductivity of Unit 4 shows

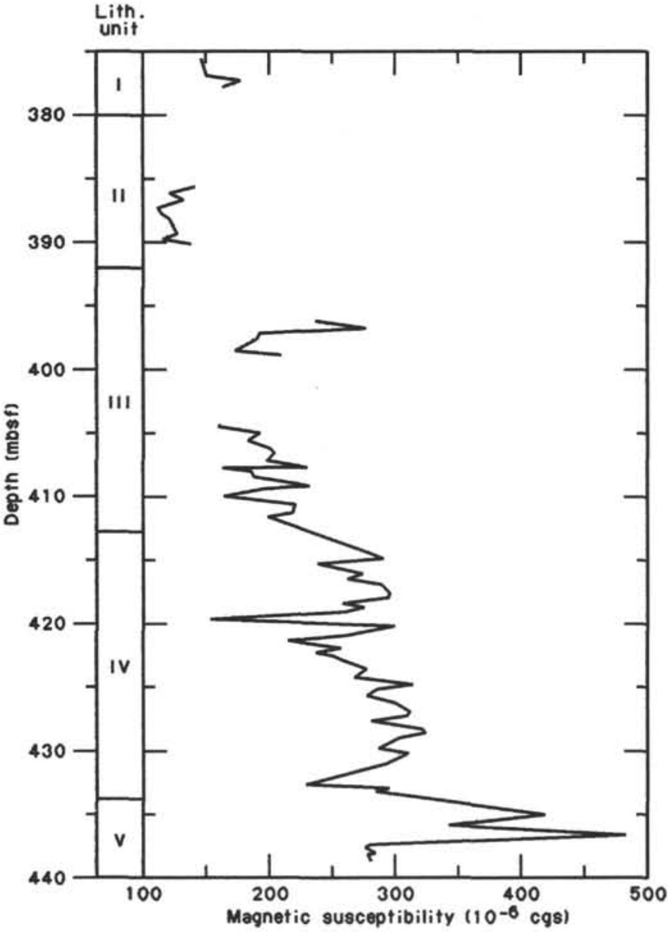

Figure 26. Magnetic susceptibility for 86 minicores cut from Site 707 basalts. The gaps reflect incomplete core recovery, and the unit numbers are those described in the text. There is an overall increase in susceptibility with depth in the core.

a fairly uniform increase with water depth, increasing from 1.58 $W \cdot m^{-1} \cdot K^{-1}$ at the top of the unit to 1.76 $W \cdot m^{-1} \cdot K^{-1}$ at the bottom. The low value below this is from the interbedded carbonate between Units 4 and 5.

Summary

We evaluated the physical properties of an ooze-chalk-limestone sequence with interbedded basalts and grainstones at Site 707. The nannofossil ooze and chalks had a relatively homogeneous composition with carbonate content between 90% and 95% and an average porosity of 70%.

Compressional-wave velocities remained fairly constant, but there was a large variation in V_s and shear strength between the hard chalks and softer ooze. It is unclear whether the chalk "chunks" observed are due to drilling disturbance and/or actual variations in *in-situ* hardness (see "Lithostratigraphy" section, this chapter).

Impedance contrasts were registered between the base of the soft ooze and successive chalks and interbedded chert. Stronger contrasts were present between the base of the chalks and the top of the limestone beds, and between the limestones and the downward-following interbedded basalt flows. The basalts showed some evidence for a progressive increase in velocity and density with successive flow units.

SEISMIC STRATIGRAPHY

Site 707 is located on the topographic high connecting the Seychelles and Saya de Malha Banks about 6 nmi to the east of a major north-trending submarine channel (Fig. 37). This channel shows up as a distinct feature on all available seismic lines throughout the region (CD-21/87, GC-24, RC17-07, and V34-06) and is characterized by substantial thinning of the sediment drape.

The original target for Site 707 (CARB-1A) was located on a single-channel seismic (SCS), air-gun line obtained by the *Charles Darwin*, cruise 21/87. This line shows moderately to poorly reflective layers which converge and diverge repeatedly or are broken up. These characteristics indicate a depositional history strongly influenced by the activity of bottom currents, leading to the erosion and redeposition of sediment over large areas on this topographic high. The intended drilling site (CARB-1A) was placed on a thick sediment sequence, estimated to be about 400 m, showing weak but fairly parallel internal reflectors.

Upon arriving in the vicinity of the projected site, we had to wait for about 4 hr before good global positioning satellite (GPS) fixes could be received. This extra time was spent surveying a profile immediately west of the projected site, using the *JOIDES Resolution's* 80-in.^{3} water gun and the 12- and 3.5-kHz depth profilers.

In this new seismic profile we identified a roughly 5-nmi-long section showing consistently parallel and, in comparison to CARB-1A, more pronounced internal reflectors. The basement was interpreted to occur at 0.41 s (two-way traveltime). Site 707 is located in the middle of that window of internally coherent reflectors, where the sediment is thickest (Fig. 38). Along the west to east seismic profile across the ridge, the basement reflector shows only gentle undulations with occasional offsets on the order of 0.1 s, or about 250 m, which we interpret as normal faults.

An uppermost seismically transparent sequence overlies a moderately strong reflector (**A**) at about 0.20 s (two-way traveltime) below the sediment-water interface (Fig. 39). This unit corresponds to the Pleistocene to upper Oligocene nannofossil oozes. Using measured *P*-wave velocities of about 1600 m/s (see "Physical Properties" section, this chapter), the thickness of this unit should be about 160 m. Core 115-707A-17H had low recovery and chert fragments in the core catcher. The two cores penetrating through this sub-bottom depth (115-707A-18H and -19H, 160.7-173.7 mbsf) had zero recovery, and the only clue as to the character of the reflector at 0.20 s is the chert fragments and a marked increase in acoustic impedance between Cores 115-707A-17H and -20X (see "Physical Properties" section, this chapter).

A second strong reflector (**B**) is seen at about 0.32 s (Fig. 39). Measured *P*-wave velocities in the material above this marker are slightly higher than in the uppermost sediments, indicating changes in lithology from oozes to consolidated chalks and occasional chert in these lower Oligocene to middle Eocene sediments. Taking a representative value of 1750 m/s, the reflector should be at about 265 mbsf. This corresponds roughly with an observed change in the cored material to more lithified and silicified carbonate rocks at 270–280 mbsf.

Between the **B** reflector and the basement (**C**) lies a region of discontinuous reflections (Fig. 39). We know from the cored material that this unit consists of glauconite-bearing foraminiferal chalks, carbonate sandstones and mudstones, and silicified limestones (see "Lithostratigraphy" section, this chapter). Measured *P*-wave velocities vary from 1900 m/s (chalks and sandstones) to 5000 m/s (silicified limestones). Furthermore, we esti-

Table 9. Index-properties data, Site 707.

Section interval (cm)	Depth (mbsf)	Water content (%)	Porosity (%)	Wet-bulk density (g/cm^3)	Dry-bulk density (g/cm^3)	Grain density (g/cm^3)	Carbonate content (wt%)
115-707A-							
1H-2, 65	2.15	46.18	69.46	1.55	0.83	2.68	93.94
1H-4, 36	4.86	51.62	73.83	1.49	0.72	2.67	91.87
2H-1, 138	7.98	55.51	77.83	1.45	0.65	2.84	91.46
2H-3, 35	9.95	54.52	76.73	1.52	0.69	2.77	91.84
2H-6, 84	14.94	52.66	73.74	1.45	0.68	2.55	89.70
3H-2, 55	18.25	49.00	71.61	1.48	0.76	2.65	89.56
3H-4, 30	21.00	47.65	65.79	1.51	0.79	2.13	85.00
4H-1, 90	26.70	51.20	68.57	1.48	0.72	2.09	94.54
4H-3, 89	29.69	47.80	70.79	1.52	0.79	2.67	88.92
4H-5, 56	32.36	49.75	73.62	1.52	0.76	2.85	95.28
5H-2, 89	37.89	47.39	70.78	1.53	0.81	2.72	87.93
5H-4, 37	40.37	48.03	70.46	1.52	0.79	2.61	94.09
5H-6, 29	43.29	43.44	67.79	1.62	0.91	2.77	94.65
6H-2, 53	47.13	47.16	70.27	1.53	0.81	2.68	93.00
6H-4, 50	50.10	45.42	70.00	1.56	0.85	2.83	91.61
6H-7, 30	54.40	41.56	66.17	1.62	0.95	2.78	86.44
7H-2, 49	56.69	40.64	65.43	1.62	0.96	2.80	94.31
7H-4, 49	59.69	43.99	67.60	1.58	0.89	2.69	84.83
7H-6, 90	63.10	47.03	71.12	1.54	0.82	2.80	94.98
8H-2, 54	66.34	49.63	72.38	1.48	0.75	2.69	94.70
8H-4, 53	69.33	46.19	69.90	1.57	0.84	2.73	95.27
8H-6, 56	72.36	46.66	72.05	1.60	0.85	2.98	94.08
9H-2, 84	76.34	42.60	66.60	1.59	0.91	2.72	94.98
9H-4, 56	79.06	44.43	68.77	1.58	0.88	2.79	92.80
9H-6, 43	81.93	43.71	67.50	1.57	0.88	2.70	94.83
10H-2, 83	85.93	42.34	66.62	1.60	0.93	2.75	90.43
10H-4, 86	88.96	44.80	68.79	1.68	0.93	2.75	87.68
10H-6, 45	91.55	44.51	67.88	1.56	0.87	2.66	89.16
12H-2, 53	104.83	47.0	70.9	1.54	0.82	2.78	94.08
12H-4, 85	108.15	41.15	64.99	1.61	0.95	2.69	86.24
12H-6, 50	110.80	42.53	67.00	1.63	0.94	2.78	86.11
13H-2, 48	114.38	41.75	66.01	1.54	0.90	2.74	94.68
13H-4, 52	117.42	46.08	69.79	1.57	0.84	2.73	95.00
14H-2, 54	124.04	47.31	68.91	1.59	0.84	2.49	93.46
14H-4, 47	126.97	51.67	72.59	1.53	0.74	2.50	95.55
15H-2, 58	133.68	52.22	73.95	1.46	0.70	2.62	92.19
15H-4, 54	136.64	52.38	74.85	1.46	0.70	2.73	92.42
16H-2, 54	143.34	38.60	63.58	1.68	1.03	2.81	96.10
16H-5, 103	148.33	40.79	64.87	1.64	0.97	2.71	93.56
17H-1, 125	152.25	42.19	66.87	1.61	0.93	2.80	84.15
20X-3, 143	178.13	38.23	62.52	1.69	1.04	2.73	92.80
21X-4, 141	189.31	34.89	59.15	1.74	1.13	2.74	93.68
22X-3, 140	197.50	34.16	58.88	1.74	1.14	2.80	92.22
22X-5, 139	200.49	37.75	61.59	1.69	1.05	2.68	90.44
23X-2, 50	204.70	35.48	60.04	1.75	1.13	2.77	90.30
23X-4, 85	208.05	32.94	55.70	1.77	1.18	2.59	91.38
23X-6, 136	211.56	35.68	59.64	1.74	1.12	2.70	88.19
115-707B-							
1H-3, 48	3.48	51.12	74.17	1.48	0.72	2.77	95.83
2H-4, 117	15.17	47.91	71.29	1.53	0.80	2.73	93.52
3H-3, 36	25.46	51.81	73.96	1.47	0.71	2.66	95.78
3H-5, 45	25.55	46.99	70.41	1.54	0.82	2.71	95.34
4H-3, 118	32.88	48.76	71.98	1.52	0.78	2.73	95.04
4H-5, 120	35.90	45.29	68.65	1.57	0.86	2.67	95.56
5H-2, 63	40.53	48.72	72.42	1.51	0.78	2.79	95.01
5H-4, 85	43.75	43.05	67.25	1.61	0.92	2.75	96.81
6H-2, 25	49.75	47.99	71.34	1.53	0.80	2.73	92.45
6H-4, 64	53.14	45.05	68.67	1.55	0.85	2.70	92.19
7H-2, 134	60.44	47.50	70.97	1.52	0.80	2.73	94.80
7H-4, 113	63.23	45.75	69.94	1.57	0.85	2.79	96.79
7H-6, 113	66.23	44.54	72.36	1.57	0.87	3.30	95.01
8H-2, 93	69.63	47.62	71.36	1.55	0.81	2.77	95.49
8H-4, 113	72.83	43.65	67.42	1.58	0.89	2.70	95.94
8H-6, 64	75.34	39.16	66.56	1.68	1.02	3.13	97.03
9H-2, 104	79.44	47.37	71.01	1.53	0.81	2.75	92.93
9H-4, 65	82.05	46.64	69.76	1.57	0.84	2.67	93.45
10H-5, 111	93.61	44.61	68.54	1.62	0.90	2.74	94.27
11H-3, 106	100.16	46.29	69.46	1.54	0.83	2.67	94.02
11H-5, 132	103.42	45.22	69.50	1.58	0.86	2.79	94.91
13H-1, 100	116.30	44.77	69.72	1.58	0.87	2.87	94.75
13H-3, 100	119.30	46.18	70.14	1.56	0.84	2.77	95.24
13H-5, 100	122.30	42.43	67.12	1.61	0.93	2.80	94.62

Table 9 (continued).

Section interval (cm)	Depth (mbsf)	Water content (%)	Porosity (%)	Wet-bulk density (g/cm^3)	Dry-bulk density (g/cm^3)	Grain density (g/cm^3)	Carbonate content (wt%)
115-707C-							
3R-2, 89	195.89	32.44	55.90	1.78	1.20	2.68	94.69
3R-4, 23	198.23	35.10	59.50	1.75	1.14	2.75	92.03
3R-6, 135	202.35	35.52	60.17	1.73	1.11	2.78	92.72
6R-3, 65	226.20	33.35	55.82	1.76	1.17	2.56	92.26
6R-3, 96	226.51	32.13	56.17	1.79	1.22	2.74	93.84
7R-3, 142	236.52	12.13	20.45	1.70	1.49	1.89	90.54
7R-5, 6	238.16	12.44	22.62	1.82	1.59	2.09	79.79
9R-1, 128	252.68	9.90	19.98	1.72	1.55	2.31	84.90
10R-2, 33	262.83	33.17	56.42	1.75	1.17	2.64	87.83
10R-4, 114	266.64	33.46	51.72	1.72	1.15	2.15	84.21

mated the average velocity to be 2500 m/s for this unit from the thickness of the cored section.

Because core recovery was low, we do not have a direct measurement of the proportions of rock types through this region. However, using the average velocity and measured samples, we estimate that 80% is chalk and carbonate sandstone and 20% is silicified limestone.

The basement reflector (C) represents the top of a thick sequence of subaerially erupted basalt flows, penetrated from 375 to 443 mbsf. These are variably altered and yield *P*-wave velocities in the range of 2800–5000 m/s (see "Physical Properties" section).

DOWNHOLE MEASUREMENTS

Introduction

Site 707 was the first site where downhole logging was attempted on Leg 115. The logging program was carried out in the deepest hole, Hole 707C, and was only partially successful. The logging plan included three runs using different combinations of standard Schlumberger logging tools. The first run was the seismic stratigraphy combination; the second was the geochemical combination; and the third, the lithoporosity combination. The drill pipe had been set to 1703 meters below rig floor (mbrf), 150 mbsf, due to worries about hole stability in the soft carbonate sediments at this site.

Operations

The seismic stratigraphy logging run was the only successful one at this site. This run was made from the bottom of the hole at 1995 to 1529 mbrf, above the level of the seafloor. The seismic combination cannot measure through the drill pipe, so the interval of useful data extends from the bottom of the hole to 1704 mbrf.

The geochemical run encountered a major bridge in the hole at 1900 mbrf, some 95 m above the bottom of the hole. The geochemical combination can obtain valid data through the drill pipe, so we decided to log the interval from the bridge to above the sea floor and then attempt to clean out the hole with a wiper trip. At this time, the Induced Gamma Ray Spectrometry Tool (the GST) failed to calibrate downhole, and we had to abandon the logging run. We brought the logging tools back to the surface and performed a wiper trip to clear out the bridges in the hole. We then rigged up the geochemical combination using the backup GST. This tool failed during the on-deck testing, so we decided to proceed to the lithoporosity combination.

The lithoporosity logging tool string encountered a major bridge in the hole at 1733 mbrf, only 30 m below the end of the drill pipe. We were unable to penetrate this bridge, so we returned the tool string to the surface.

There was insufficient time to rig up the sidewall entry sub and resume the logging because of time constraints from the GPS satellite navigation window. The GPS satellite system has enough satellites visible for site location navigation for only a few hours each day. It was essential that we pull the pipe out of the hole and make the transit to the next site so that we could arrive during that navigation time window.

Logging Results

Logging results for Hole 707C are shown in the summary log plot (Fig. 40). The caliper and natural gamma-ray data are plotted together in the left column. The three resistivity logs—shallow, deep, and focused—are plotted in the center column. The sonic travel time log, converted to velocity, is plotted in the right column. Selected parts of the data for the lower 100 m of Hole 707C are shown in more detail in Figure 41.

The diameter of Hole 707C is approximately 16 in. through most of the sedimentary and chalk sequences. A hard layer at approximately 243 mbsf is the first major reduction in hole size and represents a chalk layer in the lower part of Unit IIB. The hole is larger in the 40 m below this until a series of thin, hard layers cause reductions in hole diameter in the interval from 280 to 295 mbsf, which corresponds to the upper 15 m of Unit III. Below this interval the hole widens out again and is quite smooth, although it very gradually decreases in diameter until about 367 mbsf.

The diameter of Hole 707C decreases at 367 mbsf over a 5-m depth range and then increases again over a similar range. This is slightly above the first recovered basalt at 375.6 mbsf. The hole remains quite wide through the upper basalt and through most of the uppermost layer of interbedded sediments. The hole then narrows to 402 mbsf and rewidens gradually to 413 mbsf. The tool is at the top of the seismic string, so it did not measure below this depth.

The natural gamma-ray data are low in Unit II to 250 mbsf. They drop abruptly at the top of Unit III and then show a smooth, accelerating increase through Unit III and the upper part of Unit IV. The gamma count peaks at about 325 mbsf and drops below that until about 340 mbsf, still within Unit IV. The count increases irregularly through Unit V to a maximum at 371 mbsf, just above the contact with basalt. The counts drop in the uppermost basalt and then remain steady at about 4 API units, typical for fairly fresh basalt.

Interbedded sediments from 391 to 400 mbsf stand out clearly on Figure 40. The gamma-ray count in the basalts from 401 to 415 mbsf is slightly higher than that in the upper units, perhaps showing more alteration. The counts in the interval from 415 to 431 mbsf again are quite low. The counts start to increase from 431 to 434 mbsf as the second interbedded sediment sequence is approached. The lowest point for natural gamma data is 421 mbsf.

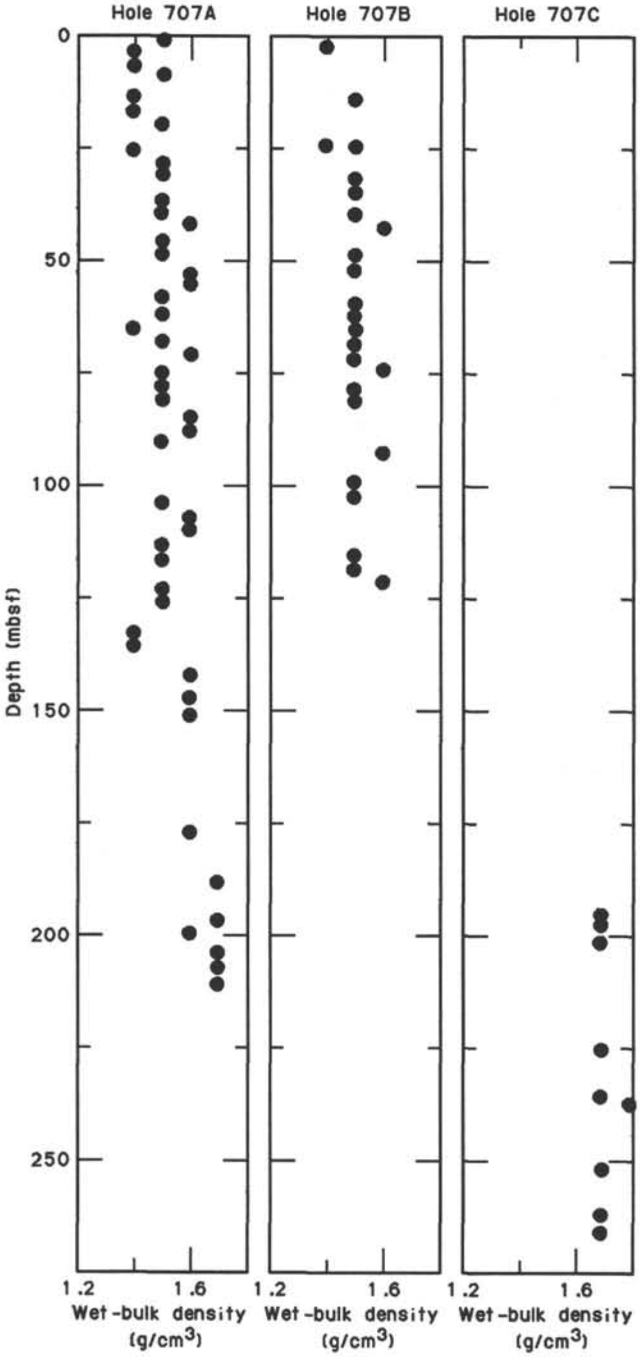

Figure 27. Wet-bulk density at Site 707.

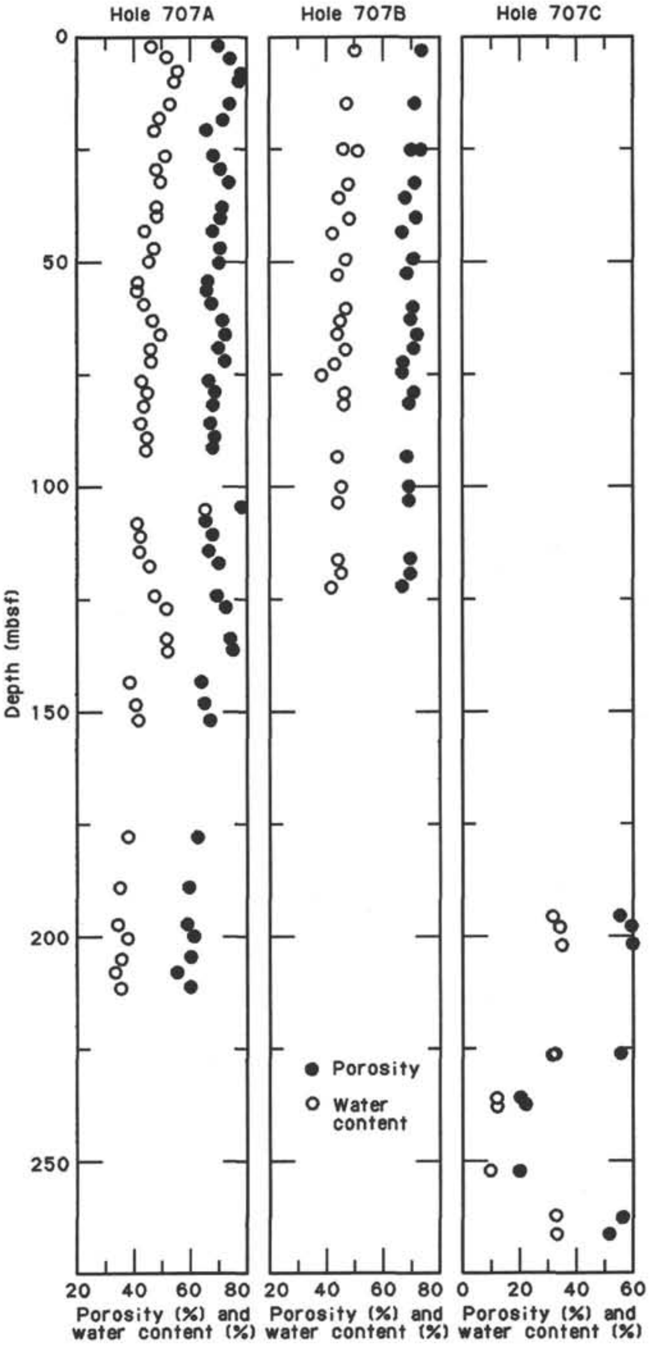

Figure 28. Porosity (%) and water content at Site 707.

Compressional-wave velocities are shown in Figure 42. The sediments have a quite uniform velocity near 1500 m/s to 190 mbsf. There is a steady increase in velocity (with some irregularities) from 190 to 250 mbsf, where the velocity is about 1950 m/s. A very large increase to 3400 m/s occurs in the hard layer at 250 mbsf. The velocity is fairly uniform near 1950 m/s below this to a depth of 280 mbsf. The velocity goes up to 2800 m/s at the top of the chalks and limestones of Unit IV and shows considerable variability in the range from 2000 to 2500 m/s throughout the unit. This is in accord with the mixed lithologies recovered here.

There is a very sharp increase in velocity to 4600 m/s in the silicified limestone just above the basalt at 372 mbsf. The velocity in the basalt shows a steady increase downhole from about 3200 m/s at 375 mbsf to 5700 m/s at 430 mbsf, the lowest point of measurement. The upper interbedded sediments stand out clearly in the 391–400 mbsf depth interval. The velocities in the well log are distinctly below those measured on selected specimens from the recovered cores (see "Physical Properties" section, this chapter). This is undoubtedly due to the fact that the log data include the effects of fractures, unit margins, and alteration. Laboratory measurements tend to be made on more massive and coherent specimens that can withstand the sampling process.

The three resistivity logs generally track very well. This indicates that there is little disturbance to the formation caused by drilling and that the formations are relatively unfractured. These data follow quite similar trends to those shown in the seismic velocity section discussed above. The resistivity is responding to density, porosity, and fracturing just like the seismic velocity.

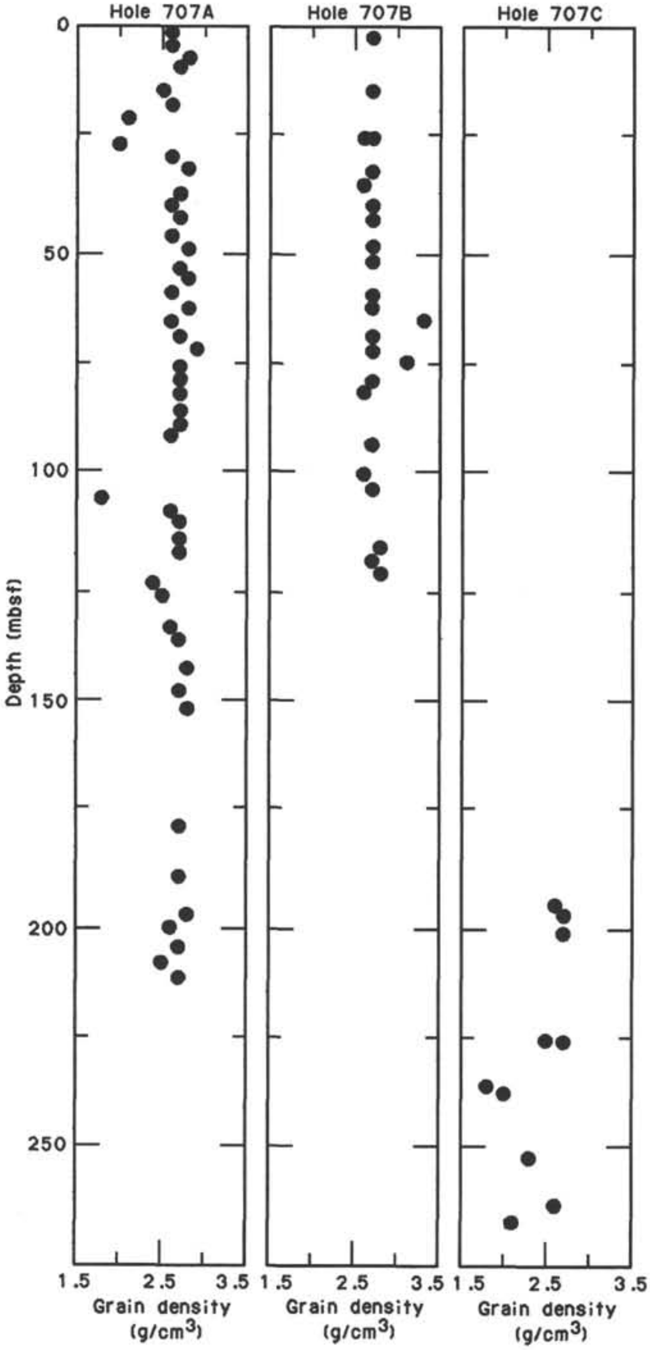

Figure 29. Grain density at Site 707.

The decrease in fracturing in the lower basalt unit from 400 to 430 mbsf is quite evident. The resistivity tool is lowest on the string.

REFERENCES

Baas Becking, L.G.M., and Moore, D., 1959. Density distribution in sediments. *J. Sediment. Petrol.*, 29:47-55.

Backman, J., and Shackleton, N. J., 1983. Quantitative biochronology of Pliocene and early Pleistocene calcareous nannofossils from the Atlantic, Indian, and Pacific Oceans. *Mar. Micropaleontol.*, 8:141-170.

Barron, J. A., and Keller, G., 1982. Widespread Miocene deep-sea hiatuses: coincidence with periods of global cooling. *Geology*, 10:577-581.

Barron, J. A., Keller, G., and Dunn, D. A., 1985a. A multiple microfossil biochronology for the Miocene. *Geol. Soc. Am. Mem.*, 163:21-36.

Barron, J. A., Nigrini, C. A., Pujos, A., Saito, T., Theyer, F., Thomas, E., and Weinreich, N., 1985b. Synthesis of biostratigraphy, central equatorial Pacific, Deep Sea Drilling Project, Leg 85: refinement of Oligocene to Quaternary biochronology. *In* Mayer, L., Theyer, F., et al., *Init. Repts. DSDP*, 85: Washington (U.S. Govt. Printing Office), 905-937.

Berggren, W. A., Kent, D. V., and Van Couvering, J. A., 1985. The Neogene: Part 2. Neogene geochronology and chronostratigraphy. *In* Snelling, N. J. (Ed.), *The Chronology of the Geological Record*, Geol. Soc. London Mem., 10:211-260.

Broecker, W. S., and Peng, T.-H., 1982. *Tracers in the Sea*: Palisades, NY (Eldigio Press).

Courtillot, V., Besse, J., Vandamme, D., Montigny, R., Jaeger, J.-J., and Cappetta, H., 1986. Deccan flood basalts at the Cretaceous-Tertiary boundary? *Earth Planet. Sci. Lett.*, 80:361-374.

Fisher, R. L., Bunce, E. T., et al., 1974. *Init. Repts. DSDP*, 24: Washington (U.S. Govt. Printing Office).

Fisher, R. L., Sclater, J. G., and McKenzie, D. P., 1971. Evolution of the Central Indian Ridge, western Indian Ocean. *Geol. Soc. Am. Bull.*, 82:553-562.

Gardner, J. V., Nelson, C. S., and Baker, P. A., 1986. Distribution and characteristics of pale green laminae in sediments from the Lord Howe Rise: a probable late Neogene and Quaternary tephrostratigraphic record. *In* Kennett, J. P., von der Borch, C. C., et al., *Init. Repts. DSDP*, 90: Washington (U.S. Govt. Printing Office), 1145-1159.

Gartner, S., 1977. Calcareous nannofossil biostratigraphy and revised zonation of the Pleistocene. *Mar. Micropaleontol.*, 2:1-25.

Hempel, P., and Mayer, L., in press. Seismic lithostratigraphy with biogenic silica on the Voring Plateau, Norwegian sea. *In* Eldholm, O., Thiede, J., Taylor, E., et al., *Proc. ODP, Sci. Results*, 104: College Station, TX (Ocean Drilling Program).

Hurd, D. C., 1983. Physical and chemical properties of siliceous skeletons. *In* Aston, S. R. (Ed.), *Silicon geochemistry and biogeochemistry*: London (Academic Press), 187-242.

Martini, E., 1971. Standard Tertiary and Quaternary calcareous nannoplankton zonation. *In* Farinacci, A. (Ed.), *Proc. II Planktonic. Conf. Roma, 1971*: Rome (Ed. Tecnoscienza), 739-777.

Nocchi, M., Parisi, G., Monaco, P., Monechi, S., Madile, M., Napoleone, G., Ripepe, M., Orlando, M., Premoli Silva, I., and Bice, D. M., 1986. The Eocene-Oligocene boundary in the Umbrian pelagic sequences, Italy. *In* Pomerol, C., and Premoli Silva, I. (Eds.), *Terminal Eocene Events*: Amsterdam (Elsevier), 25-50.

Okada, H., and Bukry, D., 1980. Supplementary modification and introduction of code numbers to the low-latitude coccolith biostratigraphic zonation (Bukry, 1973; 1975). *Mar. Micropaleontol.*, 5:321-325.

Sager, W. W., 1986. Magnetic susceptibility measurements of metal contaminants in ODP Leg 101 cores. *In* Austin, J. A., Jr., Schlager, W., et al., *Proc. ODP, Init. Repts.*, 101: College Station, TX (Ocean Drilling Program), 39-45.

Sandstrom, M., and Gieskes, J. M., 1974. Interstitial water studies, Leg 24. *In* Fisher, R. L., Bunce, E. T., et al., *Init. Repts. DSDP*, 24: Washington (U.S. Govt. Printing Office), 799-810.

Sanfilippo, A., Westberg-Smith, M. J., and Riedel, W. R., 1985. Cenozoic radiolaria. *In* Bolli, H. M., Saunders, J. B., and Perch-Nielsen, K. (Eds.), *Plankton Stratigraphy*: Cambridge (Cambridge Univ. Press), 631-712.

Takahashi, T., 1975. Carbonate chemistry of sea water and the calcite compensation depth in the oceans. *In* Sliter, W. V., Bé, A.W.H., and Berger, W. H. (Eds.), *Dissolution of Deep Sea Carbonates*: Spec. Publ. Cushman Found. Foram. Res., 13:11-26.

Vincent, E., 1974. Cenozoic planktonic biostratigraphy and paleoceanography of the tropical western Indian Ocean. *In* Fisher, R. L., Bunce, E. T., et al., *Init. Repts. DSDP*, 24: Washington (U.S. Govt. Printing Office), 1111-1150.

________, 1977. Indian Ocean Neogene planktonic foraminiferal biostratigraphy and its paleoceanographic implications. *In* Heirtzler, J. R., et al. (Eds.), *Indian Ocean Geology and Biostratigraphy*: Washington (American Geophysical Union), 469-584.

Ms 115A-106

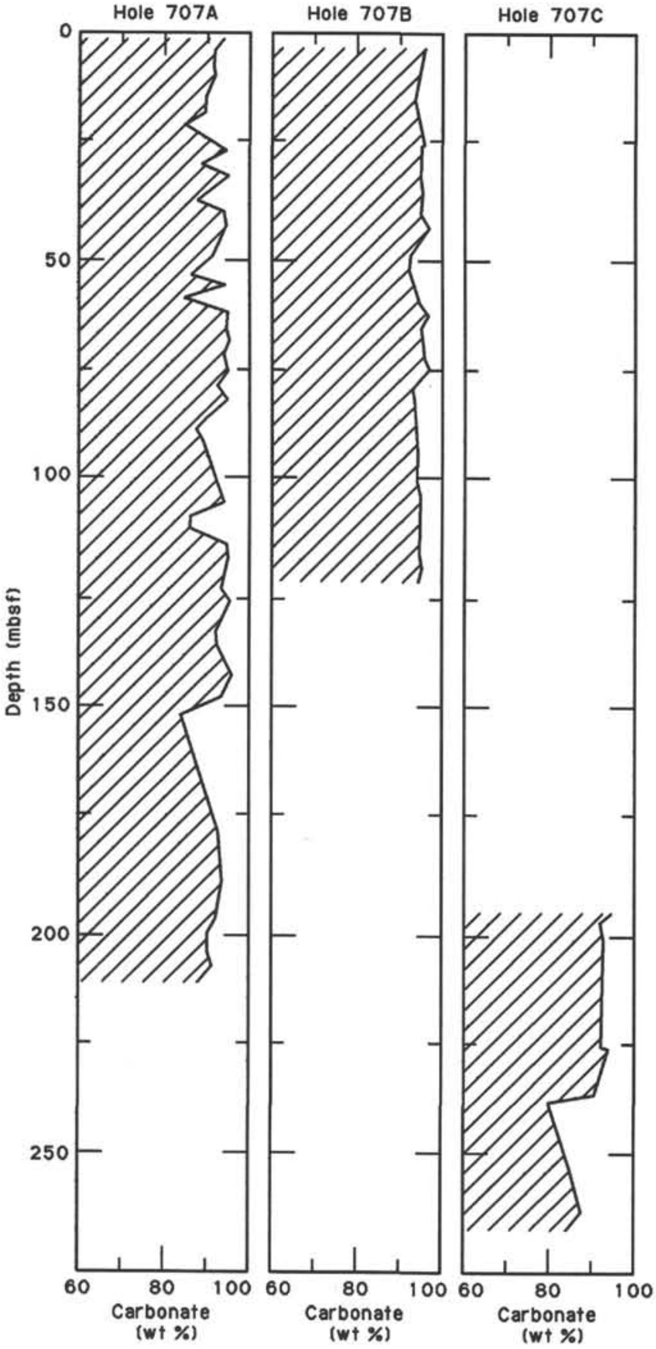

Figure 30. Carbonate content of samples for which the index properties were measured at Site 707.

Table 10. Compressional-wave velocity and acoustic impedance data, Site 707.

Section interval (cm)	Depth (mbsf)	V_p (m/s)	Acoustic impedance ($g/cm^2 \cdot s \cdot 10^5$)
115-707A-			
10H-2, 83	85.93	1502	2.40
10H-4, 86	88.96	1540	2.59
10H-6, 45	91.55	1539	2.40
12H-2, 53	104.83	1583	2.44
12H-2, 85	105.15	1509	2.43
12H-6, 50	110.80	1555	2.53
13H-2, 48	113.70	1487	2.29
14H-2, 54	124.04	1561	2.48
14H-4, 47	126.97	1665	2.55
15H-2, 58	133.68	1513	2.21
15H-4, 54	136.64	1522	2.22
16H-2, 52	143.32	1511	2.54
16H-5, 103	148.33	1571	2.58
17H-1, 125	152.25	1594	2.57
20X-3, 143	178.13	1557	2.63
21X-4, 141	189.31	1540	2.68
21X-6, 84	191.74	1556	2.68
22X-3, 140	197.50	1565	2.72
22X-5, 139	200.49	1556	2.63
23X-4, 85	208.05	1548	2.74
117-707B-			
5H-2, 63	40.53	1531	2.31
5H-4, 85	43.75	1560	2.51
6H-2, 25	49.75	1555	2.38
6H-4, 64	53.14	1545	2.39
7H-2, 134	60.44	1802	2.74
7H-4, 113	63.23	1473	2.31
7H-6, 113	66.23	1561	2.45
8H-4, 113	72.83	1560	2.46
8H-6, 64	75.34	1510	2.54
9H-2, 104	79.44	1482	2.27
9H-4, 65	82.05	1470	2.31
10H-5, 111	93.61	1571	2.55
11H-3, 106	103.16	1531	2.36
11H-5, 132	103.42	1537	2.43
115-707C-			
3R-4, 23	198.23	1547	2.75
3R-6, 135	202.37	1528	2.64
6R-3, 65	226.20	1567	2.76
6R-3, 96	226.51	1553	2.78
7R-3, 142	236.52	1557	2.65
7R-5, 6	238.16	1481	2.70
9R-1, 128	252.68	1604	2.76
10R-4, 117	266.67	1539	2.65

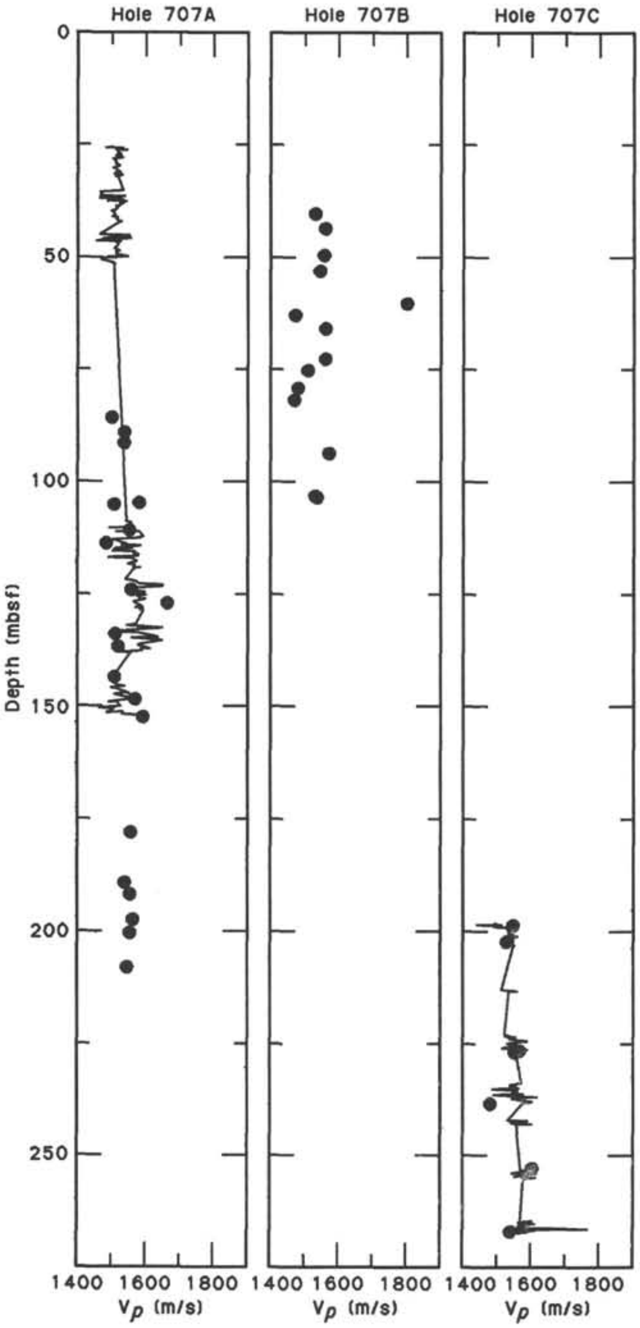

Figure 31. Compressional-wave velocity at Site 707. Shown are discrete sample measurements as well as *P*-wave logger data.

Table 11. Shear-wave velocity data, Site 707.

Section interval (cm)	Depth (mbsf)	V_s (m/s)
115-707A-		
2H-3, 30	9.90	97
4H-5, 57	32.37	30
5H-2, 95	37.95	74
5H-6, 40	43.40	95
9H-2, 40	75.90	122
9H-4, 40	78.90	132
9H-6, 30	81.80	114
10H-2, 88	85.98	150
15H-4, 118	137.28	118
16H-2, 52	143.32	56
16H-5, 103	148.33	78
17H-1, 126	152.26	106
20X-3, 142	178.12	167
21X-4, 142	189.32	72
21X-6, 85	191.75	177
22X-3, 140	197.50	116
22X-5, 140	200.50	153
23X-4, 86	208.06	110
23X-6, 137	211.57	155
115-707B-		
2H-4, 119	15.19	54
6H-4, 66	53.16	97
115-707C-		
3R-4, 24	198.24	62
3R-6, 64	201.64	88
3R-6, 137	202.37	94
6R-3, 66	226.21	225
6R-3, 93	226.48	162
7R-3, 121	236.31	117
7R-5, 6	238.16	132
10R-2, 33	262.83	229
10R-4, 44	265.94	178

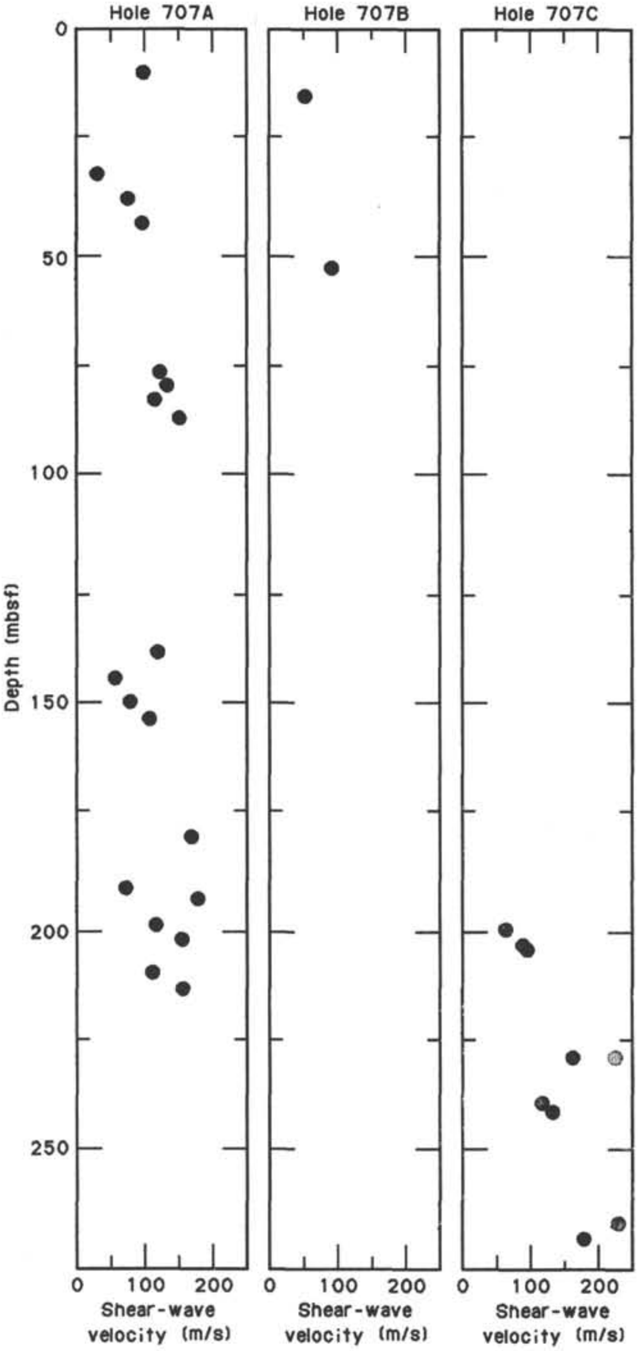

Figure 32. Shear-wave velocity at Site 707.

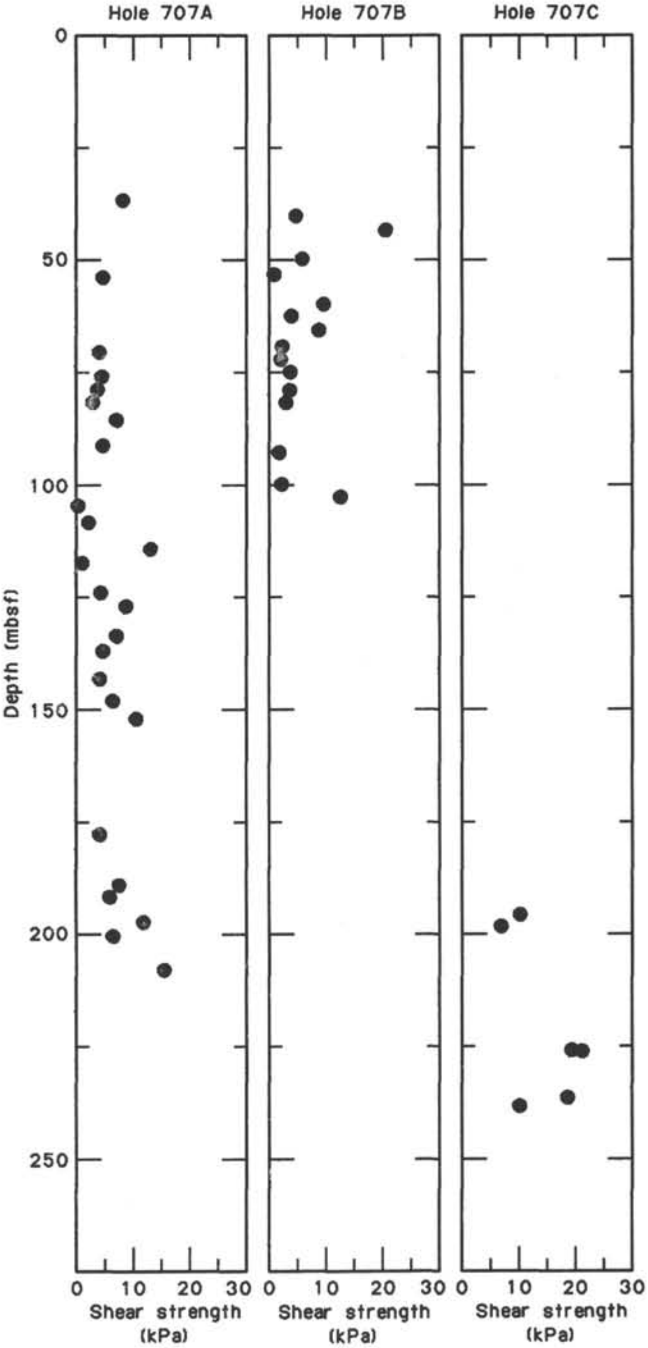

Figure 33. Shear strength at Site 707.

Table 12. Motorized shear strength data, Site 707.

Section interval (cm)	Depth (mbsf)	Peak (kPa)
115-707A-		
5H-2, 26	37.26	8.3
6H-7, 31	54.41	4.8
8H-5, 59	70.89	4.2
9H-2, 80	76.30	4.8
9H-4, 50	79.00	3.8
9H-6, 44	81.94	3.0
10H-2, 83	85.93	7.1
10H-6, 48	91.58	4.8
12H-2, 50	104.80	0.6
12H-4, 121	108.51	2.3
13H-2, 48	114.38	13.1
13H-4, 48	117.38	1.3
14H-2, 48	123.98	4.4
14H-4, 60	127.10	8.9
15H-2, 58	133.68	7.1
15H-4, 85	136.95	4.8
16H-2, 60	143.40	4.3
16H-5, 95	148.25	6.5
17H-1, 117	152.17	10.6
20X-3, 117	177.87	4.3
21X-4, 139	189.29	7.7
21X-6, 93	191.83	5.9
22X-3, 136	197.46	11.9
22X-5, 138	200.48	6.5
23X-4, 94	208.14	15.4
115-707B-		
5H-2, 64	40.54	4.7
5H-4, 95	43.85	20.1
6H-2, 65	50.15	5.9
6H-4, 95	53.45	1.2
7H-2, 95	60.05	9.5
7H-4, 55	62.65	4.0
7H-6, 76	65.86	8.5
8H-2, 75	69.45	2.4
8H-4, 65	72.35	2.1
8H-6, 55	75.25	3.8
9H-2, 75	79.15	3.7
9H-4, 56	81.96	3.1
10H-5, 76	93.26	2.0
11H-3, 85	99.95	2.4
11H-5, 85	102.95	12.4
115-707C-		
3R-4, 31	23.91	10.6
3R-2, 86	21.46	7.1
6R-3, 67	51.67	19.5
6R-3, 80	51.80	21.4
7R-3, 134	61.94	19.0
7R-5, 13	63.73	10.7

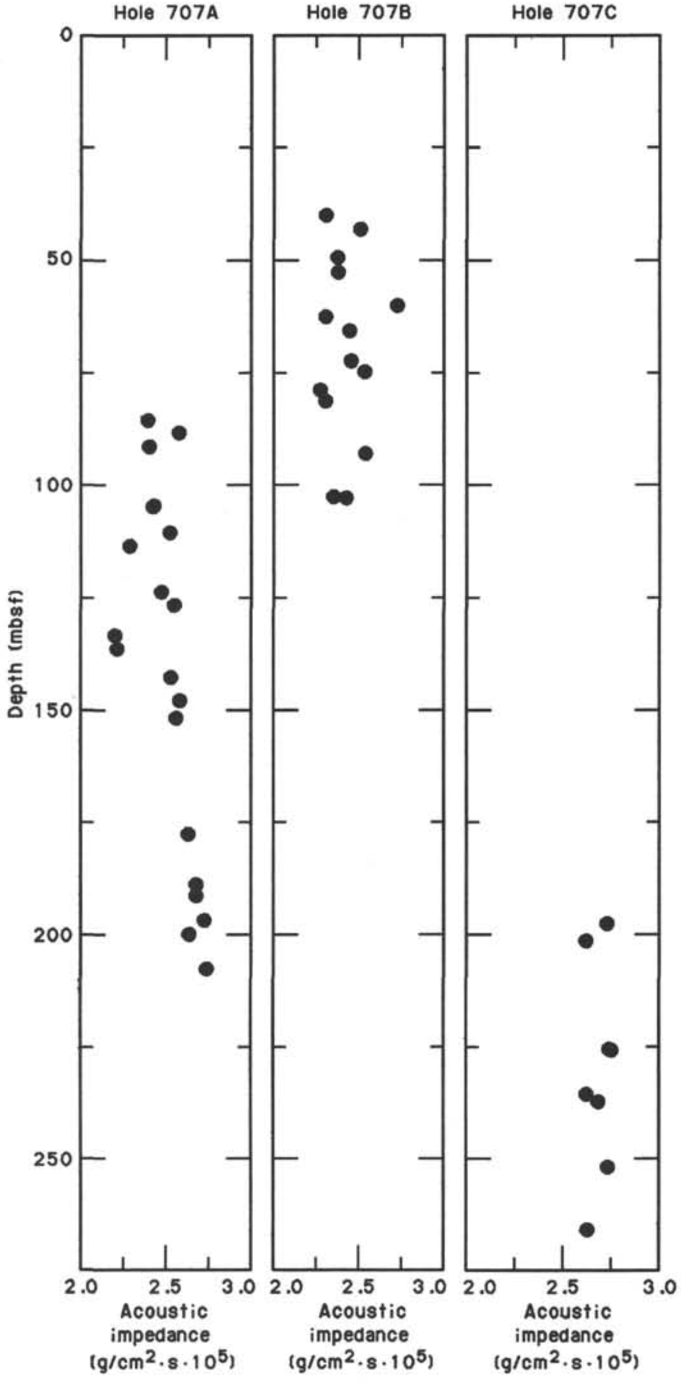

Figure 34. Calculated values of acoustic impedance at Site 707.

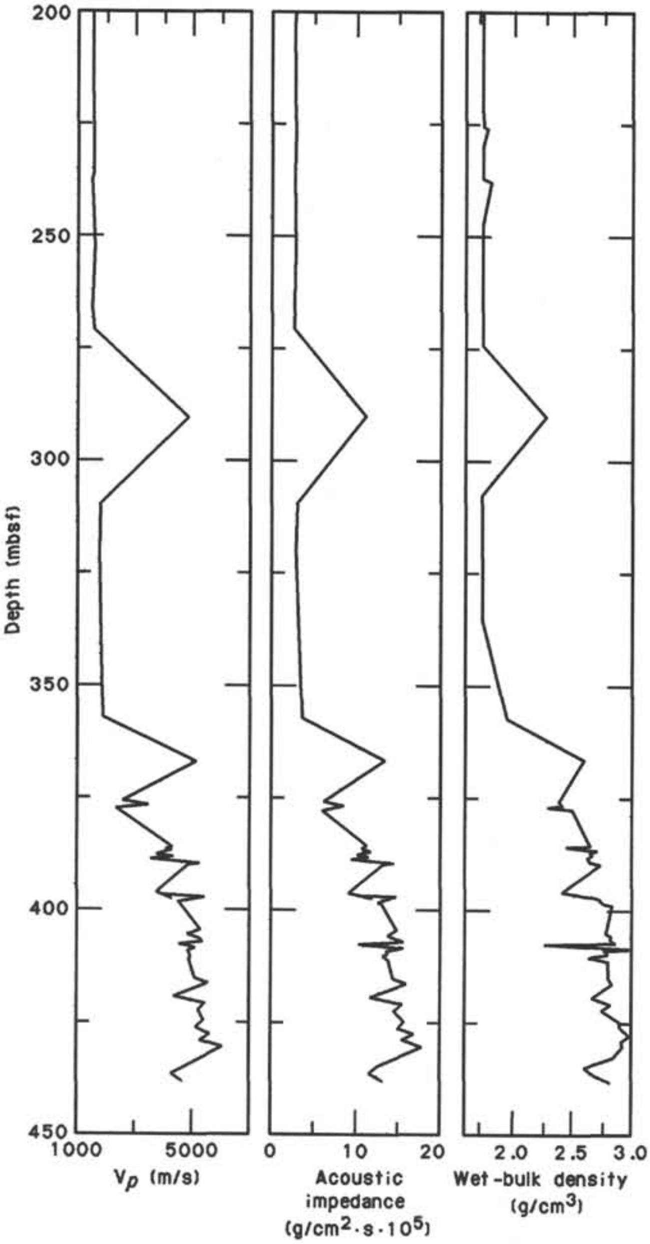

Figure 35. Compressional-wave velocity, acoustic impedance, and wet-bulk density in Hole 707C.

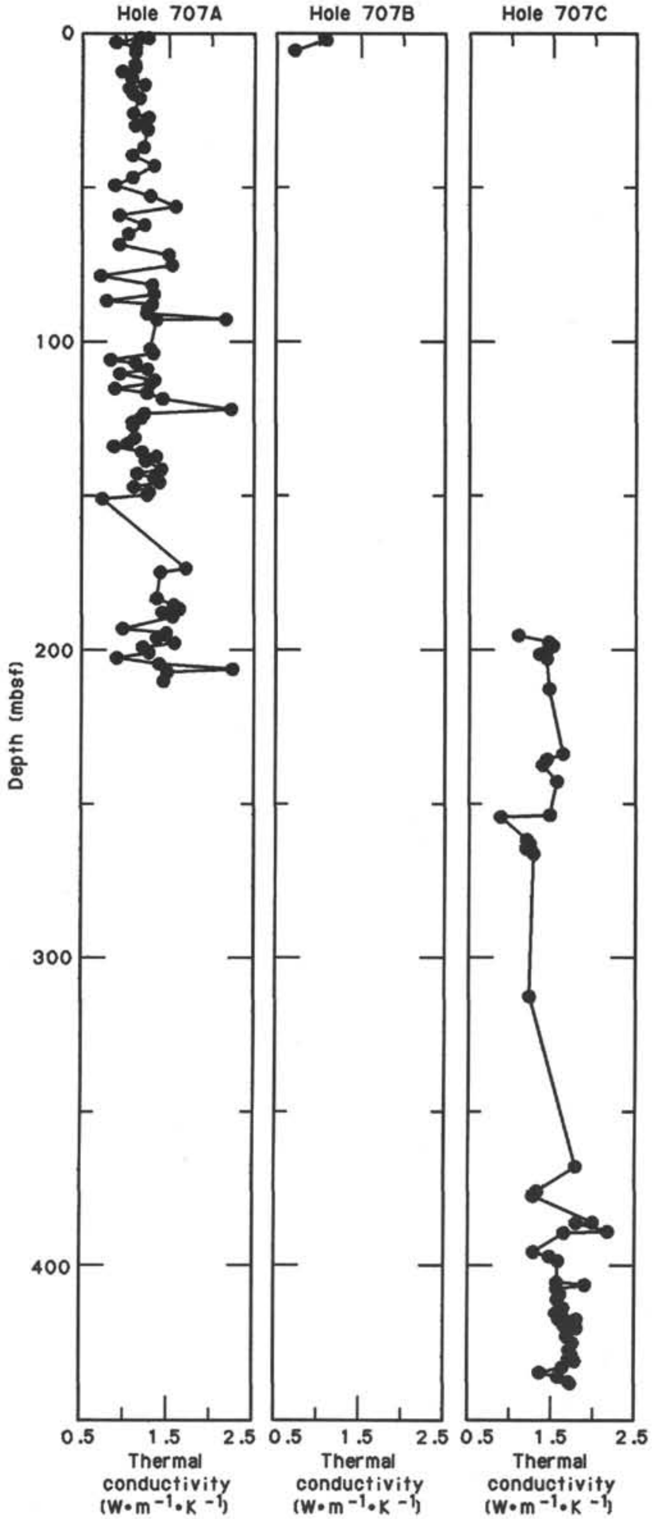

Figure 36. Thermal conductivity at Site 707.

Table 13. Thermal conductivity data, Site 707.

Section interval (cm)	Depth (mbsf)	Thermal conductivity ($W \cdot m^{-1} \cdot K^{-1}$)
115-707A-		
1H-2, 80	2.30	1.1690
1H-2, 80	2.30	1.2580
1H-3, 80	3.80	0.8870
1H-4, 80	5.30	1.1090
1H-5, 30	6.30	1.1050
2H-3, 80	10.40	1.1020
2H-4, 35	11.45	1.1060
2H-5, 35	12.95	0.9550
2H-6, 80	14.90	1.0730
3H-1, 130	17.50	1.2150
3H-2, 80	18.50	1.0420
3H-3, 80	20.00	1.0880
3H-4, 80	21.50	1.1690
4H-1, 110	26.90	1.0840
4H-2, 90	28.20	1.2670
4H-3, 80	29.60	1.2230
4H-4, 80	31.10	1.1110
4H-5, 40	32.20	1.2580
5H-2, 70	37.70	1.2112
5H-4, 70	40.70	1.0790
5H-6, 70	43.70	1.3320
6H-2, 80	47.40	1.0900
6H-4, 80	50.40	0.8820
6H-6, 80	53.40	1.2960
7H-2, 80	57.00	1.5800
7H-4, 80	60.00	0.9340
7H-6, 70	62.90	1.2230
8H-2, 80	66.60	1.0390
8H-4, 80	69.60	0.9340
8H-6, 80	72.60	1.5020
9H-2, 80	76.30	1.5420
9H-4, 70	79.20	0.7130
9H-6, 80	82.30	1.3080
10H-2, 40	85.50	1.3290
10H-3, 101	87.61	0.7880
10H-4, 80	88.90	1.3090
10H-5, 60	90.20	1.2650
10H-6, 80	91.90	1.2510
11H-1, 50	93.70	2.1720
11H-1, 66	93.86	1.3728
12H-1, 80	103.60	1.2930
12H-2, 80	105.10	1.3230
12H-3, 80	106.60	0.8300
12H-4, 80	108.10	1.1270
12H-5, 80	109.60	1.2580
12H-6, 80	111.10	0.9480
13H-1, 130	113.70	1.3460
13H-2, 80	114.70	1.2950
13H-3, 80	116.20	0.8850
13H-4, 80	117.70	1.2550
13H-5, 80	119.20	1.4390
14H-1, 80	122.80	2.2320
14H-2, 80	124.30	1.2310
14H-3, 80	125.80	1.1940
14H-4, 80	127.30	1.0890
14H-5, 40	128.40	1.0970
15H-1, 100	132.60	1.1170
15H-2, 90	134.00	1.0340
15H-3, 80	135.40	0.8720
15H-4, 80	136.90	1.1980
15H-5, 80	138.40	1.3610
15H-6, 40	139.50	1.2410
16H-1, 110	142.40	1.4210
16H-2, 80	143.60	1.1470
16H-3, 80	145.10	1.3330
16H-4, 80	146.60	1.3960
16H-5, 80	148.10	1.1040
16H-6, 80	149.60	1.2750
16H-7, 40	150.70	1.2610
17H-1, 110	152.10	0.7370
20X-1, 80	174.50	1.7090
20X-2, 80	176.00	1.4170
21X-1, 80	184.20	1.3800
21X-2, 80	185.70	1.5660
21X-3, 80	187.20	1.6340
21X-4, 80	188.70	1.4410
21X-5, 80	190.20	1.5530
22X-1, 80	193.90	0.9810
22X-2, 80	195.40	1.4850
22X-3, 80	196.90	1.3780
22X-4, 80	198.40	1.5760
22X-5, 80	199.90	1.2090
22X-6, 80	201.40	1.2810
23X-1, 80	203.50	0.9180
23X-2, 80	205.00	1.4030
23X-3, 80	206.50	2.2530
23X-4, 80	208.00	1.5060
23X-6, 80	211.00	1.4580
115-707B-		
1H-2, 80	2.30	1.0770
1H-4, 60	5.10	0.7060
115-707C-		
3R-2, 80	195.80	1.0890
3R-3, 80	197.30	1.4510
3R-4, 80	198.80	1.5030
3R-5, 80	200.30	1.4370
3R-6, 80	201.80	1.3430
3R-7, 40	202.90	1.4180
5R-1, 30	213.10	1.4560
7R-2, 42–51	234.02	1.6300
7R-3, 80	235.90	1.4370
7R-4, 80	237.40	1.3810
8R-1, 90	242.70	1.5630
9R-2, 89	253.79	1.4680
9R-3, 30	254.70	0.8790
10R-1, 104	262.04	1.1930
10R-2, 90	263.40	1.2290
10R-3, 90	264.90	1.1910
10R-4, 90	266.40	1.2700
15R-4, 1–10	312.60	1.2300
21R-2, 41–47	367.91	1.7900
22R-1, 77–85	376.37	1.3300
22R-2, 85–100	377.75	1.2800
23R-1, 81–88	386.11	1.9900
23R-2, 1–15	386.78	1.8000
23R-3, 67–80	388.88	2.1800
23R-4, 1–10	389.63	1.6600
24R-1, 103–109	395.93	1.2800
24R-2, 85–91	397.25	1.4800
24R-3, 34–46	398.09	1.5800
25R-1, 68–86	405.18	1.5700
25R-2, 34–54	406.29	1.9000
25R-3, 28–45	407.63	1.5700
25R-4, 26–36	409.11	1.6100
25R-5, 23–40	410.58	1.5900
25R-6, 123–131	412.94	1.6500
26R-1, 73–86	415.03	1.5600
26R-2, 123–134	416.91	1.8000
26R-3, 24–33	417.40	1.6200
26R-3, 24–33	417.40	1.6600
26R-4, 119–129	419.81	1.6700
26R-5, 21–27	420.23	1.8000
26R-6, 29–36	421.81	1.6900
26R-7, 29–56	423.17	1.6900
27R-1, 78–95	424.68	1.7600
27R-3, 1–12	426.91	1.7200
27R-4, 64–82	428.85	1.7600
27R-5, 83–99	430.49	1.7200
27R-6, 1–8	430.99	1.7800
27R-7, 9–22	432.57	1.6500
28R-1, 129–142	434.89	1.3700
28R-2, 67–83	435.77	1.5900
28R-3, 118–129	437.63	1.7200
28R-4, 14–27	438.04	1.7300

Table 14. Compressional-wave velocity, wet-bulk density, and acoustic impedance of basement rocks, Hole 707C.

Lithology	Section interval (cm)	Depth (mbsf)	V_p (m/s)	Wet-bulk density (g/cm^3)	Acoustic impedance (g/cm^2·s·10^5)
Chalk	11R-1, 73	271.33	1580	1.65	2.60
Chert	13R-1, 60	290.40	4884	2.28	11.13
Limestone (L)	15R-1, 88	309.78	1815	1.71	3.10
Limestone	16R-2, 74	320.44	1773	1.62	2.87
Grainstone	20R-1, 80	357.50	1900	1.96	3.73
Silicified L	21R-1, 109	367.09	5172	2.60	13.45
Basalt Unit 1	22R-1, 63	376.23	2610	2.39	6.24
Basalt Unit 1	22R-2, 10	377.00	3520	2.43	8.55
Basalt Unit 1	22R-2, 38	377.28	3185	2.30	7.33
Basalt Unit 1	22R-2, 94	377.84	2402	2.50	6.00
Basalt Unit 2	23R-1, 43	385.73	4269	2.66	11.40
Basalt Unit 3	23R-1, 94	386.24	4360	2.45	10.68
Basalt Unit 3	23R-1, 133	386.63	4100	2.69	11.03
Basalt Unit 3	23R-2, 31	387.08	4336	2.71	11.75
Basalt Unit 3	23R-2, 58	387.35	4250	2.65	11.26
Basalt Unit 3	23R-2, 98	387.75	3794	2.68	10.17
Basalt Unit 3	23R-3, 4	388.25	4388	2.64	11.58
Basalt Unit 3	23R-3, 79	389.00	3595	2.65	9.53
Basalt Unit 3	23R-3, 111	389.32	4326	2.66	11.51
Basalt Unit 3	23R-4, 9	389.71	5285	2.75	14.53
Basalt Unit 3	23R-4, 39	390.01	4924	2.72	13.39
Basalt Unit 3	24R-1, 135	396.25	3767	2.41	9.08
Basalt Unit 5	24R-2, 126	397.66	4356	2.75	11.98
Basalt Unit 5	24R-2, 36	396.76	3875	2.53	9.80
Basalt Unit 5	24R-2, 86	397.26	5470	2.70	14.77
Basalt Unit 5	24R-3, 76	398.51	4543	2.77	12.58
Basalt Unit 5	24R-3, 108	398.83	4627	2.84	13.14
Basalt Unit 5	25R-1, 8	404.58	5330	2.79	14.87
Basalt Unit 5	25R-1, 68	405.18	5157	2.78	14.34
Basalt Unit 5	25R-1, 124	405.74	4849	2.83	13.72
Basalt Unit 5	25R-2, 67	406.62	5288	2.82	14.91
Basalt Unit 5	25R-2, 131	407.26	5407	2.87	15.52
Basalt Unit 5	25R-3, 29	407.64	5043	2.73	13.77
Basalt Unit 5	25R-3, 38	407.73	4583	2.27	10.40
Basalt Unit 5	25R-3, 63	407.98	4604	2.69	12.38
Basalt Unit 5	25R-3, 113	408.48	5173	3.02	15.62
Basalt Unit 5	25R-4, 26	409.11	5045	2.76	13.92
Basalt Unit 5	25R-4, 50	409.35	4887	2.79	13.63
Basalt Unit 5	25R-4, 112	409.97	4931	2.80	13.80
Basalt Unit 5	25R-5, 26	410.61	4979	2.64	13.14
Basalt Unit 5	25R-5, 118	411.53	4946	2.80	13.85
Basalt Unit 5	26R-1, 106	415.36	5148	2.81	14.46
Basalt Unit 5	26R-2, 88	416.56	5604	2.84	15.91
Basalt Unit 5	26R-3, 84	418.00	4981	2.75	13.70
Basalt Unit 5	26R-4, 84	419.46	4408	2.67	11.77
Basalt Unit 5	26R-5, 90	420.92	5495	2.83	15.55
Basalt Unit 5	26R-6, 83	422.35	5273	2.75	14.50
Basalt Unit 5	26R-7, 79	423.67	5347	2.83	15.13
Basalt Unit 5	27R-1, 88	424.78	5449	2.90	15.80
Basalt Unit 5	27R-2, 84	426.24	5168	2.90	14.99
Basalt Unit 5	27R-3, 81	427.71	5656	2.98	16.85
Basalt Unit 5	27R-4, 79	429.00	5306	2.92	15.49
Basalt Unit 5	27R-5, 85	430.51	6090	2.93	17.84
Basalt Unit 5	27R-6, 34	431.32	5874	2.90	17.03
Basalt Unit 5	27R-7, 27	432.75	5437	2.85	15.50
Basalt Unit 6	28R-1, 135	434.95	4851	2.60	12.61
Basalt Unit 6	28R-3, 17	436.62	4328	2.69	11.64
Basalt Unit 6	28R-4, 37	438.27	4701	2.82	13.25

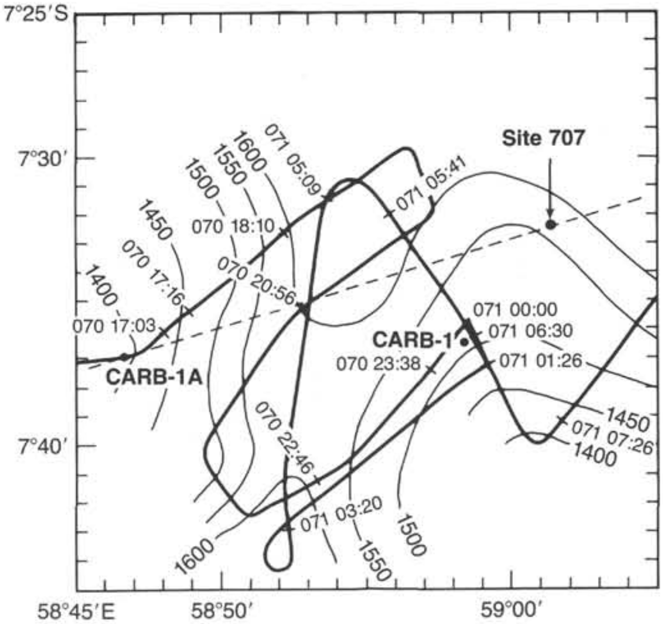

Figure 37. Bathymetry in the vicinity of Site 707 compiled from site survey data collected during the *Charles Darwin* cruise 21/87. The position of the *JOIDES Resolution's* approach and single-channel seismic (SCS) profile is also shown (dashed line). Depth in meters.

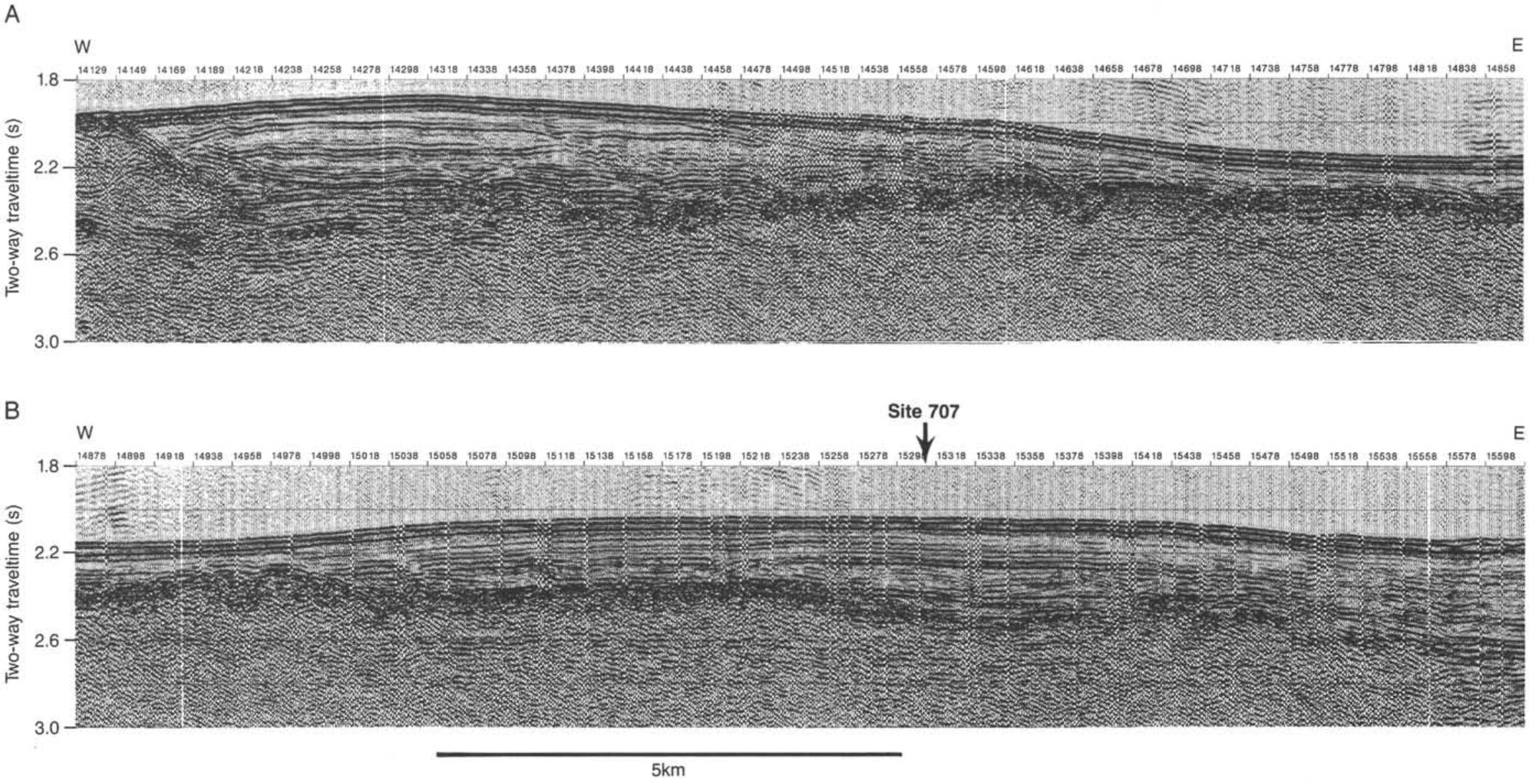

Figure 38. Single-channel seismic (SCS) survey conducted by the *JOIDES Resolution* through Site 707. The profile (located in Fig. 37) is along a west to east section across the top of the ridge which connects the Seychelles Bank and the Saya de Malha Bank (**B** follows to the east of **A**). Site 707 is located over a small sedimentary basin formed by slight offsets (probably normal faults?) in the basement.

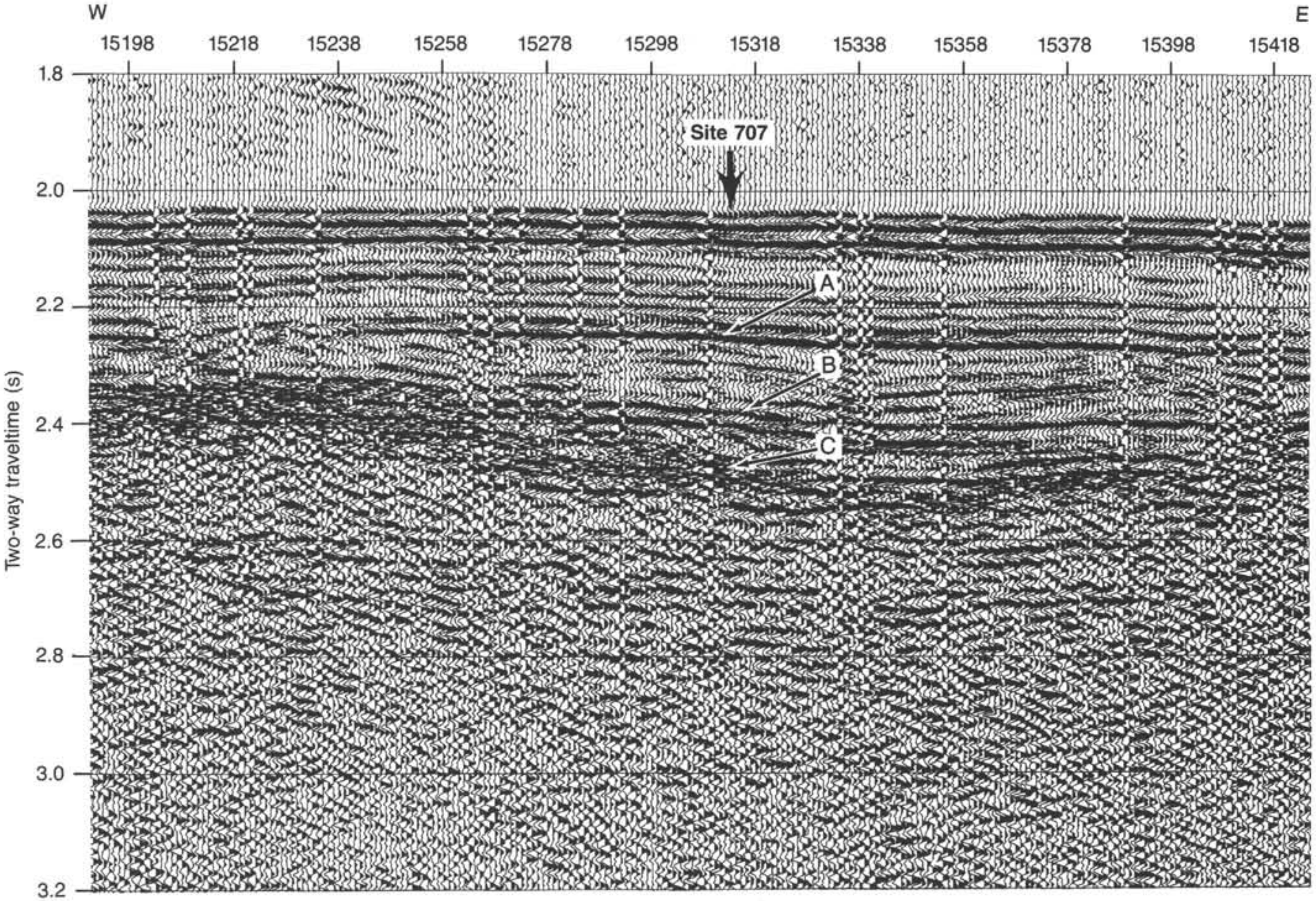

Figure 39. Seismic section at Site 707 produced from *JOIDES Resolution's* single-channel seismic (SCS) profile. A series of prominent reflectors are seen at 0.20 **A**, 0.32 **B**, and 0.41 **C** s (two-way traveltime) below the seafloor. The first two are related to impedance changes in the Cenozoic sedimentary section, the third is the basaltic basement.

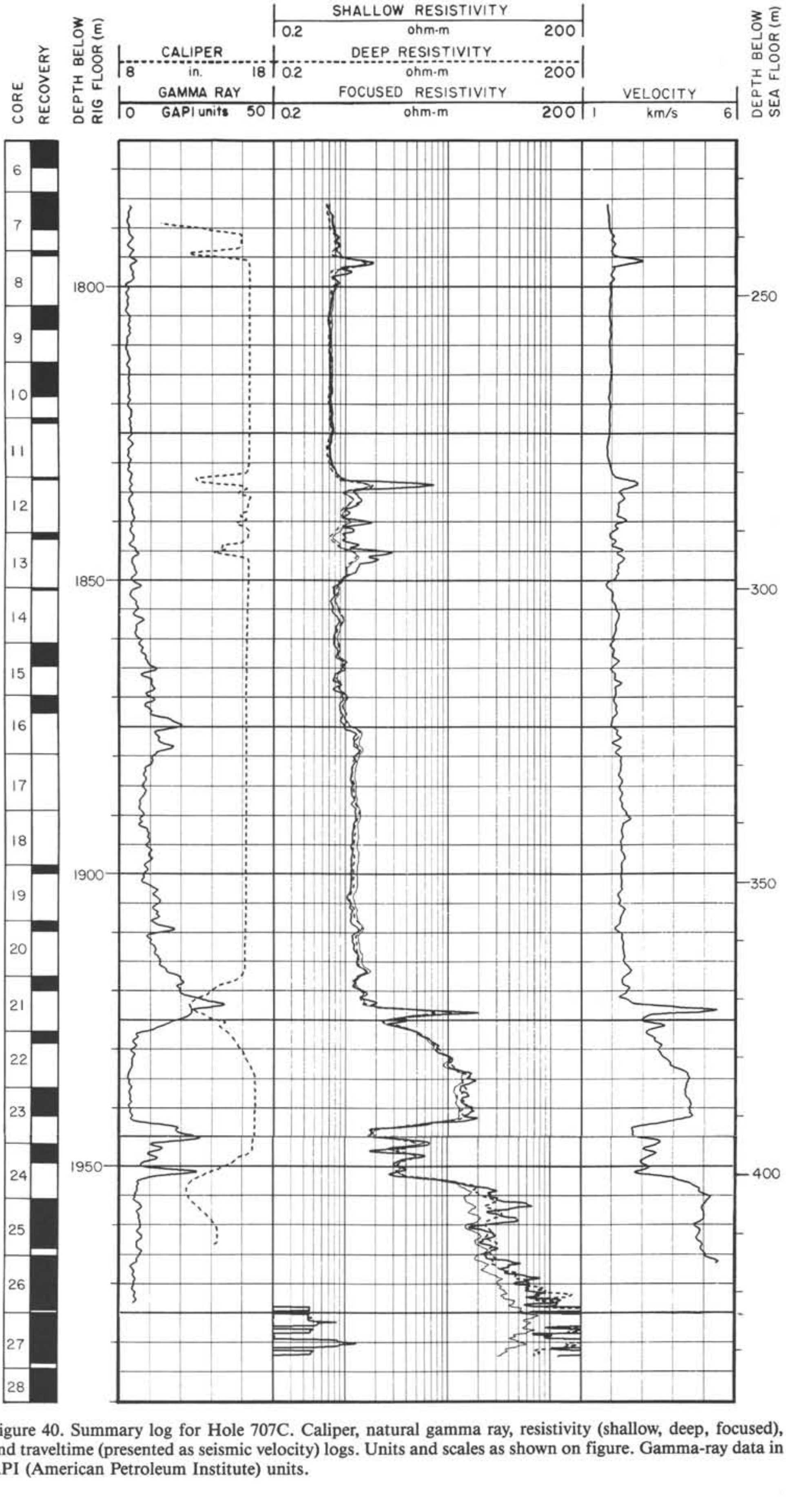

Figure 40. Summary log for Hole 707C. Caliper, natural gamma ray, resistivity (shallow, deep, focused), and traveltime (presented as seismic velocity) logs. Units and scales as shown on figure. Gamma-ray data in API (American Petroleum Institute) units.

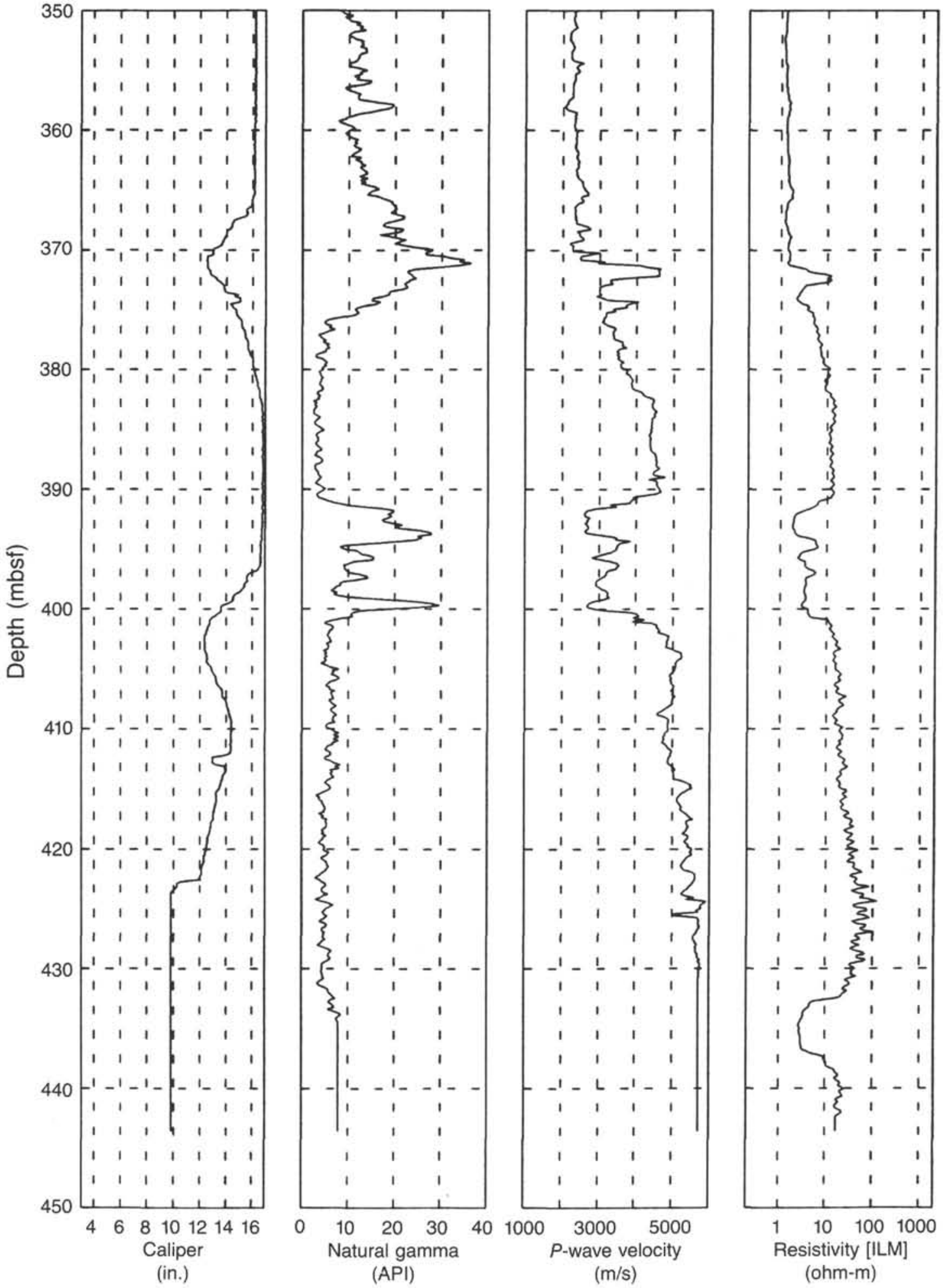

Figure 41. "Stacked" plot of caliper, natural gamma, *P*-wave velocity, and ILM resistivity for the interval from just above the sediment-basalt contact at 375 mbsf to the bottom of Hole 707C. Interbedded sediments are present from 392 to 401 mbsf and 433 to 437 mbsf.

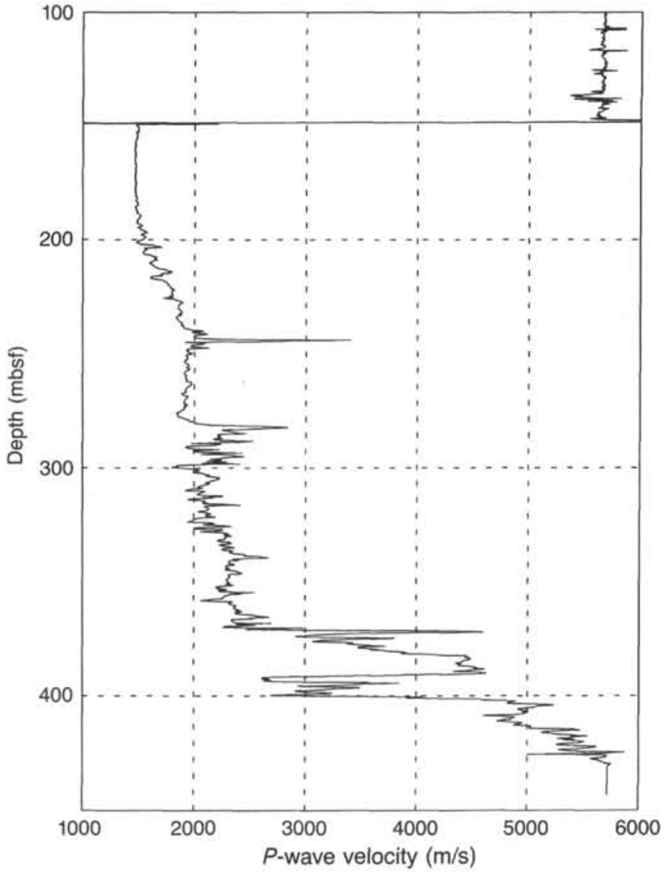

Figure 42. Compressional-wave velocity in m/s vs. depth below seafloor at Hole 707C.

SITE 707 HOLE A CORE 1H CORED INTERVAL 1541.4-1548.0 mbsl; 0.0-6.6 mbsf

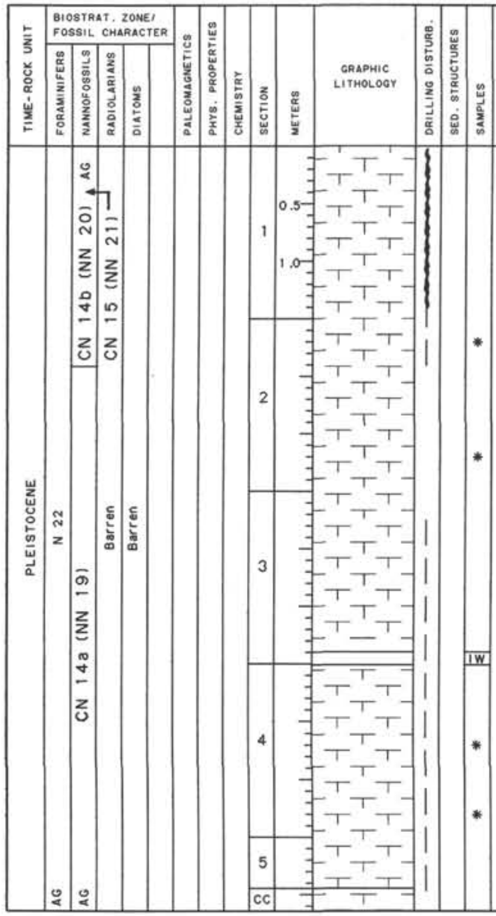

LITHOLOGIC DESCRIPTION

NANNOFOSSIL-BEARING FORAMINIFERAL OOZE

Major lithology: Nannofossil-bearing foraminiferal ooze, homogeneous, white (2.5Y 8/2, 10YR 8/2) and light gray (2.5Y 7/2) to very pale brown (10YR 8/3). No visible structures except for subtle, gradational color changes.

Section 1 of core very is disturbed with incomplete filling of core tube to 135 cm.

SMEAR SLIDE SUMMARY (%):

	2, 20 D	2, 120 D	4, 70 D	4, 130 D
TEXTURE:				
Sand	85	80	75	70
Silt	—	—	10	10
Clay	15	20	15	20
COMPOSITION:				
Feldspar	—	Tr	—	—
Foraminifers	85	84	85	80
Nannofossils	15	15	15	20
Sponge spicules	—	1	Tr	Tr

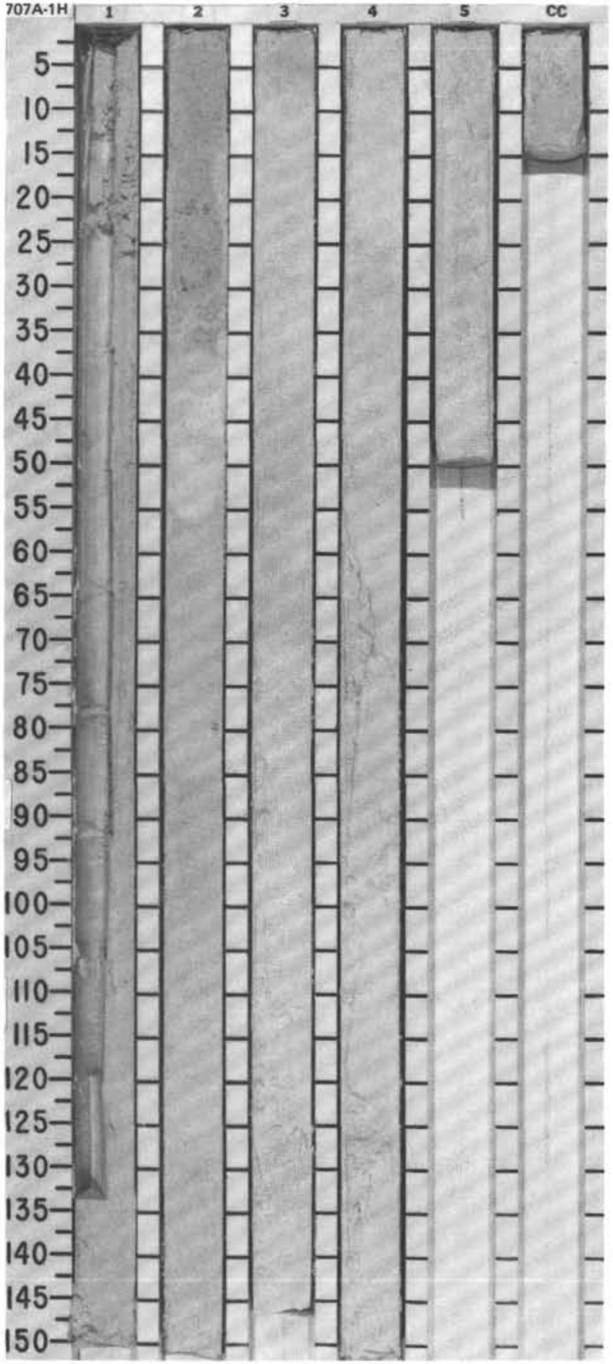

SITE 707 HOLE A CORE 2H CORED INTERVAL 1548.0-1557.6 mbsl; 6.6-16.2 mbsf

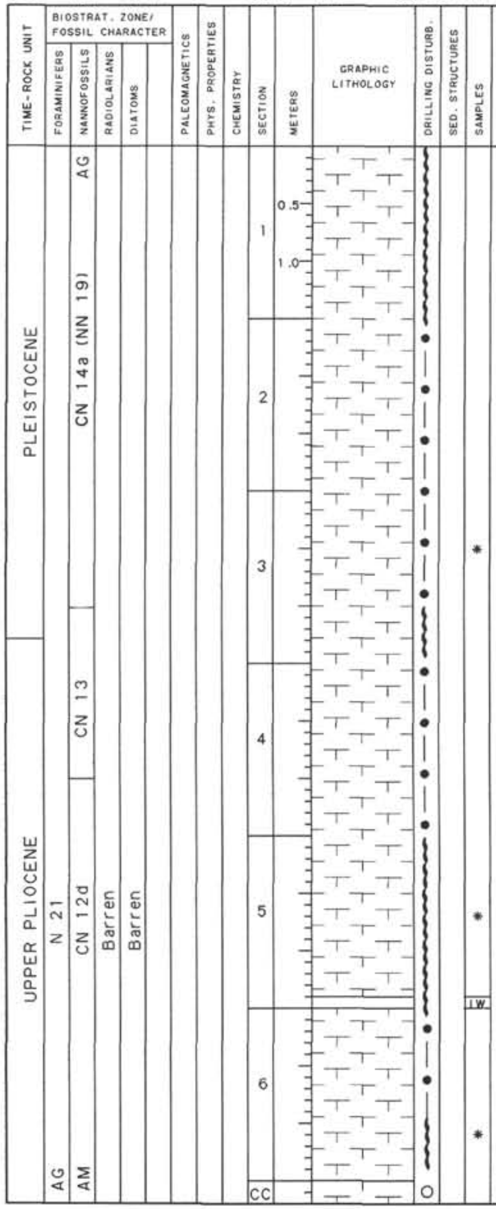

LITHOLOGIC DESCRIPTION

NANNOFOSSIL-BEARING FORAMINIFERAL OOZE

Major lithology: Nannofossil-bearing foraminiferal ooze, homogeneous white ooze throughout, but alternating slightly in shade from 10YR 8/2 to 10YR 8/1. No visible structures.

Section 1 and Section 5 are largely disturbed, as are the last 50 cm in each of Sections 3 and 6.

SMEAR SLIDE SUMMARY (%):

	3, 50 D	5, 70 D	6, 110 D
TEXTURE:			
Sand	70	60	60
Silt	10	20	20
Clay	20	20	20
COMPOSITION:			
Accessory minerals	—	Tr	—
Foraminifers	80	80	80
Nannofossils	20	20	20
Sponge spicules	Tr	Tr	—

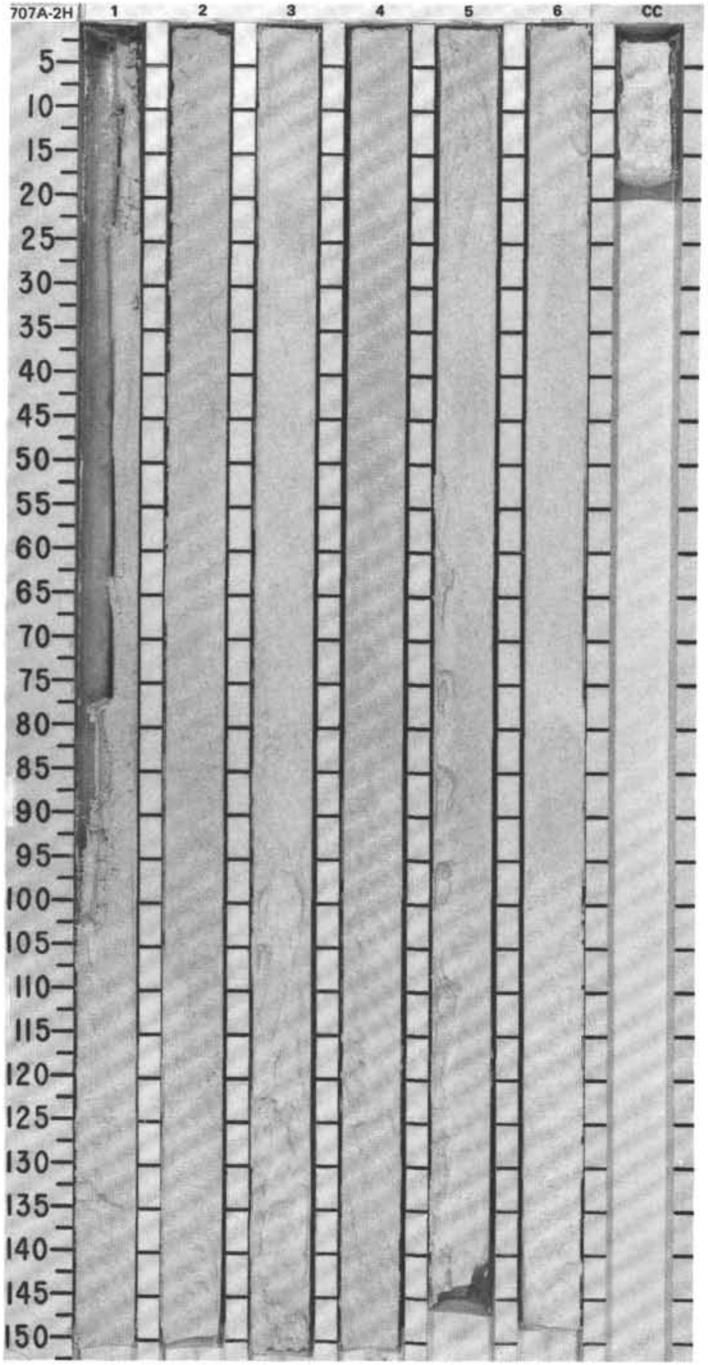

SITE 707 HOLE A CORE 3H CORED INTERVAL 1557.6-1567.2 mbsl; 16.2-25.8 mbsf

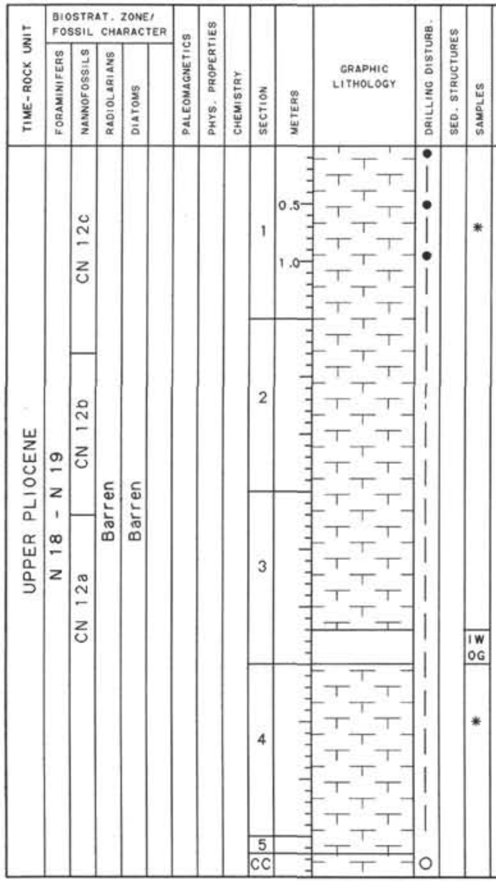

LITHOLOGIC DESCRIPTION

NANNOFOSSIL-BEARING FORAMINIFERAL OOZE

Major lithology: Nannofossil-bearing foraminiferal ooze, homogeneous, white (10YR 8/2, 2.5Y 8/2), no visible structures. Whole core is slightly disturbed.

SMEAR SLIDE SUMMARY (%):

	1, 70 D	4, 50 D
TEXTURE:		
Sand	70	70
Silt	10	10
Clay	20	20
COMPOSITION:		
Foraminifers	80	80
Nannofossils	20	20

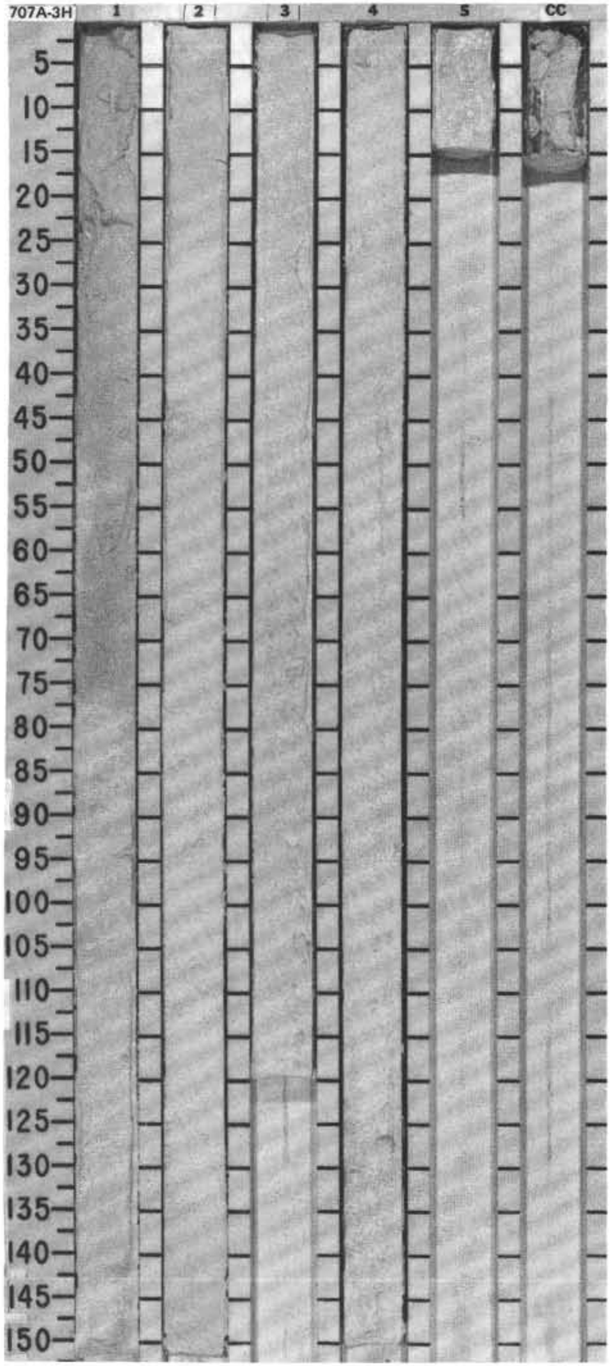

SITE 707 HOLE A CORE 4H CORED INTERVAL 1567.2-1576.9 mbsl; 25.8-35.5 mbsf

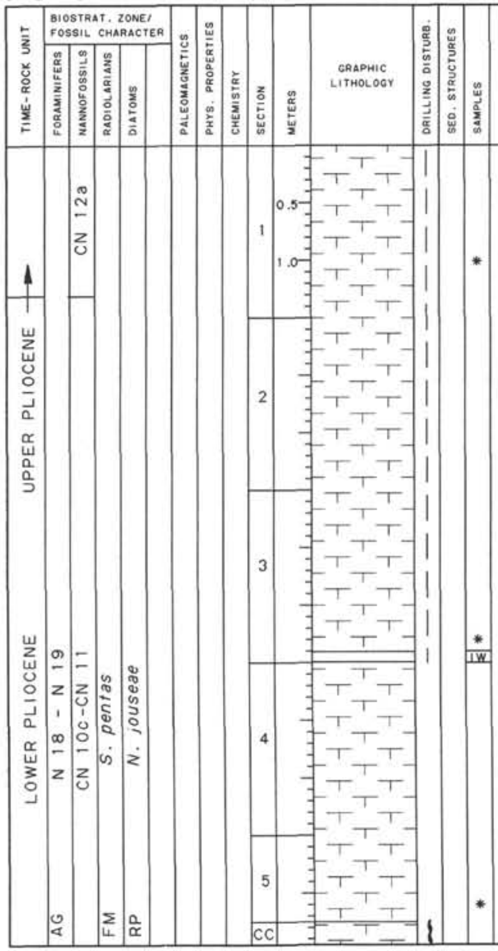

LITHOLOGIC DESCRIPTION

NANNOFOSSIL-BEARING FORAMINIFERAL OOZE

Major lithology: Nannofossil-bearing foraminiferal ooze, homogeneous, white (10YR 8/2) with light gray (10YR 7/1) horizons in Section 3, 100-146 cm; Section 4, 110, 117, and 135 cm; and Section 5, 4-10 and 52-66 cm. Contacts between these layers and the predominant white lithology are gradational and indistinct. Gray layers contain a trace of volcanic ash.

SMEAR SLIDE SUMMARY (%):

	1, 100 D	3, 130 D	5, 57 D
TEXTURE:			
Sand	70	70	70
Silt	10	10	10
Clay	20	20	20
COMPOSITION:			
Volcanic glass	—	Tr	—
Foraminifers	80	80	80
Nannofossils	20	20	20
Sponge spicules	Tr	Tr	—

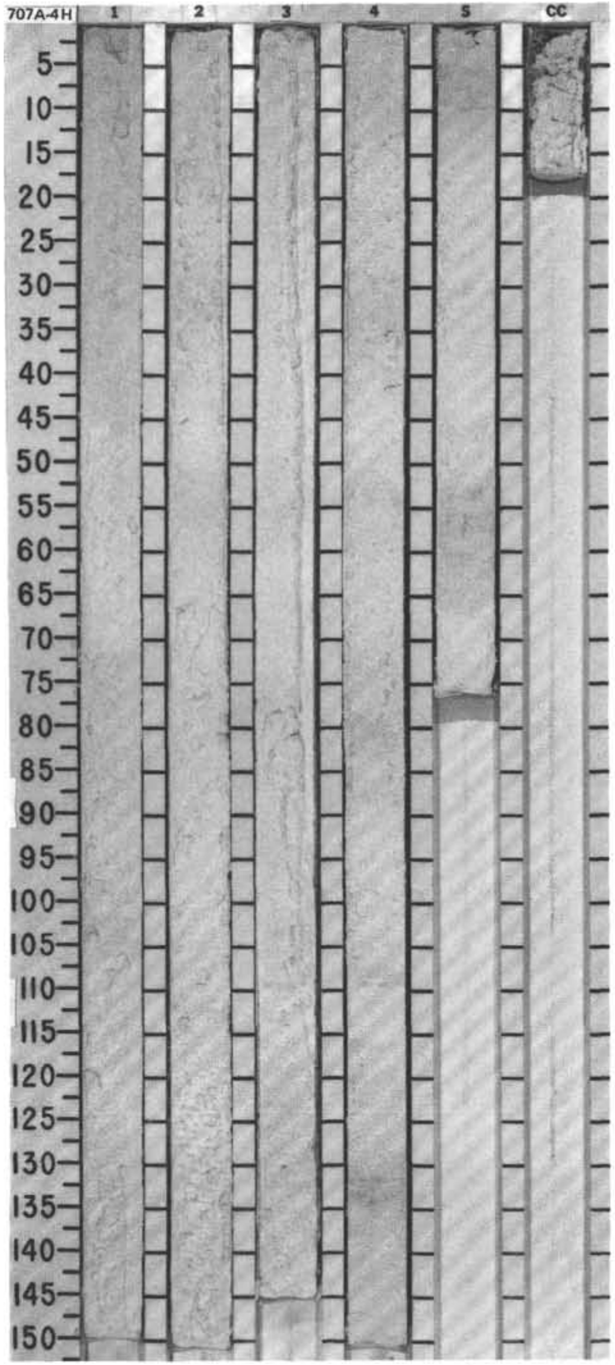

SITE 707 HOLE A CORE 5H CORED INTERVAL 1576.9-1586.5 mbsl; 35.5-45.1 mbsf

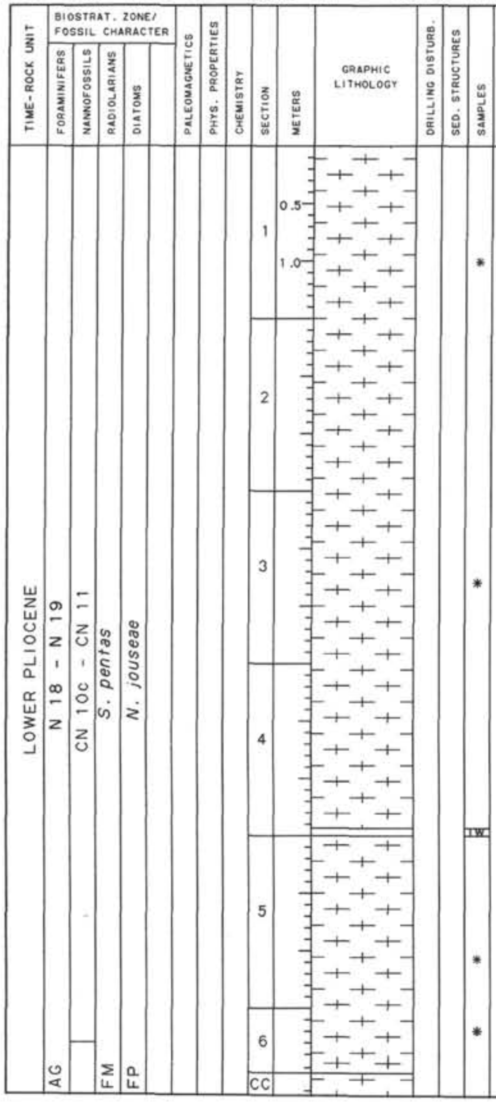

LITHOLOGIC DESCRIPTION

NANNOFOSSIL FORAMINIFERAL OOZE and FORAMINIFER-NANNOFOSSIL OOZE

Major lithology: Nannofossil foraminiferal ooze that grades to foraminifer-nannofossil ooze somewhere about Section 4. Whole core is fairly homogeneous, predominantly white (10YR 8/2), with faint light gray (10YR 7/1) horizons in Section 1, 38-40, 86-89, 120-125, and 139-143 cm; Section 2, 51-52, 80-85, and 126-130 cm; Section 3, 22-40, 64-100, and 134-136 cm; Section 4, 5-6, 22-25, 46-50, 74-77, 86-87, and 96-104 cm; and Section 5, 0-2, 12-24, 47-49, 81-93, and 118-124 cm.

SMEAR SLIDE SUMMARY (%):

	1, 86 D	3, 83 D	5, 105 D	6, 20 D
TEXTURE:				
Sand	50	60	40	30
Silt	10	—	10	15
Clay	40	40	50	55
COMPOSITION:				
Accessory minerals:				
Opaques	Tr	—	—	—
Foraminifers	60	60	40	45
Nannofossils	40	40	60	55
Sponge spicules	Tr	Tr	—	Tr

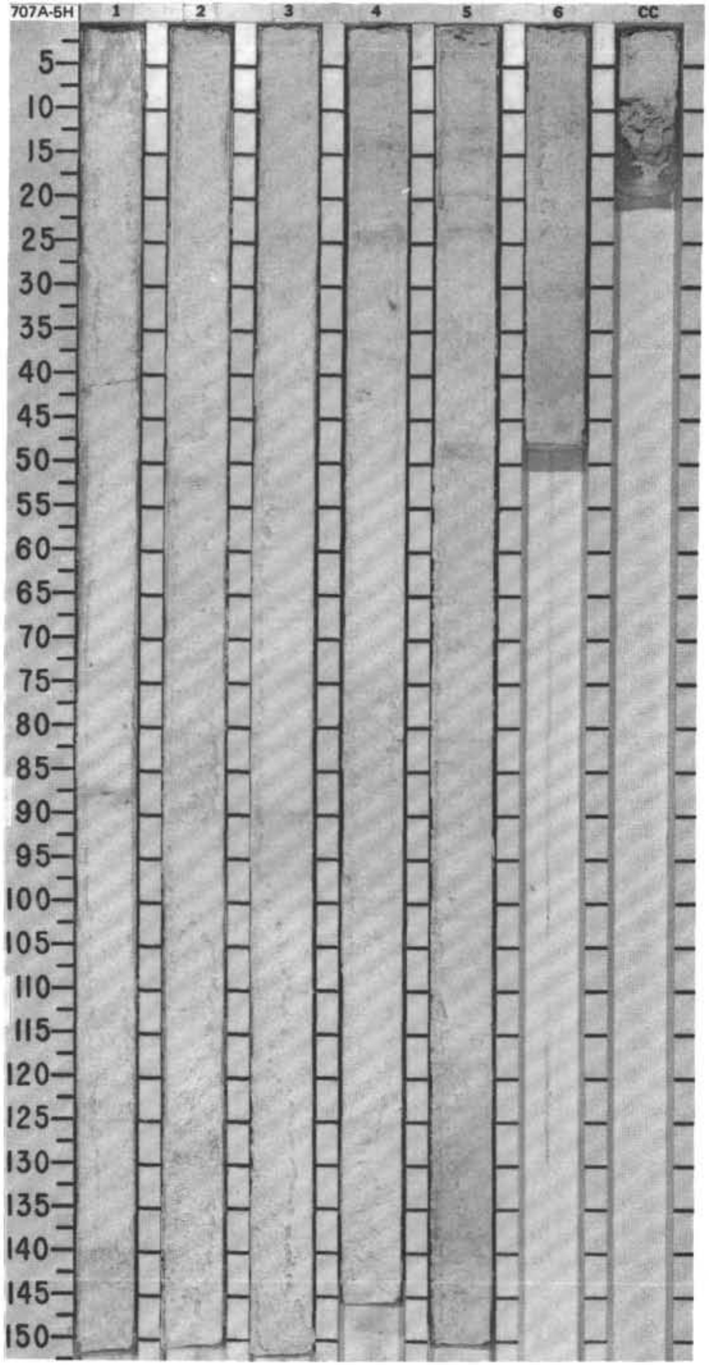

SITE 707 HOLE A CORE 6H CORED INTERVAL 1586.5-1596.1 mbsl; 45.1-54.7 mbsf

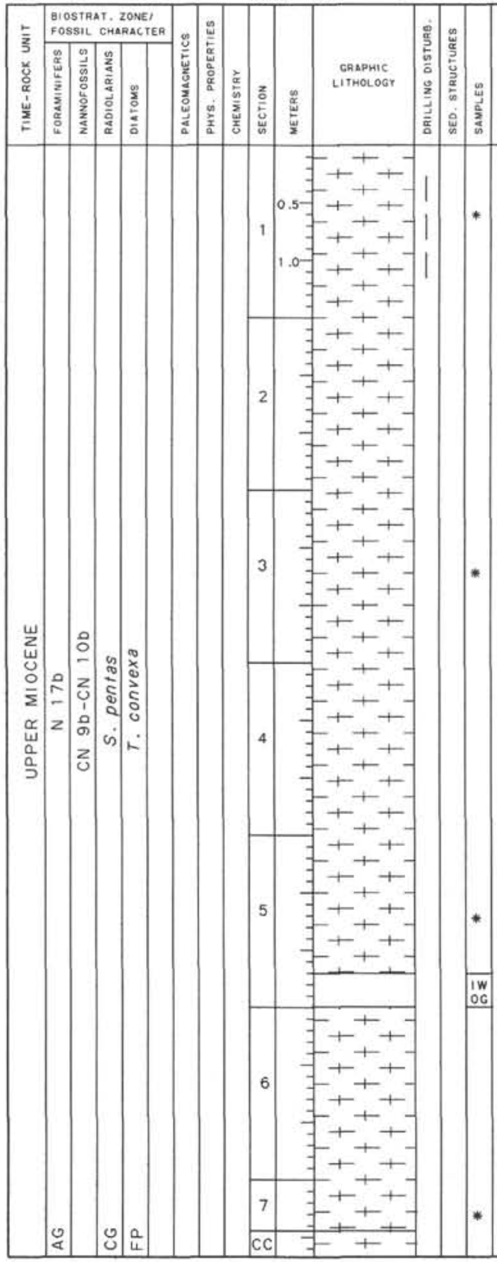

LITHOLOGIC DESCRIPTION

FORAMINIFER-NANNOFOSSIL OOZE

Major lithology: Foraminifer-nannofossil ooze, white (10YR 8/1), with light gray horizons (10YR 7/1) in Section 1, 111-128 cm; Section 2, 24-51 and 141-150 cm; Section 3, 12-13, 34-60, 113-117, and 139-140 cm; Section 4, 65-100 cm; Section 5, 101-107 cm; and Section 6, 0-58 and 110-158 cm. No visible features, except for this faint layering.

SMEAR SLIDE SUMMARY (%):

	1, 60 D	3, 70 D	5, 70 D	7, 30 D
TEXTURE:				
Sand	25	30	30	25
Silt	15	11	15	15
Clay	60	59	55	60
COMPOSITION:				
Foraminifers	40	40	45	40
Nannofossils	60	59	55	60
Sponge spicules	—	1	Tr	Tr

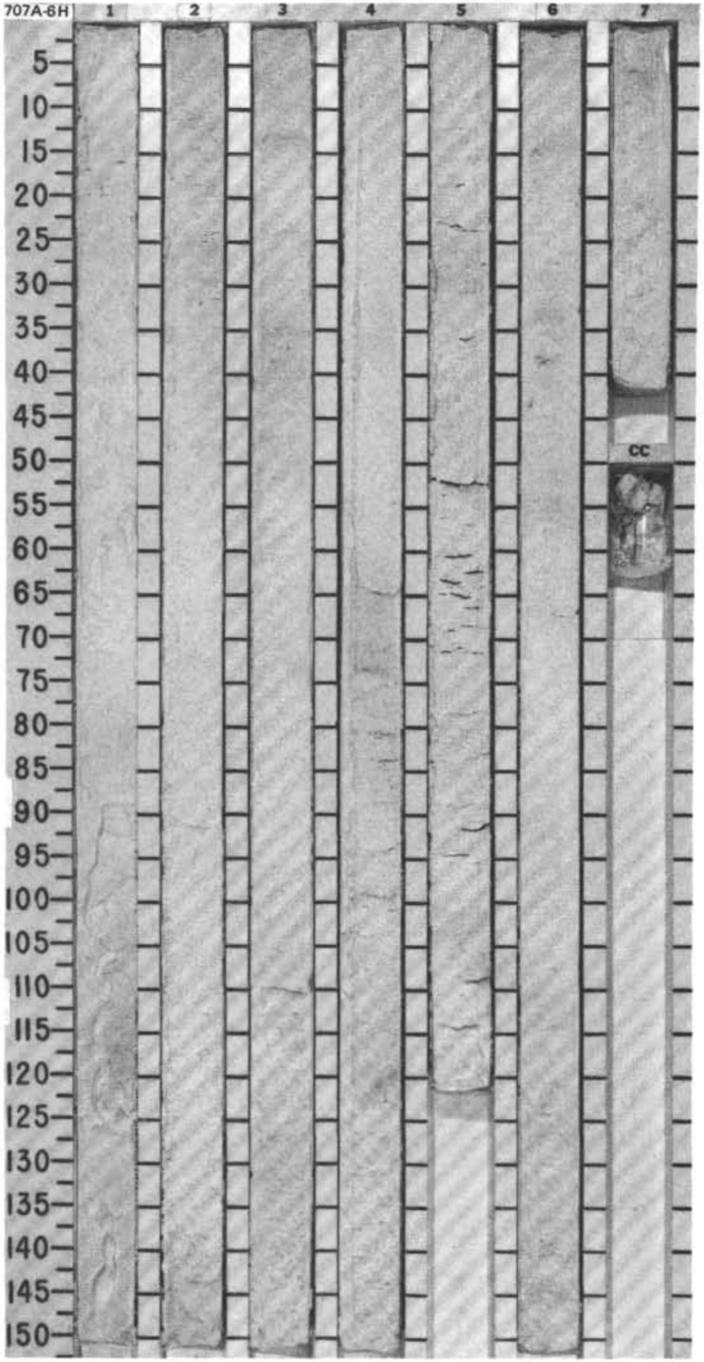

SITE 707 HOLE A CORE 7H CORED INTERVAL 1596.1-1605.7 mbsl; 54.7-64.3 mbsf

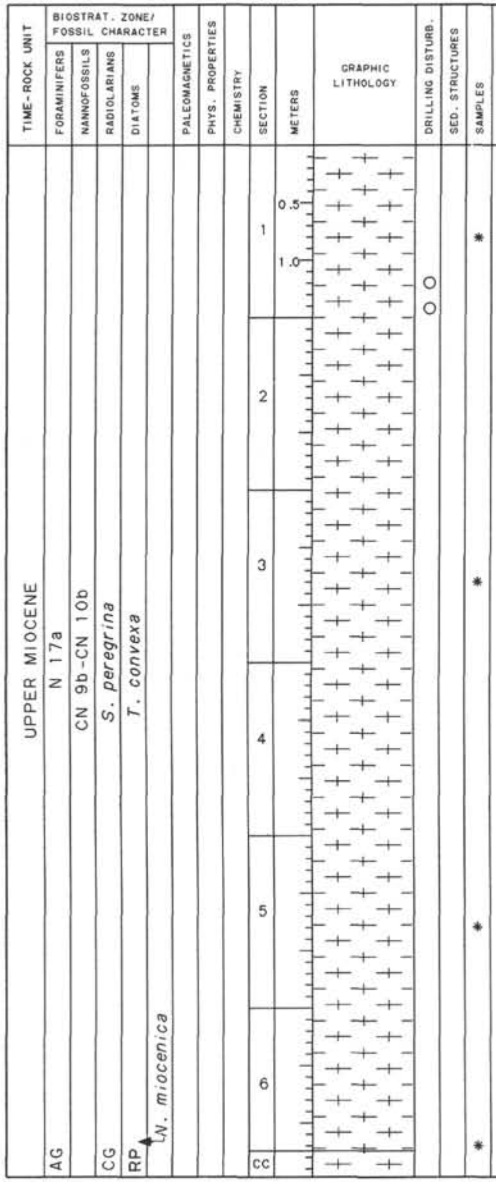

LITHOLOGIC DESCRIPTION

FORAMINIFER-NANNOFOSSIL OOZE

Major lithology: Foraminifer-nannofossil ooze, homogeneous, white (10YR 8/1, 8/2), with light gray horizons (10YR 7/1) in Section 1, 50-75 cm; Section 2, numerous thin horizons between 20-110 cm; Section 3, 66-89 cm; Section 4, 3-8, 78-88, and 116-119 cm; and Section 5, 10-22 and 138-144 cm. No other visible structures.

SMEAR SLIDE SUMMARY (%):

	1, 80 D	3, 80 D	5, 80 D	6, 120 D
TEXTURE:				
Sand	30	50	50	60
Silt	25	10	10	10
Clay	45	40	40	30
COMPOSITION:				
Foraminifers	45	40	40	40
Nannofossils	55	60	60	60
Sponge spicules	Tr	—	—	Tr

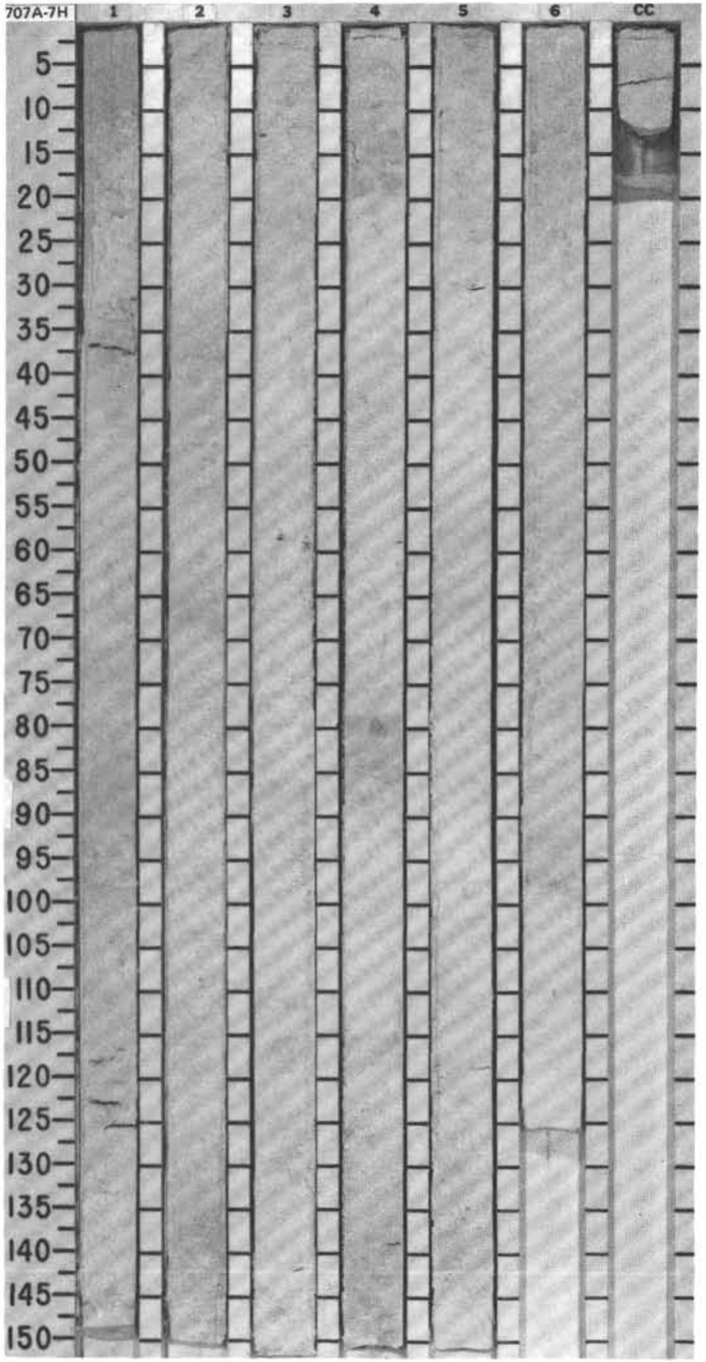

SITE 707 HOLE A CORE 8H CORED INTERVAL 1605.7-1615.4 mbsl; 64.3-74.0 mbsf

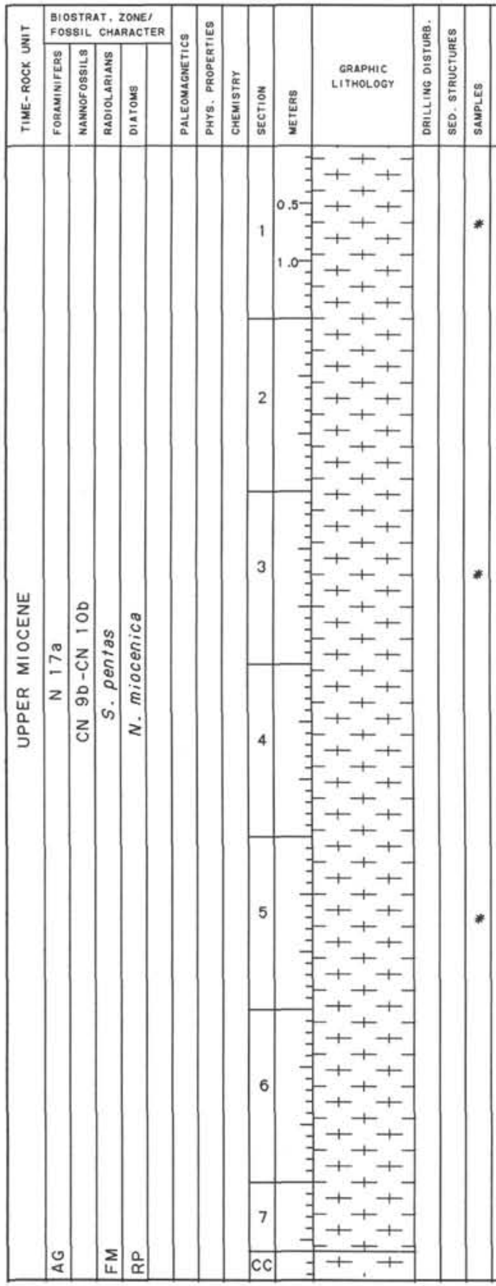

LITHOLOGIC DESCRIPTION

FORAMINIFER-NANNOFOSSIL OOZE

Major lithology: Foraminifer-nannofossil ooze, homogeneous, white (10YR 8/1), with faint light gray horizons (10YR 7/1) in Section 1, 47-60, 106-113, and 134-135 cm; Section 2, 131-144 cm; Section 4, 9-19 cm; Section 5, 32-43 cm; and Section 6, 80-98 cm.

SMEAR SLIDE SUMMARY (%):

	1, 70 D	3, 70 D	5, 70 D
TEXTURE:			
Sand	30	20	30
Silt	20	20	10
Clay	50	60	60
COMPOSITION:			
Foraminifers	40	40	40
Nannofossils	60	60	60
Sponge spicules	Tr	Tr	—

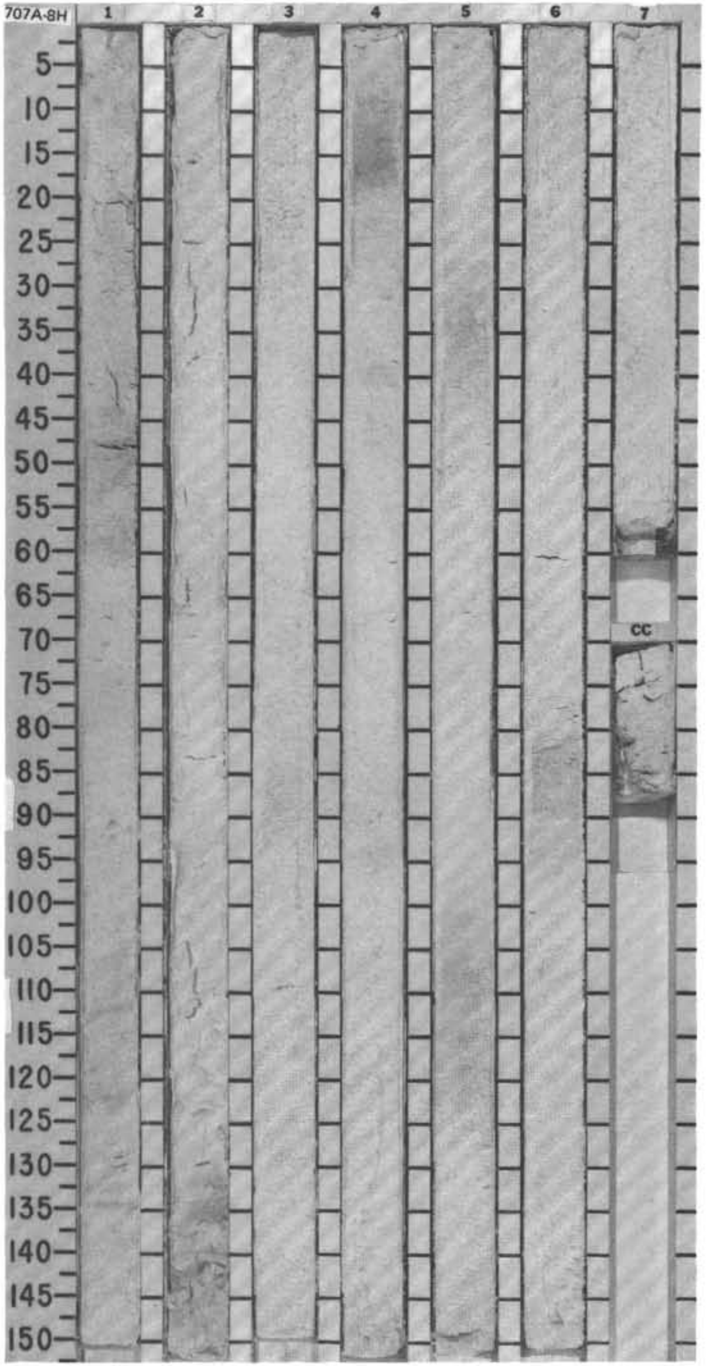

SITE 707 HOLE A CORE 9H CORED INTERVAL 1615.4-1625.0 mbsl; 74.0-83.6 mbsf

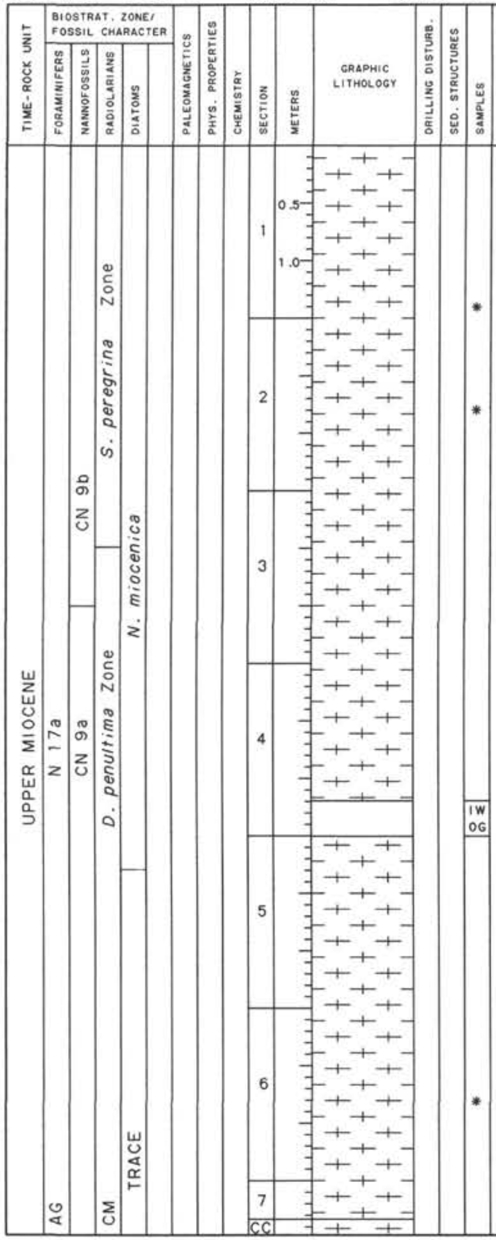

LITHOLOGIC DESCRIPTION

FORAMINIFER-NANNOFOSSIL OOZE

Major lithology: Foraminifer-nannofossil ooze, homogeneous, white (10YR 8/1, N9), with faint grayish white (N8) horizons in Section 1, 41-46 and 130-140 cm; Section 2, 10-20, 41-50, 83-85, and 133-135 cm; Section 3, 45-49, 71-73, and 112-122 cm; and Section 4, 100-104 cm.

SMEAR SLIDE SUMMARY (%):

	1, 143 M	2, 80 D	6, 80 D
TEXTURE:			
Sand	20	31	20
Silt	20	—	20
Clay	60	69	60
COMPOSITION:			
Feldspar	—	—	Tr
Volcanic glass	Tr	Tr	1
Foraminifers	30	30	30
Nannofossils	69	69	65
Radiolarians	—	1	2
Sponge spicules	1	Tr	2

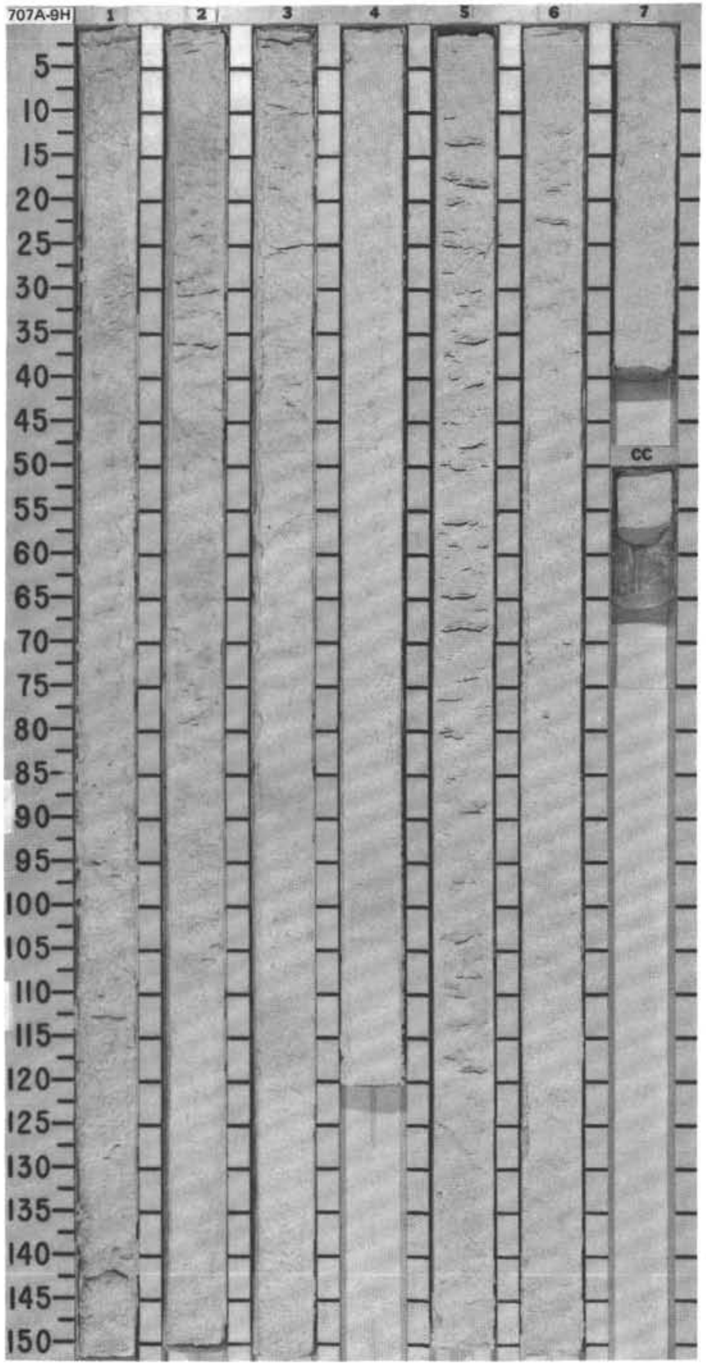

SITE 707 HOLE A CORE 10H CORED INTERVAL 1625.0-1634.6 mbsl; 83.6-93.2 mbsf

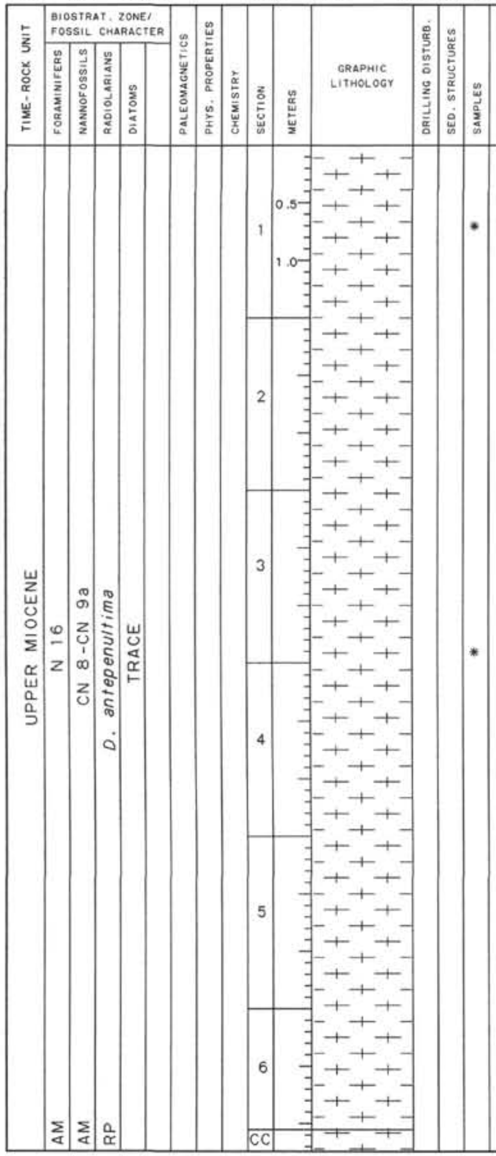

LITHOLOGIC DESCRIPTION

FORAMINIFER-NANNOFOSSIL OOZE

Major lithology: Foraminifer-nannofossil ooze, white (N9), homogeneous throughout except for faint grayish white (N8) horizons in Section 2, 37-50 cm; Section 3, 35-47, 70-72, and 137-149 cm; Section 4, 32-48 and 93-95 cm; and Section 5, 120-150 cm.

SMEAR SLIDE SUMMARY (%):

	1, 70 D	3, 148 D
TEXTURE:		
Sand	30	35
Silt	20	20
Clay	50	45
COMPOSITION:		
Foraminifers	40	45
Nannofossils	58	53
Diatoms	Tr	—
Radiolarians	Tr	Tr
Sponge spicules	2	2

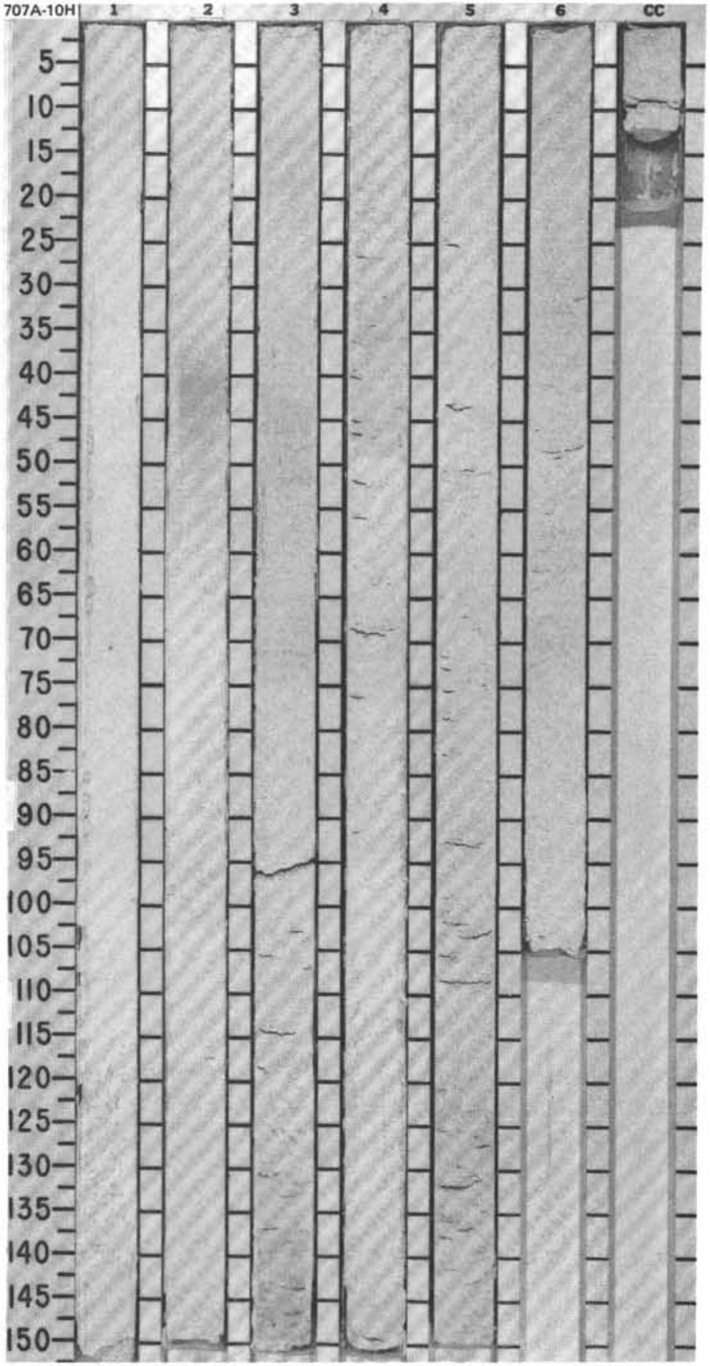

SITE 707 HOLE A CORE 11H CORED INTERVAL 1634.6-1644.2 mbsl; 93.2-102.8 mbsf

TIME-ROCK UNIT	BIOSTRAT. ZONE/ FOSSIL CHARACTER					PALEOMAGNETICS	PHYS. PROPERTIES	CHEMISTRY	SECTION	METERS	GRAPHIC LITHOLOGY	DRILLING DISTURB.	SED. STRUCTURES	SAMPLES
	FORAMINIFERS	NANNOFOSSILS	RADIOLARIANS	DIATOMS										
UPPER MIOCENE	N 15 - N 13 AM	CN 8-CN 9a AM	*D. antepenultima* Zone RP	Barren					1	0.5	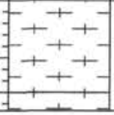			*
									CC					

LITHOLOGIC DESCRIPTION

FORAMINIFER-NANNOFOSSIL OOZE

Major lithology: Foraminifer-nannofossil ooze, white (N9), no visible structures or disturbance.

SMEAR SLIDE SUMMARY (%):

	1, 40 D
TEXTURE:	
Sand	20
Silt	20
Clay	60
COMPOSITION:	
Feldspar	Tr
Volcanic glass	Tr
Accessory minerals	1
Foraminifers	25
Nannofossils	69
Sponge spicules	5
Calcareous spicules	Tr

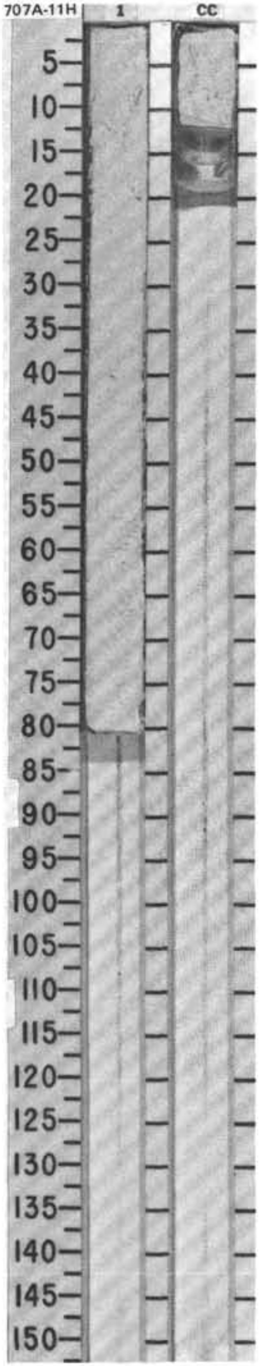

SITE 707 HOLE A CORE 12H CORED INTERVAL 1644.2-1653.8 mbsl; 102.8-112.4 mbsf

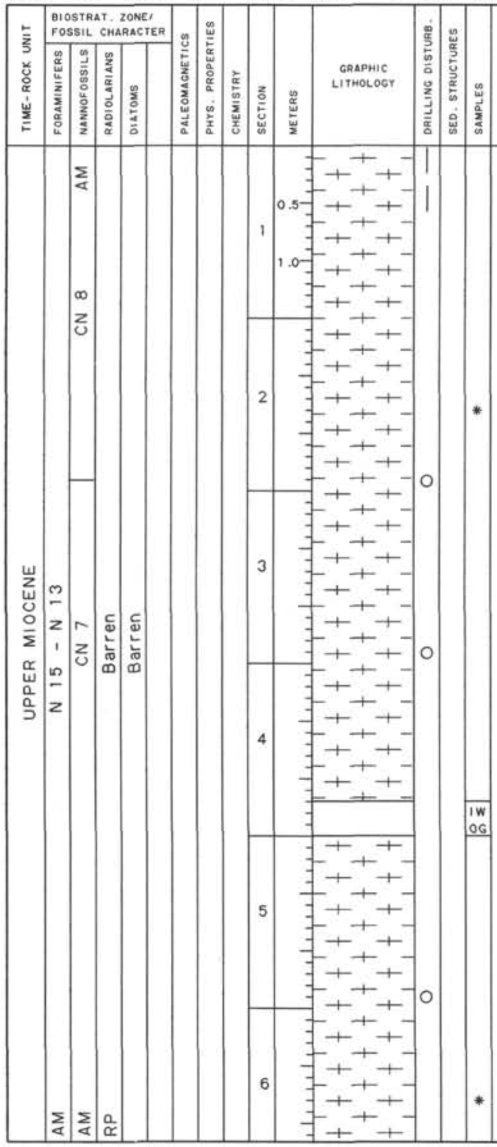

LITHOLOGIC DESCRIPTION

FORAMINIFER-NANNOFOSSIL OOZE

Major lithology: Foraminifer-nannofossil ooze, white (N9), homogeneous, with faint grayish white (N8) horizons in Section 4, 23-25 cm, and alternating with layers of the dominant color (N9) in Section 6 between 50 and 118 cm (the end of the core). No other visible structures.

Minor lithology: Foraminiferal ooze, very pale brown (10YR 8/2, 8/3), coarse grained, in Section 1, 0-4 cm; probably material caved in from uphole.

Sediments are soupy at the base of Sections 2, 3, and 5.

SMEAR SLIDE SUMMARY (%):

	2, 80 D	6, 80 D
TEXTURE:		
Sand	25	30
Silt	15	10
Clay	60	60
COMPOSITION:		
Volcanic glass	Tr	Tr
Dolomite	—	Tr
Accessory minerals	—	Tr
Foraminifers	30	30
Nannofossils	68	64
Radiolarians	—	1
Sponge spicules	2	5
Silicoflagellates	—	Tr

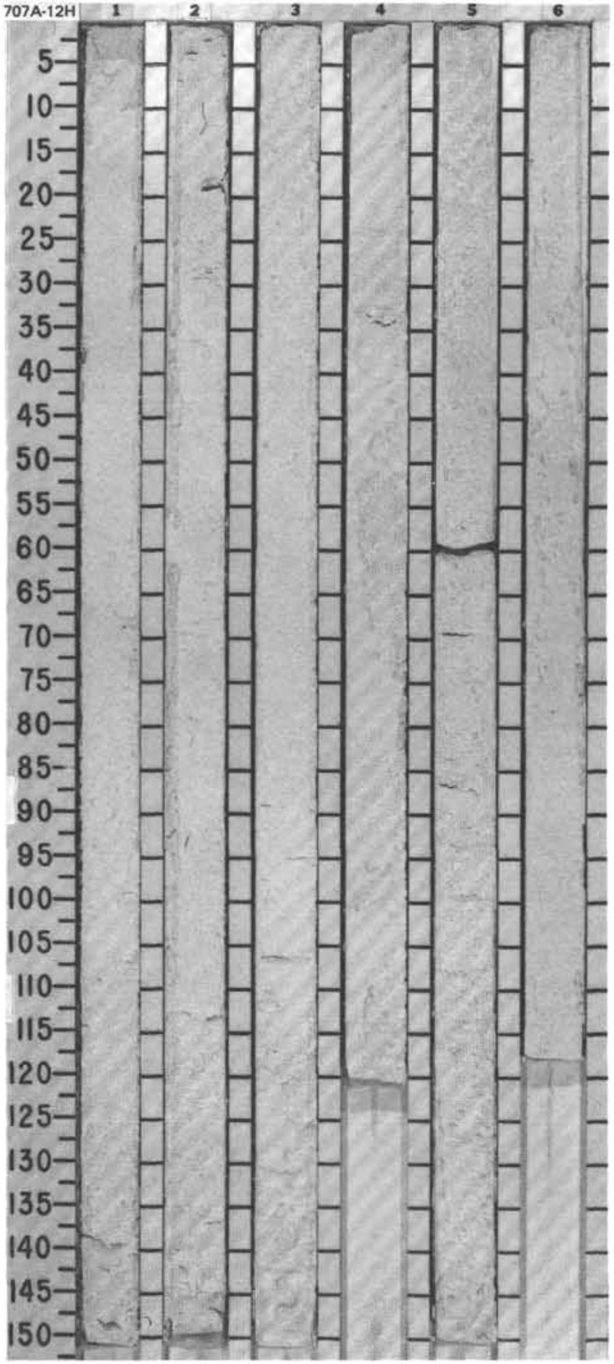

SITE 707 HOLE A CORE 13H CORED INTERVAL 1653.8-1663.4 mbsl; 112.4-122.0 mbsf

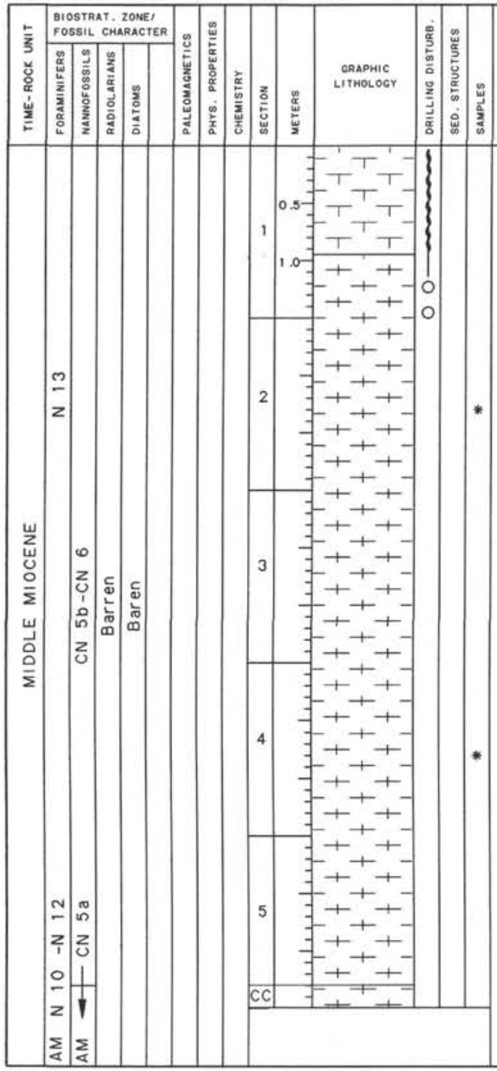

LITHOLOGIC DESCRIPTION

FORAMINIFER-NANNOFOSSIL OOZE

Major lithology: Foraminifer-nannofossil ooze, homogeneous, white to grayish white (N9, N8). No visible structures.

Section 1, 0-90 cm, is severely disturbed and represents flow-in at the top of the core from higher in the section. Sediment in this interval is a very coarse, pale brown (10YR 8/2) foraminiferal sand.

SMEAR SLIDE SUMMARY (%):

	2, 80 D	4, 80 D
TEXTURE:		
Sand	30	30
Silt	20	25
Clay	50	45
COMPOSITION:		
Volcanic glass	Tr	—
Foraminifers	45	35
Nannofossils	54	65
Radiolarians	—	Tr
Sponge spicules	1	—

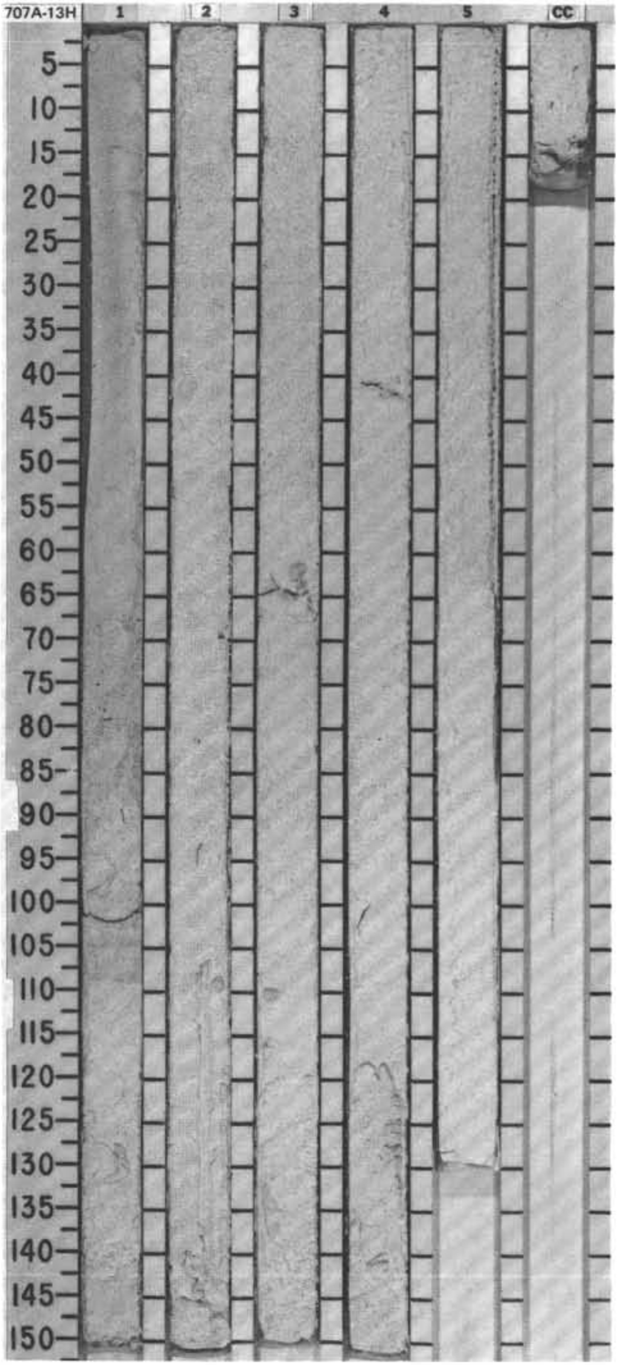

SITE 707 HOLE A CORE 14H CORED INTERVAL 1663.4-1673.0 mbsl; 122.0-131.6 mbsf

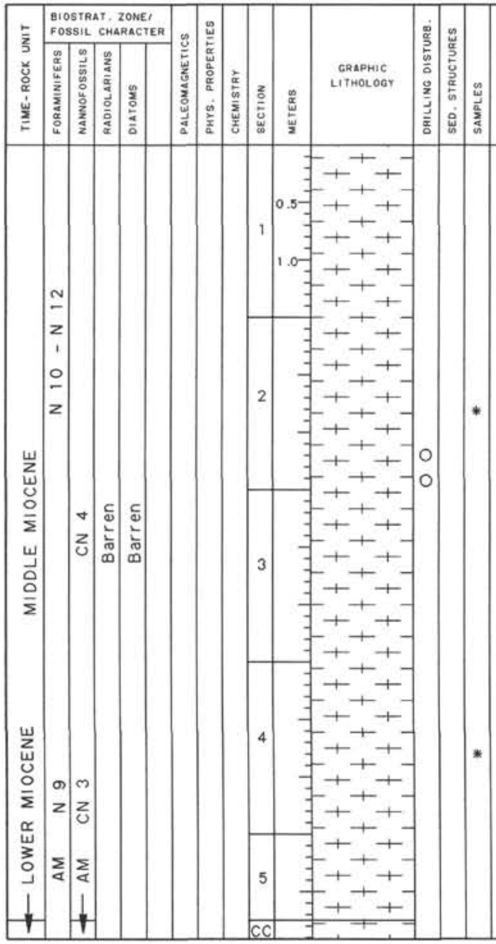

LITHOLOGIC DESCRIPTION

FORAMINIFER-NANNOFOSSIL OOZE

Major lithology: Foraminifer-nannofossil ooze, homogeneous, white to grayish white (N9, N8) throughout, with no visible structures. Base of Section 2 is somewhat soupy and disturbed.

SMEAR SLIDE SUMMARY (%):

	2, 80 D	4, 80 D
TEXTURE:		
Sand	35	40
Silt	15	10
Clay	50	50
COMPOSITION:		
Feldspar	Tr	—
Volcanic glass	Tr	Tr
Foraminifers	45	45
Nannofossils	55	55
Sponge spicules	Tr	Tr

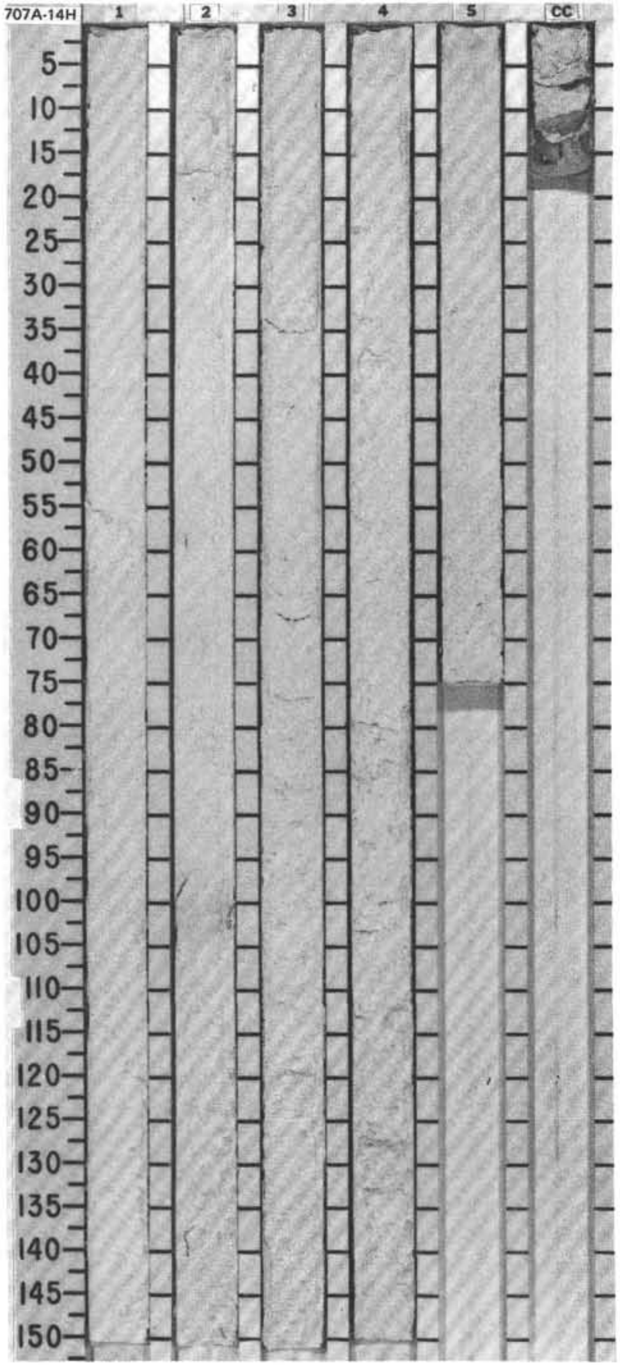

SITE 707 HOLE A CORE 15H CORED INTERVAL 1673.0-1682.7 mbsl; 131.6-141.3 mbsf

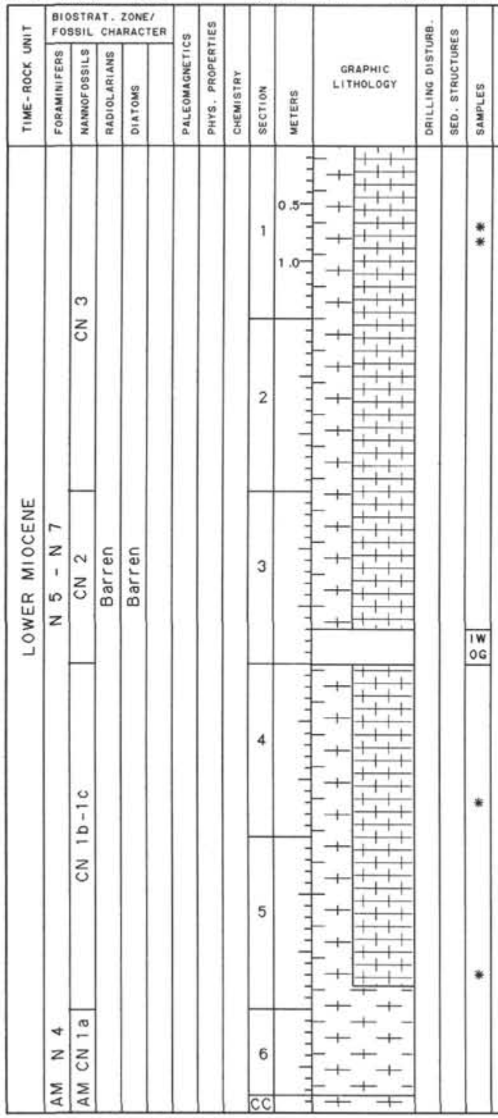

LITHOLOGIC DESCRIPTION

FORAMINIFER-NANNOFOSSIL OOZE and FORAMINIFER-NANNOFOSSIL CHALK

Major lithology: Foraminifer-nannofossil ooze, white to pale orange (N9, 10YR 8/2), interbedded with semi-indurated foraminifer-nannofossil (micrite?) chalk (Section 1 through Section 5, 130 cm). Chalk forms "nodules" surrounded by an ooze matrix, but may have originally formed layers broken by coring. Much of the fine carbonate in both the ooze and chalk in this interval is unidentifiable, but heavy overgrowths on recognizable coccoliths and discoasters suggest a nannofossil origin.

Section 5, 130 cm, to CC: Light gray to grayish white (10YR 7/1, 8/1) foraminifer-nannofossil ooze, lacking the chalky nature of the overlying interval. Nannofossils within this interval are well preserved.

SMEAR SLIDE SUMMARY (%):

	1, 73 D	1, 87 M	4, 127 D	5, 120 D
TEXTURE:				
Sand	50	40	40	30
Silt	10	—	10	10
Clay	40	60	50	60
COMPOSITION:				
Mica	—	—	—	Tr
Volcanic glass	—	—	—	Tr
Foraminifers	60	40	45	40
Nannofossils	5	5	5	60
Micrite(?)	35	55	50	—

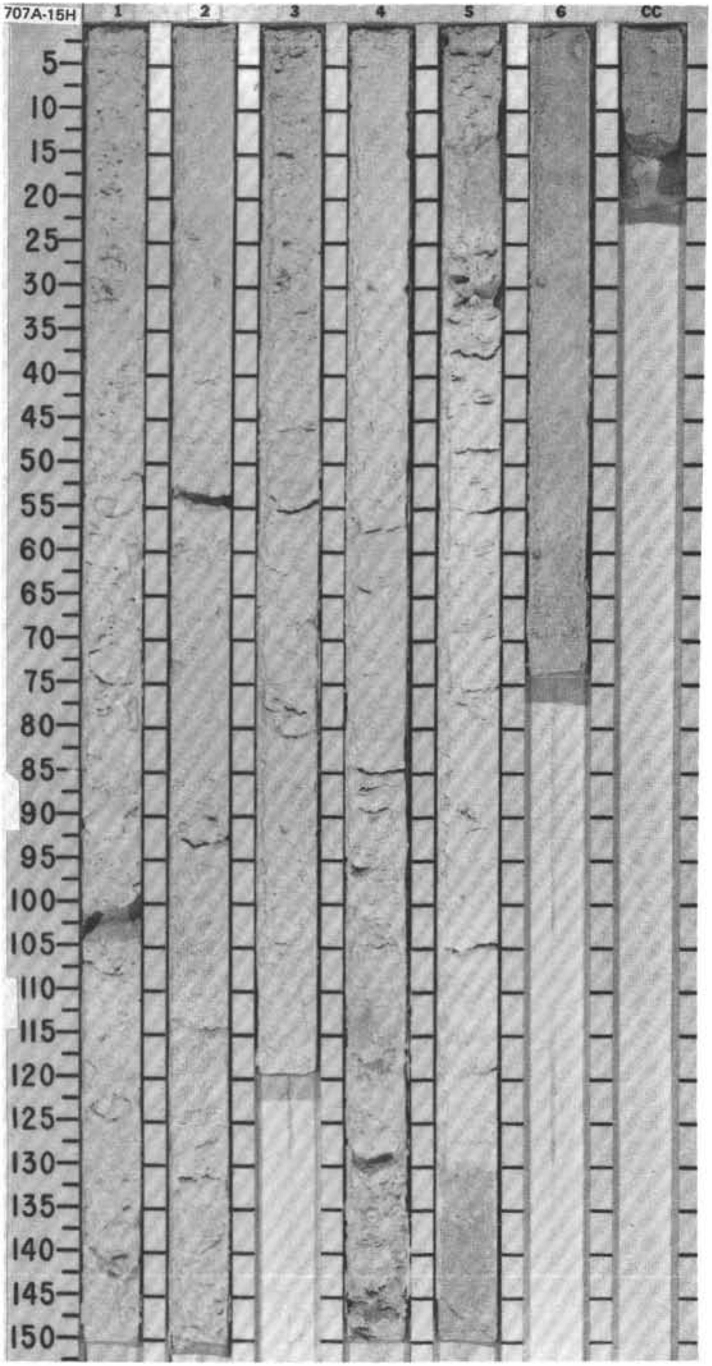

SITE 707 HOLE A CORE 16H CORED INTERVAL 1682.7-1692.4 mbsl; 141.3-151.0 mbsf

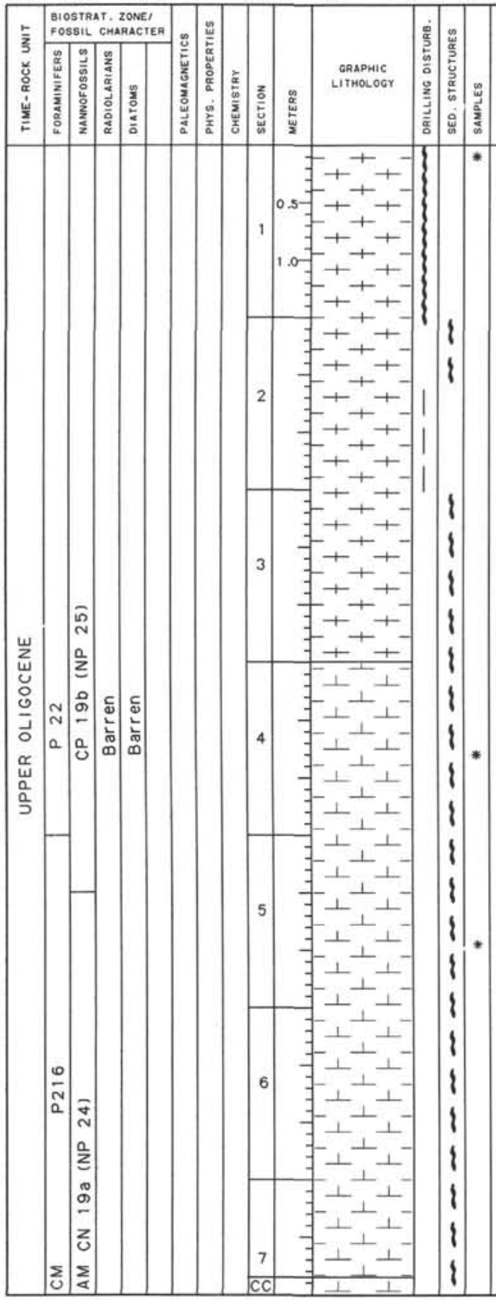

LITHOLOGIC DESCRIPTION

FORAMINIFER-NANNOFOSSIL OOZE and FORAMINIFER-BEARING NANNOFOSSIL OOZE

Major lithology: Foraminifer-nannofossil ooze, white and whitish gray to light gray (N9, 10YR 8/2, 10YR 7/2), grading into foraminifer-bearing nannofossil ooze in Section 4. There are also several very pale orange brown horizons (10YR 8/3) in Section 5, 100-112 cm, and Section 6, 40-50 cm. Moderate bioturbation throughout, with pyrite staining observed in Section 4, 80 and 100 cm.

Section 1 was very soupy and was disturbed during the splitting of the core.

SMEAR SLIDE SUMMARY (%):

	1, 10 D	4, 85 D	5, 100 D
TEXTURE:			
Sand	30	20	20
Silt	15	10	10
Clay	55	70	70
COMPOSITION:			
Volcanic glass	Tr	3	Tr
Foraminifers	30	25	25
Nannofossils	67	67	74
Radiolarians	Tr	—	—
Calcareous spicules	3	5	1

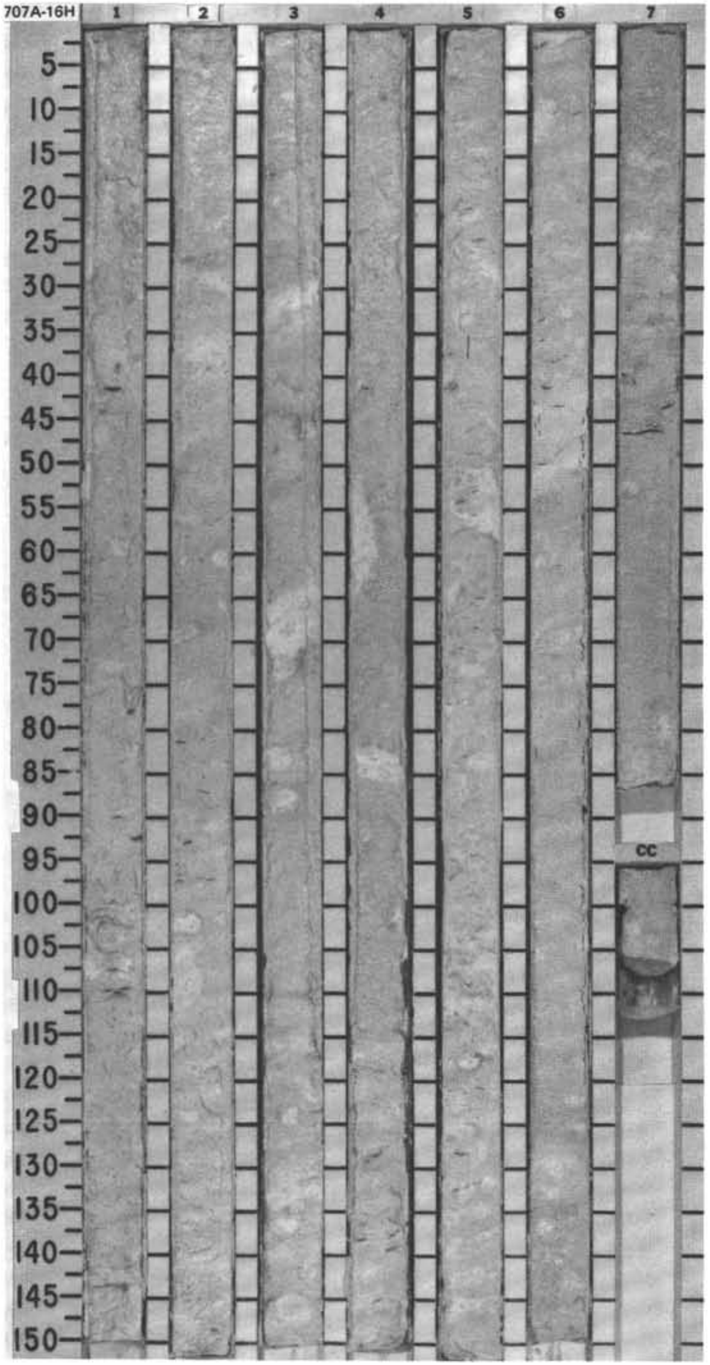

SITE 707 HOLE A CORE 17H CORED INTERVAL 1692.4-1702.1 mbsl; 151.0-160.7 mbsf

TIME-ROCK UNIT	BIOSTRAT. ZONE/ FOSSIL CHARACTER: FORAMINIFERS	NANNOFOSSILS	RADIOLARIANS	DIATOMS		PALEOMAGNETICS	PHYS. PROPERTIES	CHEMISTRY
UPPER OLIGOCENE	CM P 21a	AM CP 19a (NP 24)	*T. tuberosa*	TRACE LATE EOCENE-EARLY OLIGOCENE				

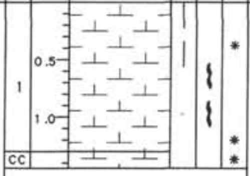

LITHOLOGIC DESCRIPTION

NANNOFOSSIL OOZE

Major lithology: Nannofossil ooze, homogeneous, white (10YR 8/1, 8/2), moderately bioturbated throughout. Slight core disturbance between 10-30 cm.

Minor lithology: Volcanic ash-bearing foraminifer-bearing nannofossil ooze, light gray (10YR 7/2), in CC.

SMEAR SLIDE SUMMARY (%):

	1, 40 D	1, 120 D	CC, 5 M
TEXTURE:			
Sand	5	8	20
Clay	95	92	80
COMPOSITION:			
Volcanic glass	—	—	15
Foraminifers	4	8	15
Nannofossils	95	90	70
Sponge spicules	1	2	—

SITE 707 HOLE A CORE 18H CORED INTERVAL 1702.1-1711.7 mbsl; 160.7-170.3 mbsf

TIME-ROCK UNIT	BIOSTRAT. ZONE/ FOSSIL CHARACTER: FORAMINIFERS	NANNOFOSSILS	RADIOLARIANS	DIATOMS		PALEOMAGNETICS	PHYS. PROPERTIES	CHEMISTRY
LOWER OLIGOCENE	CP P 21	AM CP 17 - CP 18 (NP 23)	RM *T. tuberosa*	TRACE LATE EOCENE-EARLY EOCENE				

LITHOLOGIC DESCRIPTION

NANNOFOSSIL OOZE

Major lithology: Core empty except for a few cm³ of white (10YR 8/1) nannofossil ooze in the CC.

707 A 19H NO RECOVERY

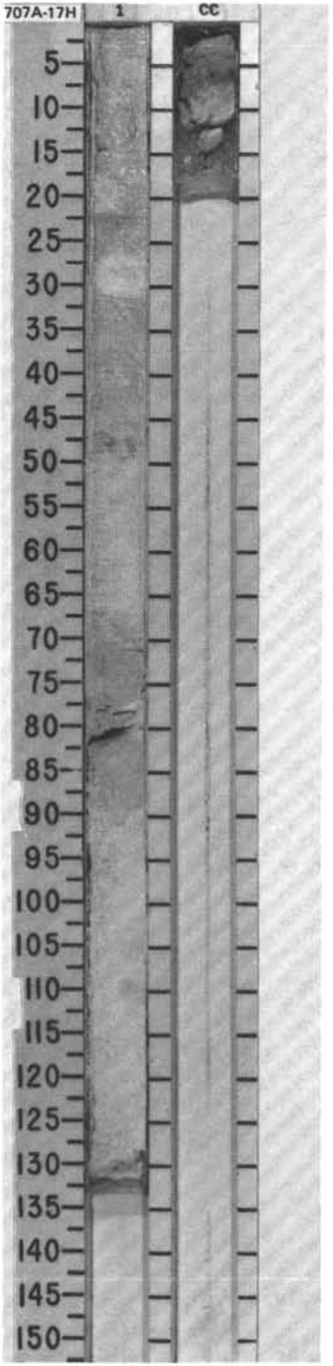

SITE 707 HOLE A CORE 20X CORED INTERVAL 1715.1-1724.8 mbsl; 173.7-183.4 mbsf

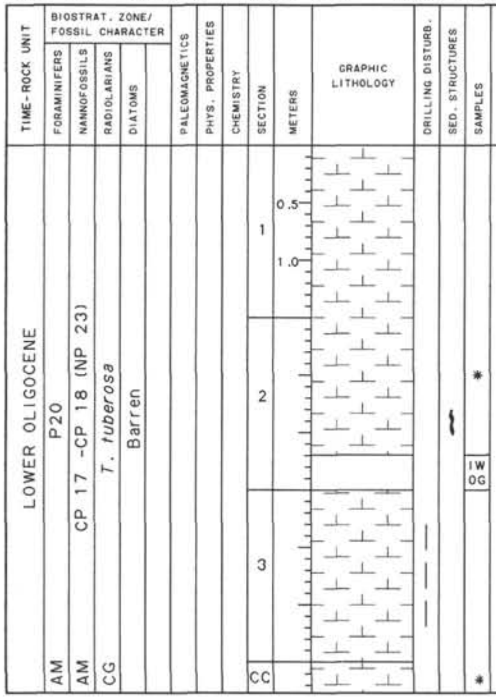

LITHOLOGIC DESCRIPTION

NANNOFOSSIL OOZE

Major lithology: Nannofossil ooze, white (N9), homogeneous, varying in degree of consolidation from soupy to firm, slightly disturbed in Section 3, 50-80 cm. Light gray horizon (10YR 7/1, 8/1) in Section 1, 97-99 cm.

SMEAR SLIDE SUMMARY (%):

	2, 50	CC, 10
	D	D
TEXTURE:		
Sand	10	10
Silt	10	10
Clay	80	80
COMPOSITION:		
Volcanic glass	Tr	Tr
Foraminifers	9	5
Nannofossils	77	88
Radiolarians	2	5
Sponge spicules	7	2
Calcareous spicules	5	Tr

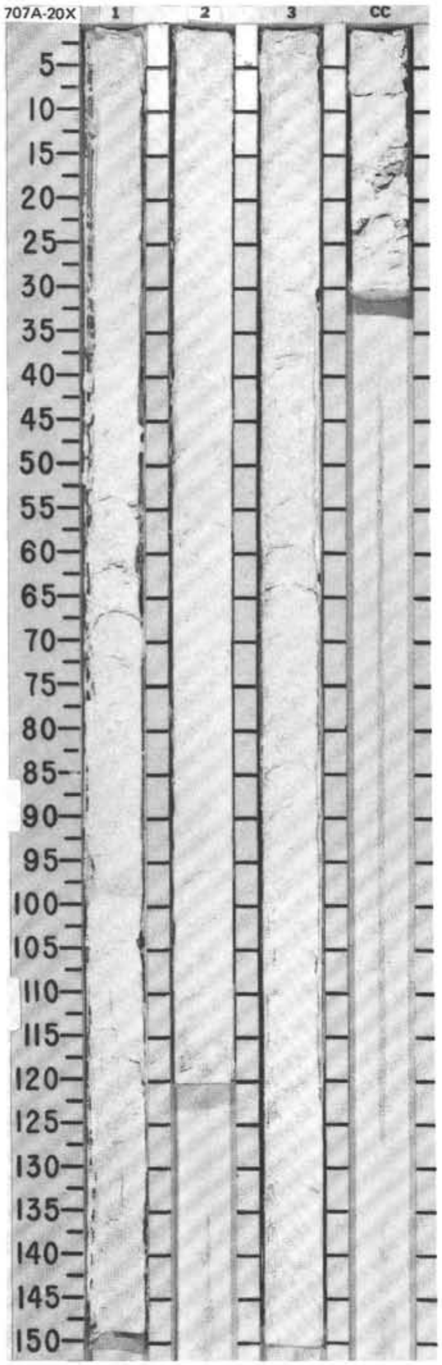

SITE 707 HOLE A CORE 21X CORED INTERVAL 1724.8-1734.5 mbsl; 183.4-193.1 mbsf

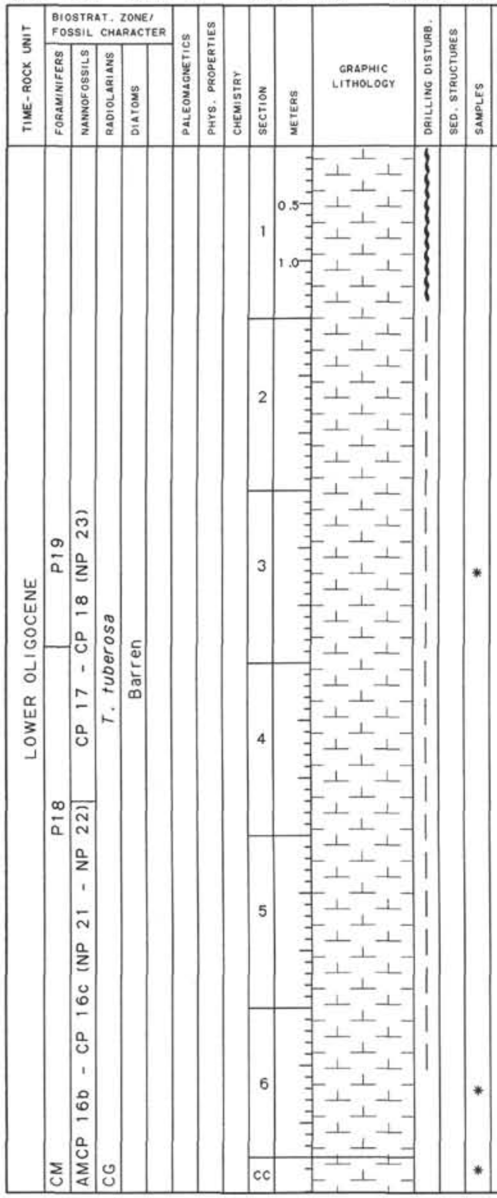

LITHOLOGIC DESCRIPTION

NANNOFOSSIL OOZE

Major lithology: Nannofossil ooze, white (N9), homogeneous, fairly soupy and moderately to slightly disturbed throughout.

SMEAR SLIDE SUMMARY (%):

	3, 75	6, 75	CC, 10
	D	D	D
TEXTURE:			
Sand	10	10	10
Clay	90	90	90
COMPOSITION:			
Volcanic glass	Tr	Tr	Tr
Accessory minerals:			
Opaques	—	—	1
Foraminifers	8	8	6
Nannofossils	89	89	88
Radiolarians	—	—	1
Sponge spicules	3	3	4

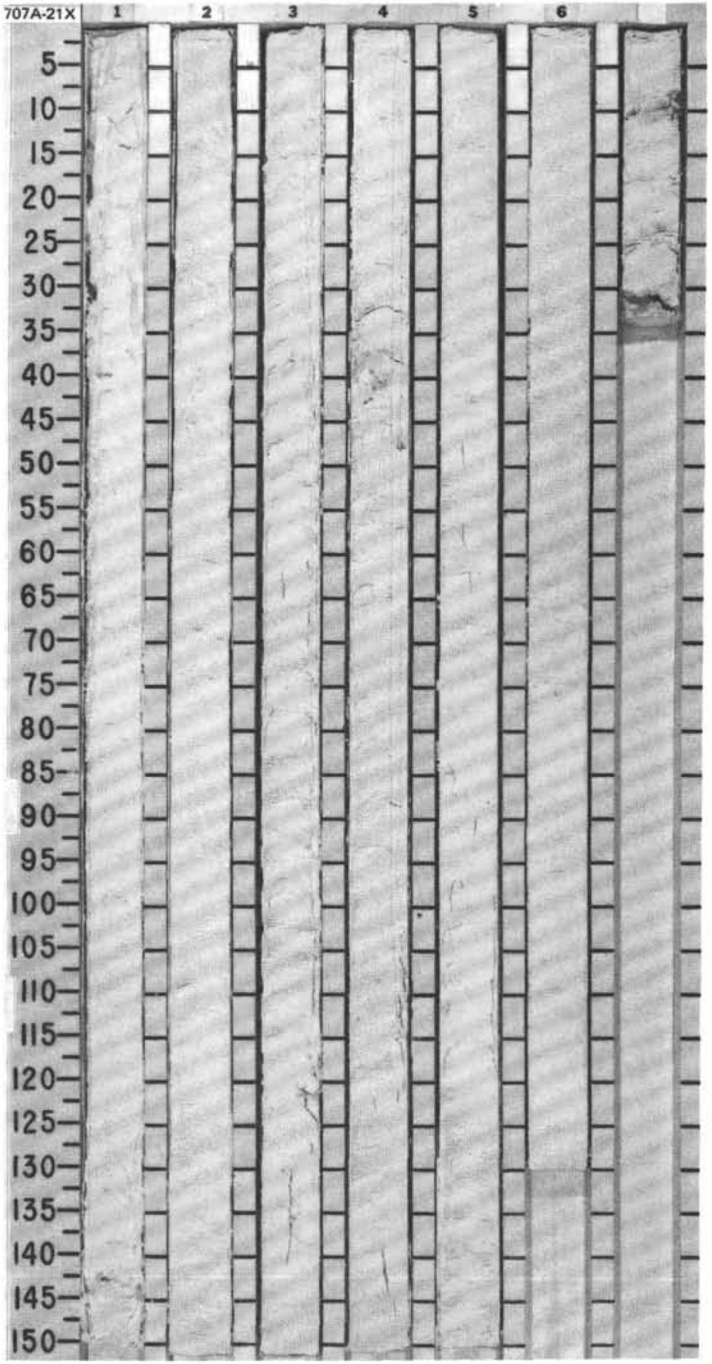

SITE 707 HOLE A CORE 22X CORED INTERVAL 1724.9-1734.5 mbsl; 193.1-202.7 mbsf

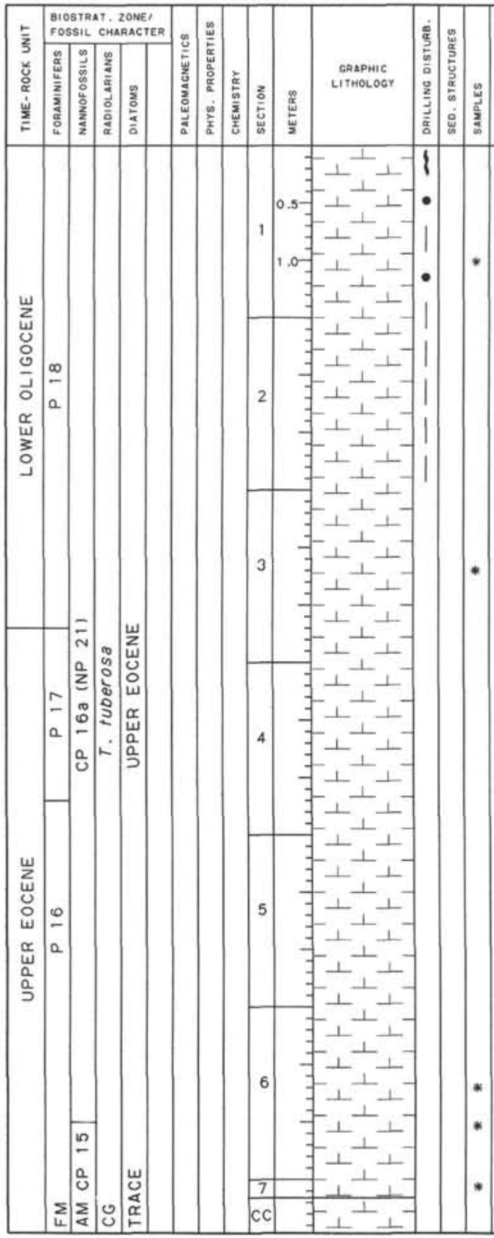

LITHOLOGIC DESCRIPTION

NANNOFOSSIL OOZE

Major lithology: Nannofossil ooze, white (N9, 2.5Y 8/2), homogeneous, varying slightly throughout in degree of consolidation. Dark grayish brown (2.5Y 4/2) mottles in Section 1, 60 cm; Section 2, 39-40 cm; and Section 6, 107-108 cm.

SMEAR SLIDE SUMMARY (%):

	1, 87 D	3, 75 D	6, 75 D	6, 105 D	7, 9 D
TEXTURE:					
Sand	5	5	5	5	5
Silt	—	—	—	10	—
Clay	95	95	95	85	95
COMPOSITION:					
Volcanic glass	—	Tr	—	—	Tr
Accessory minerals:					
Opaques	2	—	—	Tr	—
Foraminifers	3	5	5	3	3
Nannofossils	90	87	94	82	87
Sponge spicules	—	Tr	Tr	8	5
Silicoflagellates	5	8	1	7	5

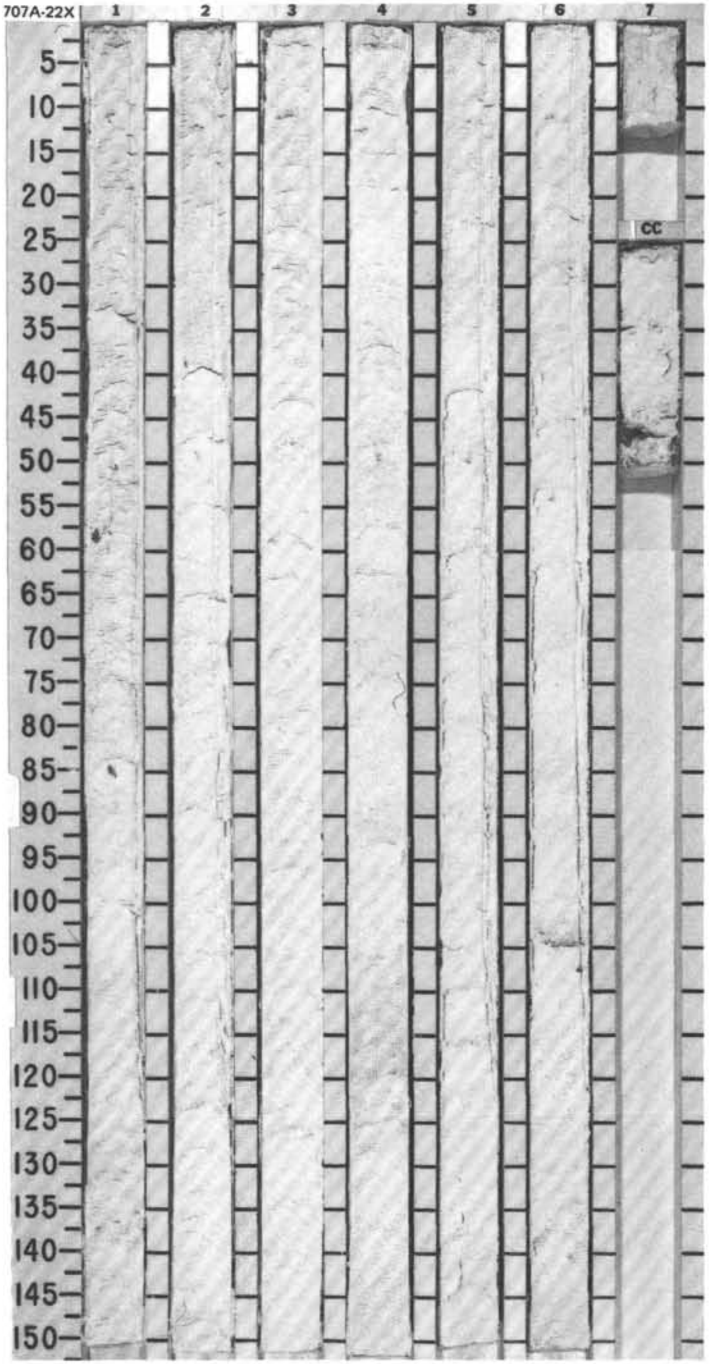

SITE 707 HOLE A CORE 23X CORED INTERVAL 1744.1-1753.7 mbsl; 202.7-212.3 mbsf

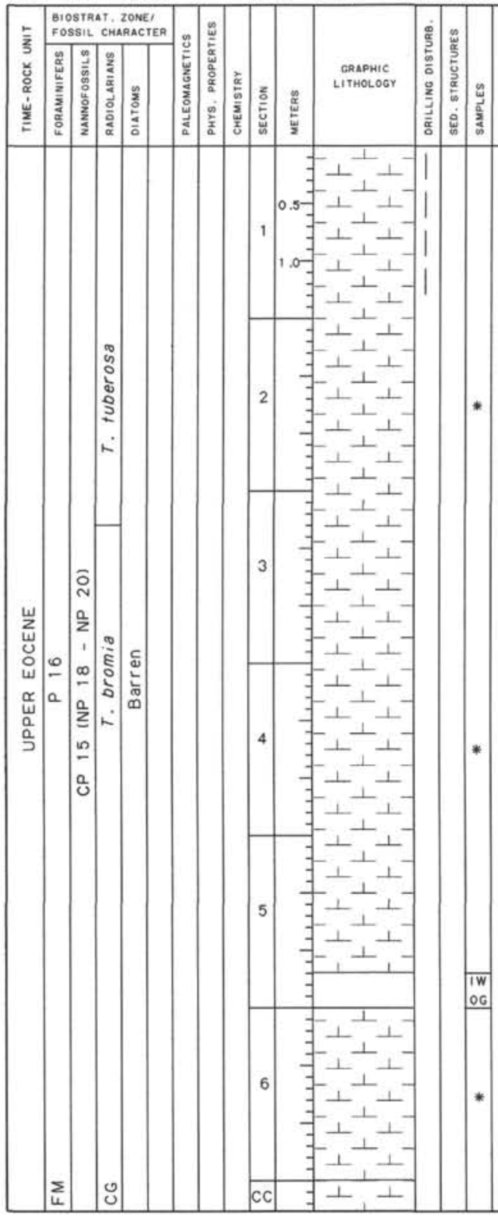

LITHOLOGIC DESCRIPTION

NANNOFOSSIL OOZE

Major lithology: Nannofossil ooze, white to light gray (N9, N7), homogeneous. No visible structures except for slight disturbance in Section 1, 0-120 cm.

SMEAR SLIDE SUMMARY (%):

	2, 75 D	4, 75 D	6, 75 D
TEXTURE:			
Sand	10	10	10
Clay	90	90	90
COMPOSITION:			
Volcanic glass	Tr	—	Tr
Foraminifers	3	2	3
Nannofossils	89	88	90
Radiolarians	3	4	2
Sponge spicules	5	6	5

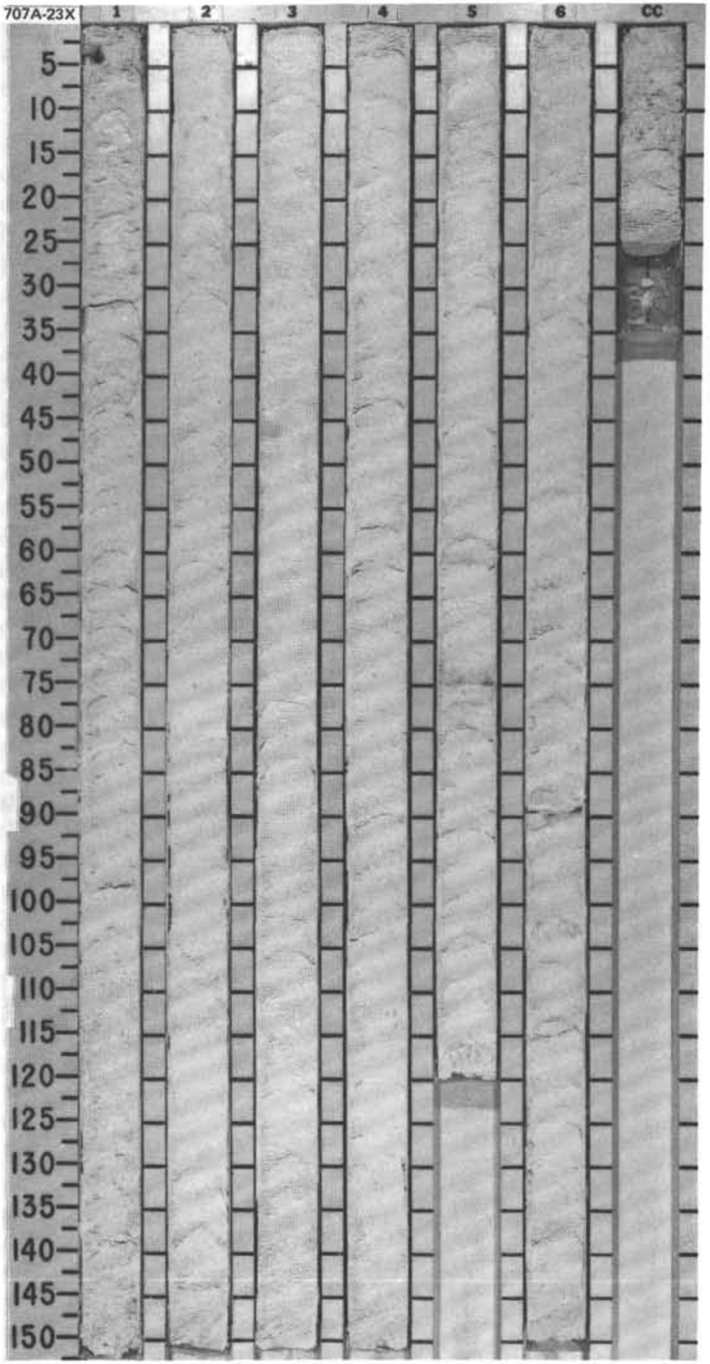

SITE 707 HOLE B CORE 1H CORED INTERVAL 1541.4-1550.9 mbsl; 0.0-9.5 mbsf

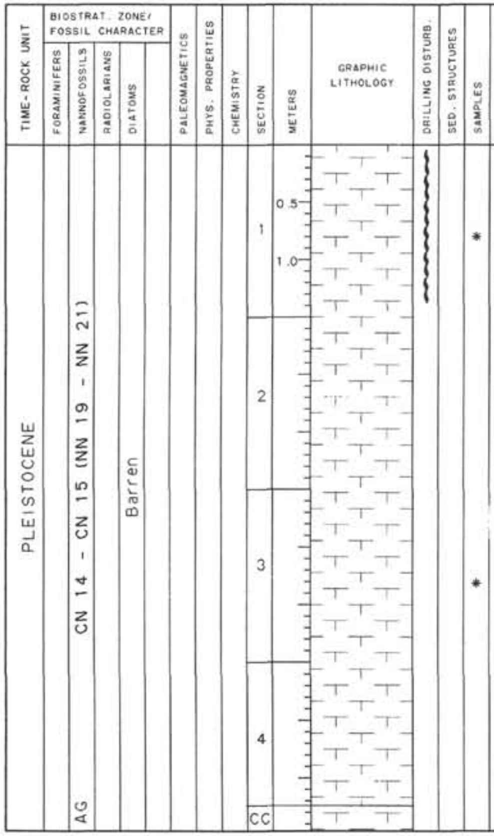

LITHOLOGIC DESCRIPTION

NANNOFOSSIL-BEARING FORAMINIFERAL OOZE

Major lithology: Nannofossil-bearing foraminiferal ooze, white (2.5Y 8/2, 10YR 8/2) and very pale brown (10YR 8/3) to light gray (10YR 7/2). Homogeneous, except for very faint, gradational color changes. No visible structures.

Section 1 in core is very soupy and disturbed.

SMEAR SLIDE SUMMARY (%):

	1, 80 D	3, 80 D
TEXTURE:		
Sand	80	80
Silt	10	10
Clay	10	10
COMPOSITION:		
Foraminifers	90	90
Nannofossils	10	10

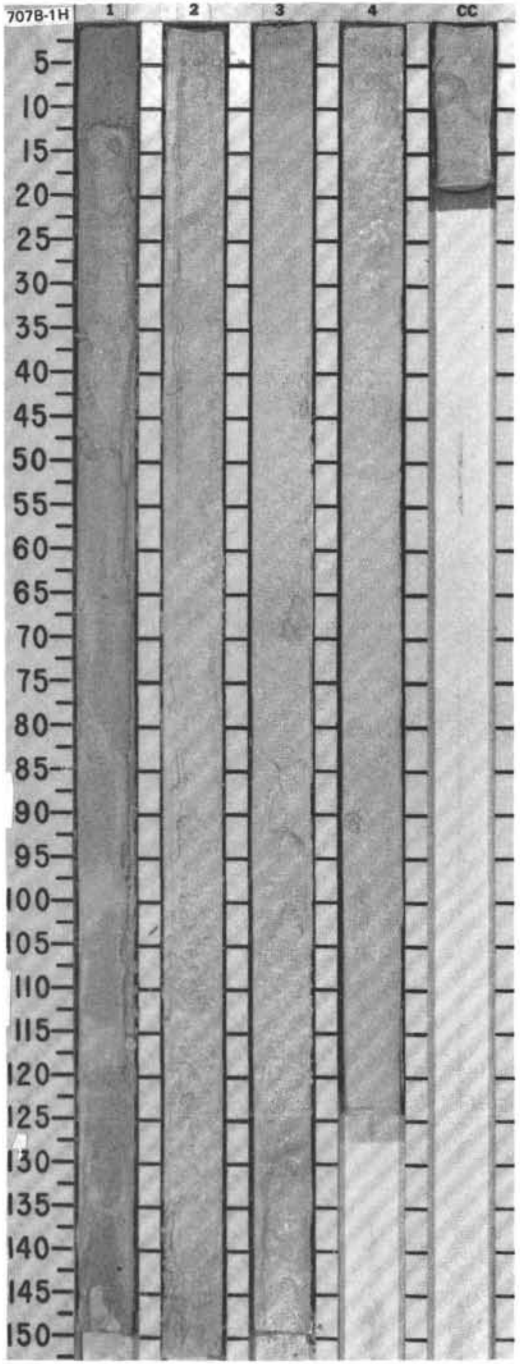

SITE 707 HOLE B CORE 2H CORED INTERVAL 1550.9-1560.5 mbsl; 9.5-19.1 mbsf

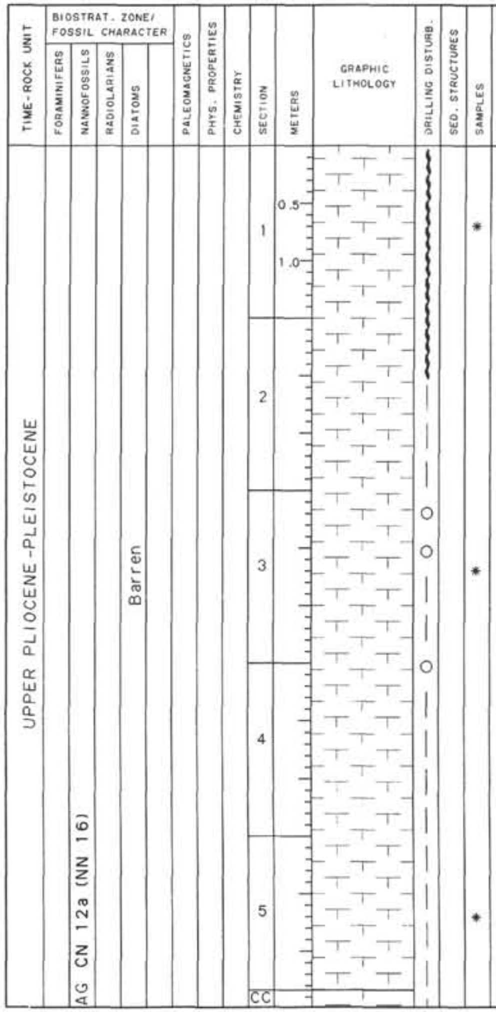

LITHOLOGIC DESCRIPTION

NANNOFOSSIL-BEARING FORAMINIFERAL OOZE

Major lithology: Nannofossil-bearing foraminiferal ooze, white (10YR 8/2), homogeneous, changing color slightly to 10YR 8/1 below Section 3, 135 cm.

Much of core is disturbed, particularly Section 1, where brown-stained foraminifer tests between 0-100 cm and soupy nature of sediments suggest *introduction of reworked(?) material.*

SMEAR SLIDE SUMMARY (%):

	1, 70 D	3, 70 D	5, 70 D
TEXTURE:			
Sand	80	80	80
Silt	10	5	10
Clay	10	15	10
COMPOSITION:			
Foraminifers	90	87	90
Nannofossils	10	13	10

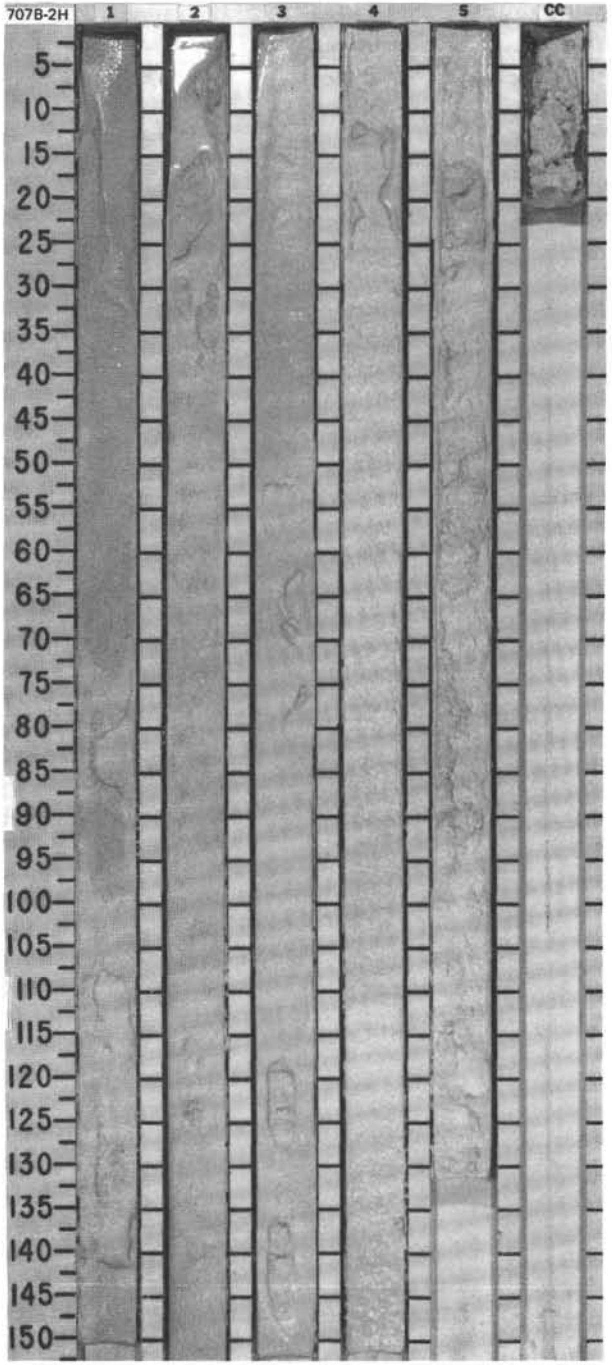

SITE 707 HOLE B CORE 3H CORED INTERVAL 1560.5-1570.1 mbsl; 19.1-28.7 mbsf

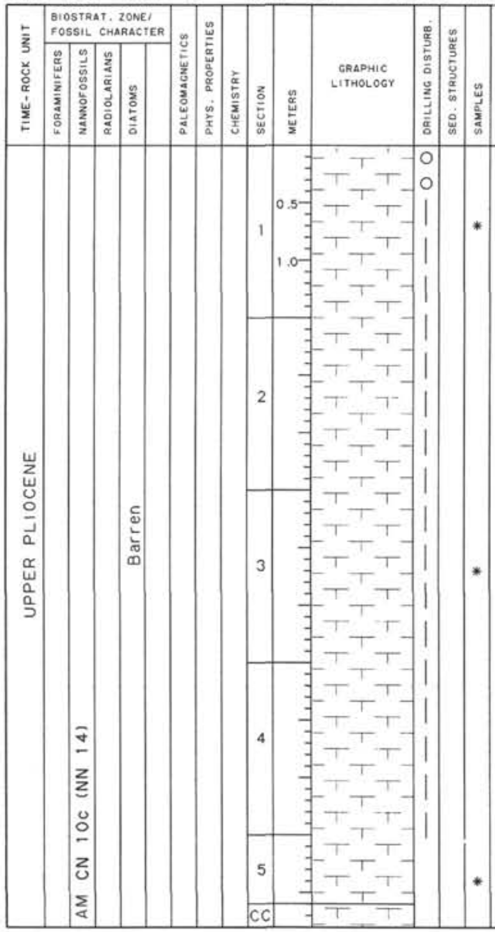

LITHOLOGIC DESCRIPTION

NANNOFOSSIL-BEARING FORAMINIFERAL OOZE

Major lithology: Nannofossil-bearing foraminiferal ooze, white (10YR 8/2, 8/1), homogeneous. Whole core shows evidence of slight disturbance.

SMEAR SLIDE SUMMARY (%):

	1, 70 D	3, 70 D	5, 40 D
TEXTURE:			
Sand	80	80	80
Silt	10	10	5
Clay	10	10	15
COMPOSITION:			
Foraminifers	90	90	90
Nannofossils	10	10	—
Sponge spicules	—	Tr	Tr

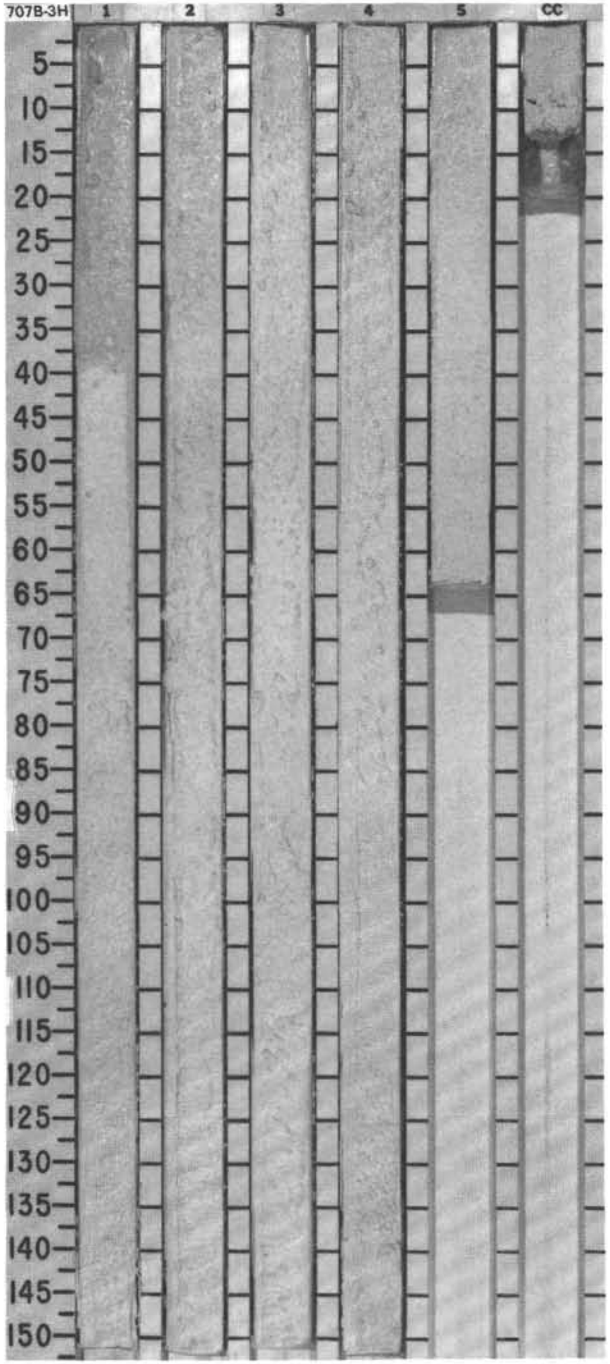

SITE 707 HOLE B CORE 4H CORED INTERVAL 1570.1-1579.8 mbsl; 28.7-38.4 mbsf

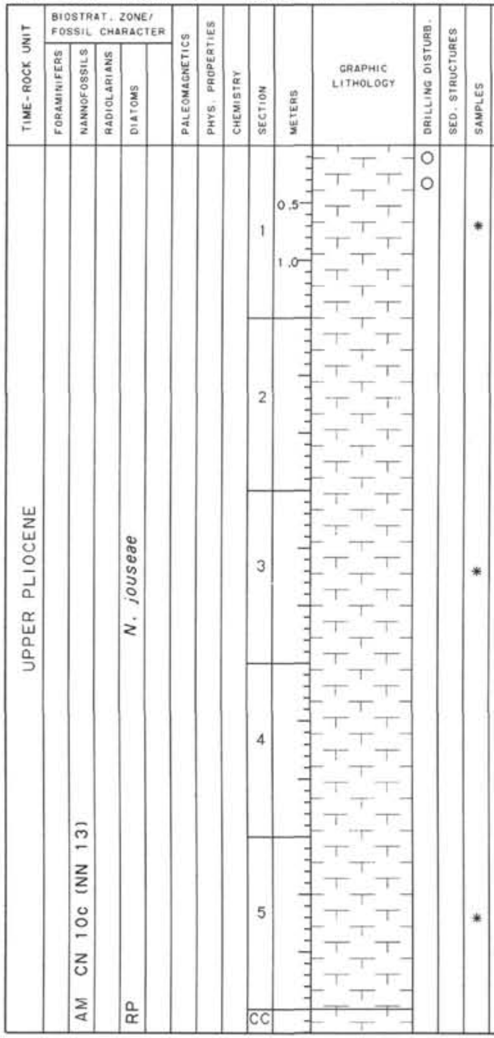

LITHOLOGIC DESCRIPTION

NANNOFOSSIL-BEARING FORAMINIFERAL OOZE

Major lithology: Nannofossil-bearing foraminiferal ooze, grayish white (10YR 8/1), grading to white (N9) below Section 1, 135 cm. Light gray (N8) horizons visible in Section 2, 10-32, 67-75, and 109-110 cm; Section 3, 8-15, 37-47, 101-105, and 146-150 cm; Section 4, 1-6, 63-64, 105-109, and 135-150 cm; and Section 5, 1-8, 67-68, 78-81, and 105-106 cm. Pyrite staining of sediments between 113-119 cm in Section 5.

SMEAR SLIDE SUMMARY (%):

	1, 70 D	3, 70 D	5, 70 D
TEXTURE:			
Sand	90	80	70
Silt	—	5	10
Clay	10	15	20
COMPOSITION:			
Foraminifers	90	85	80
Nannofossils	10	15	20
Sponge spicules	—	Tr	Tr

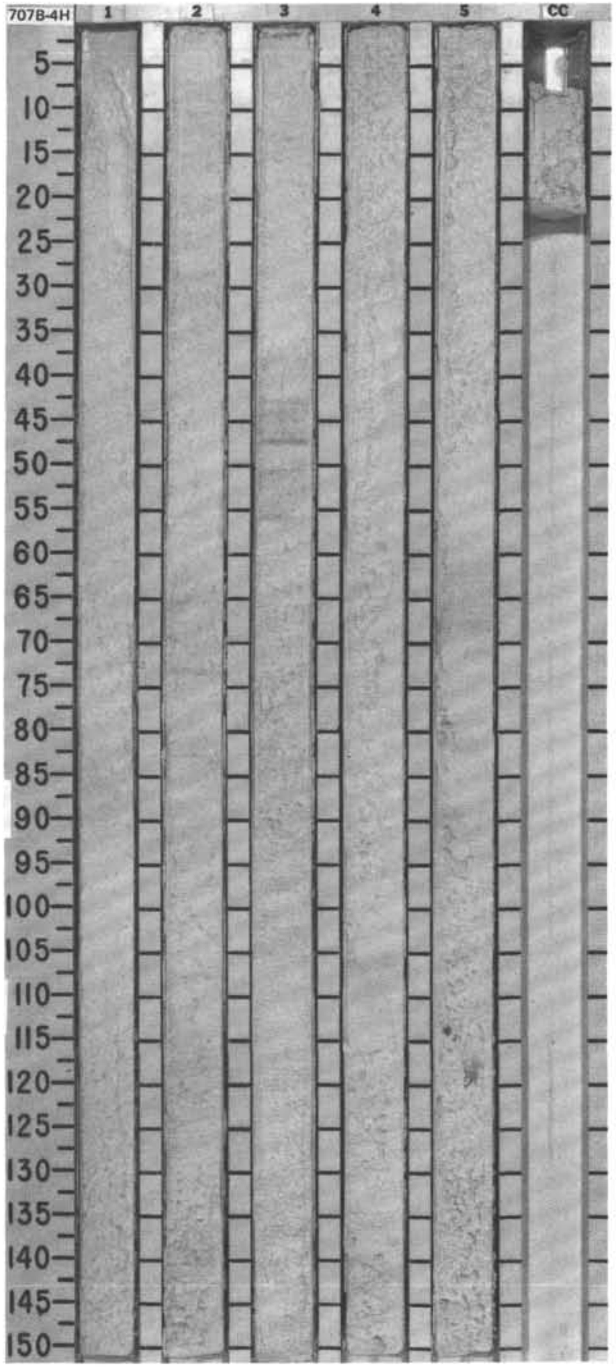

SITE 707 HOLE B CORE 5H CORED INTERVAL 1579.8-1589.4 mbsl; 38.4-48.0 mbsf

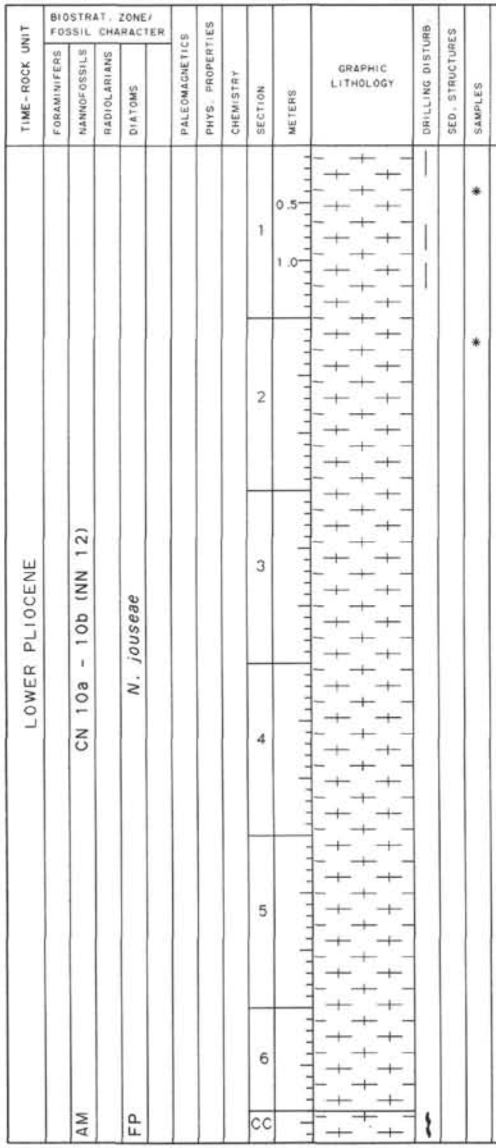

LITHOLOGIC DESCRIPTION

FORAMINIFER-NANNOFOSSIL OOZE

Major lithology: Foraminifer-nannofossil ooze, white (N9), homogeneous in composition, with indistinct light gray (N7, N8) to very light green (5G 8/2, 9/2) horizons in Section 1, 55, 75-80, and 148-150 cm; Section 2, 10, 20, 30, and 100-105 cm; Section 3, 5-7, 20, 30, 60-64, and 103-107 cm; Section 4, interbedded between 37-107 cm; Section 5, 15, 20-23, and 145 cm; and Section 6, interbedded between 20-75 cm. Pyritized burrows found in Section 3, 40 and 73 cm.

SMEAR SLIDE SUMMARY (%):

	1, 40 D	2, 18 D
TEXTURE:		
Sand	15	30
Silt	15	10
Clay	70	60
COMPOSITION:		
Volcanic glass	Tr	Tr
Foraminifers	30	38
Nannofossils	70	60
Diatoms	Tr	—
Radiolarians	Tr	Tr
Sponge spicules	Tr	2

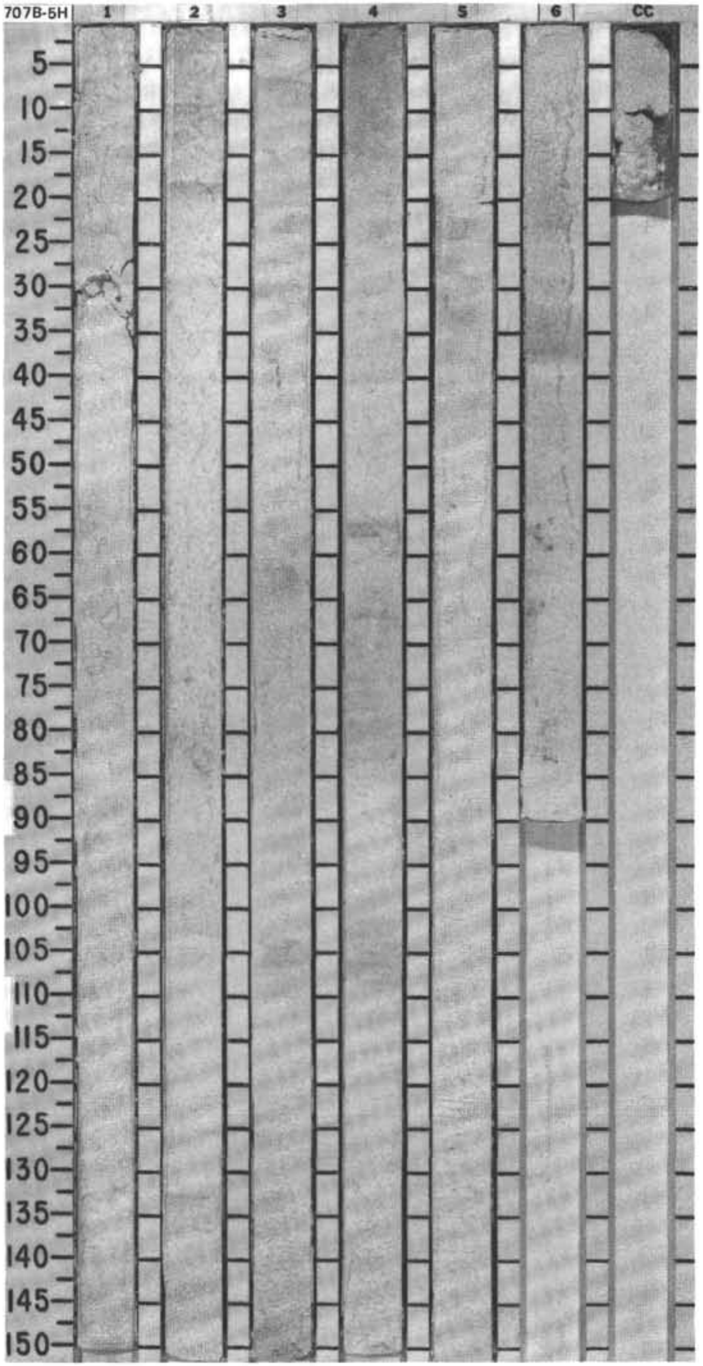

SITE 707 HOLE B CORE 6H CORED INTERVAL 1589.4-1599.0 mbsl; 48.0-57.6 mbsf

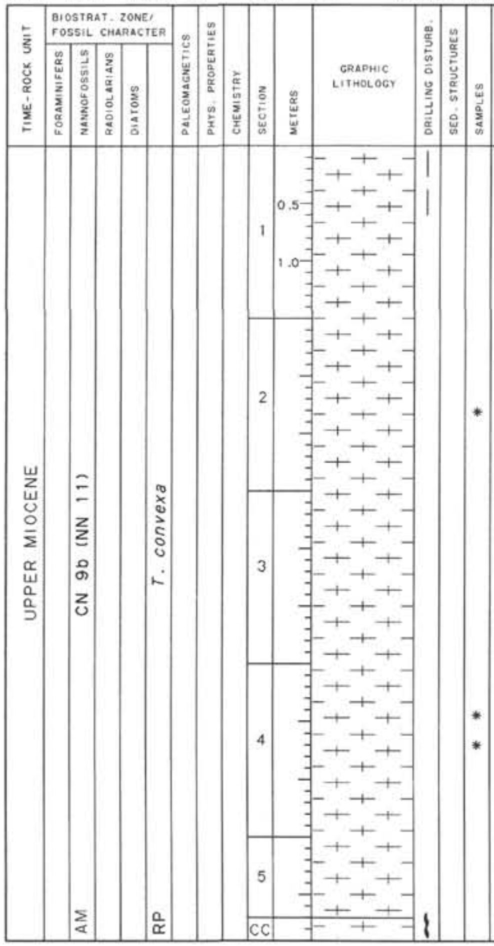

LITHOLOGIC DESCRIPTION

FORAMINIFER-NANNOFOSSIL OOZE

Major lithology: Foraminifer-nannofossil ooze, white (N9), homogeneous, with indistinct very light gray (N7, N8) to very light green (5G 8/2) horizons in Section 1, 23-25, 40, 60-64, 73, and 144-145 cm; Section 2, 50-60, 95, 125, and 139-144 cm; Section 3, 35-45, 73-80, and 110-116 cm; Section 4, 8-10, 15, 33-35, and 105 cm; and Section 5, 15-18, 37-39, and 63-65 cm. Very light yellowish gray (2.5Y 7/2) horizons observed in Section 4, 21-23, 45-46, and 134-140 cm, and Section 5, 46-48 cm.

SMEAR SLIDE SUMMARY (%):

	2, 80 D	4, 46 D	4, 70 M
TEXTURE:			
Sand	20	20	20
Silt	10	15	15
Clay	70	65	65
COMPOSITION:			
Feldspar	Tr	—	—
Volcanic glass	—	Tr	Tr
Accessory minerals:			
Pyrite framboids	—	—	2
Foraminifers	30	35	35
Nannofossils	70	65	60
Radiolarians	Tr	Tr	1
Sponge spicules	Tr	Tr	2

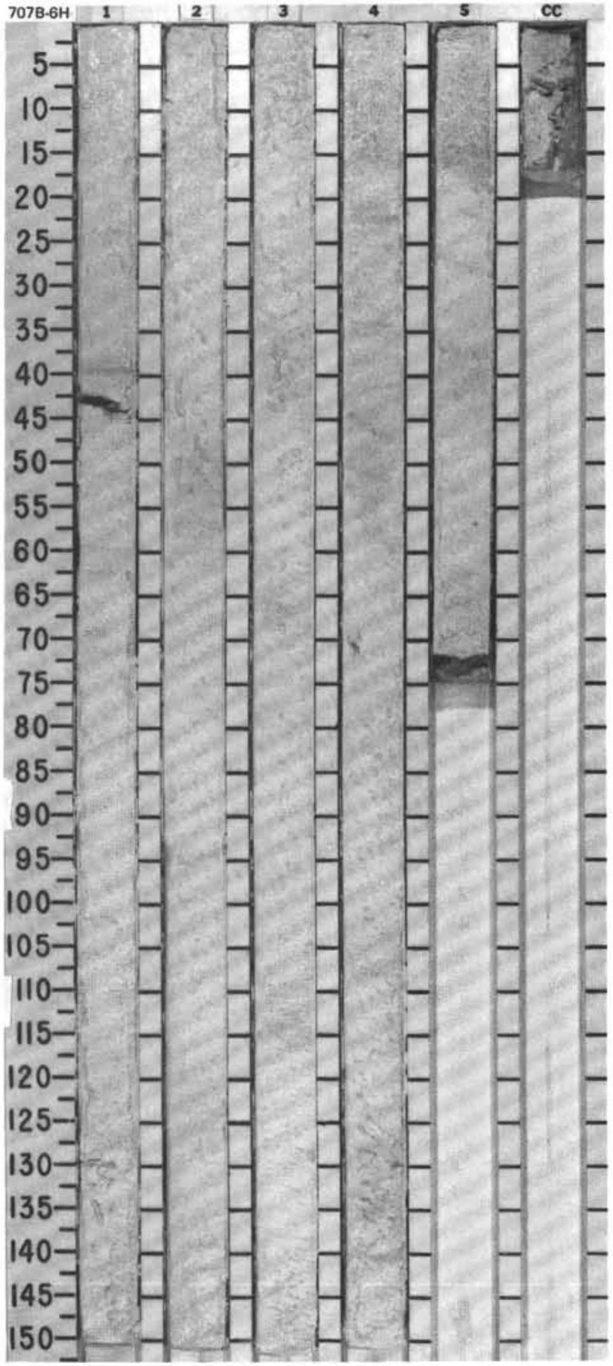

SITE 707 HOLE B CORE 7H CORED INTERVAL 1599.0-1608.6 mbsl; 57.6-67.2 mbsf

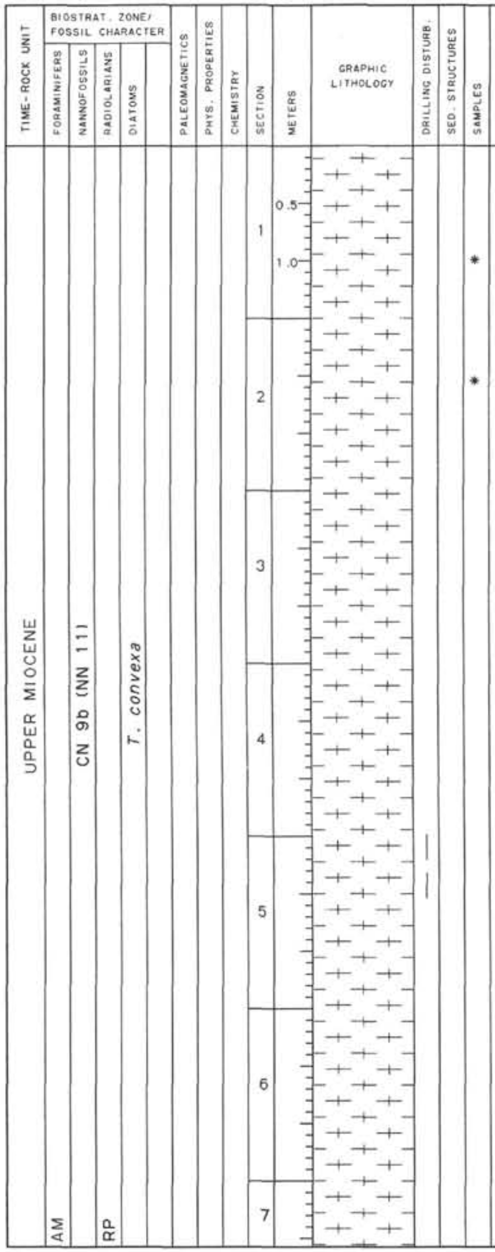

LITHOLOGIC DESCRIPTION

FORAMINIFER-NANNOFOSSIL OOZE

Major lithology: Foraminifer-nannofossil ooze, white (N9), homogeneous, with subtle very light gray (N8) to light yellowish gray (2.5Y 7/2) horizons in Section 1, 11-13, 17, 43, 75-80, and 130-140 cm; Section 2, 21-23, 50-58, and 65-75; Section 3, 28-30, 41-52, 66-76, and 144 cm; Section 4, 8, 22, 90, 97-100, and 128 cm; Section 5, 110 and 133 cm; and Section 6, 35 cm; and in Section 7, numerous thin layers between 40-55 cm. Many of these layers have a sharp base and gradational (bioturbated) upper contact. Pyritized blebs (burrows?) in Section 2, 105-106 cm; Section 4, 83 cm; and Section 6, 2-5 cm.

SMEAR SLIDE SUMMARY (%):

	1, 100 D	2, 57 D
TEXTURE:		
Sand	20	25
Silt	20	15
Clay	60	60
COMPOSITION:		
Feldspar	—	Tr
Volcanic glass	—	Tr
Foraminifers	38	38
Nannofossils	60	60
Radiolarians	Tr	—
Sponge spicules	2	2
Silicoflagellates	Tr	—

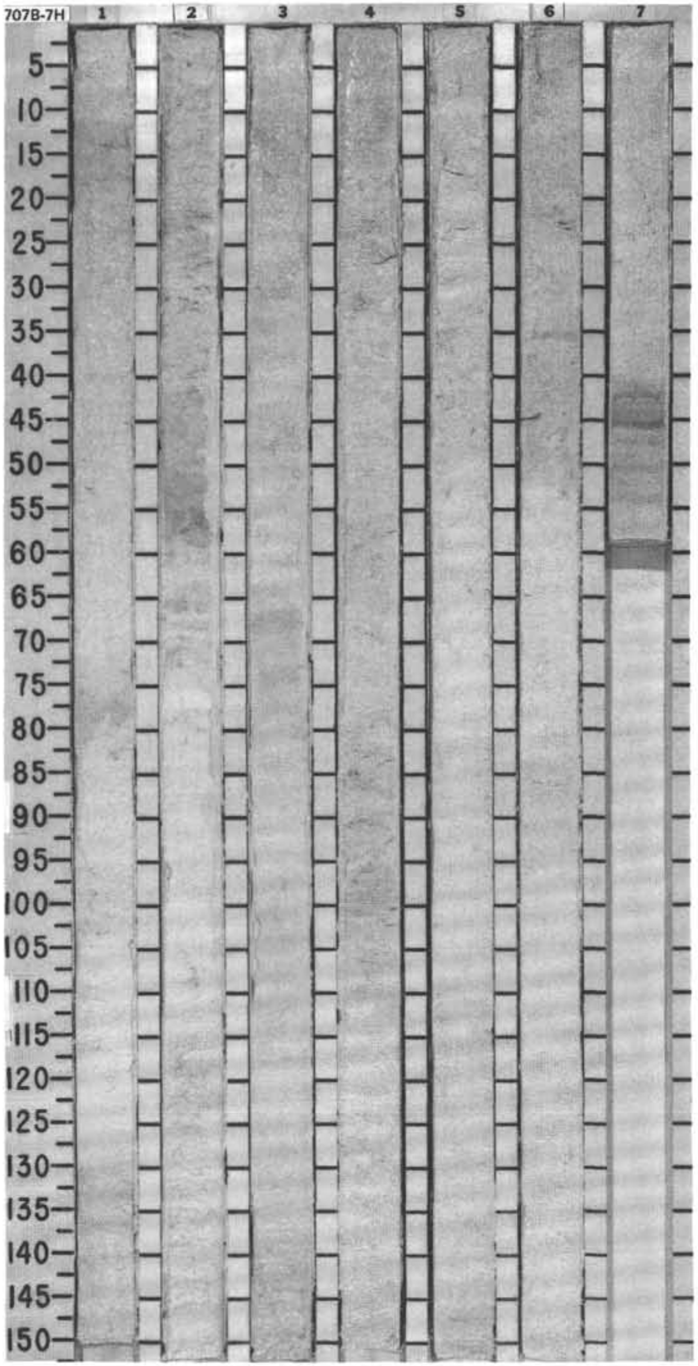

SITE 707 HOLE B CORE 8H CORED INTERVAL 1608.6-1618.3 mbsl; 67.2-76.9 mbsf

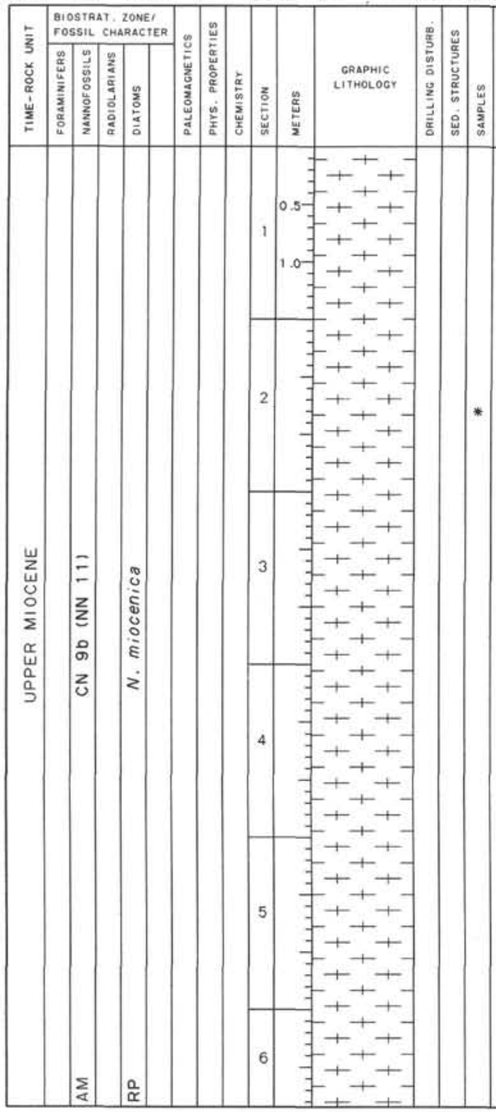

LITHOLOGIC DESCRIPTION

FORAMINIFER-NANNOFOSSIL OOZE

Major lithology: *Foraminifer-nannofossil ooze*, white (N9), homogeneous, with subtle light gray (N7, N8) to very light yellowish gray (2.5Y 7/2) horizons in Section 1, 33-37 and 50-52 cm; Section 2, 22-28, 95-102, 105-107, 112-118, and 138-140 cm; Section 3, 44-59 and 108-145 cm; Section 4, 45-50, 103-105, 110, and 116-123 cm; Section 5, 48-54, 83-85, 124-135; and Section 6, 34-36 and 52-56 cm.

SMEAR SLIDE SUMMARY (%):

	2, 80 D
TEXTURE:	
Sand	20
Silt	17
Clay	63
COMPOSITION:	
Foraminifers	35
Nannofossils	63
Radiolarians	Tr
Sponge spicules	2

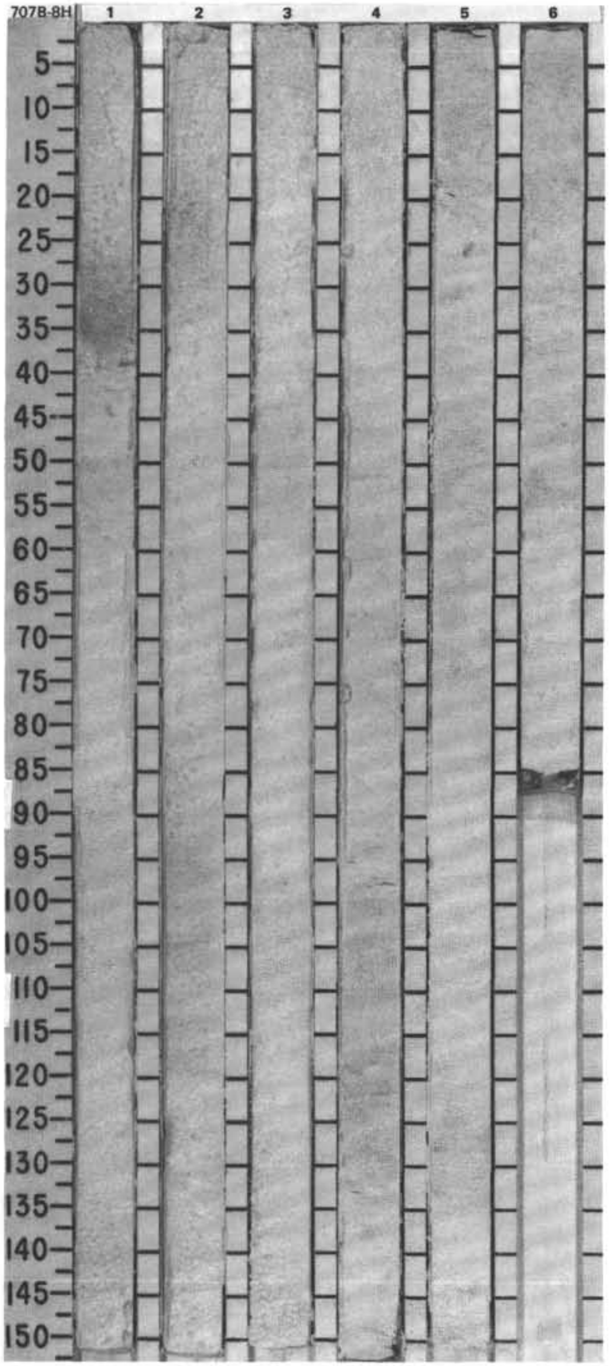

SITE 707 HOLE B CORE 9H CORED INTERVAL 1618.3-1627.9 mbsl; 76.9-86.5 mbsf

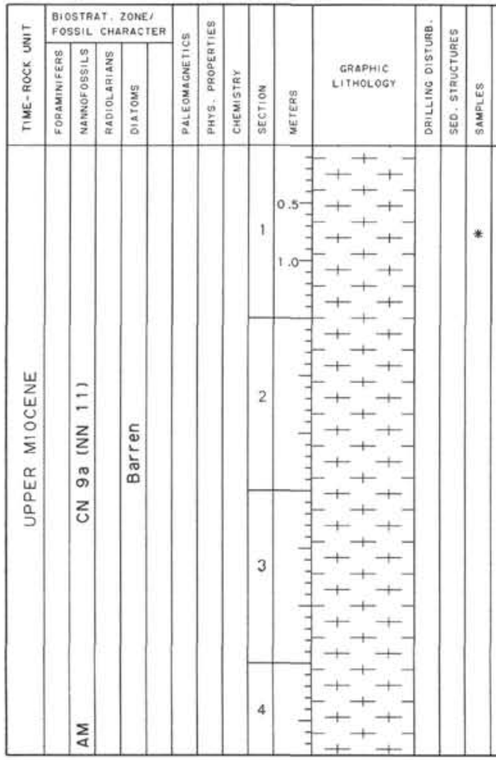

LITHOLOGIC DESCRIPTION

FORAMINIFER-NANNOFOSSIL OOZE

Major lithology: Foraminifer-nannofossil ooze, white (N9), homogeneous, with subtle light gray (N7, N8) horizons in Section 1, 35-46 cm; Section 2, 23-26 and 72-81 cm; and Section 3, 21-31 cm.

SMEAR SLIDE SUMMARY (%):

	1, 80 D
TEXTURE:	
Sand	20
Silt	15
Clay	65
COMPOSITION:	
Volcanic glass	Tr
Foraminifers	33
Nannofossils	65
Diatoms	Tr
Radiolarians	Tr
Sponge spicules	2

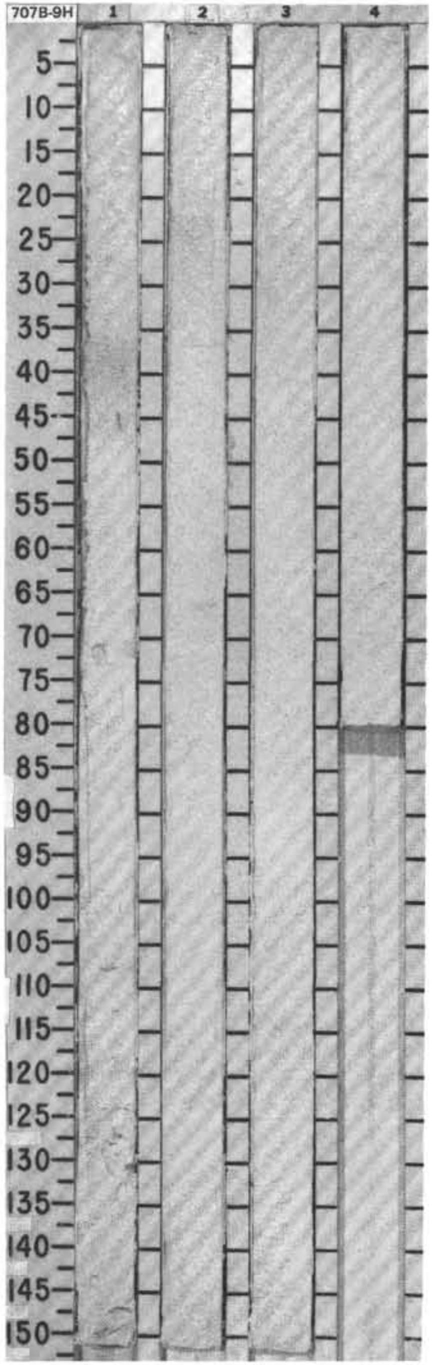

SITE 707 HOLE B CORE 10H CORED INTERVAL 1627.9-1637.5 mbsl; 86.5-96.1 mbsf

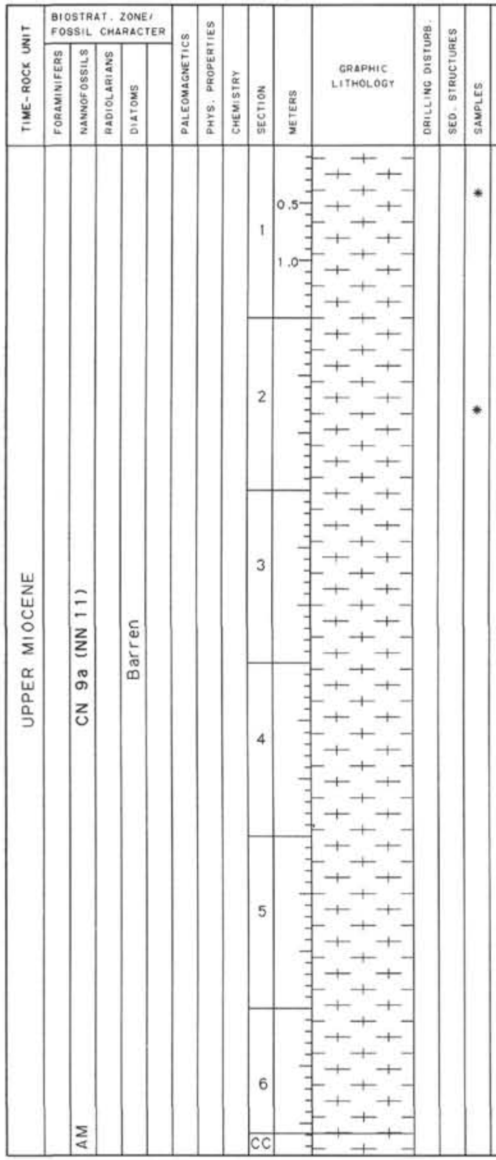

LITHOLOGIC DESCRIPTION

FORAMINIFER-NANNOFOSSIL OOZE

Major lithology: Foraminifer-nannofossil ooze, white (N9), homogeneous, with subtle light gray (N7, N8) horizons in Section 1, 30-42, 76-83, and 105-110 cm; Section 2, 118-140 cm; Section 3, 13-14, 43-45, 118, and 126 cm; and Section 4, 35-36 cm.

SMEAR SLIDE SUMMARY (%):

	1, 42 D	2, 80 D
TEXTURE:		
Sand	25	20
Silt	10	12
Clay	65	68
COMPOSITION:		
Feldspar	—	Tr
Foraminifers	33	30
Nannofossils	65	68
Diatoms	—	Tr
Radiolarians	Tr	Tr
Sponge spicules	2	2

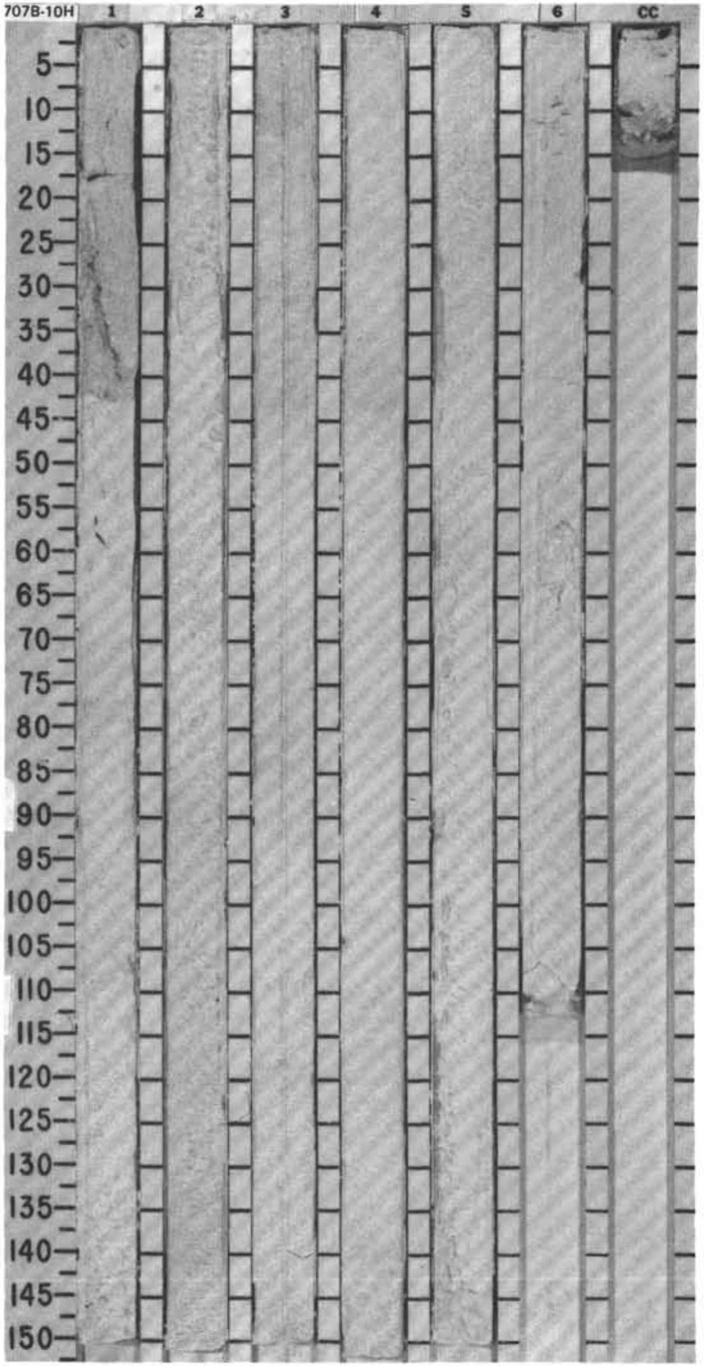

SITE 707 HOLE B CORE 11H CORED INTERVAL 1637.5-1647.1 mbsl; 96.1-105.7 mbsf

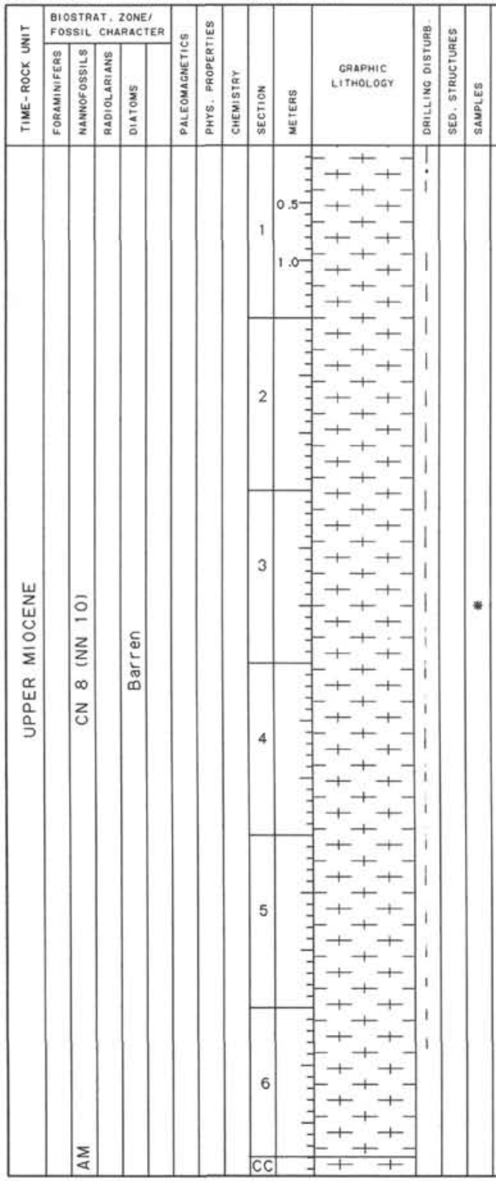

LITHOLOGIC DESCRIPTION

FORAMINIFER-NANNOFOSSIL OOZE

Major lithology: Foraminifer-nannofossil ooze, white (N9), homogeneous but soupy, with visible core disturbance as indicated. Core is first in this hole to show incipient induration over short intervals.

SMEAR SLIDE SUMMARY (%):

	3, 100 D
TEXTURE:	
Sand	15
Silt	15
Clay	70
COMPOSITION:	
Foraminifers	29
Nannofossils	70
Radiolarians	Tr
Sponge spicules	1

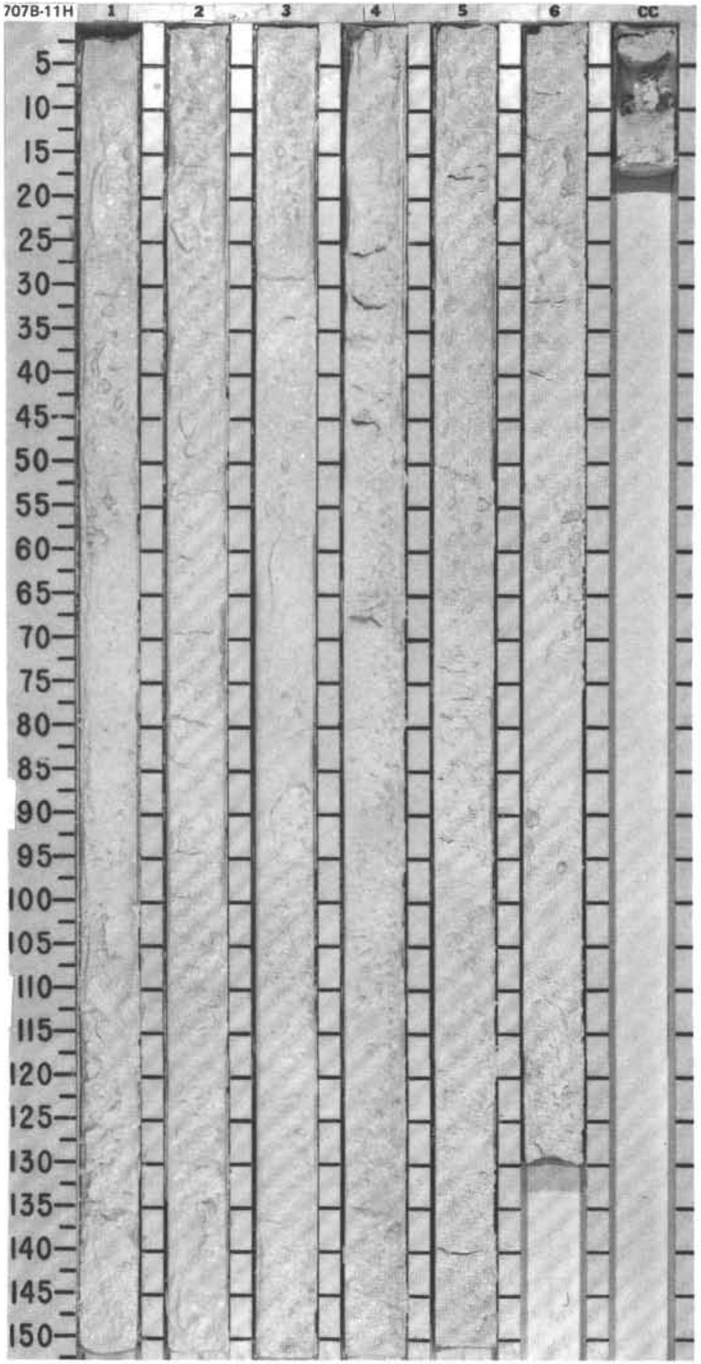

SITE 707 HOLE B CORE 12H CORED INTERVAL 1647.1-1656.7 mbsl; 105.7-115.3 mbsf

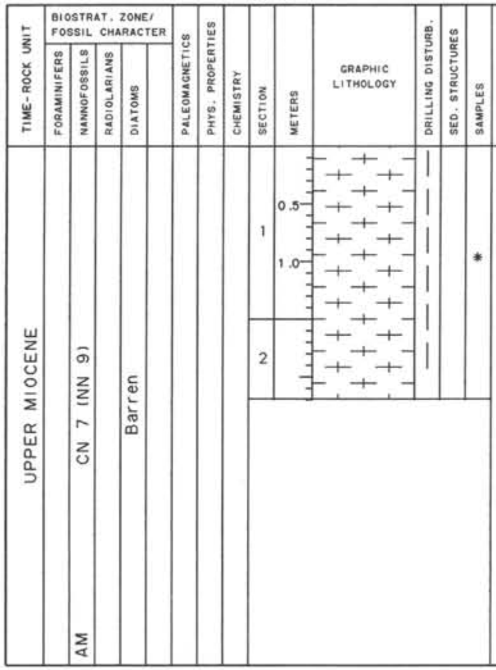

LITHOLOGIC DESCRIPTION

FORAMINIFER-NANNOFOSSIL OOZE

Major lithology: Foraminifer-nannofossil ooze, white (N9), homogeneous, with subtle light gray (N7, N8) bands in Section 2, 40-43 and 48 cm. Section 1 slightly disturbed.

SMEAR SLIDE SUMMARY (%):

	1, 80 D
TEXTURE:	
Sand	20
Silt	15
Clay	65
COMPOSITION:	
Volcanic glass	Tr
Foraminifers	34
Nannofossils	65
Diatoms	Tr
Radiolarians	Tr
Sponge spicules	1

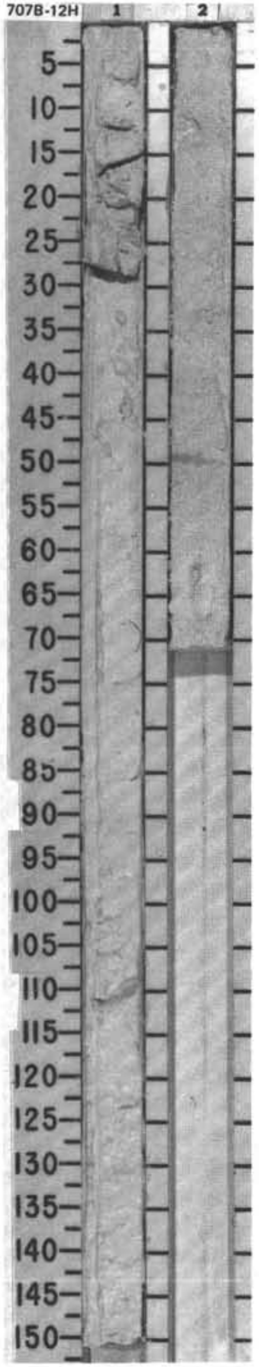

SITE 707 HOLE B CORE 13H CORED INTERVAL 1656.7-1666.3 mbsl; 115.3-124.9 mbsf

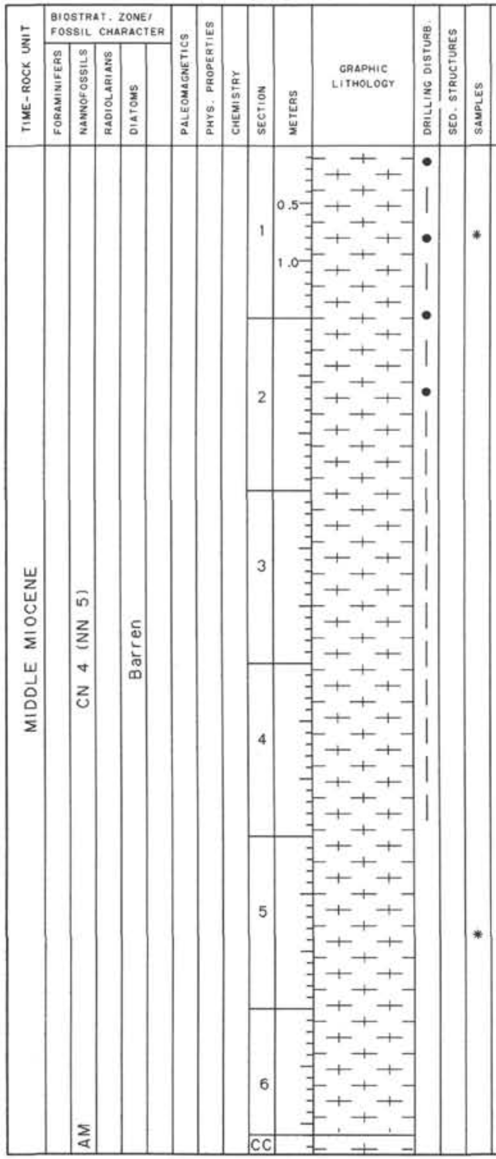

LITHOLOGIC DESCRIPTION

FORAMINIFER-NANNOFOSSIL OOZE

Major lithology: Foraminifer-nannofossil ooze, white (N9), homogeneous, with slightly indurated chalky nodules or biscuits in a soupy and predominantly ooze matrix.

SMEAR SLIDE SUMMARY (%):

	1, 63 D	5, 80 D
TEXTURE:		
Sand	20	20
Silt	10	15
Clay	70	65
COMPOSITION:		
Volcanic glass	—	Tr
Foraminifers	30	35
Nannofossils	70	65
Radiolarians	Tr	Tr
Sponge spicules	—	Tr

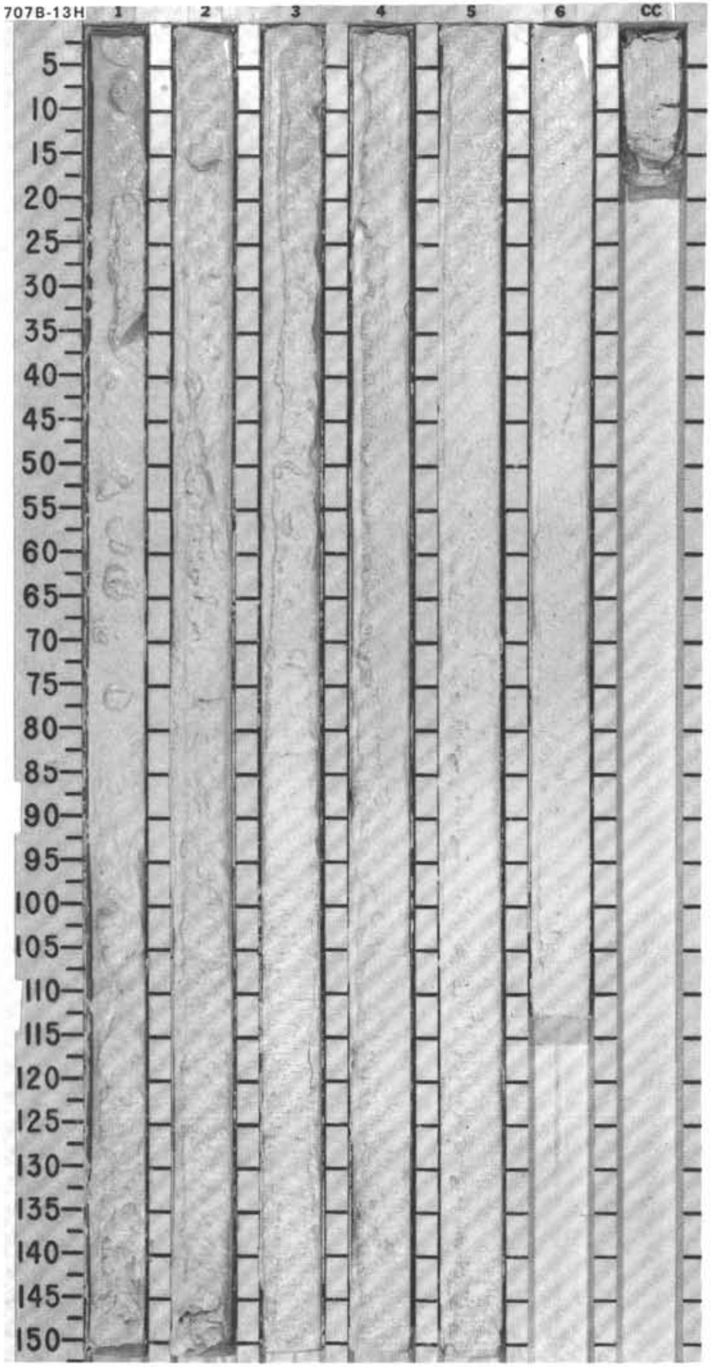

SITE 707 HOLE C CORE 1W CORED INTERVAL 1541.4-1725.2 mbsl; 0.0-183.8 mbsf

TIME-ROCK UNIT	BIOSTRAT. ZONE/ FOSSIL CHARACTER				PALEOMAGNETICS	PHYS. PROPERTIES	CHEMISTRY	SECTION	METERS	GRAPHIC LITHOLOGY	DRILLING DISTURB.	SED. STRUCTURES	SAMPLES	LITHOLOGIC DESCRIPTION
	FORAMINIFERS	NANNOFOSSILS	RADIOLARIANS	DIATOMS										
								1						FORAMINIFER-NANNOFOSSIL CHALK Major lithology: Liner empty except for a few pieces of moderately consolidated, white (N9) to pale yellow (2.5Y 9/2) foraminifer-nannofossil chalk.

707 C 2R NO RECOVERY

SITE 707 HOLE C CORE 3R CORED INTERVAL 1734.9-1744.5 mbsl; 193.5-203.1 mbsf

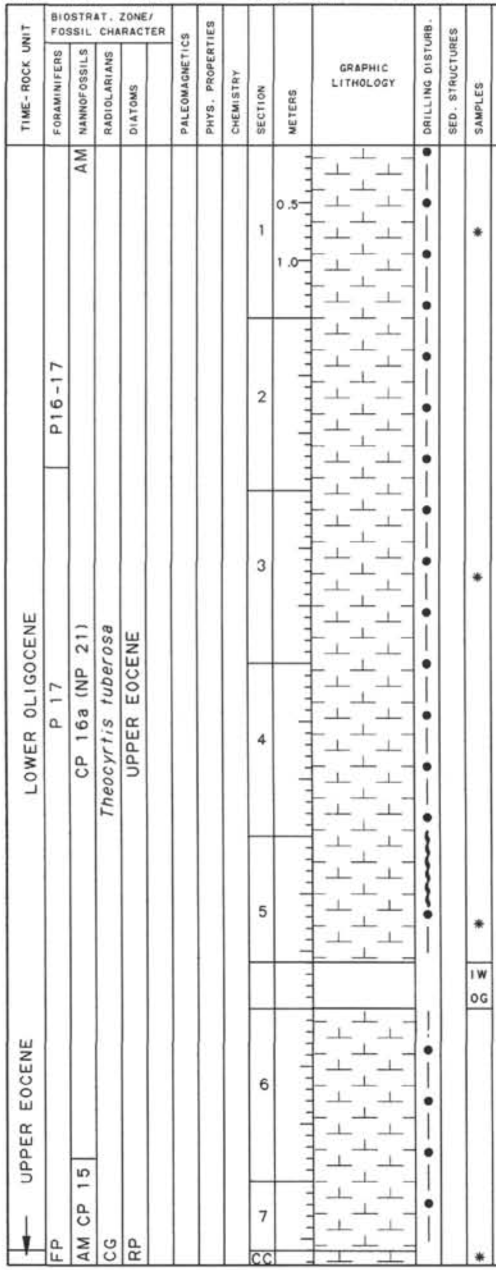

LITHOLOGIC DESCRIPTION

NANNOFOSSIL OOZE

Major lithology: Nannofossil ooze, white (N9), homogeneous, with subtle light gray (N8) bands in Section 6, 70-80 and 125-127 cm, and Section 7, 40-43 cm. Entire core is moderately disturbed.

SMEAR SLIDE SUMMARY (%):

	1, 75 D	3, 75 D	5, 75 D	CC, 5 D
TEXTURE:				
Sand	10	10	10	5
Silt	10	10	10	10
Clay	80	80	80	85
COMPOSITION:				
Clay	—	—	Tr	Tr
Volcanic glass	Tr	Tr	—	Tr
Foraminifers	5	2	2	Tr
Nannofossils	86	88	88	95
Radiolarians	Tr	3	3	2
Sponge spicules	9	7	7	3

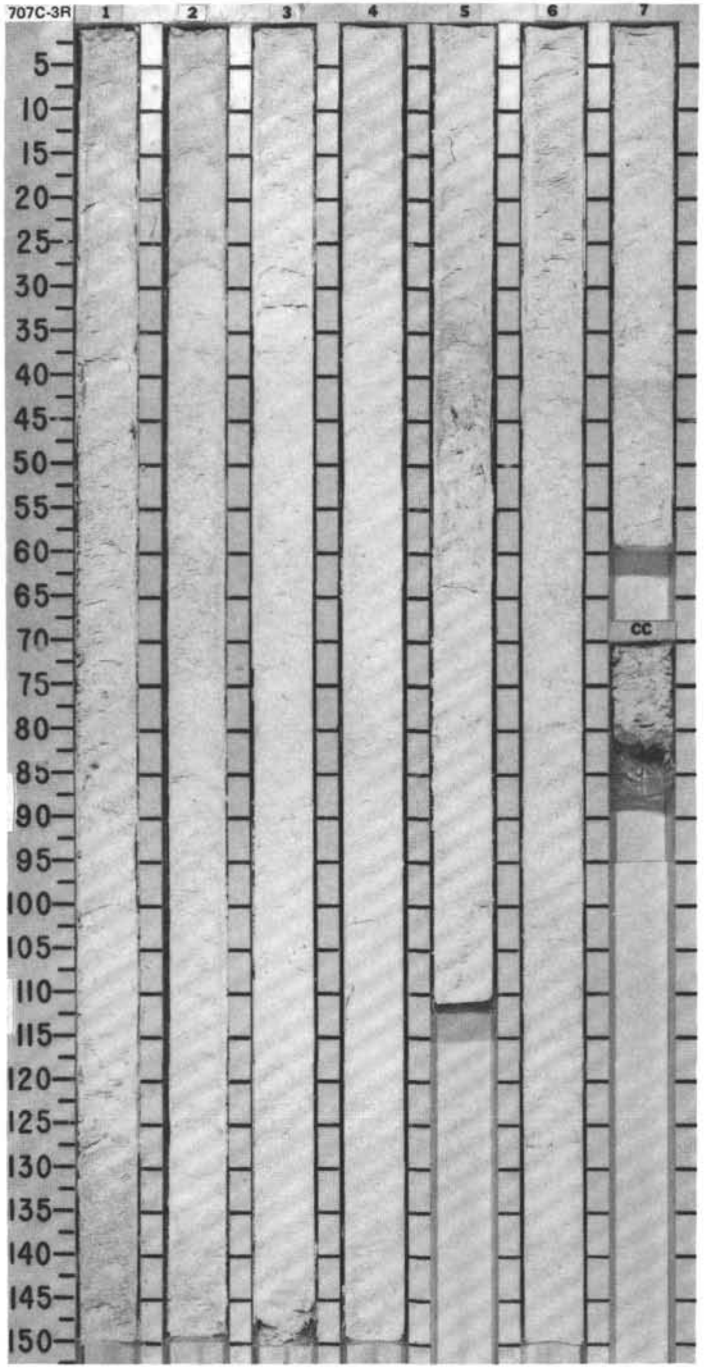

707 C 4R NO RECOVERY

SITE 707 HOLE C CORE 5R CORED INTERVAL 1754.2-1763.9 mbsl 212.8-222.5 mbsf

TIME-ROCK UNIT	BIOSTRAT. ZONE/ FOSSIL CHARACTER					PALEOMAGNETICS	PHYS. PROPERTIES	CHEMISTRY	SECTION	METERS	GRAPHIC LITHOLOGY	DRILLING DISTURB.	SED. STRUCTURES	SAMPLES
	FORAMINIFERS	NANNOFOSSILS	RADIOLARIANS	DIATOMS										
UPPER EOCENE	P 15 FP	CP 15 (NP 18 - NP 20) AM	AM *T. bromia* CG	Barren					1	0.5	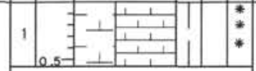			* * *

LITHOLOGIC DESCRIPTION

NANNOFOSSIL OOZE and NANNOFOSSIL CHALK

Major lithology: Nannofossil ooze alternating with thinner, more consolidated layers of nannofossil chalk, white (N9), homogeneous, slightly disturbed.

SMEAR SLIDE SUMMARY (%):

	1, 10 M	1, 30 D
TEXTURE:		
Sand	30	10
Silt	30	30
Clay	40	60
COMPOSITION:		
Accessory minerals:		
Opaques	Tr	—
Nannofossils	64	90
Radiolarians	35	8
Sponge spicules	1	2

SITE 707 HOLE C CORE 6R CORED INTERVAL 1763.9-1773.5 mbsl; 222.5-232.1 mbsf

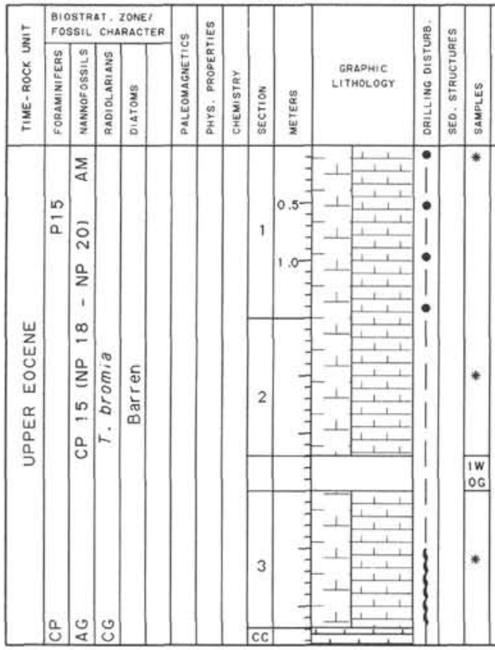

LITHOLOGIC DESCRIPTION

NANNOFOSSIL OOZE and NANNOFOSSIL CHALK

Major lithology: Nannofossil chalk alternating with thinner, irregularly spaced layers of nannofossil ooze, white (N9), homogeneous, with some pyrite(?) staining visible in Section 2, 26-33 cm. Whole core is slightly to moderately disturbed, with small voids in Section 1, 74-76, 119-120, and 143-144 cm. CC is entirely chalk.

Minor lithology: Foraminifer-nannofossil ooze, white (10YR 8/1), in Section 1, 1-8 cm. Probable contaminant from higher in the hole introduced during drilling.

SMEAR SLIDE SUMMARY (%):

	1, 11 M	2, 50 D	3, 63 D
TEXTURE:			
Sand	40	5	4
Silt	10	35	36
Clay	50	60	60
COMPOSITION:			
Foraminifers	40	4	1
Nannofossils	57	92	95
Radiolarians	2	2	3
Sponge spicules	1	2	1

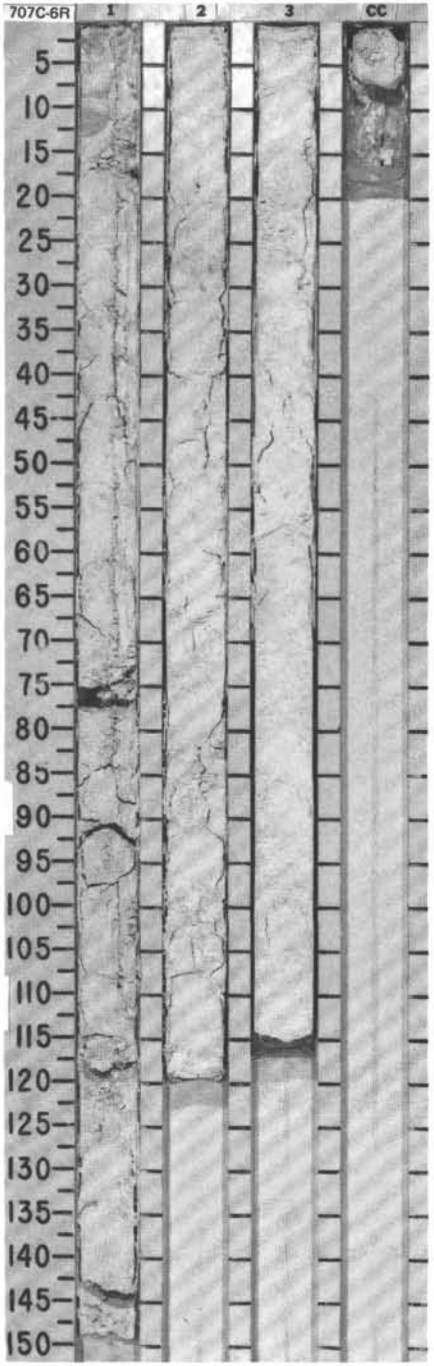

SITE 707 HOLE C CORE 7R CORED INTERVAL 1773.5-1783.2 mbsl; 232.1-241.8 mbsf

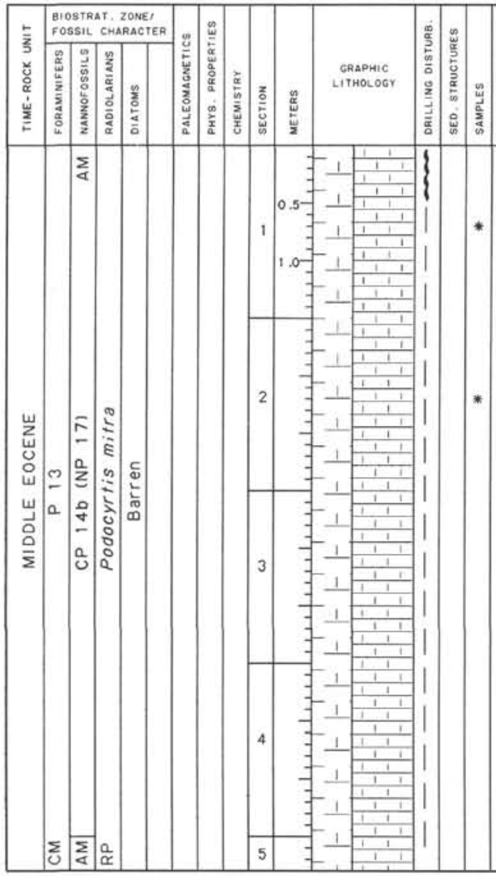

LITHOLOGIC DESCRIPTION

NANNOFOSSIL OOZE and NANNOFOSSIL CHALK

Major lithology: Nannofossil chalk alternating with thinner, irregularly spaced layers of nannofossil ooze, white (N9, 10YR 8/1), homogeneous except for variations in the degree of consolidation. Entire core is slightly disturbed.

SMEAR SLIDE SUMMARY (%):

	1, 70 D	2, 71 M
TEXTURE:		
Sand	6	5
Silt	40	15
Clay	54	80
COMPOSITION:		
Foraminifers	1	Tr
Nannofossils	93	78
Radiolarians	5	20
Sponge spicules	2	2

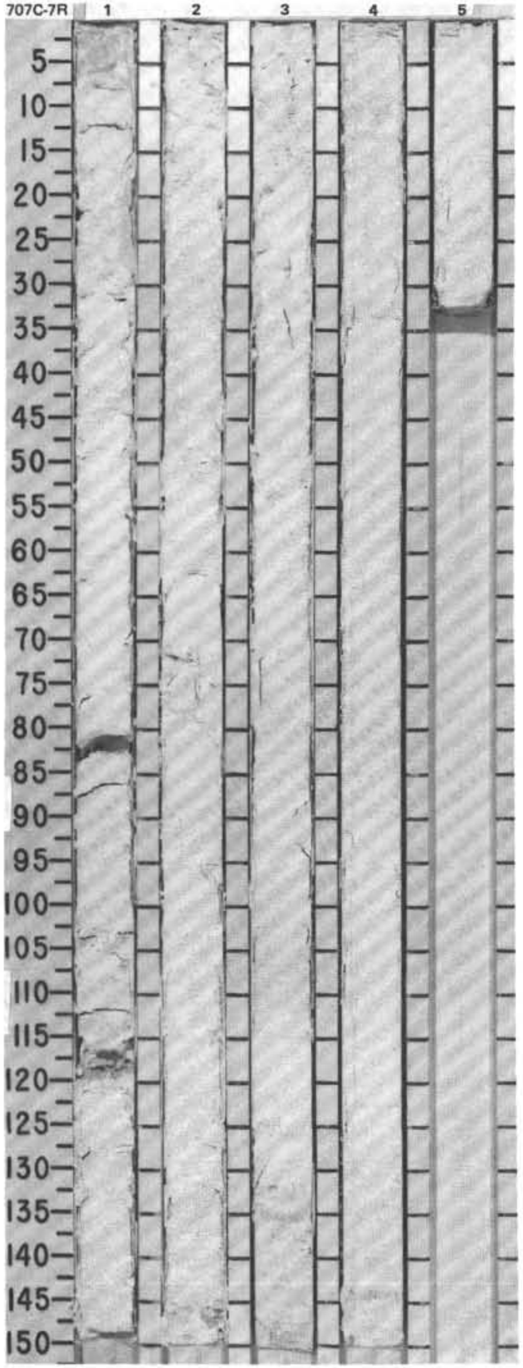

SITE 707 HOLE C CORE 8R CORED INTERVAL 1783.2-1792.8 mbsl; 241.8-251.4 mbsf

TIME-ROCK UNIT	BIOSTRAT. ZONE/ FOSSIL CHARACTER: FORAMINIFERS	NANNOFOSSILS	RADIOLARIANS	DIATOMS	PALEOMAGNETICS	PHYS. PROPERTIES	CHEMISTRY	SECTION	METERS	GRAPHIC LITHOLOGY	DRILLING DISTURB.	SED. STRUCTURES	SAMPLES
MIDDLE EOCENE	FM P 13	AM CP 14b	RP *Podocyrtis mitra*	Barren				1 CC	0.5				*

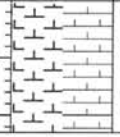

LITHOLOGIC DESCRIPTION

NANNOFOSSIL CHALK and NANNOFOSSIL OOZE

Major lithology: Nannofossil chalk alternating with thinner, irregularly spaced layers of nannofossil ooze. white (N9), homogeneous. Chalk in this core is much more indurated than the chalk in overlying cores.

Minor lithology: Chert, white (10YR 8/1), found as fragments in Section 1, 8-10, 18-19, and 24-25 cm.

SMEAR SLIDE SUMMARY (%):

	1, 55 D
TEXTURE:	
Sand	6
Clay	94
COMPOSITION:	
Foraminifers	5
Nannofossils	94
Diatoms	1

SITE 707 HOLE C CORE 9R CORED INTERVAL 1792.8-1802.4 mbsl; 251.4-261.0 mbsf

TIME-ROCK UNIT	BIOSTRAT. ZONE/ FOSSIL CHARACTER: FORAMINIFERS	NANNOFOSSILS	RADIOLARIANS	DIATOMS	PALEOMAGNETICS	PHYS. PROPERTIES	CHEMISTRY	SECTION	METERS	GRAPHIC LITHOLOGY	DRILLING DISTURB.	SED. STRUCTURES	SAMPLES
MIDDLE EOCENE	P 13 FM	CP 14b (NP 17) AM CP 14a	*Podocyrtis mitra* CG	MIDDLE EOCENE RP				1 2 3 CC	0.5 1.0				* IW OG *

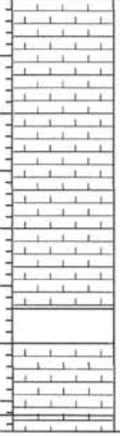

LITHOLOGIC DESCRIPTION

RADIOLARIAN-BEARING NANNOFOSSIL CHALK

Major lithology: Radiolarian-bearing nannofossil chalk, white (N9), homogeneous, with a few thin interbedded layers of softer ooze in those intervals that show signs of drilling disturbance. Pale gray (N7, N8) burrow structures visible in Section 2, 5-35 cm, and Section 3, 20-30 cm.

Minor lithology: Chert, white (10YR 8/1), found as two pebble-sized fragments at top of Section 1.

SMEAR SLIDE SUMMARY (%):

	1, 90 D	3, 45 D
TEXTURE:		
Sand	10	10
Silt	10	10
Clay	80	80
COMPOSITION:		
Foraminifers	3	3
Nannofossils	77	77
Radiolarians	15	15
Sponge spicules	5	5

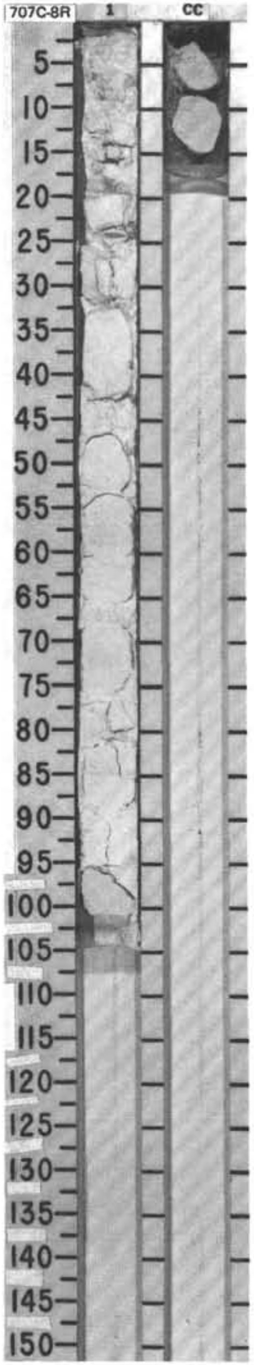

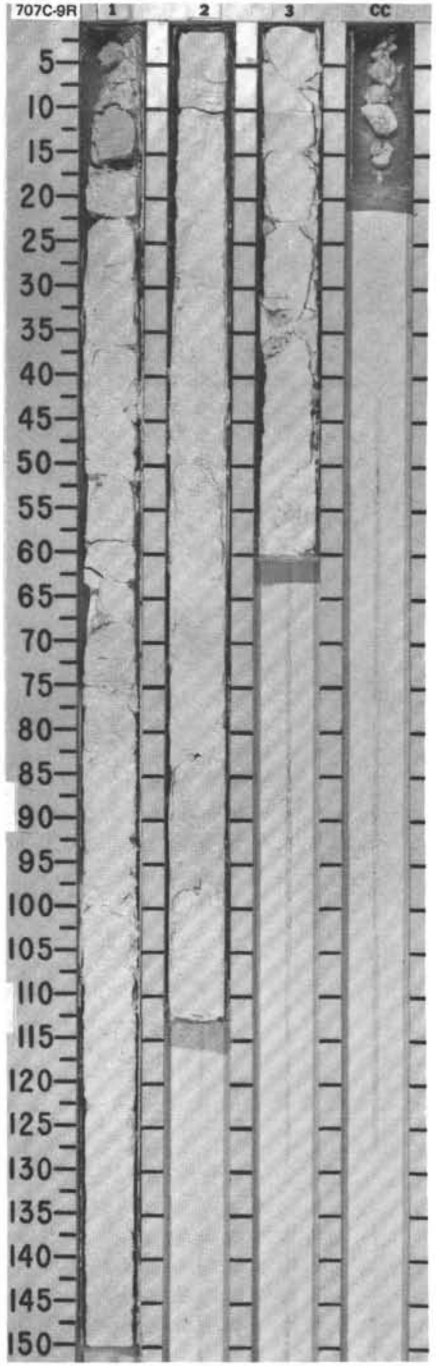

SITE 707 HOLE C CORE 10R CORED INTERVAL 1802.4-1812.0 mbsl; 261.0-270.6 mbsf

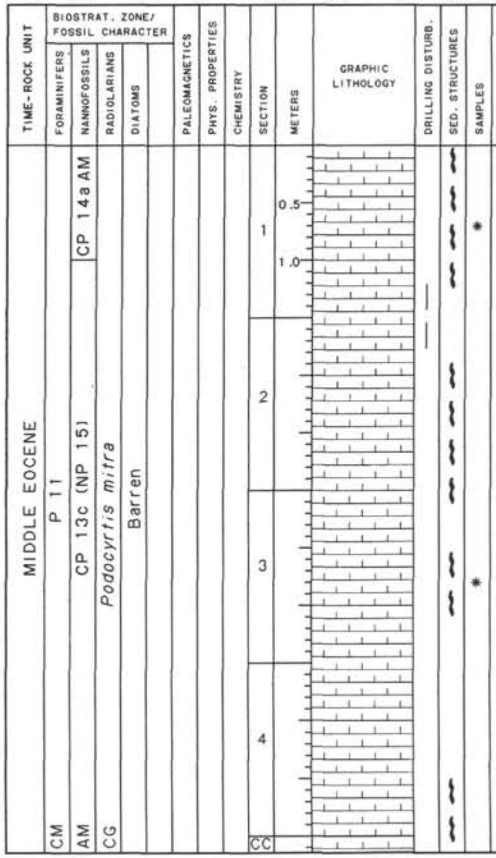

LITHOLOGIC DESCRIPTION

RADIOLARIAN-BEARING NANNOFOSSIL CHALK

Major lithology: Radiolarian-bearing nannofossil chalk, white (N9), with radiolarians making up to 25% of the sediment. Faintly burrow mottled throughout much of the core. Pale gray (N7, N8) horizons observed in Section 2, 50-55 and 75-77 cm; and as thin laminae in the CC.

SMEAR SLIDE SUMMARY (%):

	1, 70 D	3, 70 D
TEXTURE:		
Sand	20	20
Silt	10	10
Clay	70	70
COMPOSITION:		
Foraminifers	5	Tr
Nannofossils	70	70
Radiolarians	20	25
Sponge spicules	5	5

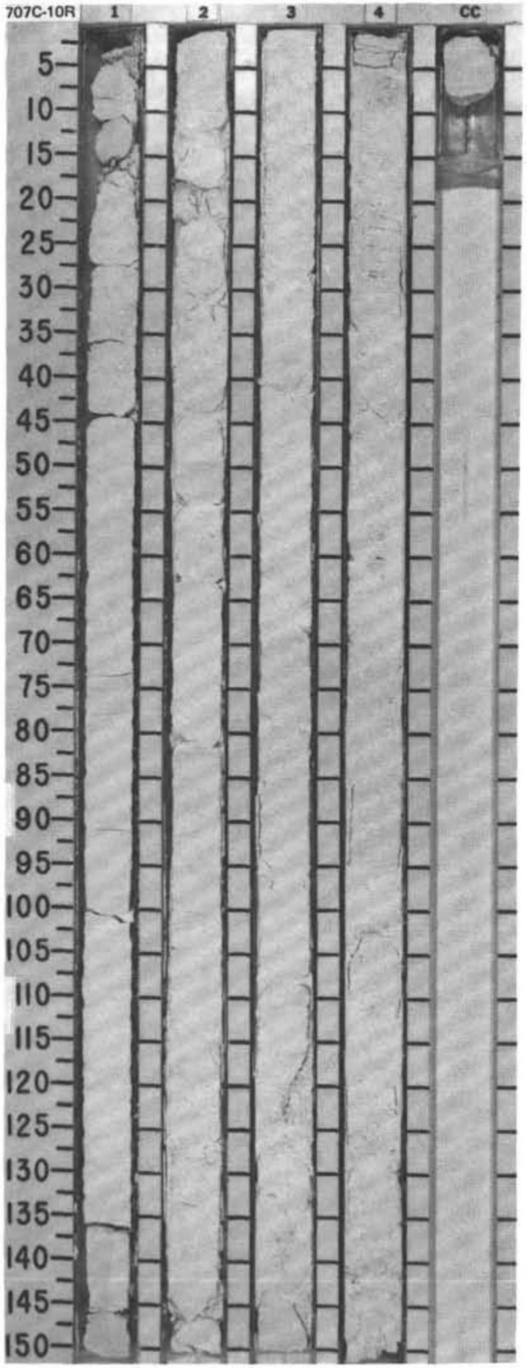

SITE 707 HOLE C CORE 11R CORED INTERVAL 1812.0-1821.7 mbsl: 270.6-280.3 mbsf

TIME-ROCK UNIT	BIOSTRAT. ZONE/ FOSSIL CHARACTER					PALEOMAGNETICS	PHYS. PROPERTIES	CHEMISTRY	SECTION	METERS	GRAPHIC LITHOLOGY	DRILLING DISTURB.	SED. STRUCTURES	SAMPLES
	FORAMINIFERS	NANNOFOSSILS	RADIOLARIANS	DIATOMS										
MIDDLE EOCENE	P 11 CM	AM CP 13b (NP 15) AM	*Podocyrtis mitra* CM	Barren					1	0.5 1.0 CC	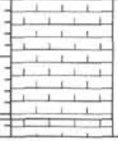			* *

LITHOLOGIC DESCRIPTION

SPONGE SPICULE-BEARING RADIOLARIAN-BEARING NANNOFOSSIL CHALK

Major lithology: Spicule-bearing radiolarian-bearing nannofossil chalk, white to very pale green (N9, 5GY 8/1), with siliceous sponge spicules and radiolarians together making up approximately 25% of the sediment. Chalk is weakly bioturbated with a few small (3-8 mm) interspersed fragments of fractured, very pale brown (10YR 7/3) chert.

SMEAR SLIDE SUMMARY (%):

	1, 80 D	CC, 2 D
TEXTURE:		
Sand	20	20
Silt	10	13
Clay	70	67
COMPOSITION:		
Quartz	Tr	3
Feldspar	—	Tr
Mica	Tr	—
Volcanic glass	Tr	Tr
Accessory minerals:		
Glauconite	—	Tr
Foraminifers	3	5
Nannofossils	70	67
Radiolarians	17	15
Sponge spicules	10	10

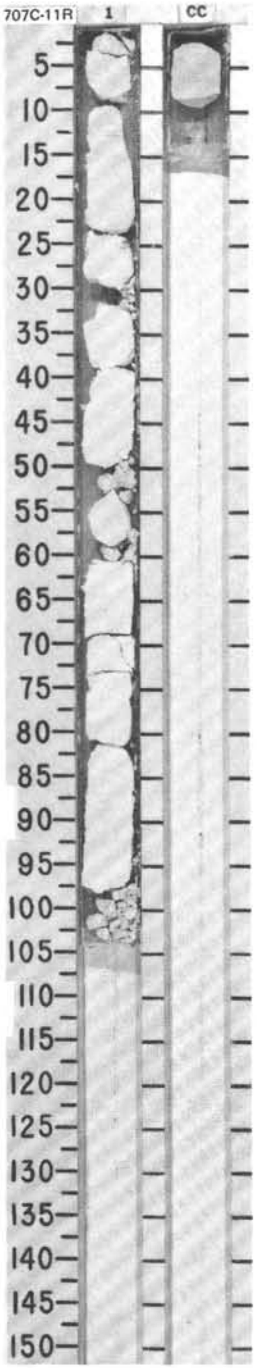

SITE 707 HOLE C CORE 12R CORED INTERVAL 1821.7-1831.2 mbsl; 280.3-289.8 mbsf

TIME-ROCK UNIT	BIOSTRAT. ZONE/ FOSSIL CHARACTER					PALEOMAGNETICS	PHYS. PROPERTIES	CHEMISTRY	SECTION	METERS	GRAPHIC LITHOLOGY	DRILLING DISTURB.	SED. STRUCTURES	SAMPLES
	FORAMINIFERS	NANNOFOSSILS	RADIOLARIANS	DIATOMS										
MIDDLE EOCENE		CP 13b AM	Barren	Barren					1	0.5	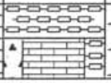	⊥ ⊥ ⊥		#* # #

LITHOLOGIC DESCRIPTION

FORAMINIFER-BEARING NANNOFOSSIL-CALCAREOUS CHALK, CHERT, and SILICIFIED LIMESTONE

Major lithologies:
Section 1, 0-30 cm: Foraminifer-bearing nannofossil-calcareous chalk, white (N9), partially lithified, faintly burrow-mottled. Much of the fine carbonate is unidentifiable (micrite), but is presumably of nannofossil origin.
Section 1, 30-68 cm: Interbedded chert and partially silicified limestone, olive brown (2.5Y 4/4) and light brownish gray (2.5Y 6/2) to white (10YR 8/1); mottled, with pockets of soft, unsilicified calcareous chalk between the chert and limestone nodules.

SMEAR SLIDE AND THIN SECTION SUMMARY (%):

	1, 15 D	1, 32 D	1, 57 D
TEXTURE:			
Sand	10		
Silt	13		
Clay	77		
COMPOSITION:			
Quartz(chert)	—	—	80
Volcanic glass	1	—	—
Foraminifers	15	60	20
Nannofossils	30	—	—
Radiolarians	2	Tr	—
Sponge spicules	5	—	—
Micrite	47	37	—
Spar cement	—	3	—

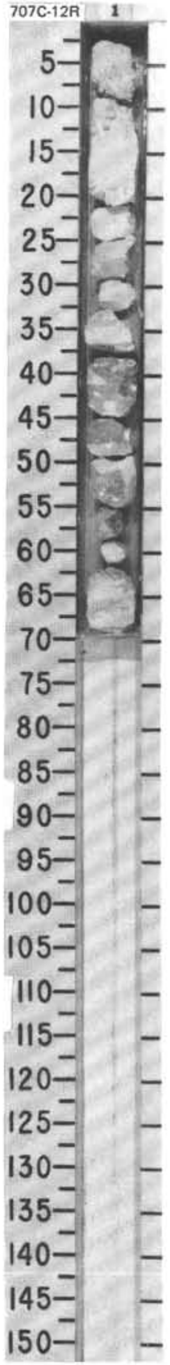

SITE 707 HOLE C CORE 13R CORED INTERVAL 1831.2-1840.7 mbsl: 289.8-299.3 mbsf

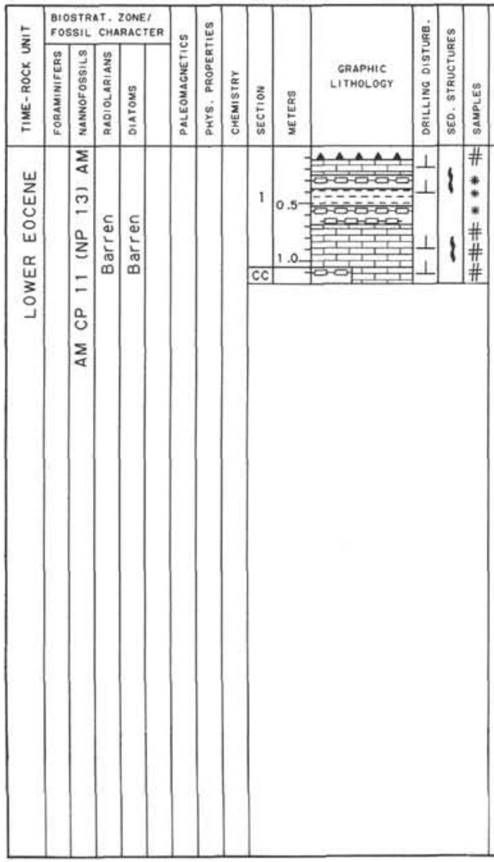

LITHOLOGIC DESCRIPTION

CHERT, FORAMINIFER-BEARING SILICIFIED LIMESTONE, FORAMINIFER-BEARING NANNOFOSSIL-BEARING CALCAREOUS CHALK, CLAYSTONE, and SILICIFIED LIMESTONE

Major lithologies:
Section 1, 0-14 cm: Chert, dark brown (7.5YR 3/2, 3/4), with minor inclusions of white (N9) silicified chalk.
Section 1, 14-23 cm: Foraminifer-bearing silicified limestone, white (10YR 8/1), horizontally bedded.
Section 1, 23-37 and 52-63 cm, and CC: Foraminifer-bearing nannofossil-bearing calcareous chalk, white to pale yellow (2.5Y 8/2, 8/4), gray (N6), and pinkish white (5YR 8/2), weakly bioturbated.
Section 1, 37-51 cm: Claystone, reddish brown (5YR 8/2), with *Zoophycos*-type burrows infilled with white (N9) calcareous chalk. Sharp bottom contact and gradational top. Possible altered ash.
Section 1, 63-105 cm, and CC: Silicified limestone, yellow (2.5Y 7/6) and brownish gray (2.5Y 6/2) to gray (N6), well indurated.

SMEAR SLIDE AND THIN SECTION SUMMARY (%):

	1, 11 D	1, 30 M	1, 45 M	1, 57 M	1, 76 D	CC, 8 M	1, 100 D	CC, 1 D
TEXTURE:								
Sand	—	10	3	10	—	5	—	—
Silt	—	25	4	25	—	35	—	—
Clay	—	65	93	65	—	60	—	—
COMPOSITION:								
Quartz	—	—	Tr	—	10	—	—	—
Chert	10	—	—	—	—	Tr	30	40
Feldspar	—	—	—	—	—	—	—	—
Clay	20	—	90	—	10	Tr	—	10
Volcanic glass	—	Tr	Tr	Tr	—	—	—	—
Opaque cash alterations	—	—	—	—	20	—	—	—
Foraminifers	40	10	4	10	30	Tr	40	30
Nannofossils	—	15	3	15	—	15	—	—
Micrite	30	75	3	75	30	85	30	20

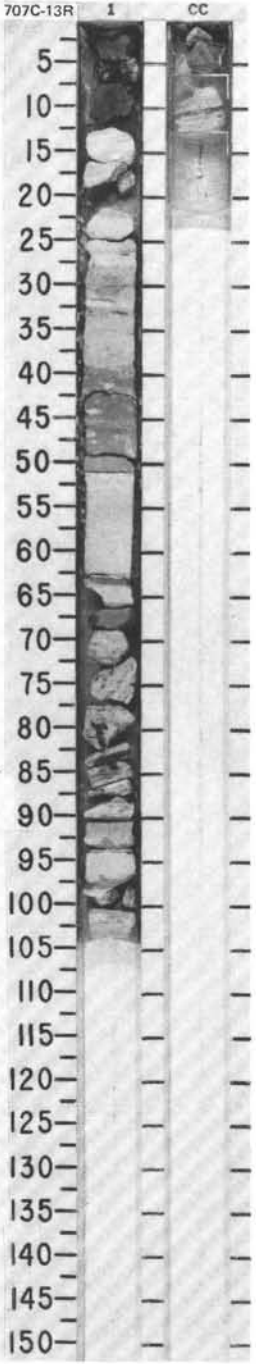

SITE 707 HOLE C CORE 14R CORED INTERVAL 1840.7-1850.3 mbsl: 299.3-308.9 mbsf

TIME-ROCK UNIT	BIOSTRAT. ZONE/ FOSSIL CHARACTER					PALEOMAGNETICS	PHYS. PROPERTIES	CHEMISTRY	SECTION	METERS	GRAPHIC LITHOLOGY	DRILLING DISTURB.	SED. STRUCTURES	SAMPLES	LITHOLOGIC DESCRIPTION
	FORAMINIFERS	NANNOFOSSILS	RADIOLARIANS	DIATOMS											
LOWER EOCENE	P 8	CM CP 10 (NP 12) AM	Barren	Barren					1			× ×		*	

SILICIFIED LIMESTONE, CHERT, and GLAUCONITIC FORAMINIFERAL LIMESTONE

Entire core consists of a drilling breccia.
Section 1, 0-10 cm: Silicified limestone, light gray (5Y 7/2), well indurated.
Section 1, 10-15 cm: Chert, dark yellowish brown (10YR 4/6) to very dark grayish brown (10YR 3/2).
Section 1, 22-50 cm: Glauconitic foraminiferal limestone, moderate yellowish green (10GY 6/4), grain supported, with glauconite making up approximately 5% of the limestone.

A 7-8 cm diameter, irregularly shaped manganese nodule was found in Section 1 between 15-22 cm.

SMEAR SLIDE SUMMARY (%):

	1, 40 D
TEXTURE:	
Sand	50
Silt	30
Clay	20
COMPOSITION:	
Quartz	Tr
Feldspar	Tr
Volcanic glass	Tr
Accessory minerals:	
Glauconite	5
Foraminifers	40
Nannofossils	15
Micrite	40

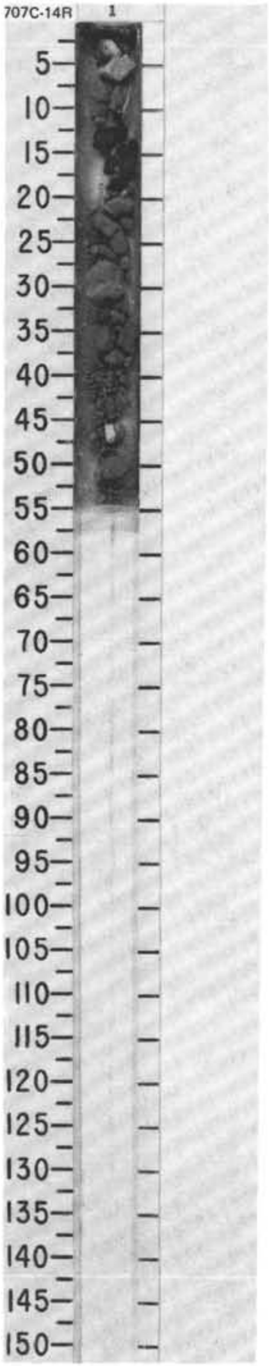

SITE 707 HOLE C CORE 15R CORED INTERVAL 1850.3-1859.6 mbsl; 308.9-318.2 mbsf

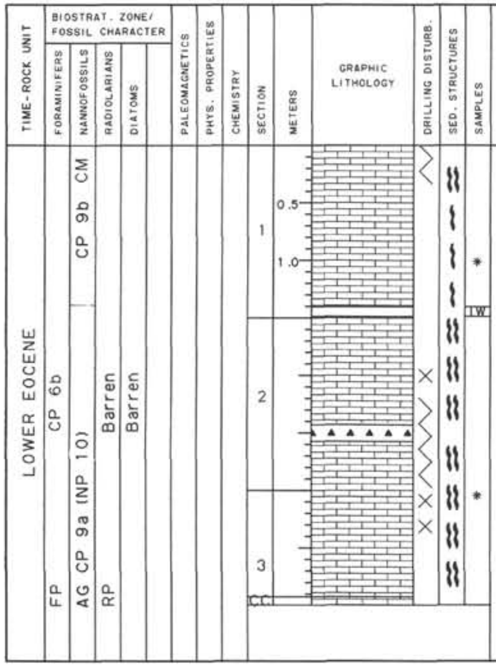

LITHOLOGIC DESCRIPTION

GLAUCONITIC FORAMINIFER-BEARING NANNOFOSSIL LIMESTONE

Major lithology: Glauconitic foraminifer-bearing nannofossil limestone, pale green to grayish green (5G 6/2, 4/2), with very dark green (5BG 2/1) glauconite grains (<2 mm) commonly visible. Weakly to moderately bioturbated throughout much of the core. Very dark green (5BG 2/1), thin (<0.5 mm) laminae occur in Section 1, 73-74 and 79-80 cm, and Section 2, 128-135 cm.

Minor lithology: Chert, grayish green (5G 5/2), with glauconite inclusions, in Section 2, 95-108 cm.

SMEAR SLIDE SUMMARY (%):

	1, 100 D	2, 146 D
TEXTURE:		
Sand	10	25
Silt	15	25
Clay	75	50
COMPOSITION:		
Quartz	Tr	Tr
Volcanic glass	1	Tr
Accessory minerals:		
Glauconite	4	—
Foraminifers	20	30
Nannofossils	40	60
Micrite	35	10

SITE 707 HOLE C CORE 16R CORED INTERVAL 1859.6-1869.3 mbsl; 318.2-327.9 mbsf

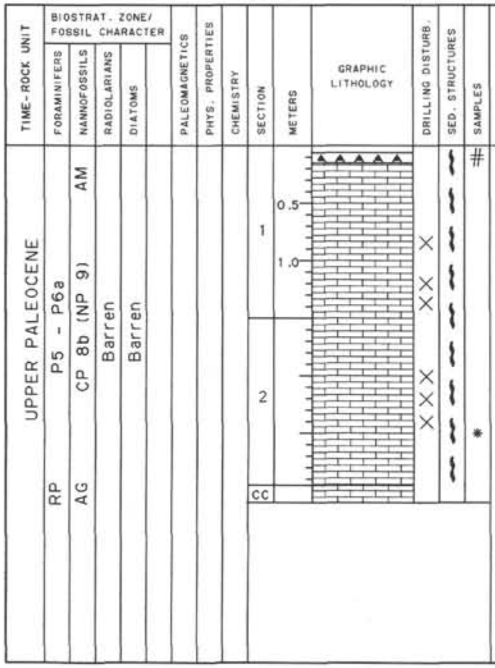

LITHOLOGIC DESCRIPTION

GLAUCONITIC FORAMINIFER-BEARING NANNOFOSSIL LIMESTONE

Major lithology: Glauconitic foraminifer-bearing nannofossil limestone, pale green to grayish green (5G 6/2, 4/2), with common very dark dusky green (5G 2/2) glauconite grains visible throughout the core. Moderately to heavily bioturbated, including well-preserved *Zoophycos*-type burrows.

Minor lithology: Chert, grayish green (5G 4/2), in Section 1, 5-12 cm.

SMEAR SLIDE AND THIN SECTION SUMMARY (%):

	1, 3 M	2, 100 D
TEXTURE:		
Sand	20	
Silt	20	
Clay	60	
COMPOSITION:		
Quartz (chert)	15	—
Clay	—	5
Accessory minerals:		
Glauconite	—	2
Foraminifer	70	20
Nannofossils	—	73
Fish remains	—	Tr
Micrite	15	—

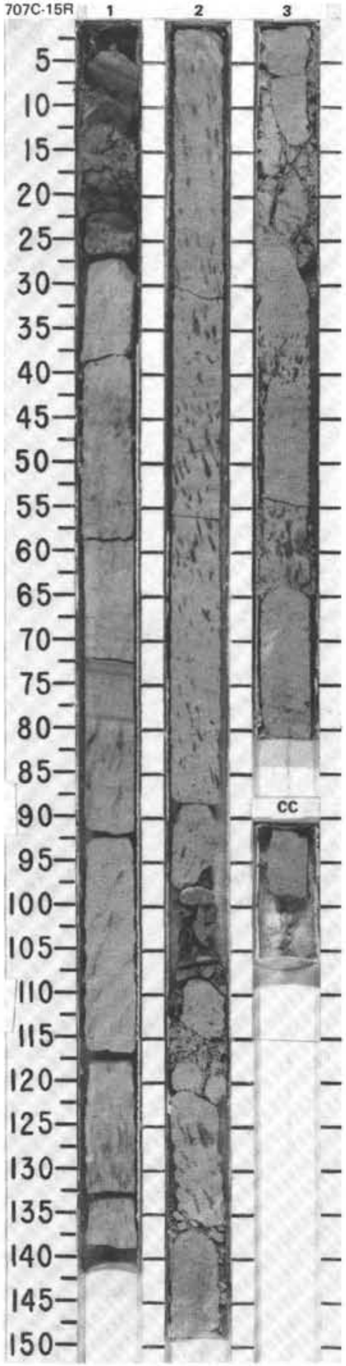

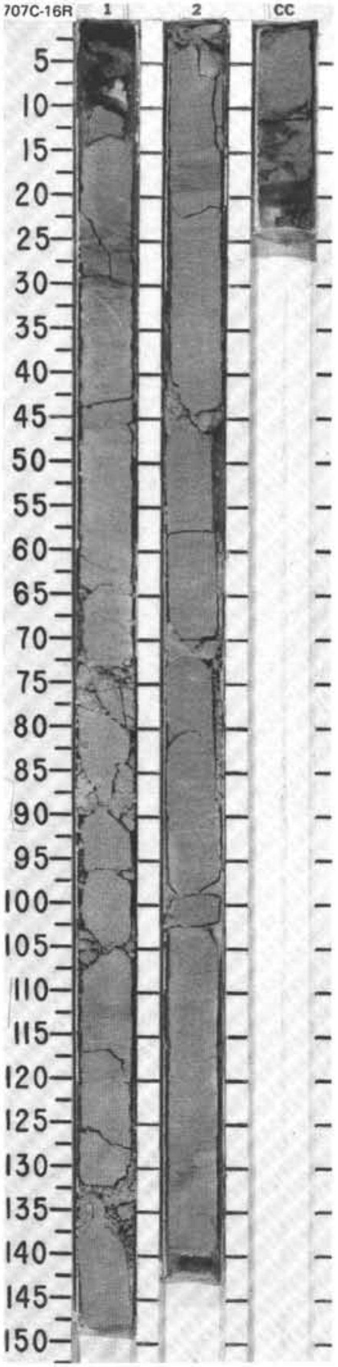

SITE 707 HOLE C CORE 17R CORED INTERVAL 1869.3-1879.9 mbsl; 327.9-337.5 mbsf

TIME-ROCK UNIT	BIOSTRAT. ZONE/ FOSSIL CHARACTER					PALEOMAGNETICS	PHYS. PROPERTIES	CHEMISTRY	SECTION	METERS	GRAPHIC LITHOLOGY	DRILLING DISTURB.	SED. STRUCTURES	SAMPLES
	FORAMINIFERS	NANNOFOSSILS	RADIOLARIANS	DIATOMS										
UPPER PALEOCENE		FM CP 7 (NP 8)	Barren	Barren					CC					#

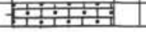

LITHOLOGIC DESCRIPTION

CALCAREOUS GRAINSTONE

Major lithology: Calcareous grainstone, greenish gray (5GY 6/1) from minor amounts of glauconite, well lithified, with grains <0.5 mm in size (medium sand).

THIN SECTION SUMMARY (%):

	CC, 11 D
COMPOSITION:	
Foraminifers	20
Bioclasts	30
Echinoderm fragments	30
Spar cement	20

707 C 18R NO RECOVERY

SITE 707 HOLE C CORE 19R CORED INTERVAL 1888.5-1898.1 mbsl; 347.1-356.7 mbsf

TIME-ROCK UNIT	BIOSTRAT. ZONE/ FOSSIL CHARACTER					PALEOMAGNETICS	PHYS. PROPERTIES	CHEMISTRY	SECTION	METERS	GRAPHIC LITHOLOGY	DRILLING DISTURB.	SED. STRUCTURES	SAMPLES
	FORAMINIFERS	NANNOFOSSILS	RADIOLARIANS	DIATOMS										
LOWER (?) PALEOCENE	RP P 4	FM CP3-CP4 (NP4-NP5)	Barren	Barren					1 CC	0.5 1.0				* #

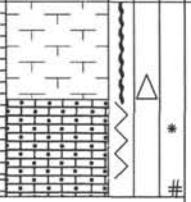

LITHOLOGIC DESCRIPTION

FORAMINIFER-BEARING CALCAREOUS GRAINSTONE

Section 1, 0-85 cm: Graded, unlithified calcareous sand, with very coarse sand at base and fining upward to very fine sand. This represents drilling disturbance and probable cave-in of material from higher in the hole.

Major lithology: Foraminifer-bearing calcareous grainstone, highly fractured, gray (5Y 6/1), homogeneous, with very fine sand-sized grains (<0.125 mm), in Section 1, 85-148 cm, and CC.

SMEAR SLIDE AND THIN SECTION (%):

	1, 110 D	CC, 15 D
TEXTURE:		
Sand	80	
Silt	15	
Clay	5	
COMPOSITION:		
Feldspar	1	—
Clay	—	20
Accessory minerals:		
Glauconite	3	—
Foraminifers	15	20
Nannofossils	Tr	—
Unidentifiable calcareous grains	80	—
Bioclasts	—	20
Micrite	—	40

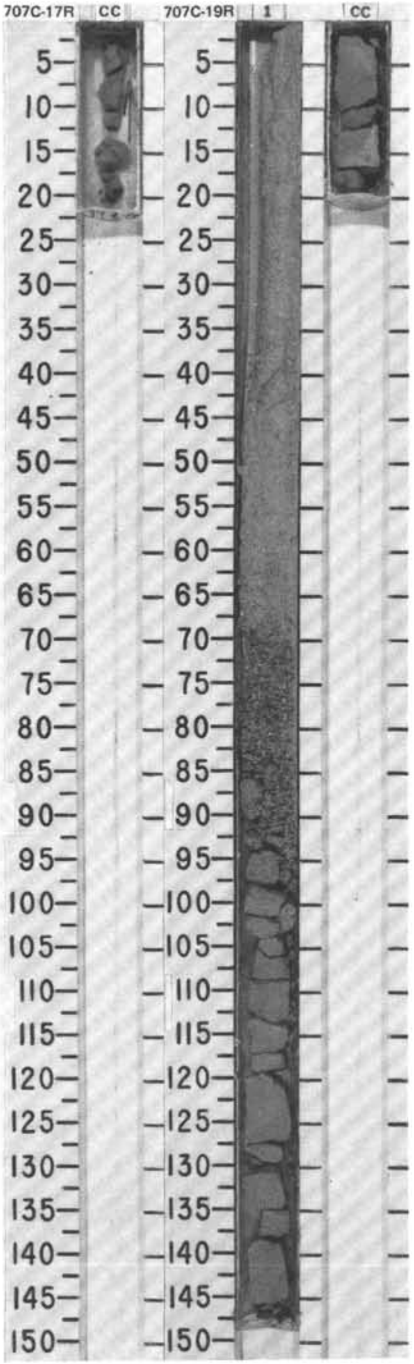

SITE 707 HOLE C CORE 20R CORED INTERVAL 1898.1-1907.4 mbsl; 356.7-366.0 mbsf

TIME-ROCK UNIT	BIOSTRAT. ZONE/ FOSSIL CHARACTER					PALEOMAGNETICS	PHYS. PROPERTIES	CHEMISTRY	SECTION	METERS
	FORAMINIFERS	NANNOFOSSILS	RADIOLARIANS	DIATOMS						
LOWER PALEOCENE	RP P3a	FM CP3-CP4 (NP4-NP5)	Barren	Barren					1 CC	0.5 1.0

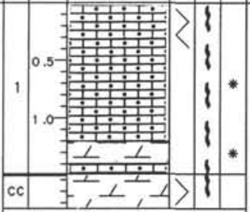

LITHOLOGIC DESCRIPTION

CALCAREOUS GRAINSTONE and CALCAREOUS DOLOMITE

Major lithology: Calcareous grainstone, gray to greenish gray (5Y 5/1, 6/1), weakly to moderately bioturbated throughout. Gradual coarsening-upward sequence in Section 1 from 140 cm to top, with fine-grained lower part of this interval (120-140 cm) a calcareous dolomite. Partially silicified horizons in Section 1 near 8 cm and 40 cm.

Minor lithology: CC contains light olive gray (5Y 6/2) dolomitized grainstone.

SMEAR SLIDE AND THIN SECTION (%):

	1, 63 D	1, 133 M	2, 21 D
TEXTURE:			
Sand	60	2	
Silt	20	38	
Clay	20	60	
COMPOSITION:			
Quartz—(chert)	—	2	—
Feldspar	1	—	10
Dolomite	—	—	85
Accessory minerals:			
Opaques	—	Tr	—
Foraminifers	5	—	5
Unidentifiable calcareous grains	94	98	—

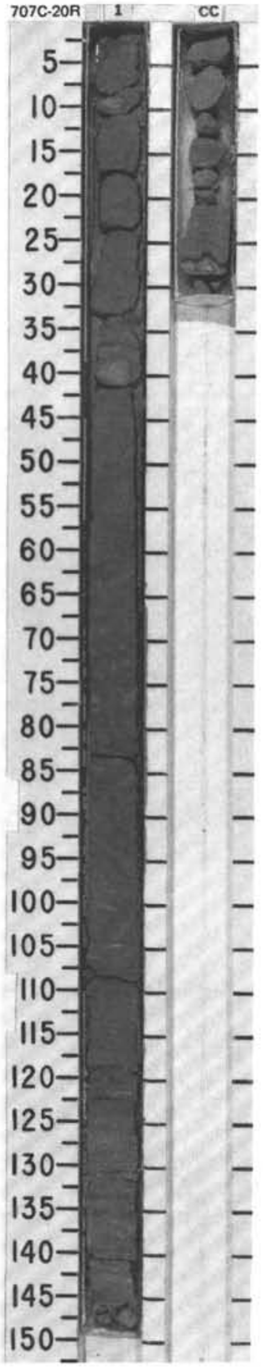

SITE 707 HOLE C CORE 21R CORED INTERVAL 1907.4-1917.0 mbsl; 366.0-375.6 mbsf

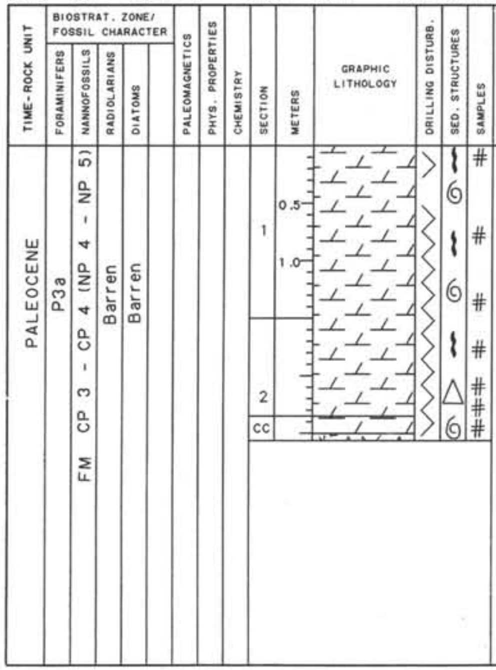

LITHOLOGIC DESCRIPTION

DOLOMITE

Major lithology: Dolostone, light olive gray (5Y 6/2) and dark olive gray (5Y 3/2) to dark gray (5Y 4/1). Fractured and fragmented, weakly bioturbated, commonly shelly, with fine flaser structure in Section 1, 0-70 cm, and decreasing grain size upward from Section 2, 67 cm, to Section 1, 70 cm. Section 2, 0-60 cm, is glauconite rich.

CC: Three pieces of shelly dolomite with numerous bivalve molds, overlying a single piece of oceanic basalt.

THIN SECTION SUMMARY:

	1, 11 D	1, 73 D	1, 141 D	2, 30 D	2, 58 D	CC, 2 D	CC, 2 M
COMPOSITION:							
Quartz (chert)	Tr	Tr	—	Tr	Tr	2	20
Dolomite	20	100	98	92	95	80	15
Accessory minerals: (gluconite)	—	—	1	5	3	—	—
Foraminifers	30	—	—	—	—	—	15
Bioclasts	40	—	2	—	—	18	17
Spar Cement	10	—	—	—	—	—	—
Micrite	—	—	—	—	—	—	30
Echinoderm fragments	—	—	—	3	2	Tr	3

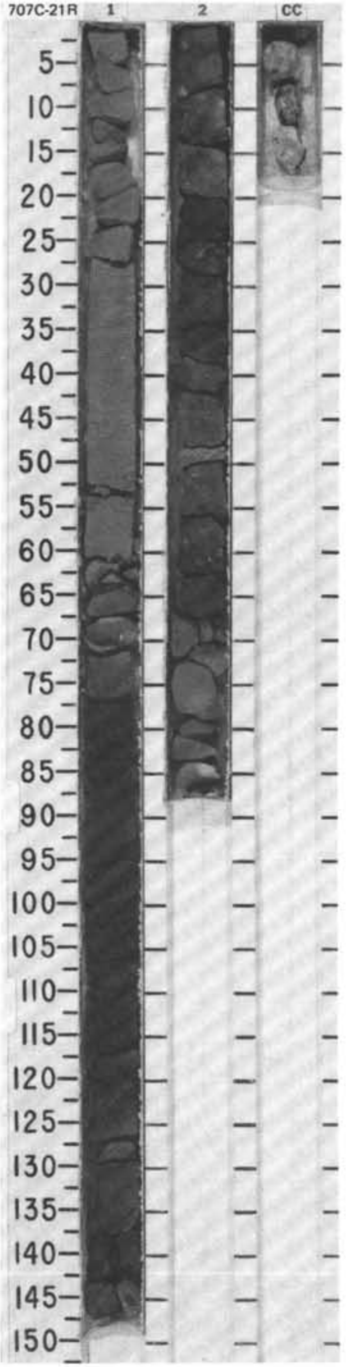

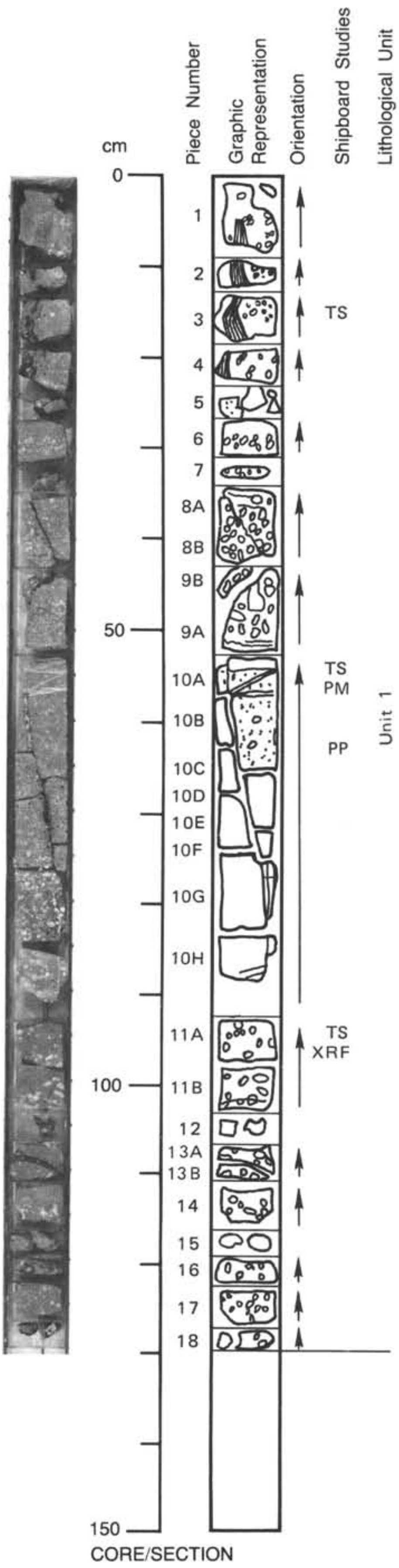

115-707C-22R-1

UNIT 1: FINE-GRAINED VESICULAR BASALT

Pieces 1-18

GLASS: Pieces 1, 2, 3, and 4 may have altered glassy pillow rims.
PHENOCRYSTS: None.
GROUNDMASS: Fine-grained matrix. Feldspar ≈0.5 mm, pyroxene <0.5 mm.
COLOR: Dark gray (5Y 4/1).
VESICLES: Round, 0.5-15.0 mm in size, some connected to form dumbbells. Bands of vesicles occur in Piece 6. Abundance is variable, 3-5% in Piece 11A, 15-20% in Pieces 8 and 9.
SECONDARY PHASES: Vesicles filled with clay and/or calcite, light gray or white.
ALTERATION: Moderately altered, groundmass to clay. Green clay in voids.
VEINS/FRACTURES: Steeply dipping fractures, 60-80°, filled with 2-3 mm thick clay, light gray (5Y 7/2). Horizontal veins, <1-2 mm thick, white crosscut clay-filled veins, calcite. Veins and fractures make up 1% of Unit 1.

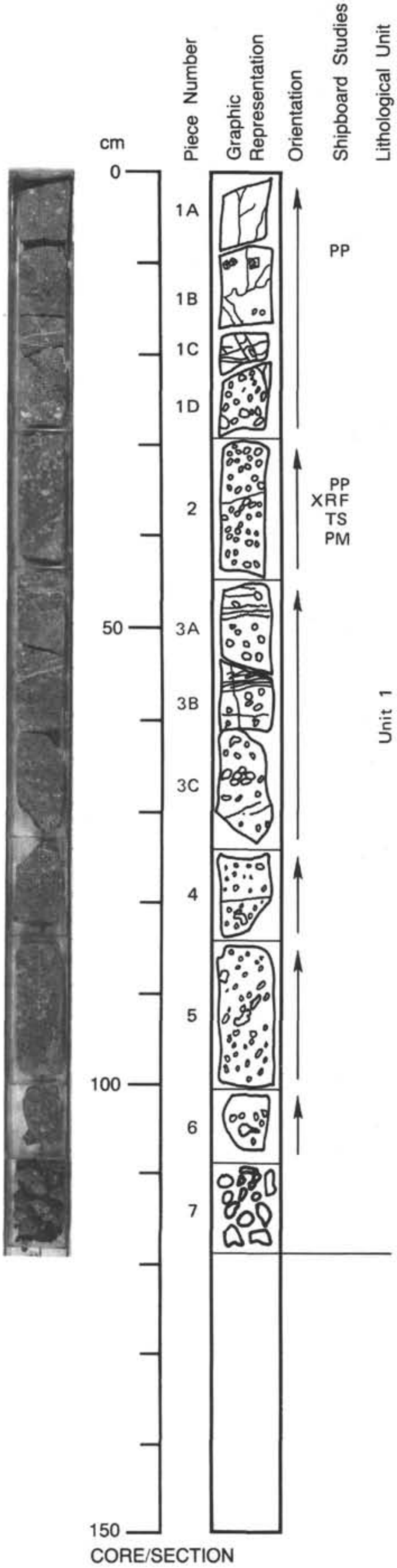

115-707C-22R-2

UNIT 1 (CONTINUED): FINE-GRAINED VESICULAR BASALT

Pieces 1-7

Continuous with 115-707C-22R-1, Unit 1

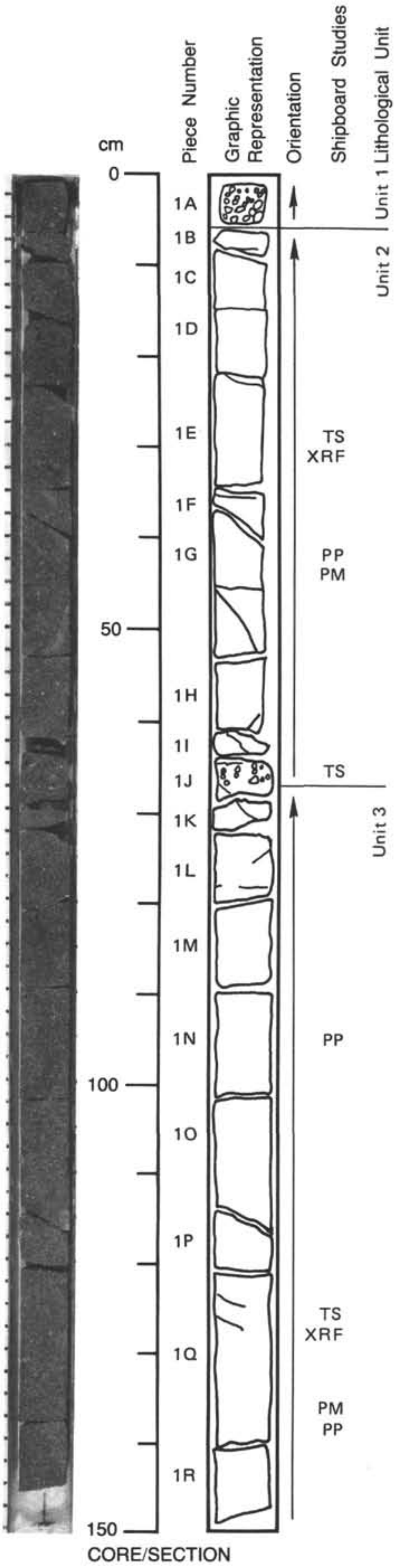

115-707C-23R-1

UNIT 1 (CONTINUED): FINE-GRAINED VESICULAR BASALT

Piece 1A

Continuous with 115-707C-22R-2, Unit 1

UNIT 2: FINE-GRAINED PLAGIOCLASE BASALT

Pieces 1B–1J

PHENOCRYSTS: Feldspar, 2 mm. Pyroxene, as large as 2 mm.
GROUNDMASS: Fine grained, plagioclase.
COLOR: Dark gray to black.
VESICLES: None.
ALTERATION: Moderately to highly altered. Groundmass + pyroxene being altered, feldspar still fresh. Possible lower greenschist facies.
VEINS/FRACTURES: Pervasive veining. Dark veins in all orientations, from horizontal to vertical.

UNIT 3: MODERATELY ALTERED PLAGIOCLASE-PHYRIC BASALT

Pieces 1K–1R

PHENOCRYSTS: Plagioclase, subhedral, <5 mm, fresh.
GROUNDMASS: Medium grained, with plagioclase, clinopyroxene, altered glass. Textures intersertal, glassy.
COLOR: Very dark gray (N3).
VESICLES: None, occasional voids.
ALTERATION: Glass and feldspar altered to clay minerals in matrix.
VEINS/FRACTURES: Fractures perpendicular and at high angle to core, filled with white fibrous ?amphibole and calcite. Seams as wide as 3 mm.

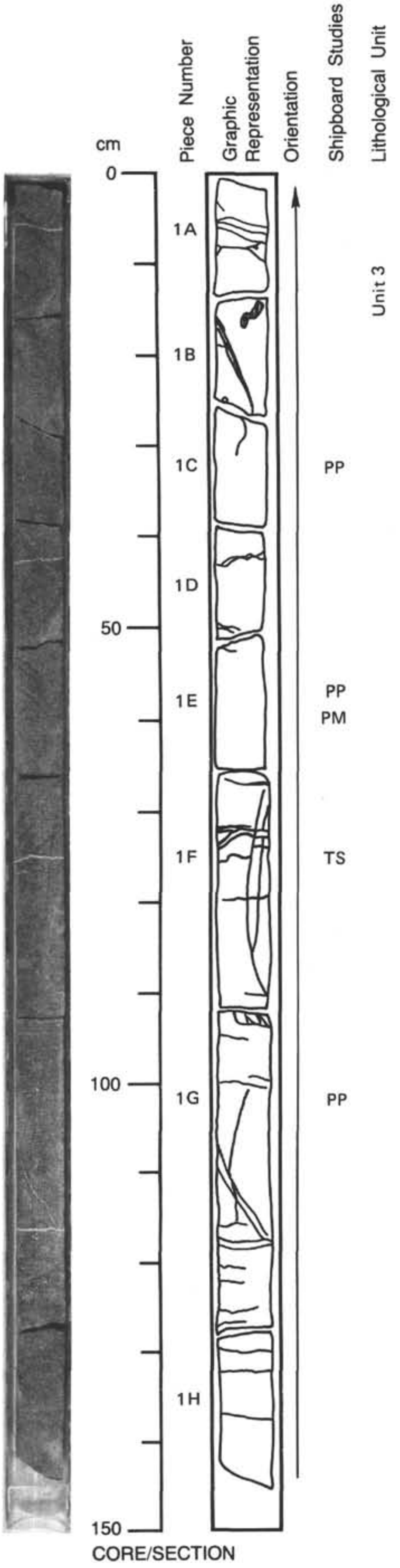

115-707C-23R-2

UNIT 3 (CONTINUED): MODERATELY ALTERED PLAGIOCLASE-PHYRIC BASALT

Pieces 1A–1H

Continuous with 115-707C-23R-1, Unit 3

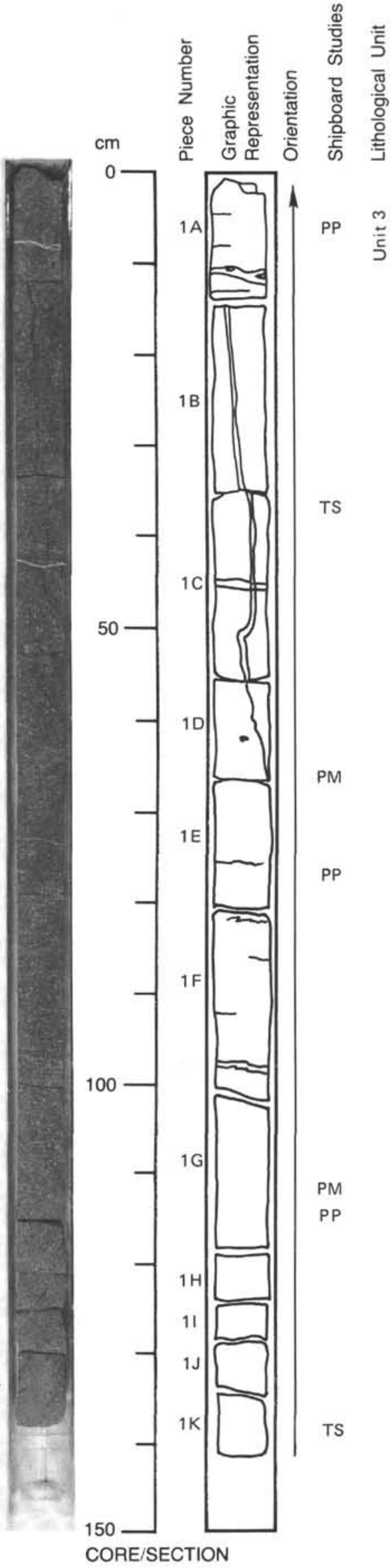

115-707C-23R-3

UNIT 3 (CONTINUED): MODERATELY ALTERED PLAGIOCLASE-PHYRIC BASALT

Pieces 1A–1K

Continuous with 115-707C-23R-2, Unit 3

GROUNDMASS: Piece 1K: Reduction in grain size is evident.

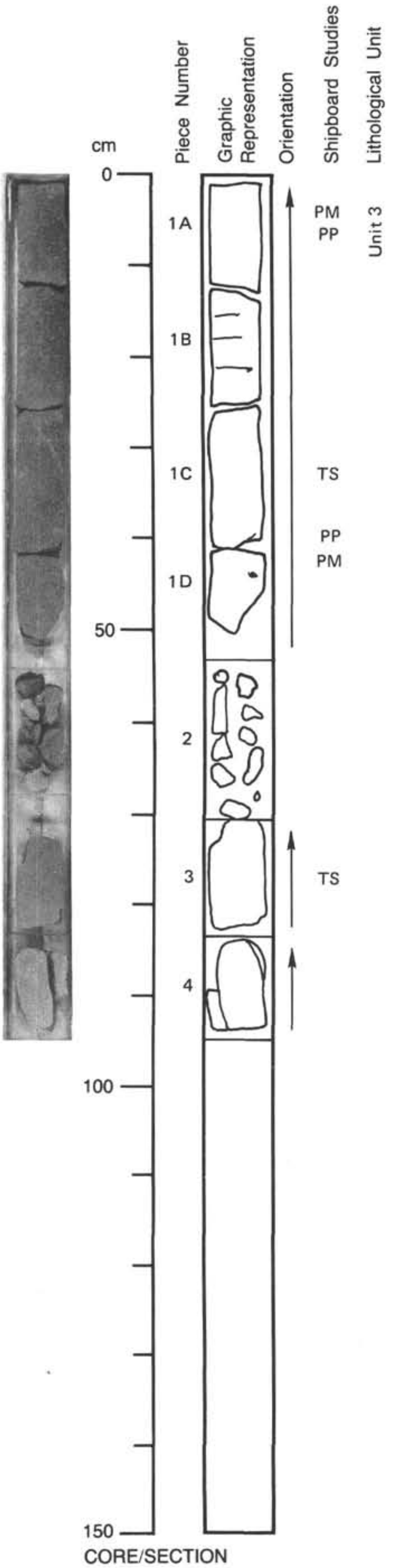

115-707C-23R-4

UNIT 3 (CONTINUED): MODERATELY ALTERED PLAGIOCLASE-PHYRIC BASALT

Pieces 1A–4B

Continuous with 115-707C-23R-3, Unit 3

GROUNDMASS: Grain size reduction seen in 115-707C-23R-3, Piece 1K, is continued here. Compare fine-grained groundmass of Piece 4A with Piece 1A in this section.

SITE 707 HOLE C CORE 24R CORED INTERVAL 1936.3-1945.9 mbsl; 394.9-404.5 mbsf

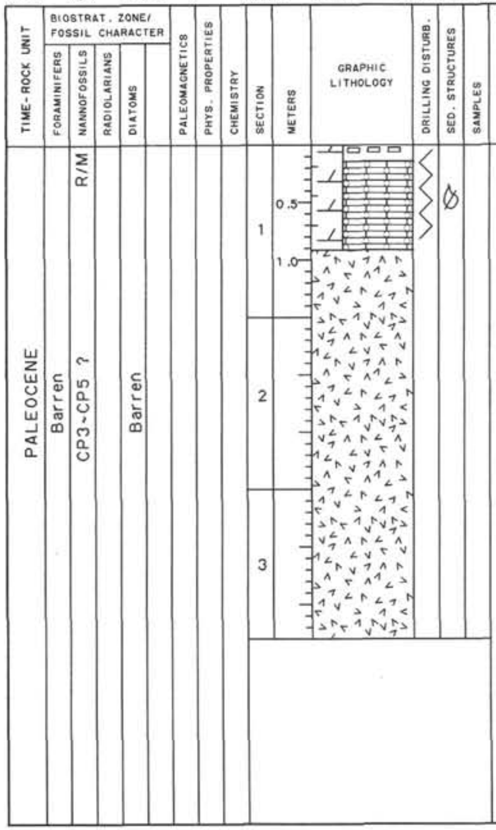

LITHOLOGIC DESCRIPTION

Major lithologies:

0-15 cm: Glauconite-bearing calcerous mudstone, particularly dolomitized, grayish brown to dark grayish brown (2.5Y 5/2-4/2). Silt sized particles showing flaser structure, with burrows infilled by coarser shelly grainstone. Several molds of large oyster shells. 15-91 cm: Shelly rudstone, partially dolomitized, greenish gray (5GY 7/1-6/1), with grainstone matrix and common small bivalves, branchipods, gastropods, worm tubes, and minor amounts of glauconite.

Sediment is underlain by oceanic basalt in this core and overlain by basalt in Core 115-707C-23R.

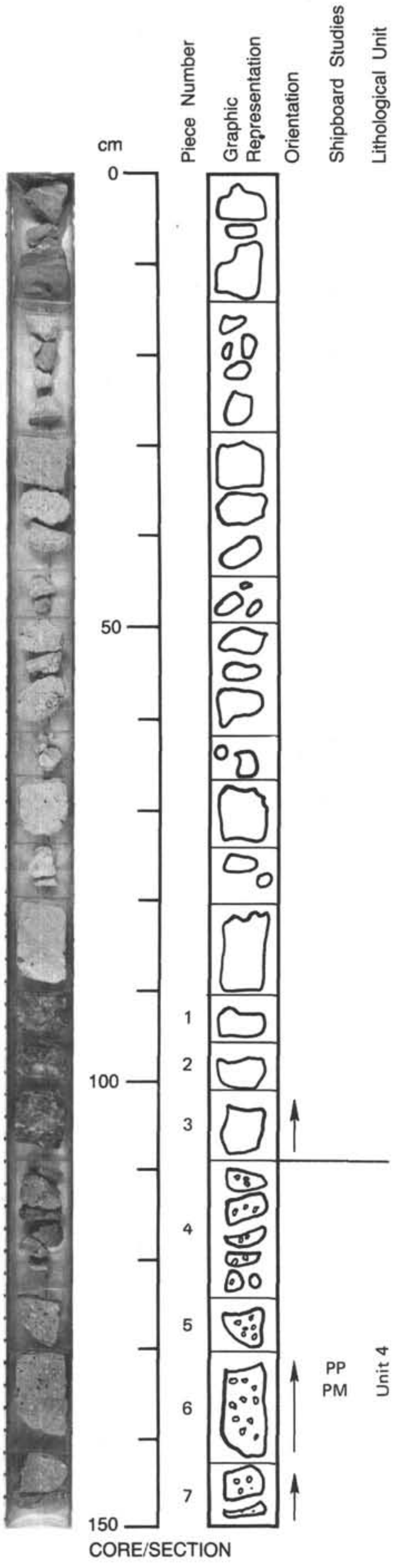

115-707C-24R-1

SEDIMENT: PARTIALLY DOLOMITIZED GLAUCONITE-BEARING CALCAREOUS MUDSTONE GRADING IN TO BASALTIC BRECCIA.

0-109 cm

Section 1, 0-15 cm: Glauconite-bearing calcareous mudstone, partially dolomitized, grayish brown to dark grayish brown (2.5Y 5/2, 4/2). Silt-sized particles showing flaser structure, with burrows infilled by coarser shelly grainstone. Several molds of large oyster shells.

Section 1, 15-91 cm: Shelly rudstone, partially dolomitized, greenish gray (5GY 7/1, 6/1), with grainstone matrix and common small bivalves, brachiopods, gastropods, worm tubes, and minor amounts of glauconite.

Section 1, 91-109 cm: Silica-cemented basaltic breccia: consits of subungular fragments, often with crenulate margins. Vesicles filled with clay, as large as 2 mm.

NOTE: Sediment is overlain by basalt in 115-707C-23R-4 and underlain by basalt in this core.

UNIT 4: PLAGIOCLASE BASALT

Pieces 4-7

PHENOCRYSTS: Plagioclase, subhedral, as large as 2 mm.
GROUNDMASS: Fine grained, with augite + plagioclase.
COLOR: Dark gray (N4).
VESICLES: Moderately vesicular, irregular-ellipsoid, >1 cm diameter, ≈10%. Variously empty or infilled with calcite + green (celadonite?) clay phases.
ALTERATION: Moderate. Calcite + green celadonite(?). Clots of apparently unaltered intersertal-textured groundmass present, as large as 5 mm.
VEINS/FRACTURES: None.

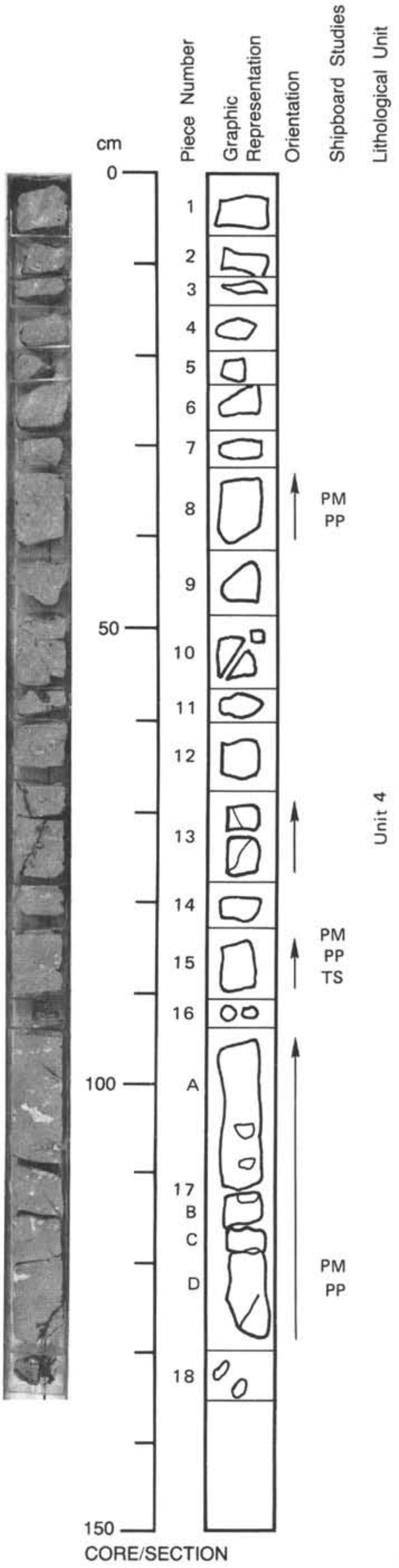

115-707C-24R-2

UNIT 4 (CONTINUED): PLAGIOCLASE BASALT

Pieces 1-18

Continuous with 115-707C-24R-1, Unit 4

115-707C-24R-3

UNIT 4 (CONTINUED): PLAGIOCLASE BASALT

Pieces 1-9

Continuous with 115-707C-24R-2, Unit 4

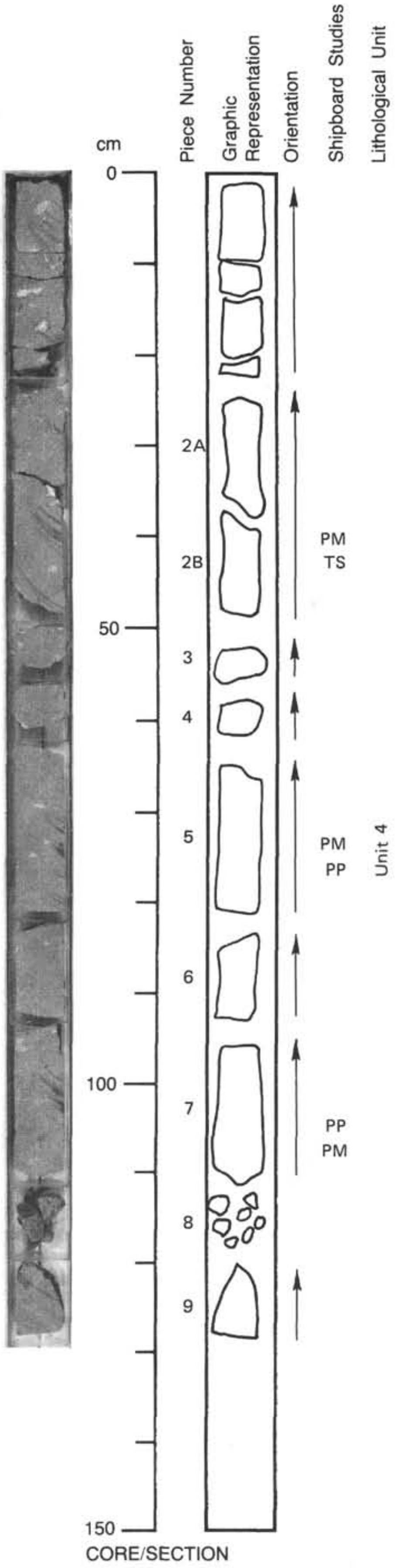

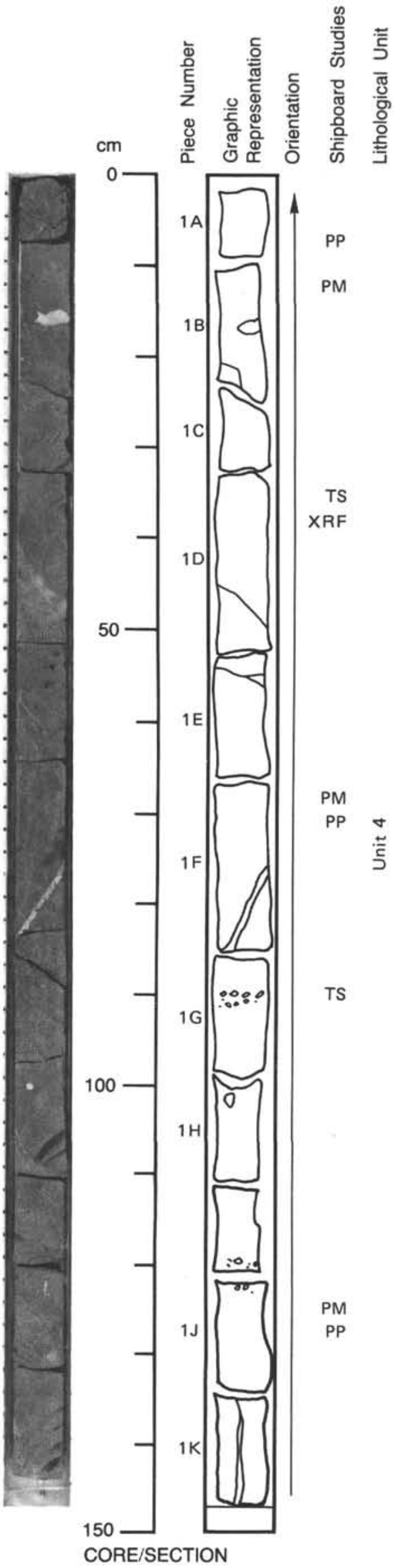

115-707C-25R-1

UNIT 4 (CONTINUED): PLAGIOCLASE BASALT

Piece 1

Continuous with 115-707C-24R-3, Unit 4

VESICLES: Two bands with larger number of vesicles are observed.
VEINS/FRACTURES: Some with high-angle veins filled with calcite and green clay.

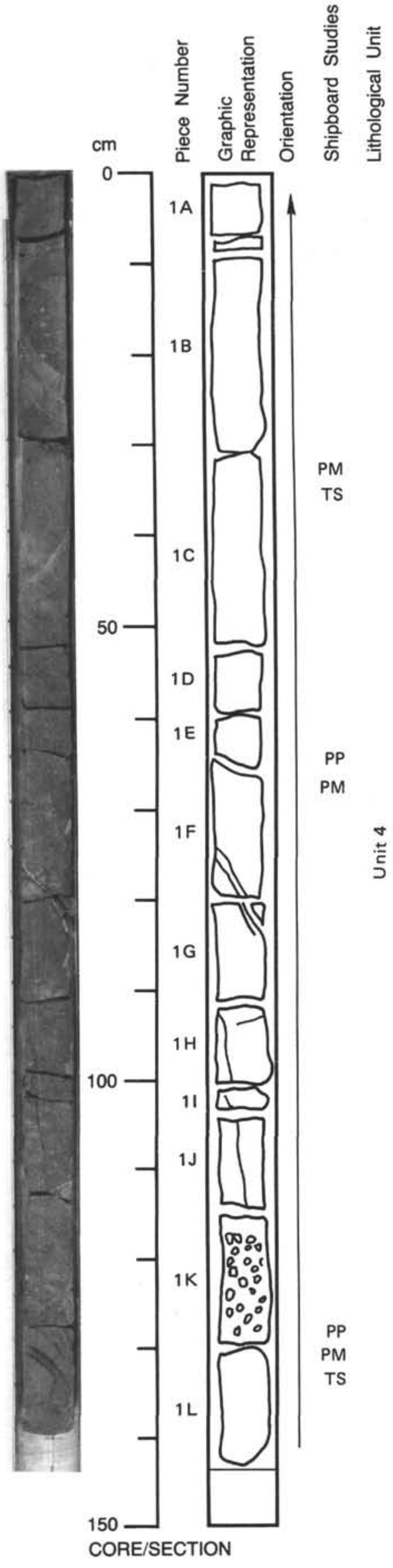

115-707C-25R-2

UNIT 4 (CONTINUED): PLAGIOCLASE BASALT

Pieces 1A–1L

Continuous with 115-707C-25R-1, Unit 4

COLOR: Slightly darker than previous core.
VESICLES: Piece 1K is rich in vesicles.
VEINS/FRACTURES: Pieces 1F and 1G are cut by high-angle vein of olive green clay.

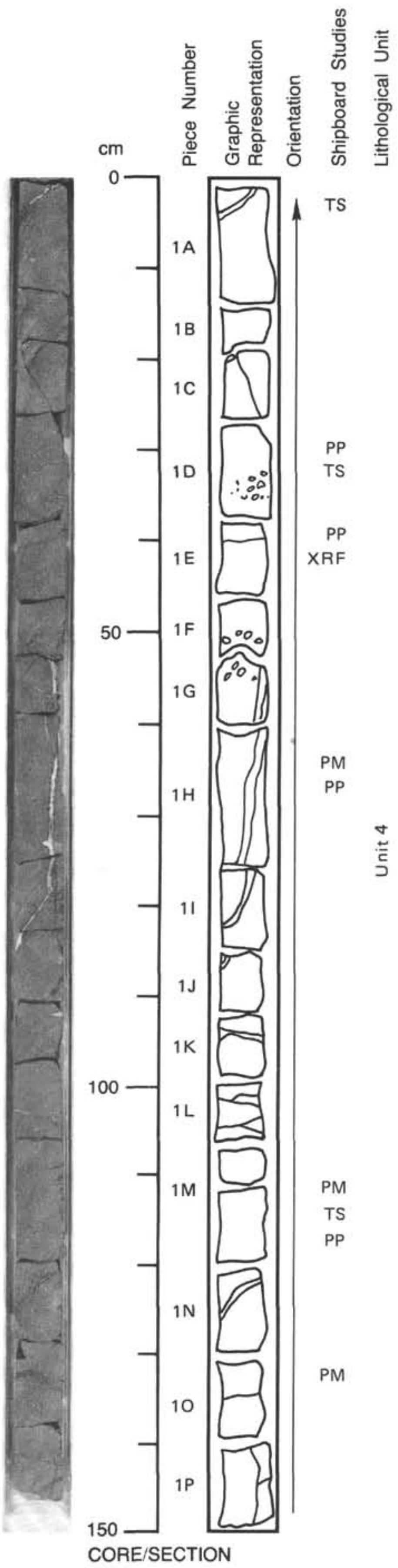

115-707C-25R-3

UNIT 4 (CONTINUED): PLAGIOCLASE BASALT

Pieces 1A–1P

Continuous with 115-707C-25R-2, Unit 4

VESICLES: Some vesicle-rich bands.
VEINS/FRACTURES: Some veins.

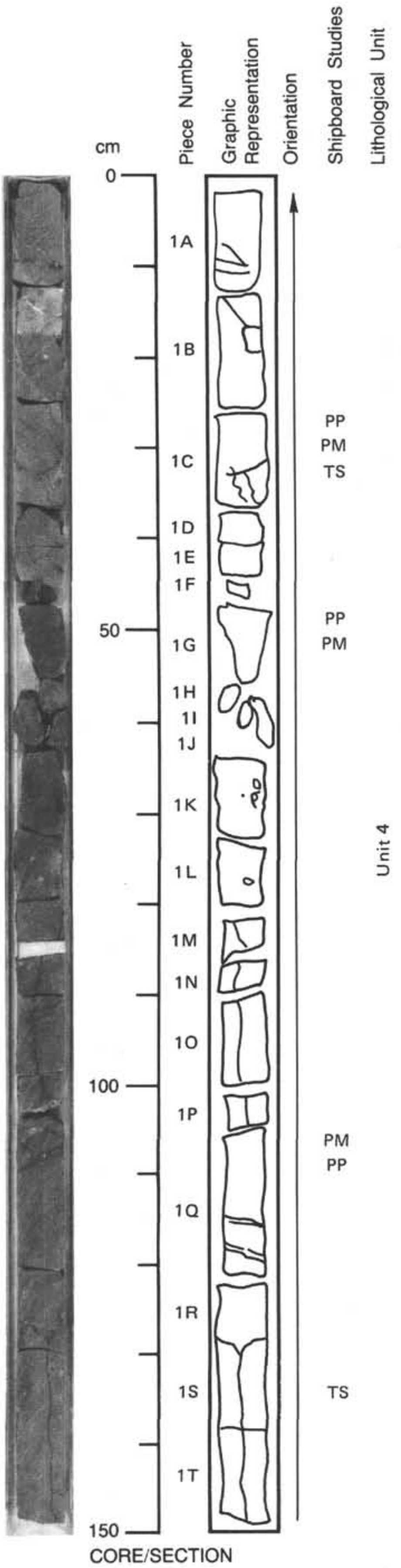

115-707C-25R-4

UNIT 4 (CONTINUED): PLAGIOCLASE BASALT

Pieces 1A–1T

Continuous with 115-707C-25R-3, Unit 4

PHENOCRYSTS: In lower part, tiny (<0.5 mm) green-brown olivine-like minerals occur.
VESICLES: Piece 1K is more vesicular.
VEINS/FRACTURES: High-angle veins are filled by chlorite + calcite.

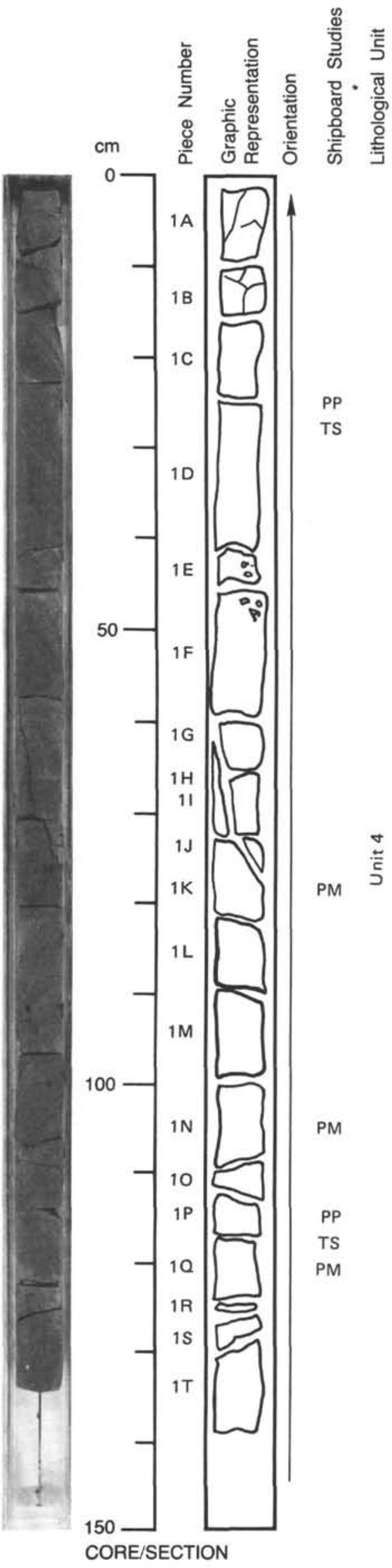

115-707C-25R-5

UNIT 4 (CONTINUED): PLAGIOCLASE BASALT

Pieces 1A–1T

Continuous with 115-707C-25R-4, Unit 4

PHENOCRYSTS: Tiny brown crystals are found.
VESICLES: Parts of Pieces 1E and 1F are vesicular.
VEINS/FRACTURES: Wide, high-angle veins filled with chlorite + calcite.

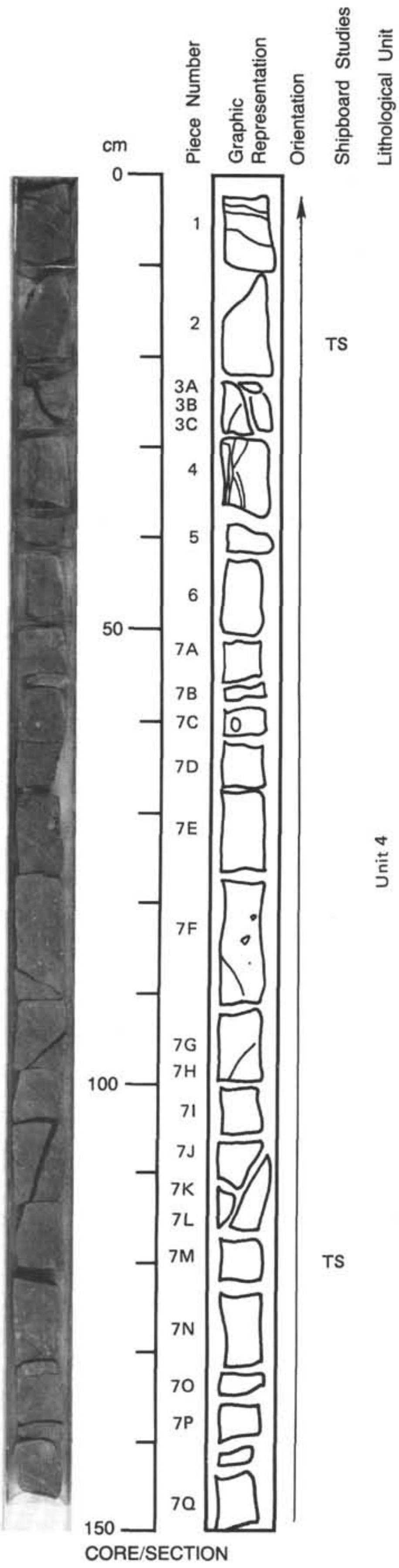

115-707C-25R-6

UNIT 4 (CONTINUED): PLAGIOCLASE BASALT

Pieces 1-7Q

Continuous with 115-707C-25R-5, Unit 4

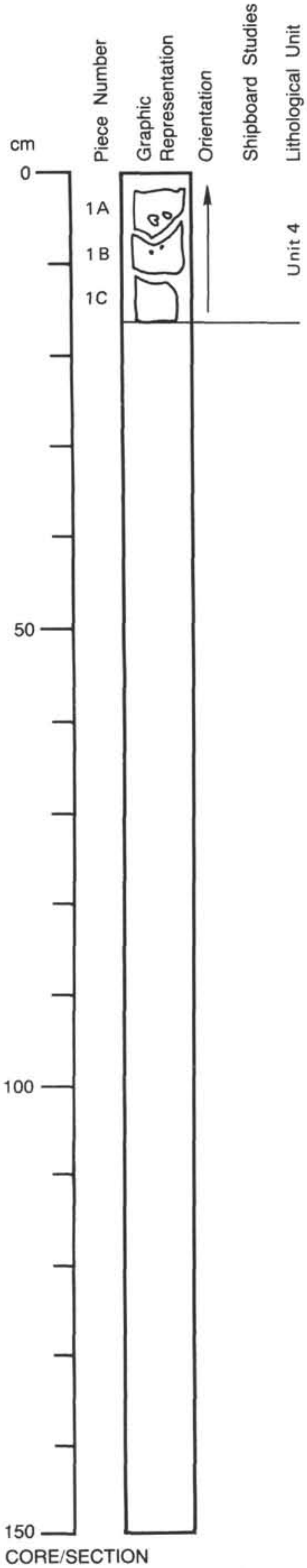

115-707C-25R-7

UNIT 4 (CONTINUED): PLAGIOCLASE BASALT

Pieces 1A–1C

Continuous with 115-707C-25R-6, Unit 4

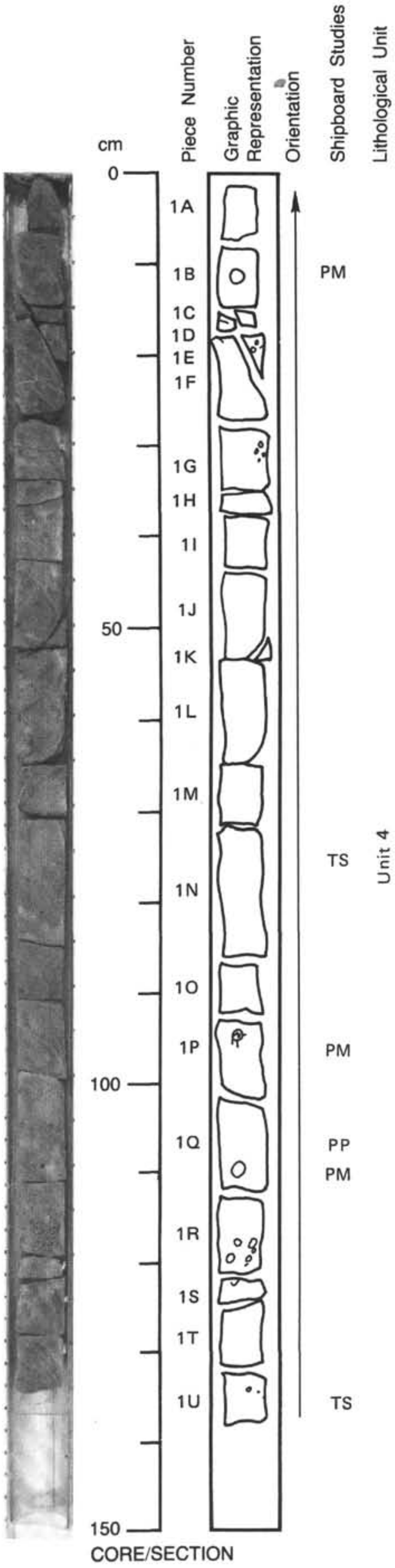

115-707C-26R-1

UNIT 4 (CONTINUED): PLAGIOCLASE BASALT

Pieces 1A–1U

Continuous with 115-707C-25R-7, Unit 4

VESICLES: Pieces 1E, 1G, and 1R are rich in vesicles filled with green clay.

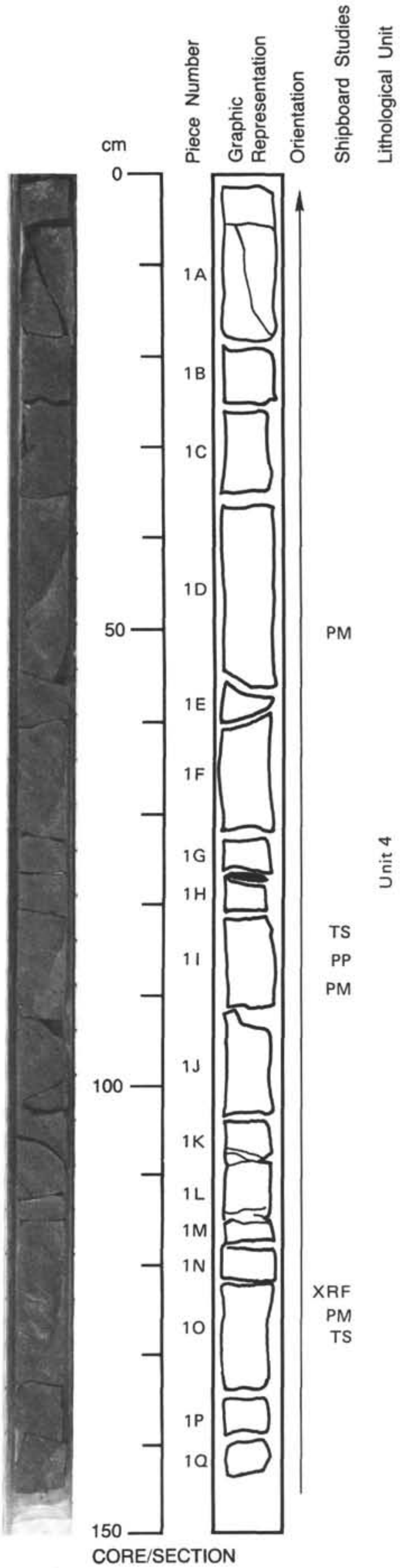

115-707C-26R-2

UNIT 4 (CONTINUED): PLAGIOCLASE BASALT

Pieces 1A–1Q

Continuous with 115-707C-26R-1, Unit 4

VEINS/FRACTURES: Boundary between Pieces 1G and 1K is calcite-filled vein.

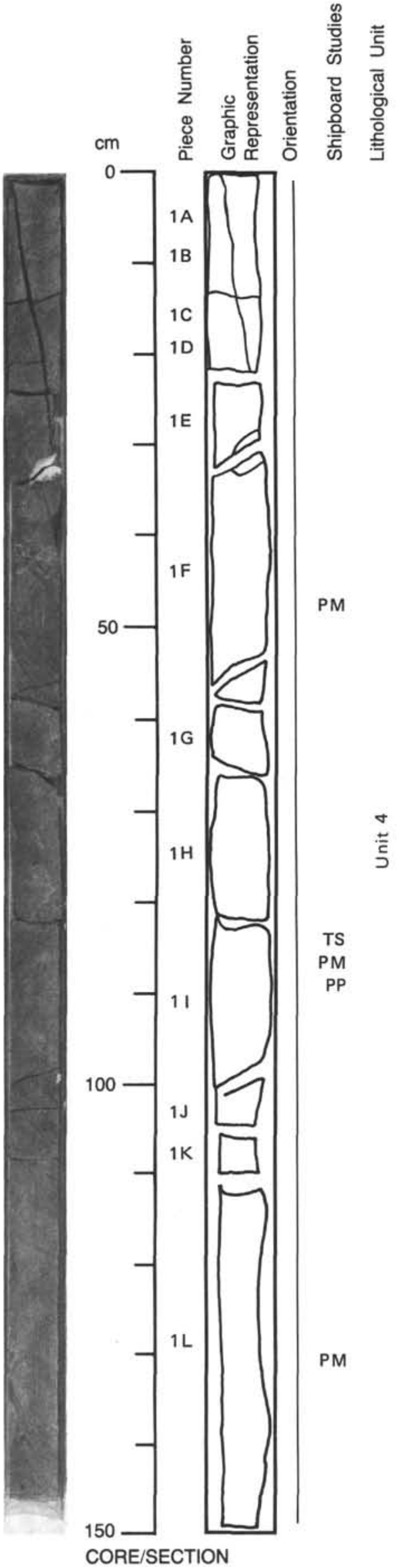

115-707C-26R-3

UNIT 4 (CONTINUED): PLAGIOCLASE BASALT

Pieces 1A–1L

Continuous with 115-707C-26R-2, Unit 4

VEINS/FRACTURES: Calcite vein at boundary of Pieces 1E and 1F.

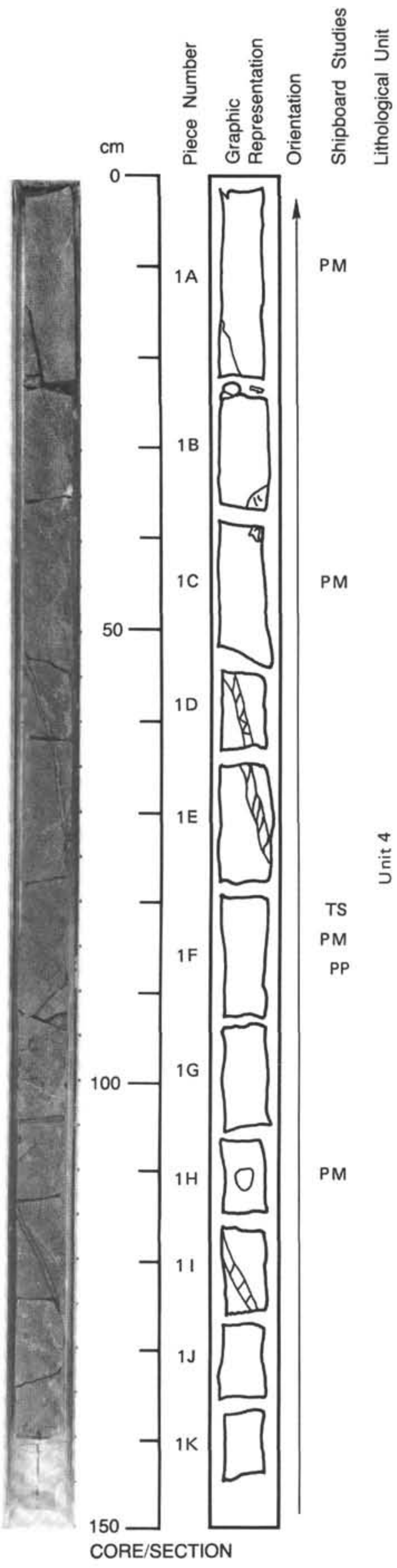

115-707C-26R-4

UNIT 4 (CONTINUED): PLAGIOCLASE BASALT

Pieces 1A–1K

Continuous with 115-707C-26R-3, Unit 4

VEINS/FRACTURES: High-angle veins with calcite and green clay in Pieces 1D, 1E, and 1I.

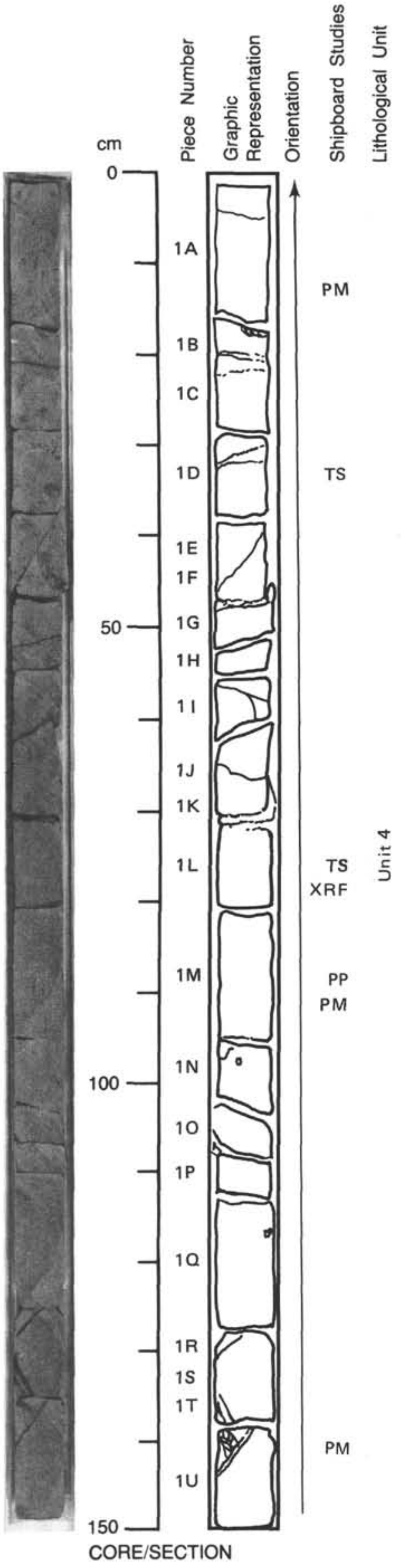

115-707C-26R-5

UNIT 4 (CONTINUED): PLAGIOCLASE BASALT

Pieces 1A–1U

Continuous with 115-707C-26R-4, Unit 4

GROUNDMASS: Similar to upper parts of Unit 5 but few amygdules (<1%).
VEINS/FRACTURES: Few fractures, <1%. Infilled with calcite + clay, as large as 8 mm across, with almost no thin calcite veins.

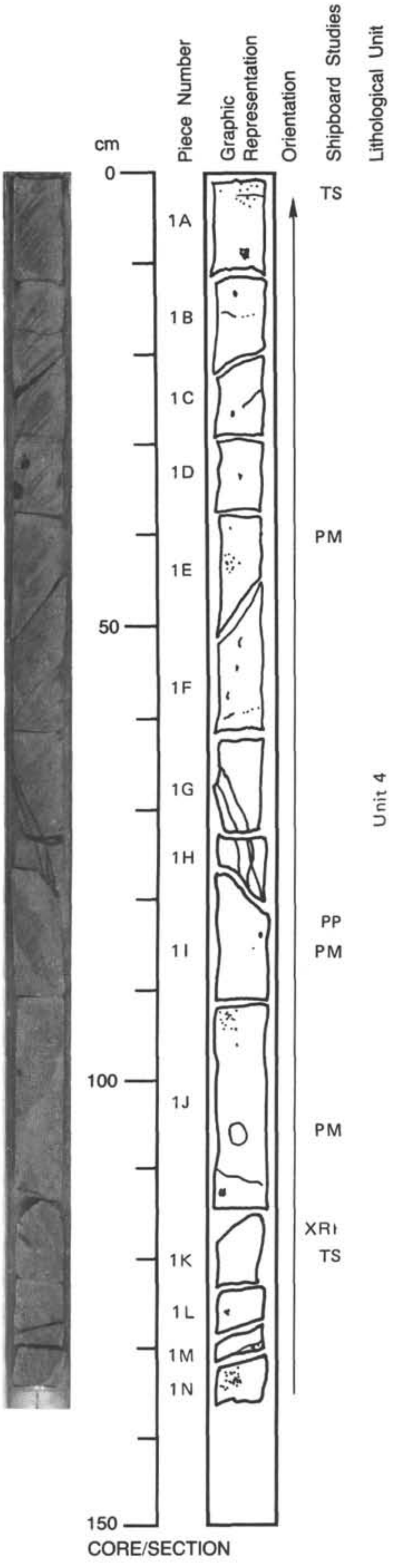

115-707C-26R-6

UNIT 4 (CONTINUED): PLAGIOCLASE BASALT

Pieces 1A–1N

Continuous with 115-707C-26R-5, Unit 4

GROUNDMASS: Similar to basalt above, massive. Amygdules noted on graphic representation.

VEINS/FRACTURES: Piece 1B has 1 mm fracture filled with black alteration mineral. Fractures filled with black clay mineral, 2–3 mm wide. Pieces 1H and 1L broken along 1 mm wide calcite-filled fracture.

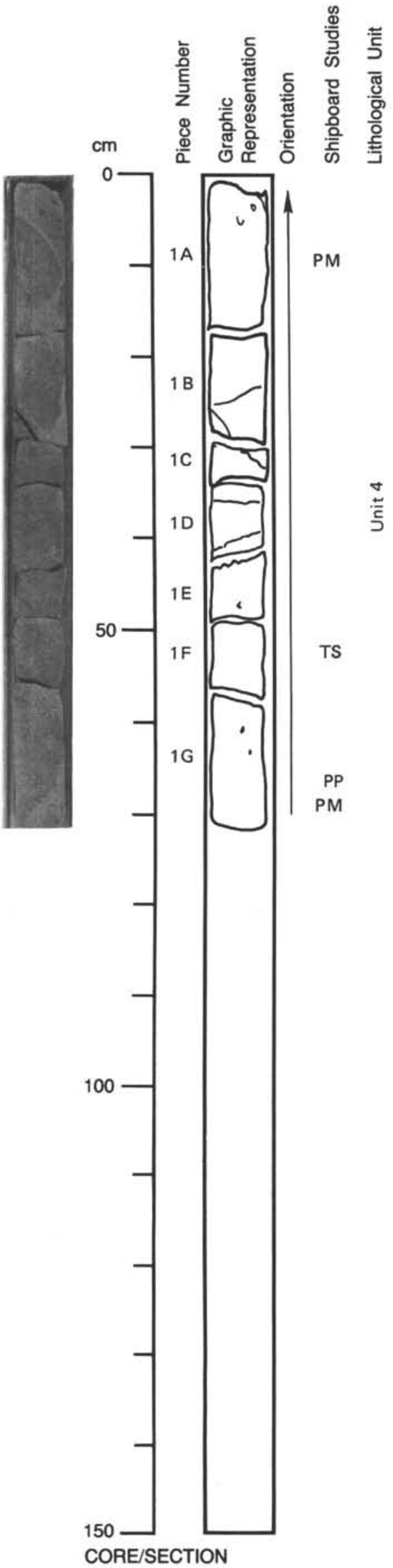

115-707C-26R-7

UNIT 4 (CONTINUED): PLAGIOCLASE BASALT

Pieces 1A–1G

Continuous with 115-707C-26R-6, Unit 4

GROUNDMASS: Rare amygdules.
VEINS/FRACTURES: Similar to 115-707C-26R-6, but only rare cracks. One filled with calcite <1 mm wide.

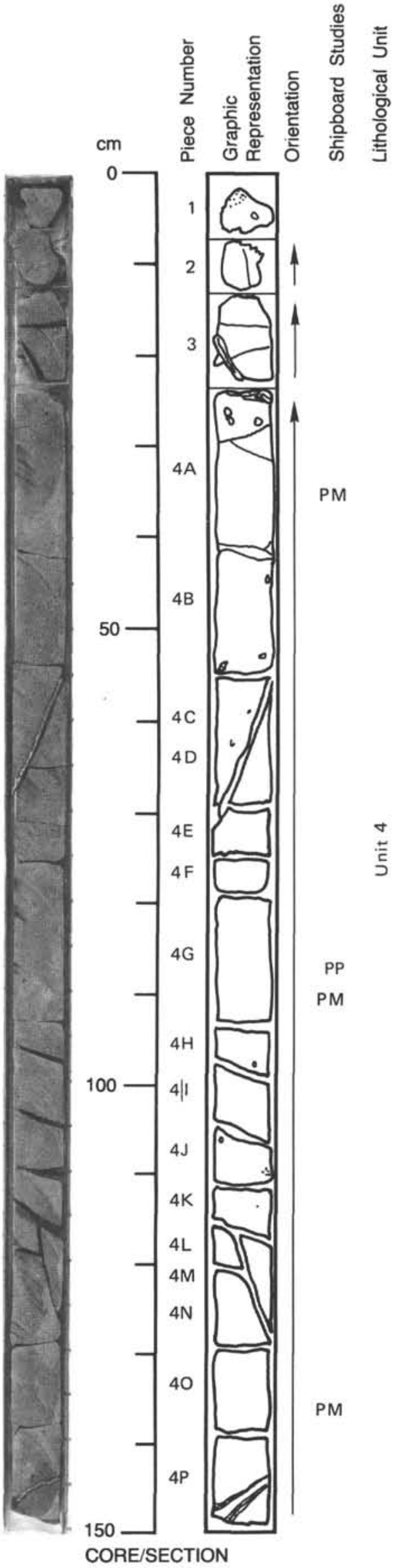

115-707C-27R-1

UNIT 4 (CONTINUED): PLAGIOCLASE BASALT

Pieces 1-4P

Continuous with 115-707C-26R-7, Unit 4

VEINS/FRACTURES: Crosscutting veins in Piece 3. Large vein between Pieces 4C and 4D. Vein with black margins and grey interior in Piece 48.

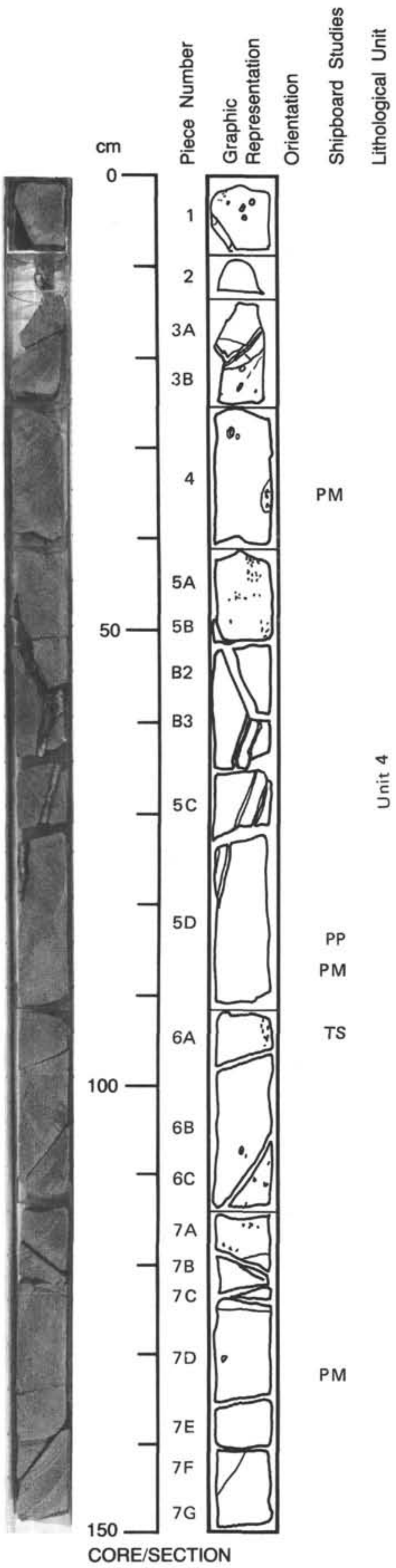

115-707C-27R-2

UNIT 4 (CONTINUED): PLAGIOCLASE BASALT

Pieces 1-7G

Continuous with 115-707C-27R-1, Unit 4

VEINS/FRACTURES: Vein in Piece 1. Fragile black vein filling in Pieces 5A and 5B1. Vein with black margin and gray interior in Pieces 5B2, 5B3, and 5D. Vein between Pieces 7F and 7G.

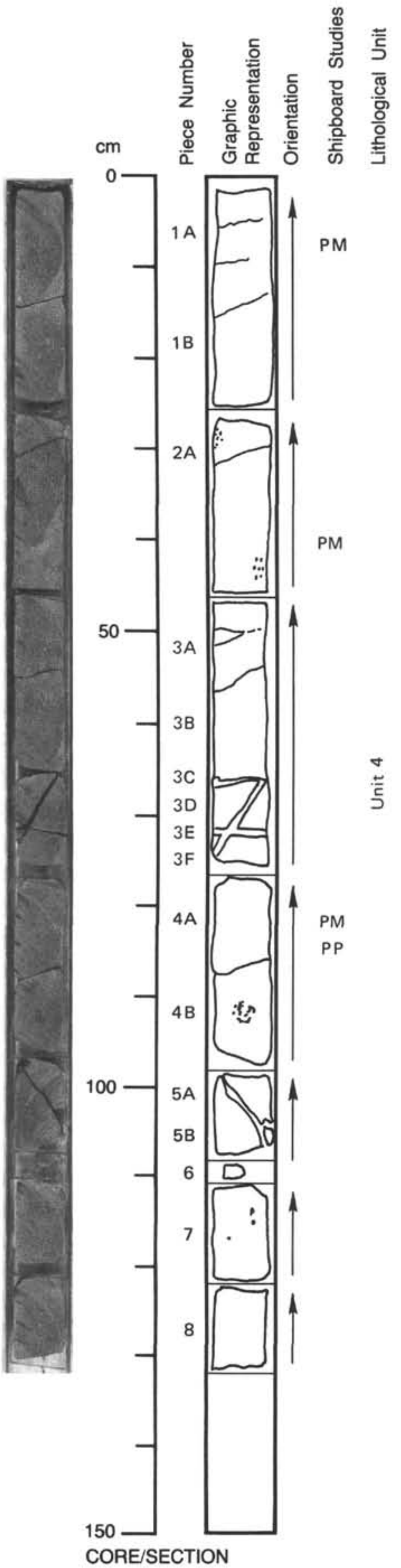

115-707C-27R-3

UNIT 4 (CONTINUED): PLAGIOCLASE BASALT

Pieces 1A–8

Continuous with 115-707C-27R-2, Unit 4

VEINS/FRACTURES: Crosscutting veins in Pieces 3C, 3D, 3E, and 3F.

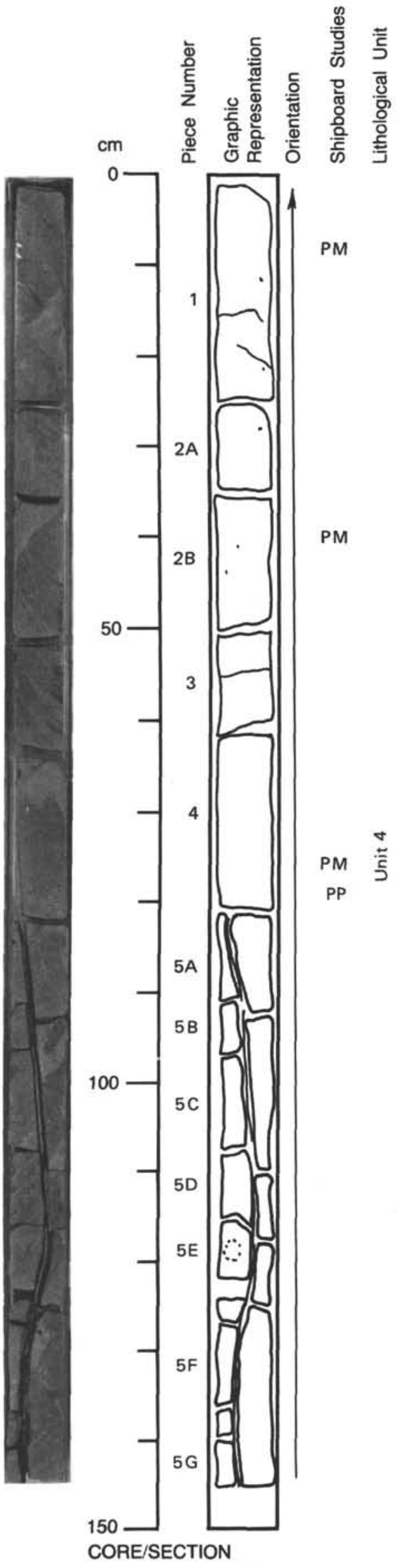

115-707C-27R-4

UNIT 4 (CONTINUED): PLAGIOCLASE BASALT

Pieces 1–5L

Continuous with 115-707C-27R-3, Unit 4

VESICLES: Occasional clay-filled vesicles in Piece 2B. Concentration of filled vesicles, probably due to gas-streaming segregation; crystals slightly larger around in area, in Piece 5E.

VEINS/FRACTURES: Fine fractures filled with calcite in Piece 1. Loose vein material in Piece 5. Mega-crack, ≈2 mm wide, filled with dark green, very hard clay and calcite in Pieces 5A–5G.

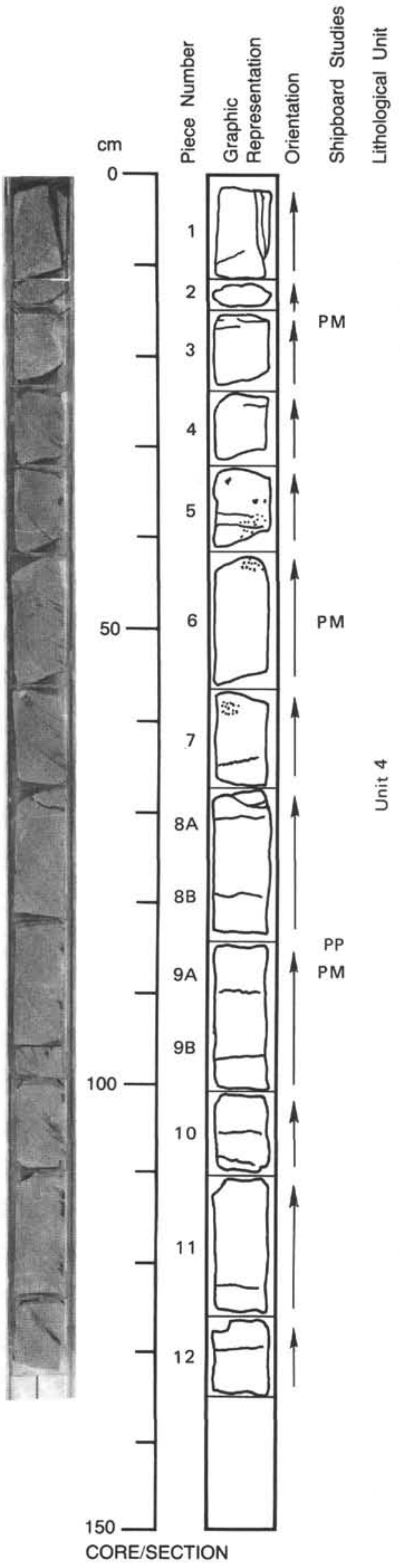

115-707C-27R-5

UNIT 4 (CONTINUED): PLAGIOCLASE BASALT

Pieces 1–12

Continuous with 115-707C-27R-4, Unit 4

ALTERATION: Moderately altered throughout.
VEINS/FRACTURES: Few veins, calcite filled, <1 mm thick.

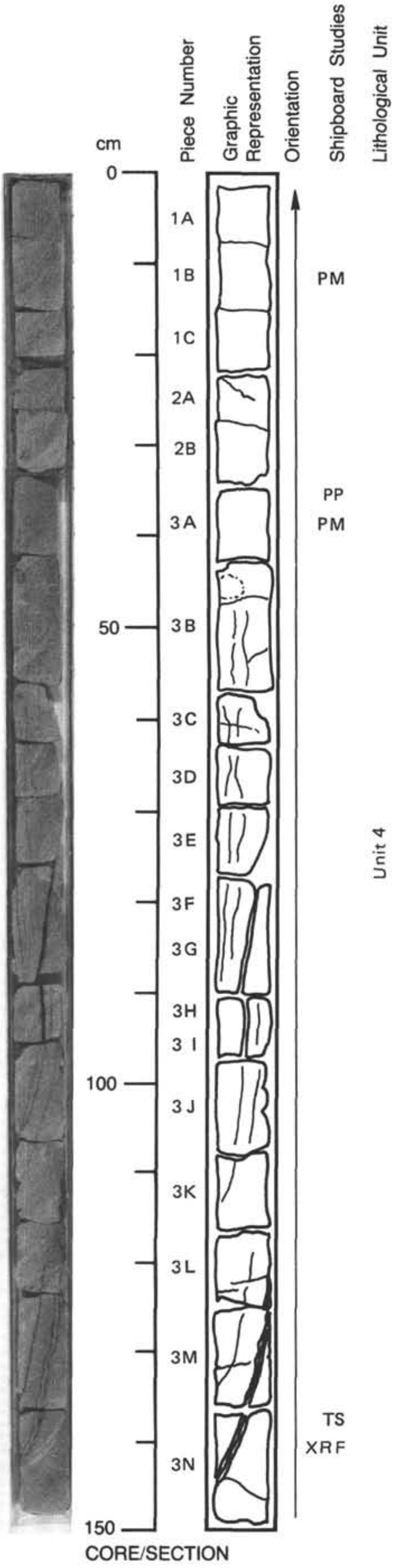

115-707C-27R-6

UNIT 4 (CONTINUED): PLAGIOCLASE BASALT

Pieces 1A–3N

Continuous with 115-707C-27R-5, Unit 4

VESICLES: Concentration of gas vesicles, filled with clay and calcite, in Piece 3B.
VEINS/FRACTURES: Fine calcite-lined veins in Pieces 3B through 3N. Large 3–5 mm fracture filled with clay + calcite.

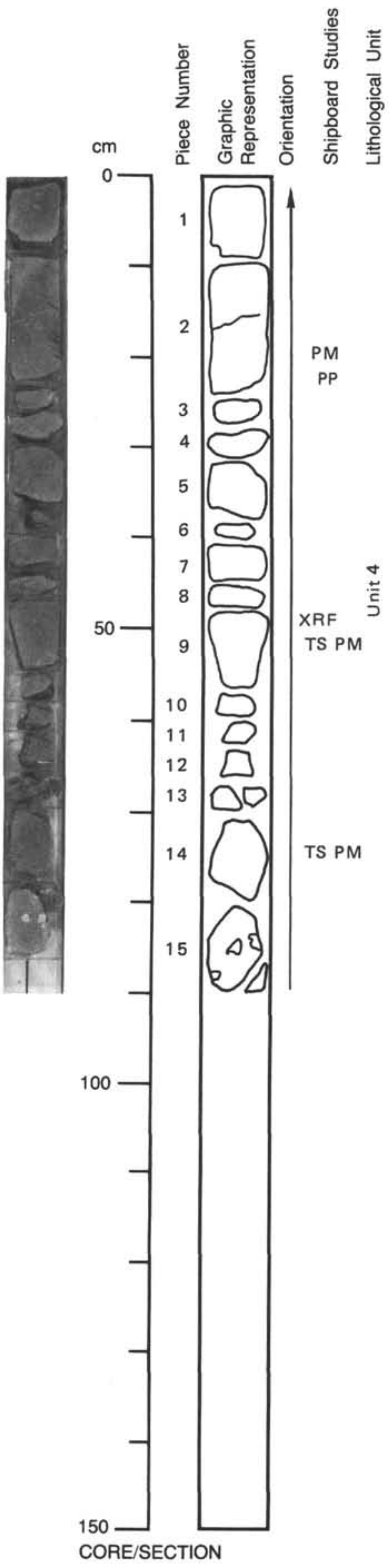

115-707C-27R-7

UNIT 4 (CONTINUED): PLAGIOCLASE BASALT

Pieces 1–15

Continuous with 115-707C-27R-6, Unit 4

ALTERATION: Increasing alteration downcore.
VEINS/FRACTURES: Fine fractures in Piece 2. Voids filled with calcite and clay, Piece 15.

SITE 707 HOLE C CORE 28R CORED INTERVAL 1975.2-1984.6 mbsl; 433.6-443.2 mbsf

TIME-ROCK UNIT	BIOSTRAT. ZONE/ FOSSIL CHARACTER				PALEOMAGNETICS	PHYS. PROPERTIES	CHEMISTRY	SECTION	METERS	GRAPHIC LITHOLOGY	DRILLING DISTURB.	SED. STRUCTURES	SAMPLES	LITHOLOGIC DESCRIPTION
	FORAMINIFERS	NANNOFOSSILS	RADIOLARIANS	DIATOMS										
PALEOCENE	Barren	CP3-CP5 ? R/M		Barren				1 2 3	0.5 1.0					PARTIALLY DOLOMITIZED CALCAREOUS GRAINSTONE

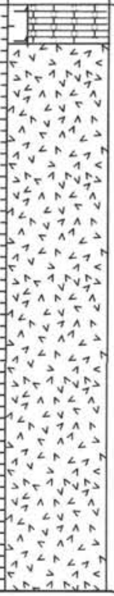

PARTIALLY DOLOMITIZED CALCAREOUS GRAINSTONE

Major lithology: Calcareous grainstone cobbles and pebbles, partially dolomitized, greenish gray (5GY 6/1-7/1), and glauconite rich. Grainstones consist mainly of bioclasts and a few broken (oyster?) shells.

Sediment is underlain by oceanic basalt.

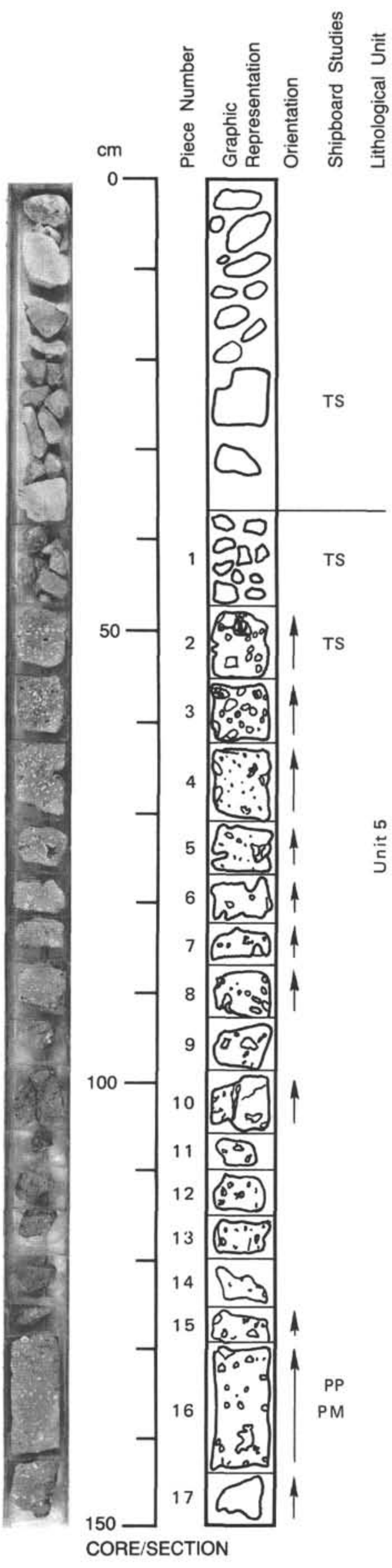

115-707C-28R-1

SEDIMENT: PARTIALLY DOLOMITIZED CALCAREOUS GRAINSTONE AND BRECCIA

0-37 cm: Calcareous grainstone cobbles and pebbles, partially dolomitized, greenish gray (5GY 6/1, 7/1), and glauconite rich. Grainstone consists mainly of bioclasts and a few broken (oyster?) shells. Sandstone, chert, and carbonate breccia.

NOTE: Sediment is underlain by basalt.

UNIT 5: CLINOPYROXENE-PLAGIOCLASE BASALT

Pieces 1-17

CONTACTS: No contact observed, vesicular top.
PHENOCRYSTS: Plagioclase microphenocryst - ≈1 mm in size.
Clinopyroxene - 1-2 mm in size, slightly altered.
GROUNDMASS: Fine grained, porphyritic.
COLOR: Dark gray.
VESICLES: Highly vesicular, 1.0-10.0 mm large, 10-20%.
ALTERATION: Epidote + quartz present, clay and calcite fill voids + vesicles.
VEINS/FRACTURES: <1%, filled with black clay or calcite.
VOIDS: Irregularly shaped, large (>5 mm, and as large as 20 mm). Lined with spherical olive (5Y 5/6) crystals, ≈1%.

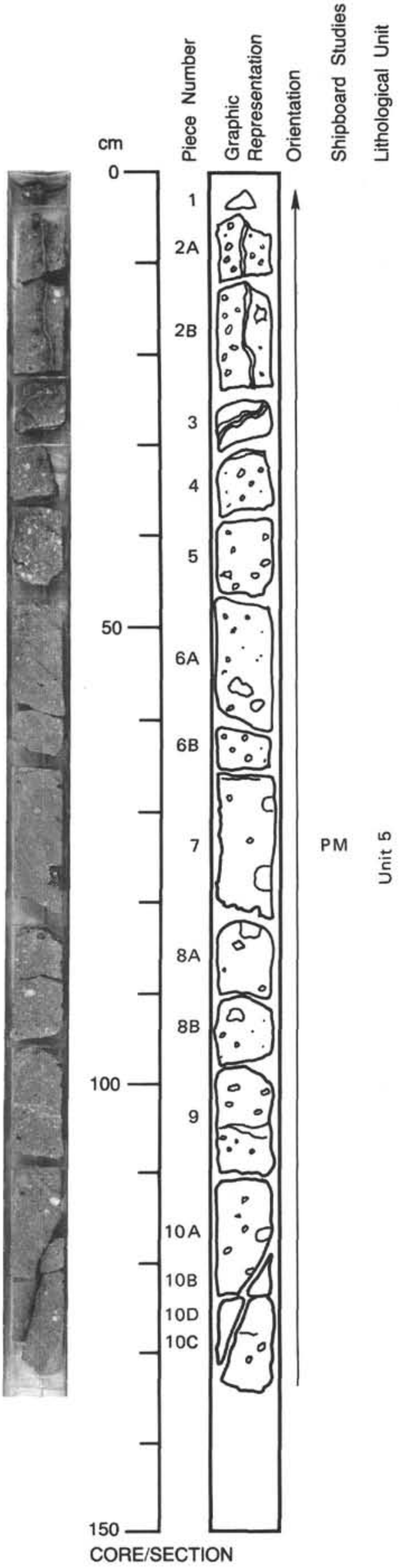

115-707C-28R-2

UNIT 5 (CONTINUED): CLINOPYROXENE PLAGIOCLASE BASALT

Pieces 1-10C

Continuous with 115-707C-28R-1, Unit 5

GROUNDMASS: Grain size increases slightly with depth.

VESICLES: Vesicles decrease in number and size downcore, ranging from 10-20% at top of core, 1.0-10 mm in size, to 1% at Pieces 10A-10D, generally 2-3 mm in size. Large vesicle, filled with calcite, in Piece 10A.

VEINS/FRACTURES: Piece 2B: Large, 2-4 mm in size, fracture filled with calcite and green clay.

Piece 6A: Large vug filled with botryoidal silica(?).

Piece 7: Large, open vesicle/vug infilled with botryoidal silica(?), bottom.

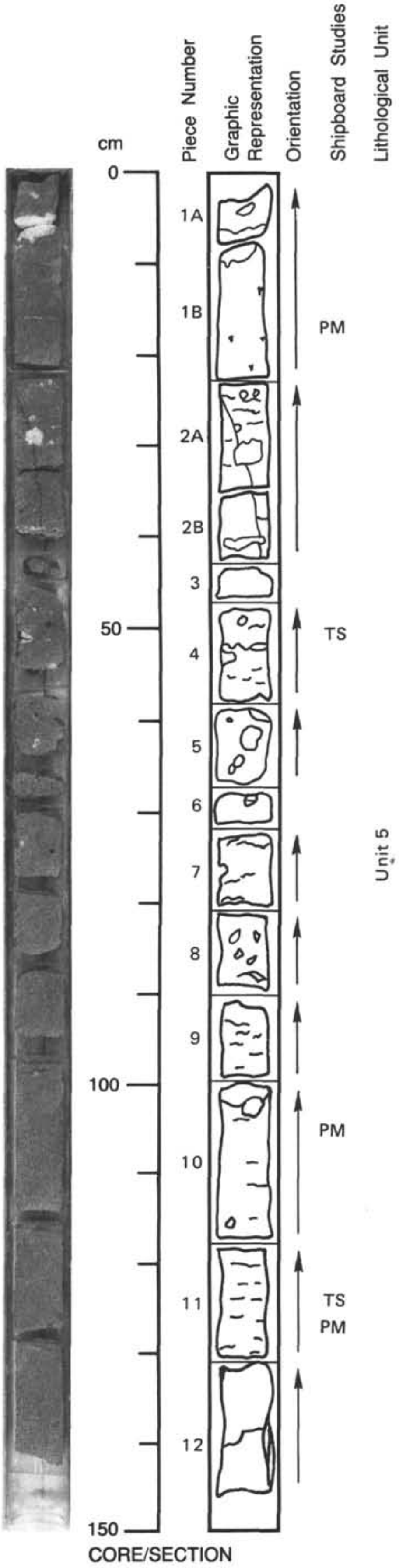

115-707C-28R-3

UNIT 5 (CONTINUED): CLINOPYROXENE-PLAGIOCLASE BASALT

Pieces 1A–12

Continuous with 115-707C-28R-2, Unit 5

GROUNDMASS: Massive, fine grained (especially Pieces 9–12).

VESICLES: Large vesicles contain olive (5Y 5/6) botryoidal mineral (probably too soft to be chalcedony, or quartz, ≈5). Few vesicles in lower part, Pieces 9–12.

VEINS/FRACTURES: Between Pieces 1A and 1B, large 1 cm wide calcite vein.

Many tiny horizontal calcite-filled cracks, and a large calcite-filled vug (labelled "cc") cut Piece 2A. 1 mm wide crack (labeled "c") is filled with black alteration mineral in Pieces 2A and 2B.

Few veins in lower part, Pieces 9–12.

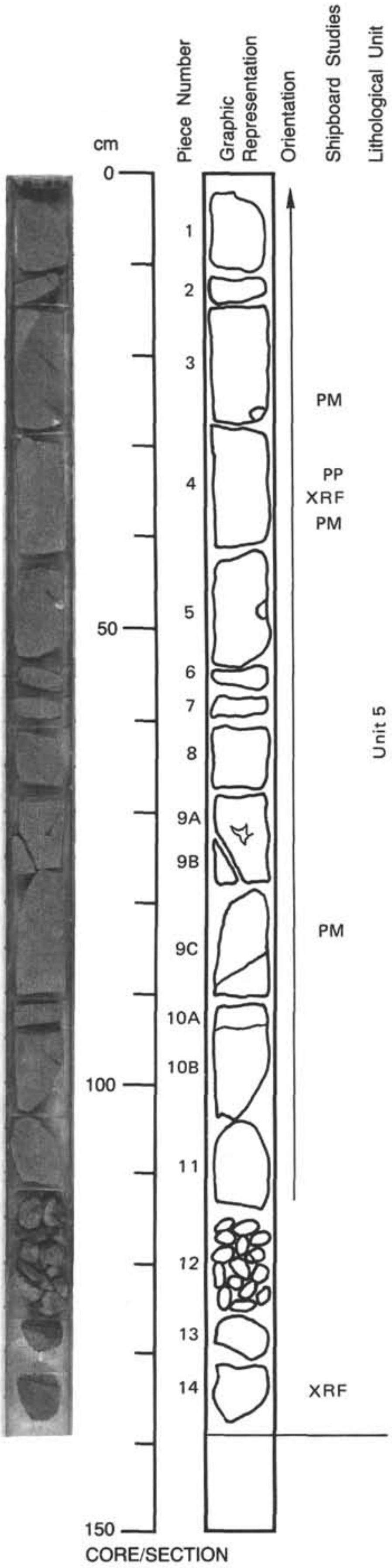

115-707C-28R-4

UNIT 5 (CONTINUED): CLINOPYROXENE-PLAGIOCLASE BASALT

Pieces 1–14

Continuous with 115-707C-28R-3, Unit 5

PHENOCRYSTS: Plagioclase - 2–3 mm.
Clinopyroxene - <1 mm.
GROUNDMASS: Much more compact than overlying rock, with fewer vesicles. Holocrystalline.
VEINS/FRACTURES: Calcite-filled vugs at base of Piece 3 and side of Piece 5.

THIN SECTION DESCRIPTION

115-707C-22R-1 (Piece 3, 15-17 cm)

ROCK NAME: Sparsely plagioclase clinopyroxene phyric basalt

WHERE SAMPLED: Unit 1, flow top

TEXTURE: Vesicular, sparsely porphyritic

GRAIN SIZE: Fine

OBSERVER: MRF

PRIMARY MINERALOGY	PERCENT PRESENT	PERCENT ORIGINAL	SIZE RANGE (mm)	APPROX. COMPOSITION	MORPHOLOGY	COMMENTS
PHENOCRYSTS						
Plagioclase	1-2	1-2	1-2		Euhedral, rounded	Glomerocrysts with round crystals inside and euhedral crystals outside.
Clinopyroxene	1-2	1-2	0.1		Equant, subhedral	Glomerophyric cluster, 1 mm long.
GROUNDMASS						
Plagioclase	20	40	0.05-0.15		Blades	
Clinopyroxene	5	20	0.01-0.10		Equant	Green to brown. Marginal zonation to aegirine-augite.
Magnetite	2	15	0.01-0.10		Euhedral, cubes, dendritic	
Glass(?)	—	20	1		Irregular	Quenched matrix, occurs in patches, completely altered.

SECONDARY MINERALOGY	PERCENT	REPLACING/ FILLING	COMMENTS
Clays	30	Glass, cpx	Replaces groundmass cpx.
Carbonate	40	Groundmass, vesicles	Calcite.

VESICLES/ CAVITIES	PERCENT	LOCATION	SIZE RANGE (mm)	FILLING	SHAPE	COMMENTS
Vesicles	15	Variable	0.5-1.5	Calcite, clay	Round	Vesicles are concentrated at one end of the slide, away from what was interpreted as a glassy margin in hand specimen.

COMMENTS: Semi-diffuse segregation zones developed up to 1 mm in diameter.
This section is rich in more sodic plag relative to other sections and is associated with Na-rich cpx; contains more abundant magnetite.
More evolved than the rest of the section.

THIN SECTION DESCRIPTION

115–707C–22R–1 (Piece 10A, 53–55 cm)

ROCK NAME: Sparsely plagioclase clinopyroxene phyric basalt

WHERE SAMPLED: Unit 1, Top of piece 10A (flow top?)

TEXTURE: Intersertal, sparsely porphyritic

GRAIN SIZE: Fine to microcrystalline

OBSERVER: MRF

PRIMARY MINERALOGY	PERCENT PRESENT	PERCENT ORIGINAL	SIZE RANGE (mm)	APPROX. COMPO-SITION	MORPHOLOGY	COMMENTS
PHENOCRYSTS						
Plagioclase	1	1	<0.6		Blades	Crystal size gradational, from phenocrysts to groundmass crystals.
Clinopyroxene	1	5	0.3		Equant, Subhedral–euhedral	
GROUNDMASS						
Plagioclase	20	25	≈0.05		Blades	
Clinopyroxene	5	30	0.20		Equant	
Magnetite	3	3	0.05		Equant	
Glass(?)	—	5				Quenched matrix, completely altered.

SECONDARY MINERALOGY	PERCENT	REPLACING/ FILLING	COMMENTS
Clays	50	Glass, cpx, plag	
Clays	20	Vesicles	
Carbonate	Tr	Cracks	Calcite present in cracks near the bottom surface.

VESICLES/ CAVITIES	PERCENT	LOCATION	SIZE RANGE (mm)	FILLING	SHAPE	COMMENTS
Vesicles	>3	Even	1–5	Clay	Round	Some vesicles are interconnected. 3-mm blades of calcite in 6-mm vesicle; blades surrounded by clay.

COMMENTS: Consecutive bands of clay, calcite, and basalt at bottom of section, each about 1 mm wide.

THIN SECTION DESCRIPTION

115-707C-22R-1 (Piece 11A, 94-95 cm)

ROCK NAME: Sparsely plagioclase clinopyroxene phyric basalt

WHERE SAMPLED: Unit 1

TEXTURE: Intersertal, vesicular, sparsely porphyritic

GRAIN SIZE: Fine

OBSERVER: MRF

PRIMARY MINERALOGY	PERCENT PRESENT	PERCENT ORIGINAL	SIZE RANGE (mm)	APPROX. COMPO-SITION	MORPHOLOGY	COMMENTS
PHENOCRYSTS						
Plagioclase	1	1	<2		Subhedral	Glomerocrysts of anhedral crystals with glass inclusions.
Clinopyroxene	3	5	0.3		Anhedral, equant	
GROUNDMASS						
Plagioclase	20	20	<0.1		Blades	
Clinopyroxene	10	30	<0.1		Equant, subhedral–anhedral	
Magnetite	1	1	<0.03			
Glass(?)	—	28				Quenched matrix, completely altered.

SECONDARY MINERALOGY	PERCENT	REPLACING/ FILLING	COMMENTS
Clays	50	Glass, groundmass	Reddish brown clay.
Clays	10	Vesicles	
Carbonate	5	Vesicles	Calcite.

VESICLES/ CAVITIES	PERCENT	LOCATION	SIZE RANGE (mm)	FILLING	SHAPE	COMMENTS
Vesicles	15	Uneven	10	Calcite, clay	Round	Only a few large vesicles.

THIN SECTION DESCRIPTION

115-707C-22R-2 (Piece 2, 37-38 cm)

ROCK NAME: Sparsely plagioclase clinopyroxene phyric basalt

WHERE SAMPLED: Unit 1

TEXTURE: Intersertal, vesicular, sparsely porphyritic

GRAIN SIZE: Fine

OBSERVER: MRF

PRIMARY MINERALOGY	PERCENT PRESENT	PERCENT ORIGINAL	SIZE RANGE (mm)	APPROX. COMPO-SITION	MORPHOLOGY	COMMENTS
PHENOCRYSTS						
Plagooclase	1	1	1–2		Blades, subhedral–anhedral	Glomerocrysts.
Clinopyroxene	3	5	0.1–0.5		Equant, subhedral	
GROUNDMASS						
Plagioclase	20	25	≈0.05		Blades	Some crystals slightly altered to clay.
Clinopyroxene	5	25	<0.05		Equant	
Magnetite	1	1	<0.05		Equant, euhedral	
Glass(?)	—	13				Quenched matrix, completely altered.

SECONDARY MINERALOGY	PERCENT	REPLACING/ FILLING
Clays	40	Glass, groundmass
Clays	30	Vesicles

VESICLES/ CAVITIES	PERCENT	LOCATION	SIZE RANGE (mm)	FILLING	SHAPE
Vesicles	30		3	Clay	Round

THIN SECTION DESCRIPTION

115-707C-23R-1 (Piece 1E, 24-25 cm)

ROCK NAME: Highly clinopyroxene plagioclase phyric basalt

WHERE SAMPLED: Unit 2, middle of unit

TEXTURE: Highly phyric

GRAIN SIZE: Medium to fine

OBSERVER: MRF

PRIMARY MINERALOGY	PERCENT PRESENT	PERCENT ORIGINAL	SIZE RANGE (mm)	APPROX. COMPO-SITION	MORPHOLOGY	COMMENTS
PHENOCRYSTS						
Plagioclase	20	20	3		Subhedral	Glomerocrysts with cpx, up to 10 mm diameter.
Clinopyroxene	10	15	51		Subhedral	Monomineralic glomerocrysts and glomerocrysts with plag.
GROUNDMASS						
Plagioclase	10	30	<0.01			
Clinopyroxene	10	30	<0.01			
Magnetite	1	2	<0.01			
Glass(?)	—	3				Quenched matrix, completely altered.

SECONDARY MINERALOGY	PERCENT	REPLACING/ FILLING
Clays	49	Groundmass, voids
Carbonate	<1	Void

VESICLES/ CAVITIES	PERCENT	LOCATION	SIZE RANGE (mm)	FILLING	SHAPE
Vesicles	3	Even	1	Carbonate	Irregular

THIN SECTION DESCRIPTION

115-707C-23R-1 (Piece 1J, 65-66 cm)

ROCK NAME: Highly clinopyroxene plagioclase phyric basalt

WHERE SAMPLED: Unit 2

TEXTURE: Highly porphyritic

GRAIN SIZE: Medium to fine

OBSERVER: YT

PRIMARY MINERALOGY	PERCENT PRESENT	PERCENT ORIGINAL	SIZE RANGE (mm)	APPROX. COMPO-SITION	MORPHOLOGY	COMMENTS
PHENOCRYSTS						
Plagioclase	20	25	0.3–1.0	An 50	Euhedral–subhedral	Sometimes replaced by brown clay. Zoned.
Clinopyroxene	10	10	0.3–0.5	Augite	Euhedral–subhedral	Glomerocrysts with plag.
GROUNDMASS						
Plagioclase	2	30	<0.3		Subhedral	Altered to brown clay + magnetite. Cpx is augite.
Clinopyroxene	3	10				
Opaque	5	5	<0.3	Magnetite	Euhedral	Alteration product(?).

SECONDARY MINERALOGY	PERCENT	REPLACING/ FILLING
Clays	55	Plag, cpx, vesicles
Carbonate	5	Vesicles

VESICLES/ CAVITIES	PERCENT	LOCATION	SIZE RANGE (mm)	FILLING	SHAPE	COMMENTS
Vesicles	20	Even	0.5–2.0	Carbonate, clay	Elliptical, irregular	Carbonate >> brown clay. Carbonate fills in clay-rimmed vesicles.

COMMENTS: Carbonate vein runs along the side of the thin section.

THIN SECTION DESCRIPTION

115-707C-23R-1 (Piece 1Q, 126-127 cm)

ROCK NAME: Highly clinopyroxene plagioclase phyric basalt

WHERE SAMPLED: Unit 23

TEXTURE: Highly porphyritic

GRAIN SIZE: Medium

OBSERVER: YT

PRIMARY MINERALOGY	PERCENT PRESENT	PERCENT ORIGINAL	SIZE RANGE (mm)	APPROX. COMPOSITION	MORPHOLOGY	COMMENTS
PHENOCRYSTS						
Plagioclase	20	20	0.5–5	≈An 55	Subhedral	Fresh. Zoned. Larger crystal has dusty inclusions.
Clinopyroxene	10	10	0.5–0.7	Augite	Subhedral	
GROUNDMASS						
Plagioclase	30	45	<0.5	An 50	Subhedral–anhedral	
Clinopyroxene	10	20	<0.5	Augite	Subhedral–anhedral	
Opaque	5	5	<0.2	Magnetite	Euhedral	Alteration products(?).

SECONDARY MINERALOGY	PERCENT	REPLACING/ FILLING	COMMENTS
Clays	20	Plag, cpx	Alteration products of groundmass minerals.
Carbonate	5	Vein	

COMMENTS: Groundmass is coarse-grained. In this context, this rock looks like dolerite. Phenocrysts are not isolated grains, but glomerocrysts.

THIN SECTION DESCRIPTION

115-707C-23R-2 (Piece 1F, 75-77 cm)

ROCK NAME: Highly olivine clinopyroxene plagioclase phyric basalt

WHERE SAMPLED: Unit 3

TEXTURE: Highly porphyritic

GRAIN SIZE: Fine to medium, phaneritic

OBSERVER: ANB

PRIMARY MINERALOGY	PERCENT PRESENT	PERCENT ORIGINAL	SIZE RANGE (mm)	APPROX. COMPOSITION	MORPHOLOGY	COMMENTS
PHENOCRYSTS						
Olivine	—	2	<0.5		Subhedral	Completely altered or replaced by calcite.
Plagioclase	10	10	<2	An 60	Subhedral	Strong normal and oscillatory zoning.
Clinopyroxene	2	2	<0.5	Augite	Subhedral	
GROUNDMASS						
Olivine	—	2	<0.2		Anhedral	
Clinopyroxene	20	23	<0.5	Augite	Subhedral	
Plagioclase	40	40	<0.5	An 60	Subhedral–euhedral	Strongly zoned.
Spinel	1	1	<0.5	Magnetite	Subhedral	

SECONDARY MINERALOGY	PERCENT	REPLACING/ FILLING	COMMENTS
Clays	17	Cpx, vesicles	Brown clay associated with calcite in groundmass interstices.
Carbonate	10	Cpx, ol, vesicles	Infills vesicles, fractures, and interstices.

VESICLES/ CAVITIES	PERCENT	LOCATION	SIZE RANGE (mm)	FILLING	SHAPE
Vesicles	20	Random	<8	Calcite, brown clay	Irregular

COMMENTS: General transition in Core 23 (from top to bottom):
1) Clearly porphyritic.
2) Both porphyritic and glomerocrystic.
3) Medium-grained, intersertal groundmass of plag ± cpx phenocrysts (this thin section).

THIN SECTION DESCRIPTION

115-707C-23R-3 (Piece 1C, 33-35 cm)

ROCK NAME: Highly plagioclase clinopyroxene phyric basalt

WHERE SAMPLED: Unit 3

TEXTURE: Highly porphyritic, holocrystalline

GRAIN SIZE: Medium

OBSERVER: YT

PRIMARY MINERALOGY	PERCENT PRESENT	PERCENT ORIGINAL	SIZE RANGE (mm)	APPROX. COMPO-SITION	MORPHOLOGY	COMMENTS
PHENOCRYSTS						
Plagioclase	7	7	0.2–0.8	≈An 55	Euhedral–subhedral	Fresh. Zoned.
Clinopyroxene	7	7	0.2–0.5	Augite	Euhedral–subhedral	Fresh. Sometimes zoned.
Glomerocrysts	29	29	1–5			Glomerocrysts of plag (An 60–50) ± cpx.
GROUNDMASS						
Plagioclase	29	38	<0.2		Subhedral	
Clinopyroxene	10	14	<0.2	Augite	Subhedral	
Opaque	4	4	<0.1	Magnetite	Euhedral	
Glass(?)	—	<1				Quenched matrix, completely altered.

SECONDARY MINERALOGY	PERCENT	REPLACING/ FILLING	COMMENTS
Clays	14	Plag, cpx, glass	Plag ± cpx sometimes altered to brownish clay.

THIN SECTION DESCRIPTION

115-707C-23R-3 (Piece 1K, 137-140 cm)

ROCK NAME: Highly clinopyroxene plagioclase phyric basalt

WHERE SAMPLED: Unit 3

TEXTURE: Highly porphyritic, granular

GRAIN SIZE: Medium

OBSERVER: RBH

PRIMARY MINERALOGY	PERCENT PRESENT	PERCENT ORIGINAL	SIZE RANGE (mm)	APPROX. COMPO-SITION	MORPHOLOGY	COMMENTS
PHENOCRYSTS						
Plagioclase	10	10	53.0		Subhedral, laths	Some glomerocrysts.
Clinopyroxene	7	8	51	Augite	Equant, subhedral	Some monomineralic glomerocrysts, some with plag. Some discrete phenocrysts.
GROUNDMASS						
Opaques	2	2	0.15	Titano-magnetite	Equant	Ragged crystal edges. Some skeletal crystals.
Plagioclase	35	35	0.3			
Clinopyroxene	25	35				
Glass(?)	—	10				Quenched groundmass crystals replaced by clay.

SECONDARY MINERALOGY	PERCENT	REPLACING/ FILLING	COMMENTS
Clays	21	Groundmass, cpx	Patchy alteration of medium-grained groundmass + ol(?) or glass(?) + cpx.

COMMENTS: This section may have quite a number of unaltered ol(?) or opx(?) crystals. Many of these grains have low birefringence, but give optic-axis figures. On better scope, can estimate 2Vz = 60° from curvature of isogyre. These grains are almost certainly cpx.

THIN SECTION DESCRIPTION

115-707C-23R-4 (Piece 1C, 32-34 cm)

ROCK NAME: Highly olivine clinopyroxene plagioclase phyric basalt

WHERE SAMPLED: Unit 3

TEXTURE: Highly porphyritic

GRAIN SIZE: Fine

OBSERVER: ANB

PRIMARY MINERALOGY	PERCENT PRESENT	PERCENT ORIGINAL	SIZE RANGE (mm)	APPROX. COMPO-SITION	MORPHOLOGY	COMMENTS
PHENOCRYSTS						
Olivine	—	1	<0.5		Subhedral	Replaced by iddingsite.
Plagioclase	15	15	<1	An 65	Subhedral	
Clinopyroxene	10	10	<1	Augite	Subhedral–anhedral	
Glomerocrysts	25	25				Glomerocrysts of cpx + plag.
GROUNDMASS						
Plagioclase	20	20	<0.2		Subhedral	
Clinopyroxene	5	5	<0.2	Augite	Anhedral	
Spinel	1	1	<0.2	Magnetite	Subhedral–anhedral	

SECONDARY MINERALOGY	PERCENT	REPLACING/ FILLING	COMMENTS
Clays	13	Interstices, groundmass	Radial and subradial brown clays, associated with calcite.
Carbonate	10	Interstices, groundmass	Associated with clay alteration in interstices.

THIN SECTION DESCRIPTION

115-707C-23R-4 (Piece 3, 78-80 cm)

ROCK NAME: Moderately olivine-bearing clinopyroxene plagioclase phyric basalt

WHERE SAMPLED: Unit 3

TEXTURE: Moderately porphyritic

GRAIN SIZE: Medium to fine

OBSERVER: YT

PRIMARY MINERALOGY	PERCENT PRESENT	PERCENT ORIGINAL	SIZE RANGE (mm)	APPROX. COMPO-SITION	MORPHOLOGY	COMMENTS
PHENOCRYSTS						
Olivine	—	<1	0.3			Completely altered to clay.
Plagioclase	9	9	0.3–4.0	An 50	Subhedral	Fresh. Zoned, An 60 to An 40.
Clinopyroxene	3	3	0.3–4.0	Augite	Subhedral	Fresh.
Glomerocrysts	12	12	1–5			Glomerocrysts of plag ± cpx.
GROUNDMASS						
Plagioclase	31	45	<0.3	An 40	Subhedral	
Clinopyroxene	19	20	<0.3	Augite	Subhedral	
Opaque	1	1	<0.2	Magnetite	Euhedral	Associated with clay.

SECONDARY MINERALOGY	PERCENT	REPLACING/ FILLING	COMMENTS
Clays	25	Plag, cpx, vesicles	Brown clays.

VESICLES/ CAVITIES	PERCENT	LOCATION	SIZE RANGE (mm)	FILLING	SHAPE
Vesicles	10	Even	0.2–2.0	Brown clay	Round

THIN SECTION DESCRIPTION

115-707C-24R-2 (Piece 15, 85-87 cm)

ROCK NAME: Highly olivine-bearing clinopyroxene plagioclase phyric basalt

WHERE SAMPLED: Unit 4

TEXTURE: Highly porphyritic, intersertal

GRAIN SIZE: Fine, phaneritic

OBSERVER: ANB

PRIMARY MINERALOGY	PERCENT PRESENT	PERCENT ORIGINAL	SIZE RANGE (mm)	APPROX. COMPO-SITION	MORPHOLOGY	COMMENTS
PHENOCRYSTS						
Olivine	—	Tr	<0.5		Subhedral	Replaced by calcite.
Plagioclase	12	12	<1	An 65	Euhedral–subhedral	Incipient sericite developing along fractures.
Clinopyroxene	2	2	<0.5	Augite	Subhedral	
Glomerocrysts	2	2	<5			Plag ± cpx.
GROUNDMASS						
Clinopyroxene	10	19	<0.2	Augite	Anhedral	Rather granular, altered-looking crystals.
Plagioclase	25	40	<0.3	An 60	Subhedral	
Spinel	10	10	<0.2	Magnetite	Subhedral–anhedral	

SECONDARY MINERALOGY	PERCENT	REPLACING/ FILLING	COMMENTS
Clays	30	Groundmass, vesicles	In interstices in groundmass. Amorphous olive-brown phase, possibly after glass.
Carbonate	9	Groundmass, vesicles	Associated with clays.

VESICLES/ CAVITIES	PERCENT	LOCATION	SIZE RANGE (mm)	FILLING	SHAPE	COMMENTS
Vesicles	15	Random	<20	Calcite, clay	Elliptical	Brown calcite rims; radial clay growing inward.

COMMENTS: Sub-fluidal alignment of groundmass plag.

THIN SECTION DESCRIPTION

115-707C-24R-3 (Piece 2B, 38-40 cm)

ROCK NAME: Highly olivine-bearing clinopyroxene plagioclase phyric basalt

WHERE SAMPLED: Unit 4

TEXTURE: Highly porphyritic, intersertal

GRAIN SIZE: Fine, phaneritic

OBSERVER: ANB

PRIMARY MINERALOGY	PERCENT PRESENT	PERCENT ORIGINAL	SIZE RANGE (mm)	APPROX. COMPO-SITION	MORPHOLOGY	COMMENTS
PHENOCRYSTS						
Olivine	—	Tr	<0.5		Subhedral	Completely altered to iddingsite.
Plagioclase	10	10	<2	An 65	Subhedral	Fresh. Some large crystals show oscillatory zoning.
Clinopyroxene	1	1	<0.8	Augite	Subhedral	Fresh.
GROUNDMASS						
Plagioclase	25	30	<0.5	An 60(?)	Subhedral	Partially altered to clays.
Clinopyroxene	15	20	<0.5	Augite	Anhedral	Intersertal texture with plag.
Spinel	5	5	<0.5	Magnetite	Subhedral–anhedral	
Glass(?)	—	14				Quenched matrix, completely replaced by clays.

SECONDARY MINERALOGY	PERCENT	REPLACING/ FILLING	COMMENTS
Clays	29	Glass(?)	Brown clay. Alteration of interstitial groundmass material, and possibly glass.
Carbonate	5	Groundmass, vesicles	

VESICLES/ CAVITIES	PERCENT	LOCATION	SIZE RANGE (mm)	FILLING	SHAPE	COMMENTS
Vesicles	20	Random	<1	Clay, calcite	Irregular	10% rimmed by brown clays + calcite. Interiors are generally empty.

THIN SECTION DESCRIPTION

115–707C–25R–1 (Piece 1D, 39–43 cm)

ROCK NAME: Highly clinopyroxene plagioclase phyric basalt

WHERE SAMPLED: Unit 4

TEXTURE: Highly porphyritic

GRAIN SIZE: Fine

OBSERVER: YT

PRIMARY MINERALOGY	PERCENT PRESENT	PERCENT ORIGINAL	SIZE RANGE (mm)	APPROX. COMPOSITION	MORPHOLOGY	COMMENTS
PHENOCRYSTS						
Olivine	—	(?)				If any, completely altered. No more than 1% orignally.
Plagioclase	7	7	0.2–1.0	An 50	Euhedral–subhedral	Fresh. Zoned.
Clinopyroxene	3	3	0.2–0.5	Augite	Subhedral	Some glomerocrysts with plag.
GROUNDMASS						
Plagioclase	45	58	<0.2		Subhedral	Some alteration to brown clay.
Clinopyroxene	17	29	<0.2	Augite	Subhedral	
Opaques	3	3		Magnetite	Euhedral	

SECONDARY MINERALOGY	PERCENT	REPLACING/ FILLING
Clays	25	Plag, cpx

THIN SECTION DESCRIPTION

115–707C–25R–1 (Piece 1G, 90–93 cm)

ROCK NAME: Highly olivine clinopyroxene plagioclase phyric basalt

WHERE SAMPLED: Unit 4

TEXTURE: Highly porphyritic

GRAIN SIZE: Fine to medium

OBSERVER: YT

PRIMARY MINERALOGY	PERCENT PRESENT	PERCENT ORIGINAL	SIZE RANGE (mm)	APPROX. COMPOSITION	MORPHOLOGY	COMMENTS
PHENOCRYSTS						
Olivine	—	1	<0.3		Euhedral	Completely altered to brown clay.
Plagioclase	20	20	0.3–1.4	An 55	Euhedral–subhedral	Fresh. Zoned. Rarely showing honeycomb structure. Some glomerocrysts. A few crystals show reverse zoning and have dusty inclusions.
Clinopyroxene	5	5	0.3–0.5	Augite	Subhedral	Fresh. Glomerocrysts with plag common.
GROUNDMASS						
Plagioclase	35	50	<0.3		Subhedral	Partial replacement by brown clay. Cpx is augite.
Clinopyroxene	16	20				
Opaques	3	3	<0.2	Magnetite	Euhedral	

SECONDARY MINERALOGY	PERCENT	REPLACING/ FILLING	COMMENTS
Clays	1	Ol	
Clays	20	Plag, cpx	Replacing groundmass plag ± cpx.

THIN SECTION DESCRIPTION

115-707C-25R-2 (Piece 1C, 34-38 cm)

ROCK NAME: Highly olivine-bearing clinopyroxene plagioclase phyric basalt

WHERE SAMPLED: Unit 4

TEXTURE: Highly porphyritic, intersertal

GRAIN SIZE: Fine, phaneritic

OBSERVER: ANB

PRIMARY MINERALOGY	PERCENT PRESENT	PERCENT ORIGINAL	SIZE RANGE (mm)	APPROX. COMPO-SITION	MORPHOLOGY	COMMENTS
PHENOCRYSTS						
Olivine	—	<1	<0.1		Subhedral	Completely replaced by serpentine/iddingsite.
Plagioclase	15	15	<1.0	An 60	Euhedral–subhedral	Inclusions of brown glass.
Clinopyroxene	5	5	<0.8		Subhedral	
Glomerocrysts	1	1	<0.5			Glomerocrysts of plag and cpx.
GROUNDMASS						
Olivine	—	1	<0.1		Anhedral	
Plagioclase	25	25	<0.3	An 60(?)	Subhedral	
Clinopyroxene	15	15	<0.3	Augite	Anhedral	
Spinel	10	10	<0.3	Magnetite	Subhedral–anhedral	
Glass(?)	—	28				Quenched matrix, completely altered to brown clays.

SECONDARY MINERALOGY	PERCENT	REPLACING/ FILLING	COMMENTS
Clays	25	Groundmass, glass(?)	Amorphous olive brown mineral replaces quenched groundmass and possibly glass.
Carbonate	3	Groundmass	
Serpentine/ iddingsite	1	Ol	

VESICLES/ CAVITIES	PERCENT	LOCATION	SIZE RANGE (mm)	FILLING	SHAPE
Vesicles	1	Random	<0.5	Calcite	Subspherical

THIN SECTION DESCRIPTION

115-707C-25R-2 (Piece 1L, 130-132 cm)

ROCK NAME: Highly olivine clinopyroxene plagioclase phyric basalt

WHERE SAMPLED: Unit 4

TEXTURE: Highly porphyritic

GRAIN SIZE: Fine to medium

OBSERVER: YT

PRIMARY MINERALOGY	PERCENT PRESENT	PERCENT ORIGINAL	SIZE RANGE (mm)	APPROX. COMPO-SITION	MORPHOLOGY	COMMENTS
PHENOCRYSTS						
Olivine	—	3	0.2–0.3		Euhedral	Completely altered to brown clay.
Plagioclase	20	20	0.2–1.2	An 55	Euhedral–subhedral	Some glomerocrysts.
Clinopyroxene	7	7	0.2–0.5	Augite	Euhedral subhedral	Commonly as glomerocrysts with plag.
GROUNDMASS						
Plagioclase	35	43	<0.2		Subhedral	Some alteration to brown clays. Cpx is augite.
Clinopyroxene	16	20				
Opaques	7	7	<0.1	Magnetite(?)		Fine-grained aggregates with another unidentifiable opaque.

SECONDARY MINERALOGY	PERCENT	REPLACING/ FILLING	COMMENTS
Clays	12	Plag, cpx	Groundmass alteration.
Clays	3	Ol	Brown clay.

VESICLES/ CAVITIES	PERCENT	LOCATION	SIZE RANGE (mm)	FILLING	SHAPE	COMMENTS
Vesicles	<1		0.5	Clay	Round	Brown clay.

THIN SECTION DESCRIPTION

115–707C–25R–3 (Piece 1A, 0–1 cm)

ROCK NAME: Highly olivine clinopyroxene plagioclase phyric basalt

WHERE SAMPLED: Unit 4, top of piece

TEXTURE: Highly porphyritic

GRAIN SIZE: Fine

OBSERVER: MRF

PRIMARY MINERALOGY	PERCENT PRESENT	PERCENT ORIGINAL	SIZE RANGE (mm)	APPROX. COMPO-SITION	MORPHOLOGY	COMMENTS
PHENOCRYSTS						
Olivine	—	1	<1		Euhedral	Replaced by clay.
Plagioclase	15	15	1–2		Euhedral–subhedral	L:W = 2:1
Clinopyroxene	4	4	0.1–0.2		Equant, subhedral	
GROUNDMASS						
Plagioclase	30	30	0.05–0.20		Blades, euhedral–subhedral	
Clinopyroxene	30	30	0.05–0.10		Equant, anhedral	
Magnetite	5	5	0.02–0.05		Equant, subhedral	
Glass(?)	—	15				Quenched groundmass, completely altered to clay.

SECONDARY MINERALOGY	PERCENT	REPLACING/ FILLING	COMMENTS
Clays	1	Ol	Green to brown. Chlorite(?).
Clays	15	Groundmass, glass(?)	

COMMENTS: 6-mm-wide vein cuts the top of the sample. Filled with a succession of phases, from edge to center: black rim with skeletal magnetite; yellow-orange clay which grades into iddingsite; calcite.

THIN SECTION DESCRIPTION

115–707C–25R–3 (Piece 1D, 29–31 cm)

ROCK NAME: Highly olivine clinopyroxene plagioclase phyric basalt

WHERE SAMPLED: Unit 4

TEXTURE: Highly porphyritic

GRAIN SIZE: Fine

OBSERVER: MRF

PRIMARY MINERALOGY	PERCENT PRESENT	PERCENT ORIGINAL	SIZE RANGE (mm)	APPROX. COMPO-SITION	MORPHOLOGY	COMMENTS
PHENOCRYSTS						
Olivine	—	1	<1		Euhedral	
Plagioclase	15	15	1–2		Euhedral–subhedral	
Clinopyroxene	3	3	0.1–0.2		Equant, subhedral	Some glomerocrysts with plag.
GROUNDMASS						
Plagioclase	30	30	0.05–0.20		Blades, euhedral–subhedral	
Clinopyroxene	30	30	0.05–0.10		Equant, anhedral	
Magnetite	5	5	0.02–0.05		Equant, subhedral	
Glass(?)	—	16				Quenched groundmass, completely altered to clay.

SECONDARY MINERALOGY	PERCENT	REPLACING/ FILLING	COMMENTS
Clays	1	Ol	
Clays	16	Groundmass	

COMMENTS: This section is identical to 115-707C-25R-3 (Piece 1A, 0–1 cm), except for the absence of the vein in this sample.

THIN SECTION DESCRIPTION

115-707C-25R-3 (Piece 1M, 116-118 cm)

ROCK NAME: Highly clinopyroxene plagioclase phyric basalt

WHERE SAMPLED: Unit 4

TEXTURE: Highly porphyritic, intersertal(?)

GRAIN SIZE: Fine

OBSERVER: MRF

PRIMARY MINERALOGY	PERCENT PRESENT	PERCENT ORIGINAL	SIZE RANGE (mm)	APPROX. COMPO-SITION	MORPHOLOGY	COMMENTS
PHENOCRYSTS						
Plagioclase	15	15	0.5–2.0		Euhedral	Blades to equant rounded grains.
Clinopyroxene	2	5	0.04–0.20		Euhedral–subhedral, equant	
GROUNDMASS						
Plagioclase	40	40	0.02–0.15		Euhedral, blades	
Clinopyroxene	15	20	0.01–0.08		Subhedral, equant	
Magnetite	5	5	0.04		Subhedral, equant	
Glass(?)	—	15				Quenched groundmass, completely altered.

SECONDARY MINERALOGY	PERCENT	REPLACING/ FILLING	COMMENTS
Chlorite	20	Quenched groundmass, cpx	Brown to green.
Clay??	3	Cpx	Replacing cpx phenocrysts.

THIN SECTION DESCRIPTION

115-707C-25R-4 (Piece 1C, 26-28 cm)

ROCK NAME: Highly olivine clinopyroxene plagioclase phyric basalt

WHERE SAMPLED: Unit 4

TEXTURE: Highly porphyritic

GRAIN SIZE: Fine to medium

OBSERVER: RBH

PRIMARY MINERALOGY	PERCENT PRESENT	PERCENT ORIGINAL	SIZE RANGE (mm)	APPROX. COMPO-SITION	MORPHOLOGY	COMMENTS
PHENOCRYSTS						
Olivine(?)	—	3	0.5		Euhedral	Completely altered to yellow-green clay ± opx(?). Probably altered ol.
Plagioclase	10	10	1.5		Subhedral	Glomerocrysts.
Clinopyroxene	3	3	0.5		Subhedral	Associated with plag and glomerocrysts.
GROUNDMASS						
Titanomagnetite	6	6	0.02–0.15		Skeletal	Every crystal is more or less skeletal. Some dendritic crystals. Seem to be homogeneous in composition.
Plagioclase	28	28	0.3			
Clinopyroxene	20	20	0.2			
Glass(?)	—	30	0.3			Quenched matrix, completely altered.

SECONDARY MINERALOGY	PERCENT	REPLACING/ FILLING	COMMENTS
Clays	33	Ol, matrix	Yellowish brown clay replacing ol and interstitial material.

COMMENTS: Opaques are skeletal titanomagnetite. May be more abundant than estimated above.
It is not obvious whether the altered ferromagnesian mineral is ol or opx (or both). Probably ol.

THIN SECTION DESCRIPTION

115-707C-25R-4 (Piece 1S, 132-136 cm)

ROCK NAME: Highly clinopyroxene plagioclase phyric basalt

WHERE SAMPLED: Unit 4

TEXTURE: Highly porphyritic

GRAIN SIZE: Fine to medium

OBSERVER: YT

PRIMARY MINERALOGY	PERCENT PRESENT	PERCENT ORIGINAL	SIZE RANGE (mm)	APPROX. COMPO-SITION	MORPHOLOGY	COMMENTS
PHENOCRYSTS						
Plagioclase	17	17	0.2–1.2	≈An 50	Euhedral–subhedral	Fresh. Zoned. Glomerocrysts common. Some crystals show honeycomb-like structure.
Clinopyroxene	6	6	0.2–0.5	Augite	Subhedral	Fresh. Glomerocrysts with plag quite common.
GROUNDMASS						
Plagioclase	28	46	<0.2	≈An 40	Subhedral	
Clinopyroxene	17	27	<0.2	Augite	Subhedral	
Opaques	4	4	<0.2	Magnetite	Euhedral	

SECONDARY MINERALOGY	PERCENT	REPLACING/ FILLING	COMMENTS
Clays	28	Plag, cpx	Groundmass plag and cpx are replaced by brown clay.

THIN SECTION DESCRIPTION

115-707C-25R-5 (Piece 1D, 26-28 cm)

ROCK NAME: Highly olivine clinopyroxene plagioclase phyric basalt

WHERE SAMPLED: Unit 4

TEXTURE: Highly porphyritic

GRAIN SIZE: Fine to medium

OBSERVER: YT

PRIMARY MINERALOGY	PERCENT PRESENT	PERCENT ORIGINAL	SIZE RANGE (mm)	APPROX. COMPO-SITION	MORPHOLOGY	COMMENTS
PHENOCRYSTS						
Olivine	—	3	0.2–0.4		Euhedral–subhedral	Completely altered to brown clays.
Plagioclase	15	15	0.2–1.2	An 60	Euhedral–subhedral	Fresh. Zoned. An 40 to An 60. Glomerocrysts.
Clinopyroxene	3	3	0.2–0.3	Augite	Subhedral	Fresh. Glomerocrysts with plag common.
GROUNDMASS						
Plagioclase	40	50	<0.2	An 40	Subhedral	
Clinopyroxene	19	24	<0.2	Augite	Subhedral	
Opaques	5	5	<0.2	Magnetite	Euhedral	

SECONDARY MINERALOGY	PERCENT	REPLACING/ FILLING
Clays	3	Ol
Clays	15	Plag, cpx

THIN SECTION DESCRIPTION

115-707C-25R-5 (Piece 1Q, 119-121 cm)

ROCK NAME: Highly olivine clinopyroxene plagioclase phyric basalt

WHERE SAMPLED: Unit 4

TEXTURE: Highly porphyritic, intersertal

GRAIN SIZE: Fine, phaneritic

OBSERVER: ANB

PRIMARY MINERALOGY	PERCENT PRESENT	PERCENT ORIGINAL	SIZE RANGE (mm)	APPROX. COMPO-SITION	MORPHOLOGY	COMMENTS
PHENOCRYSTS						
Olivine	—	1	<0.5		Subhedral	Replaced by serpentine + calcite.
Plagioclase	15	15	<1.5	An 60(?)	Euhedral–subhedral	Fresh. Glass inclusions.
Clinopyroxene	2	2	<0.5	Augite	Subhedral	
Glomerocrysts	1	1	<1			Glomerocrysts of plag + cpx.
GROUNDMASS						
Olivine	—	Tr	<0.2		Subhedral	Replaced by brown serpentine/iddingsite.
Plagioclase	30	30	<0.3	An 60(?)	Subhedral	
Clinopyroxene	20	20	<0.2	Augite	Anhedral	
Spinel	7	7	<0.2	Magnetite	Subhedral	
Glass(?)	—	24				Quenched matrix, completely altered to olive-brown clays.

SECONDARY MINERALOGY	PERCENT	REPLACING/ FILLING	COMMENTS
Clays	22	Matrix	Olive-brown amorphous clay filling interstices in groundmass. Replacing quenched matrix.
Carbonate	2	Matrix, ol	Calcite. Partially infilling interstices in groundmass.
Serpentine/ iddingsite	1	Ol	

THIN SECTION DESCRIPTION

115-707C-25R-6 (Piece 2, 14-18 cm)

ROCK NAME: Highly olivine clinopyroxene plagioclase phyric basalt

WHERE SAMPLED: Unit 4

TEXTURE: Highly porphyritic

GRAIN SIZE: Fine

OBSERVER: MRF

PRIMARY MINERALOGY	PERCENT PRESENT	PERCENT ORIGINAL	SIZE RANGE (mm)	APPROX. COMPO-SITION	MORPHOLOGY	COMMENTS
PHENOCRYSTS						
Olivine	—	2	0.3		Equant	Replaced by chlorite.
Plagioclase	15	15	0.3–2.0		Equant, blades	Glomerocrysts up to 3 mm diameter.
Clinopyroxene	3	3	0.1–0.6			
GROUNDMASS						
Plagioclase	25	25				
Clinopyroxene	25	25				
Magnetite	1	1	0.01–0.05		Equant, skeletal, subhedral	
Glass(?)	—	29				Quenched matrix, completely altered to opaques.

SECONDARY MINERALOGY	PERCENT	REPLACING/ FILLING
Clays	29	Quenched matrix
Chlorite	2	Ol

THIN SECTION DESCRIPTION

115-707C-25R-6 (Piece 7M, 119-122 cm)

ROCK NAME: Highly olivine-bearing clinopyroxene plagioclase phyric basalt
WHERE SAMPLED: Unit 4
TEXTURE: Highly porphyritic
GRAIN SIZE: Fine
OBSERVER: MRF

PRIMARY MINERALOGY	PERCENT PRESENT	PERCENT ORIGINAL	SIZE RANGE (mm)	APPROX. COMPOSITION	MORPHOLOGY	COMMENTS
PHENOCRYSTS						
Olivine	—	1(?)				*Completely altered to clay.*
Plagioclase	10	10	0.3–2.0		Subhedral, blades	L:W = 1:2
Clinopyroxene	3	3	0.1–0.6			
Glomerocrysts	1	1				Composed of cpx + plag (in a 1:1 ratio) + clay (altered ol?). 1 mm diameter. One 3-mm-diameter glomerocryst.
GROUNDMASS						
Plagioclase	30	30	0.05–0.30		Blades, subhedral	L:W = 1:4
Clinopyroxene	30	30	0.25–0.75		Equant, anhedral	
Magnetite	1	1	0.01–0.10		Equant, skeletal	
Glass(?)	—	24				Quenched matrix, completely altered to clays.

SECONDARY MINERALOGY	PERCENT	REPLACING/ FILLING	COMMENTS
Clays	1	Ol	
Clays	24	Glass, cpx	Alteration of groundmass cpx?

THIN SECTION DESCRIPTION

115-707C-26R-1 (Piece 1N, 74-76 cm)

ROCK NAME: Highly clinopyroxene plagioclase phyric basalt
WHERE SAMPLED: Unit 4
TEXTURE: Highly porphyritic
GRAIN SIZE: Fine
OBSERVER: JDG

PRIMARY MINERALOGY	PERCENT PRESENT	PERCENT ORIGINAL	SIZE RANGE (mm)	APPROX. COMPOSITION	MORPHOLOGY	COMMENTS
PHENOCRYSTS						
Plagioclase	10	10	<3.0	An 80	Euhedral	Glomerocrysts.
Clinopyroxene	1	1	50.3	Augite		
GROUNDMASS						
Plagioclase	38	38	≈0.1		Subhedral	
Clinopyroxene	38	48	≈0.05	Augite	Anhedral	
Opaques	3	3	≈0.1		Subhedral	

SECONDARY MINERALOGY	PERCENT	REPLACING/ FILLING	COMMENTS
Clays	10	Cpx	Brown clay.

THIN SECTION DESCRIPTION

115-707C-26R-1 (Piece 1U, 134-136 cm)

ROCK NAME: Highly olivine clinopyroxene plagioclase phyric basalt

WHERE SAMPLED: Unit 4

TEXTURE: Highly porphyritic

GRAIN SIZE: Fine

OBSERVER: MRF

PRIMARY MINERALOGY	PERCENT PRESENT	PERCENT ORIGINAL	SIZE RANGE (mm)	APPROX. COMPOSITION	MORPHOLOGY	COMMENTS
PHENOCRYSTS						
Olivine	—	2	0.3		Equant	Completely altered to clays.
Plagioclase	15	15	0.2–2.0		Blades, equant	Glomerocrysts up to 6 mm diameter.
Clinopyroxene	3	3	0.05–0.40	Augite	Equant, subhedral–anhedral	
Spinel	<1	<1	0.05–0.10	Magnetite	Equant, subhedral	
GROUNDMASS						
Plagioclase	20	20				
Clinopyroxene	39	39				
Magnetite	1	1	0.005–0.025		Equant	
Glass(?)	—	20				Quenched matrix, completely altered.

SECONDARY MINERALOGY	PERCENT	REPLACING/ FILLING
Clays	2	Ol
Clays	20	Glass

THIN SECTION DESCRIPTION

115-707C-26R-2 (Piece 1I, 88-90 cm)

ROCK NAME: Highly olivine clinopyroxene plagioclase phyric basalt

WHERE SAMPLED: Unit 4

TEXTURE: Highly porphyritic

GRAIN SIZE: Fine

OBSERVER: MRF

PRIMARY MINERALOGY	PERCENT PRESENT	PERCENT ORIGINAL	SIZE RANGE (mm)	APPROX. COMPOSITION	MORPHOLOGY	COMMENTS
PHENOCRYSTS						
Olivine	—	1	0.4		Equant	
Plagioclase	14	14	0.3–2.0		Equant, blades, subhedral	
Clinopyroxene	3	3	0.05–0.30		Equant, subhedral–anhedral	
Spinel	1	1	0.05–0.30	Magnetite	Equant, subhedral	
GROUNDMASS						
Plagioclase	28	28	<0.3		Blades, subhedral	
Clinopyroxene	28	28	<0.1		Anhedral	
Magnetite	1	1	<0.5		Anhedral	
Glass(?)	—	25				Quenched matrix, completely replaced by clay.

SECONDARY MINERALOGY	PERCENT	REPLACING/ FILLING
Clays	25	Glass
Clays	1	Ol

THIN SECTION DESCRIPTION

115-707C-26R-2 (Piece 1O, 126-128 cm)

ROCK NAME: Highly clinopyroxene plagioclase phyric basalt
WHERE SAMPLED: Unit 4
TEXTURE: Highly porphyritic
GRAIN SIZE: Fine to medium
OBSERVER: JDG

PRIMARY MINERALOGY	PERCENT PRESENT	PERCENT ORIGINAL	SIZE RANGE (mm)	APPROX. COMPO-SITION	MORPHOLOGY	COMMENTS
PHENOCRYSTS						
Plagioclase	10	10	52.5	An 82	Euhedral	Fresh. Glomerocrysts.
Clinopyroxene	1	1	0.2	Augite	Euhedral	Fresh.
GROUNDMASS						
Plagioclase	38	38			Subhedral	
Clinopyroxene	38	48(?)		Augite	Anhedral	Percent cpx may be higher than estimated.
Opaques	3	3	0.1		Subhedral	

SECONDARY MINERALOGY	PERCENT	REPLACING/ FILLING	COMMENTS
Clays	10	Cpx(?)	Dark brown, microcrystalline clay. Interstitial.

VESICLES/ CAVITIES	PERCENT	LOCATION	SIZE RANGE (mm)	FILLING	SHAPE	COMMENTS
Vesicles	<1	Random	2	Clays	Oval	Appear to be vesicles.

COMMENTS: Clays are indicated above as replacing cpx. This is not certain.

THIN SECTION DESCRIPTION

115-707C-26R-3 (Piece 1I, 84-86 cm)

ROCK NAME: Highly clinopyroxene plagioclase phyric basalt
WHERE SAMPLED: Unit 4
TEXTURE: Highly porphyritic
GRAIN SIZE: Fine
OBSERVER: JDG

PRIMARY MINERALOGY	PERCENT PRESENT	PERCENT ORIGINAL	SIZE RANGE (mm)	APPROX. COMPO-SITION	MORPHOLOGY	COMMENTS
PHENOCRYSTS						
Plagioclase	10	10	52.5	An 70	Euhedral	An content determined on small grain; could be more calcic. Glomerocrysts.
Clinopyroxene	1	1	50.2	Augite		
GROUNDMASS						
Plagioclase	38	38	0.1		Anhedral–subhedral	Crystals are more calcic than An 70.
Clinopyroxene	38	48(?)	0.04	Augite	Anhedral	
Opaques	3	3	0.1		Subhedral–euhedral	

SECONDARY MINERALOGY	PERCENT	REPLACING/ FILLING	COMMENTS
Clays	10	Cpx(?)	Dark brown cryptocrystalline clay. Uncertain if result of cpx alteration.

THIN SECTION DESCRIPTION

115-707C-26R-4 (Piece 1F, 85-86 cm)

ROCK NAME: Highly clinopyroxene plagioclase phyric basalt

WHERE SAMPLED: Unit 4

TEXTURE: Porphyritic, vesicular

GRAIN SIZE: Fine

OBSERVER: JDG

PRIMARY MINERALOGY	PERCENT PRESENT	PERCENT ORIGINAL	SIZE RANGE (mm)	APPROX. COMPOSITION	MORPHOLOGY	COMMENTS
PHENOCRYSTS						
Plagioclase	10	10	53.0	An 80	Euhedral	Fresh. Zoned crystals. Glomerocrysts.
Clinopyroxene	1	1	50.2	Augite	Euhedral	Fresh.
GROUNDMASS						
Plagioclase	38	38	0.1		Subhedral	
Clinopyroxene	38	48	0.03	Augite	Anhedral	
Opaques	3	3	0.1		Subhedral	

SECONDARY MINERALOGY	PERCENT	REPLACING/ FILLING	COMMENTS
Clays	10	Cpx	Brown clay. Also present in vesicles.

VESICLES/ CAVITIES	PERCENT	LOCATION	SIZE RANGE (mm)	FILLING	SHAPE
Vesicles	15	Random	<2	Brown clays	Oval

THIN SECTION DESCRIPTION

115–707C–26R–5 (Piece 1D, 35–37 cm)

ROCK NAME: Highly olivine-bearing clinopyroxene plagioclase phyric basalt
WHERE SAMPLED: Unit 4
TEXTURE: Highly porphyritic
GRAIN SIZE: Fine
OBSERVER: MRF

PRIMARY MINERALOGY	PERCENT PRESENT	PERCENT ORIGINAL	SIZE RANGE (mm)	APPROX. COMPOSITION	MORPHOLOGY	COMMENTS
PHENOCRYSTS						
Olivine	—	<1	0.3		Equant	
Plagioclase	15	15	0.3–1.0		Subhedral, blades	Glomerocrysts up to 3 mm in diameter. Strongly zoned. Both glass and mineral inclusions near crystal margins.
Clinopyroxene	3	3	0.1–0.3			
Spinel	3	3	0.05–0.20	Magnetite	Subhedral–anhedral	
GROUNDMASS						
Plagioclase	30	30	0.05–0.20		Blades	
Clinopyroxene	39	39	0.02–0.10		Anhedral	
Spinel	<1	<1	0.01	Magnetite	Anhedral–subhedral	
Glass	—	10	0.01		Irregular	

SECONDARY MINERALOGY	PERCENT	REPLACING/ FILLING
Clays	10	Glass, ol

THIN SECTION DESCRIPTION

115–707C–26R–5 (Piece 1L, 79–80 cm)

ROCK NAME: Highly olivine-bearing clinopyroxene plagioclase phyric basalt
WHERE SAMPLED: Unit 4, center of piece
TEXTURE: Highly porphyritic
GRAIN SIZE: Fine
OBSERVER: MRF

PRIMARY MINERALOGY	PERCENT PRESENT	PERCENT ORIGINAL	SIZE RANGE (mm)	APPROX. COMPOSITION	MORPHOLOGY	COMMENTS
PHENOCRYSTS						
Olivine	—	<1	0.3		Equant, subhedral	Replaced by clay.
Plagioclase	10	10	0.3–2.0		Equant, subhedral	Glomerocrysts up to 4 mm diameter.
Clinopyroxene	3	3	0.2–0.5	Augite	Equant, subhedral–anhedral	Also in glomerocrysts with plag.
Spinel	2	2	0.05–0.20	Magnetite		
GROUNDMASS						
Plagioclase	30	30	0.05–0.50		Blades, subhedral	
Clinopyroxene	20	20	0.05–0.10		Equant, anhedral	
Spinel	<1	<1	0.01			
Glass	—	35				Completely altered to clay.

SECONDARY MINERALOGY	PERCENT	REPLACING/ FILLING
Clays	35	Glass

THIN SECTION DESCRIPTION

115-707C-26R-6 (Piece 1A, 1-2 cm)

ROCK NAME: Highly clinopyroxene plagioclase phyric basalt
WHERE SAMPLED: Unit 4
TEXTURE: Highly porphyritic
GRAIN SIZE: Fine; coarse at top of sample
OBSERVER: MRF

PRIMARY MINERALOGY	PERCENT PRESENT	PERCENT ORIGINAL	SIZE RANGE (mm)	APPROX. COMPOSITION	MORPHOLOGY	COMMENTS
PHENOCRYSTS						
Plagioclase	10	10	0.3–1.0		Subhedral–equant	Glomerocrysts up to 3 mm diameter. Percentage increases to 20% at the top of the section.
Clinopyroxene	3	3	0.1–0.3	Augite	Subhedral–anhedral, equant	
Spinel	2	2	0.05–0.20	Magnetite	Euhedral–subhedral equant	
GROUNDMASS						
Plagioclase	50	50	0.1–0.3			
Clinopyroxene	30	30				
Spinel	3	3	0.03–0.10	Magnetite		
Glass	—	2	0.1			

SECONDARY MINERALOGY	PERCENT	REPLACING/ FILLING
Clays	2	Glass

VESICLES/ CAVITIES	PERCENT	LOCATION	SIZE RANGE (mm)	FILLING	SHAPE
Vesicles	<1		2	None	Round

THIN SECTION DESCRIPTION

115-707C-26R-6 (Piece 1K, 121-123 cm)

ROCK NAME: Highly olivine clinopyroxene plagioclase phyric basalt
WHERE SAMPLED: Unit 4
TEXTURE: Highly porphyritic
GRAIN SIZE: Fine
OBSERVER: MRF

PRIMARY MINERALOGY	PERCENT PRESENT	PERCENT ORIGINAL	SIZE RANGE (mm)	APPROX. COMPOSITION	MORPHOLOGY	COMMENTS
PHENOCRYSTS						
Olivine	—	1	0.3		Equant, subhedral	Replaced by clay.
Plagioclase	15	15	0.3–2.0		Subhedral	Also form glomerocrysts.
Clinopyroxene	3	3	0.1–0.6		Subhedral–anhedral, equant	
Spinel	3	3	0.1–0.3	Magnetite	Subhedral, equant	
GROUNDMASS						
Plagioclase	30	30	0.05–0.10		Blades, subhedral	
Clinopyroxene	39	39	0.05–0.10		Subhedral–anhedral, equant	
Spinel	5	5	0.03–0.10		Subhedral, equant	
Glass	—	4				

SECONDARY MINERALOGY	PERCENT	REPLACING/ FILLING
Clays	4	Glass
Clays	1	Ol

VESICLES/ CAVITIES	PERCENT	LOCATION	SIZE RANGE (mm)	FILLING	SHAPE
Vesicles	<1	Random	2	Calcite	Round

THIN SECTION DESCRIPTION

115-707C-26R-7 (Piece 1F, 55-57 cm)

ROCK NAME: Highly olivine clinopyroxene plagioclase phyric basalt

WHERE SAMPLED: Unit 4

TEXTURE: Porphyritic

GRAIN SIZE: Fine

OBSERVER: MRF

PRIMARY MINERALOGY	PERCENT PRESENT	PERCENT ORIGINAL	SIZE RANGE (mm)	APPROX. COMPO-SITION	MORPHOLOGY	COMMENTS
PHENOCRYSTS						
Olivine	—	1	1.0			Replaced by calcite.
Plagioclase	15	15	0.5–1.0		Euhedral–subhedral	Individual crystals up to 1 mm. Some crystals are strongly zoned. Glomerocrysts up to 2 mm.
Clinopyroxene	5	5	0.2–1.0	Augite	Subhedral–anhedral	
Spinel	3	3	0.1–0.6	Magnetite	Equant, skeletal	
GROUNDMASS						
Plagioclase	30	30	0.05–0.15		Blades, subhedral	
Clinopyroxene	30	30	0.01–0.10		Subhedral	
Spinel	5	5	0.01–0.10	Magnetite	Subhedral	
Glass	—	11				

SECONDARY MINERALOGY	PERCENT	REPLACING/ FILLING	COMMENTS
Chlorite	11	Glass	Brown clay.
Carbonate	1	Ol	Calcite.

THIN SECTION DESCRIPTION

115-707C-27R-2 (Piece 6A, 96-98 cm)

ROCK NAME: Highly olivine clinopyroxene plagioclase phyric basalt

WHERE SAMPLED: Unit 4

TEXTURE: Porphyritic, intersertal

GRAIN SIZE: Fine, phaneritic

OBSERVER: ANB

PRIMARY MINERALOGY	PERCENT PRESENT	PERCENT ORIGINAL	SIZE RANGE (mm)	APPROX. COMPO-SITION	MORPHOLOGY	COMMENTS
PHENOCRYSTS						
Olivine	—	1	<1		Subhedral	Replaced by calcite + serpentine.
Plagioclase	10	10	<2	An 65	Euhedral–subhedral	Glass inclusions.
Clinopyroxene	3	3	<0.6	Augite	Subhedral	
Glomerocrysts	3	3	<2			Glomerocrysts of plag + cpx.
GROUNDMASS						
Plagioclase	30	30	<0.5	An 55(?)	Subhedral	
Clinopyroxene	25	25	<0.3	Augite	Subhedral–anhedral	
Spinel	2	2	<0.3	Magnetite	Subhedral	
Glass(?)	—	26				Completely replaced by clays.

SECONDARY MINERALOGY	PERCENT	REPLACING/ FILLING	COMMENTS
Clays	26	Glass(?)	Green, very fine-grained clay. Possibly after glass.
Carbonate	1	Ol	Calcite.

VESICLES/ CAVITIES	PERCENT	LOCATION	SIZE RANGE (mm)	FILLING	SHAPE
Vesicles	1	Random	<1	Calcite	Spherical

THIN SECTION DESCRIPTION

115-707C-27R-6 (Piece 3N, 138-143 cm)

ROCK NAME: Highly olivine clinopyroxene plagioclase phyric basalt

WHERE SAMPLED: Unit 4

TEXTURE: Highly porphyritic

GRAIN SIZE: Fine

OBSERVER: ANB

PRIMARY MINERALOGY	PERCENT PRESENT	PERCENT ORIGINAL	SIZE RANGE (mm)	APPROX. COMPO-SITION	MORPHOLOGY	COMMENTS
PHENOCRYSTS						
Olivine	—	Tr				Replaced by green serpentine minerals.
Plagioclase	7	7	<1	An 60	Euhedral–Subhedral	
Clinopyroxene	2	2	<0.5	Augite	Subhedral	
Spinel	Tr	Tr	<0.5	Magnetite	Euhedral	Just discernible as phenocrysts.
GROUNDMASS						
Clinopyroxene	30	30	<0.2	Augite	Anhedral	
Plagioclase	35	35	<0.2	An 60(?)	Subhedral	
Spinel	7	7	<0.2	Magnetite	Anhedral	
Glass(?)	—	19				Completely replaced by clays.

SECONDARY MINERALOGY	PERCENT	REPLACING/ FILLING	COMMENTS
Clays	19	Glass(?)	Green-brown clay. Possibly after glass. Fills interstices in groundmass.
Serpentine	Tr	Ol	

COMMENTS: Vein cuts across slide. Approximately 6 mm wide. Filled predominately by 2 phases: marginal microcrystalline, green chlorite (celadonite?); inner, radial, very fine-grained zeolite associated with minor calcite. Zone of alteration extends into rock matrix for several mm each side of the vein, involving the same minerals.

THIN SECTION DESCRIPTION

115-707C-27R-7 (Piece 9, 49-51 cm)

ROCK NAME: Highly plagioclase clinopyroxene phyric basalt

WHERE SAMPLED: Unit 4

TEXTURE: Highly porphyritic

GRAIN SIZE: Fine, phaneritic

OBSERVER: ANB

PRIMARY MINERALOGY	PERCENT PRESENT	PERCENT ORIGINAL	SIZE RANGE (mm)	APPROX. COMPO-SITION	MORPHOLOGY	COMMENTS
PHENOCRYSTS						
Olivine	—	1	<0.5		Subhedral	Replaced by green-brown serpentine minerals.
Plagioclase	7	7	<2	An 65	Euhedral–subhedral	
Clinopyroxene	3	3	<0.5	Augite	Subhedral	
Glomerocrysts	5	5	<2			Glomerocrysts of cpx + plag.
GROUNDMASS						
Plagioclase	26	26	<0.5	An 60(?)	Subhedral	
Clinopyroxene	15	15	<0.2	Augite	Anhedral	
Spinel	4	4	<0.2	Magnetite	Subhedral	
Glass(?)	—	39				Completely replaced by clays.

SECONDARY MINERALOGY	PERCENT	REPLACING/ FILLING	COMMENTS
Serpentine	1	Ol	
Clays	39	Glass(?)	Brown-green clays in groundmass interstices. Possibly after glass.

VESICLES/ CAVITIES	PERCENT	LOCATION	SIZE RANGE (mm)	FILLING	SHAPE
Vesicles	2	Even	<0.5	Clay, calcite	Spherical

THIN SECTION DESCRIPTION

115-707C-27R-7 (Piece 14, 73-75 cm)

ROCK NAME: Highly plagioclase clinopyroxene olivine phyric basalt

WHERE SAMPLED: Unit 4

TEXTURE: Highly porphyritic

GRAIN SIZE: Fine, phaneritic

OBSERVER: ANB

PRIMARY MINERALOGY	PERCENT PRESENT	PERCENT ORIGINAL	SIZE RANGE (mm)	APPROX. COMPO-SITION	MORPHOLOGY	COMMENTS
PHENOCRYSTS						
Olivine	—	1	<0.6		Subhedral	Completely altered to olive-green/brown serpentine.
Plagioclase	10	10	<2	An 65	Euhedral–subhedral	Fresh. Strong normal zoning. Oscillatory zoning also.
Clinopyroxene	2	2	<0.5	Augite	Subhedral	
GROUNDMASS						
Plagioclase	40	40	<0.5	An 60	Subhedral	
Clinopyroxene	25	25	<0.3	Augite	Anhedral	
Spinel	5	5	<0.3	Magnetite	Subhedral	Octahedra.
Glass(?)		17				Completely replaced by clays.

SECONDARY MINERALOGY	PERCENT	REPLACING/ FILLING	COMMENTS
Clays	17	Glass(?)	Brown clay. Possibly replacing glass in groundmass.
Serpentine	1	Ol	

VESICLES/ CAVITIES	PERCENT	LOCATION	SIZE RANGE (mm)	FILLING	SHAPE	COMMENTS
Vesicles	5	Even	<1	Clays, calcite	Spherical	Filled by brown clays ± calcite.

THIN SECTION DESCRIPTION

115-707C-27R-7 (Piece 14, 73-75 cm)

ROCK NAME: Highly clinopyroxene plagioclase phyric basalt

WHERE SAMPLED: Unit 4

TEXTURE: Glomeroporphyritic

GRAIN SIZE: Fine

OBSERVER: RBH

PRIMARY MINERALOGY	PERCENT PRESENT	PERCENT ORIGINAL	SIZE RANGE (mm)	APPROX. COMPO-SITION	MORPHOLOGY	COMMENTS
PHENOCRYSTS						
Plagioclase	10	10			Subhedral, laths	Discrete crystals and glomerocrysts.
Clinopyroxene	2	2			Subhedral, equant	
GROUNDMASS						
Plagioclase	40	40	0.25		Laths	
Clinopyroxene	23	23	0.15		Equant	
Spinel	5	5	0.05	Titano–magnetite	Skeletal	Skeletal/dendritic crystals. Appear fresh. Crystals up to 0.1 mm.
Glass	—	20				

SECONDARY MINERALOGY	PERCENT	REPLACING/ FILLING	COMMENTS
Clays	20	Glass	Brownish clay after glass in groundmass. Also fills voids. Circumferential layers first, followed by radial pattern to infilling.

THIN SECTION DESCRIPTION

115-707C-28R-1 (27-29 cm)

ROCK NAME: Moderately clinopyroxene plagioclase phyric basalt

WHERE SAMPLED: Unit 4, clast in sedimentary breccia

TEXTURE: Moderately porphyritic

GRAIN SIZE: Fine to medium

OBSERVER: RBH

PRIMARY MINERALOGY	PERCENT PRESENT	PERCENT ORIGINAL	SIZE RANGE (mm)	APPROX. COMPO-SITION	MORPHOLOGY	COMMENTS
PHENOCRYSTS						
Plagioclase	>5	>5	<1.5		Subhedral	These are distinctly larger than the groundmass crystals.
Clinopyroxene	1	1	0.8		Equant, subhedral	
GROUNDMASS						
Plagioclase	32	32	0.5		Subhedral, laths	
Clinopyroxene	37	42	0.3		Granular	
Spinel	—	4	0.1		Skeletal	Completely replaced by maghemite.
Glass(?)	—	16				Completely replaced by clays.

SECONDARY MINERALOGY	PERCENT	REPLACING/ FILLING	COMMENTS
Clays	16	Glass(?)	Replacing glass or cryptocrystalline groundmass.
Pyrite	5	Cpx	Replacing cpx in quenched matrix. Some pyrite fills voids.
Maghemite	4	Titano-magnetite	

COMMENTS: This sample is from a clast in a sedimentary basaltic breccia. Feathery cpx in quenched groundmass has been pyritized. Skeletal titanomagnetite appears to have been maghemitized (g Fe_2O_3) but has not been pyritized. Pyrite in voids is distinctly famboidal in places, but disaggregation is common.

THIN SECTION DESCRIPTION

115-707C-28R-1 (Piece 1, 41-44 cm)

ROCK NAME: Moderately clinopyroxene plagioclase phyric basalt

WHERE SAMPLED: Unit 5

TEXTURE: Moderately porphyritic

GRAIN SIZE: Fine

OBSERVER: JDG

PRIMARY MINERALOGY	PERCENT PRESENT	PERCENT ORIGINAL	SIZE RANGE (mm)	APPROX. COMPO-SITION	MORPHOLOGY	COMMENTS
PHENOCRYSTS						
Plagioclase	6	6	<3		Euhedral	Some glomerocrysts. Zoned crystals.
Clinopyroxene	<1	1	<0.4	Augite	Euhedral	Mostly altered to clays.
GROUNDMASS						
Plagioclase	37	41	0.1		Subhedral	A few crystals are altered.
Clinopyroxene	3	48	0.04	Augite	Anhedral	
Opaques	3	3	0.1		Subhedral	
Glass	—	2				Completely replaced by clays.

SECONDARY MINERALOGY	PERCENT	REPLACING/ FILLING	COMMENTS
Clays	51	Plag, cpx, glass	Cryptocrystalline. Altered cpx.

VESICLES/ CAVITIES	PERCENT	LOCATION	SIZE RANGE (mm)	FILLING	SHAPE	COMMENTS
Vesicles	15	Random	<5	Clays	Irregular	Light brown clay. Finely fibrous rosettes.

COMMENTS: Highly altered sample. Ferromagnesian minerals are especially altered.

THIN SECTION DESCRIPTION

115-707C-28R-1 (Piece 2, 50–54 cm)

ROCK NAME: Highly olivine clinopyroxene plagioclase phyric basalt

WHERE SAMPLED: Unit 5

TEXTURE: Highly porphyritic

GRAIN SIZE: Fine to medium

OBSERVER: YT

PRIMARY MINERALOGY	PERCENT PRESENT	PERCENT ORIGINAL	SIZE RANGE (mm)	APPROX. COMPOSITION	MORPHOLOGY	COMMENTS
PHENOCRYSTS						
Olivine	—	1	0.3		Subhedral	Completely altered to clay.
Plagioclase	7	7	0.3–1.3	An 70	Euhedral–subhedral	Slightly altered. Zoned crystals. Some glomerocrysts.
Clinopyroxene	3	3	0.3–0.8	Augite	Subhedral	Fresh. Forms glomerocrysts with plag.
GROUNDMASS						
Plagioclase	25	25	<0.3	<An 60	Subhedral	
Clinopyroxene	10	10	<0.3	Augite	Subhedral	
Glass	—	54				Completely altered to clay + opaques.

SECONDARY MINERALOGY	PERCENT	REPLACING/ FILLING	COMMENTS
Clays	1	Ol	
Clays	54	Glass	Clays + opaques replace glass.

VESICLES/ CAVITIES	PERCENT	LOCATION	SIZE RANGE (mm)	FILLING	SHAPE
Vesicles	25	Even	1–6	Clay, zeolite(?)	Round

COMMENTS: Plag is An rich!

THIN SECTION DESCRIPTION

115-707C-28R-3 (Piece 4, 48–50 cm)

ROCK NAME: Highly plagioclase clinopyroxene olivine phyric basalt

WHERE SAMPLED: Unit 5

TEXTURE: Highly porphyritic, glomerophyric, intersertal

GRAIN SIZE: Medium, phaneritic

OBSERVER: ANB

PRIMARY MINERALOGY	PERCENT PRESENT	PERCENT ORIGINAL	SIZE RANGE (mm)	APPROX. COMPOSITION	MORPHOLOGY	COMMENTS
PHENOCRYSTS						
Olivine	1	1	1<0.5		Subhedral	
Plagioclase	22	22	<1	An 60	Euhedral–subhedral	
Clinopyroxene	5	10	<0.5	Augite	Subhedral	Replaced by clay.
Glomerocrysts	22	22	<7			Glomerocrysts of plag + cpx. Fresh.
GROUNDMASS						
Plagioclase	22	22				Fresh.
Clinopyroxene	6	6		Augite		
Glass(?)	—	17				Interstitial. Completely altered to clay + carbonate.

SECONDARY MINERALOGY	PERCENT	REPLACING/ FILLING	COMMENTS
Clays	11	Cpx, glass	Alteration of interstitial glass(?) or infill.
Carbonate	11	Glass(?)	Alteration of interstitial glass(?) or infill.

VESICLES/ CAVITIES	PERCENT	LOCATION	SIZE RANGE (mm)	FILLING	SHAPE
Vesicles	2	Random	<1	Calcite	Elliptical

THIN SECTION DESCRIPTION

115–707C–28R–3 (Piece 11, 124–126 cm)

ROCK NAME: Highly plagioclase phyric basalt

WHERE SAMPLED: Unit 5

TEXTURE: Porphyritic

GRAIN SIZE: *Fine to medium*

OBSERVER: YT

PRIMARY MINERALOGY	PERCENT PRESENT	PERCENT ORIGINAL	SIZE RANGE (mm)	APPROX. COMPO-SITION	MORPHOLOGY	COMMENTS
PHENOCRYSTS						
Plagioclase	10	10	0.4–1.2	An 40 to An 55.	Euhedral–subhedral	Fresh, zoned crystals. Some glomerocrysts.
GROUNDMASS						
Plagioclase	20	45	<0.4	An 40	Subhedral	Altered to brown clay.
Clinopyroxene	13	33	<0.4	Augite	Subhedral	Altered to brown clay.
Opaques	7	7	<0.3	Magnetite	Euhedral–subhedral	Alteration products(?).

SECONDARY MINERALOGY	PERCENT	REPLACING/ FILLING	COMMENTS
Clays	50	Plag, cpx, matrix	Alteration products of groundmass plag + cpx + quenched matrix.

VESICLES/ CAVITIES	PERCENT	LOCATION	SIZE RANGE (mm)	FILLING	SHAPE
Vesicles	5	Even	0.5–2.0	Brown clay	Elliptical